Advances in Printing and Media Technology

Vol. XLV(V)

Edited by Patrick Gane

Associate editor: Cathy Ridgway

Darmstadt
MMXVIII

Advances in Printing and Media Technology

Proceedings of the 45th International Research Conference of iarigai
Warsaw, Poland, October 2018

Published by the International Association of
Research Organizations for the Information,
Media and Graphic Arts Industries
Darmstadt, Germany, 2018

Edited by Patrick Gane, Aalto, Finland
Associate editor: Cathy Ridgway, Oftringen, Switzerland

Online edition
ISBN 978-3-948039-00-4
ISSN 2409-4021

Contents

Welcome letter 1

Zuzanna Żołek-Tryznowska

Plenary session 1 PRINTING I: Print and user Interaction

Man-machine Interfaces using Screen Printing **2**
Gunter Hübner, Thomas Fischer and Ricardo Martinez

Augmented Print – Cross-media Learning Tools for Primary School Children **10**
Helmut Wittenzellner, Manuela Blass and Eva Paap

Plenary session 2 MEDIA AND GRAPHIC I: Graphic Design

The Method for Legibility Assessment and its Application
for Model Pharmaceutical Leaflets **20**
Petr Roudný and Markéta Držková

Reality Check: What to expect when buying different Print Products for a Campaign –
Brand Color Reproduction across Print Substrates and Technologies **27**
Michael Abildgaard Pedersen

Key Elements of Developing a Customized Web-to-Print Platform **36**
Yung-Cheng Hsieh, Cheng-Cheng Jiang, Xin-Yi Wong

Plenary session 3 PACKAGING AND SUBSTRATES I: Substrate and Materials

The Influence of Nanocellulose Addition on Printing Properties of Recycled Paper **49**
Gregor Lavrič and Igor Karlovits

Development of a unidirectional Switchable Photochromic Ink for Smart Packaging **55**
Mustafa Bilgin and Johannes Backhaus

Plenary session 4 PRINTING II: Printing Processes and Products – industrial processes and product development

Interpretation of Ink Tack Stability Testing Results for Improved Offset Printability **64**
Dominik Kapović, Branka Lozo and Wilco De Groot

Direct Observation of High-speed Fluid Transfer Phenomena in the Nip
of a Gravure Printing Machine **72**
Julian Schäfer, Hans Martin Sauer and Edgar Dörsam

Study of the Effect of the Adhesion Promoter on the Coefficient of Friction,
COF, of OPP Film **82**
Małgorzata Zakrzewska and Halina Podsiadło

Plenary session 5 PRINTING III: Print Quality

Evaluating Contact Angle on Complex Surfaces to obtain a meaningful Surface Energy for Print Adhesion **88**
Patrick Gane, Cathy Ridgway and Dirk Kisters

Assessing the Quality of Pad-printed Images by evaluating Edge Sharpness **97**
Christina Bodenstein, Hans Martin Sauer, Felipe Fernandes, Edgar Dörsam and Elisabeth Warsitz

Using FEM Simulation as a Tool to develop Pad Printing **107**
Ahmad Al Aboud, Edgar Dörsam, Arash Hakimi Tehrani and Dieter Spiehl

Session 6A PACKAGING AND SUBSTRATES II: Substrate and Materials

Cardboards printed with Water-based Inkjet Inks **115**
Sandra Rosalen and Johannes Backhaus

Design of a Lightfastness Calculator for Printed Materials **125**
Fons Put and Michiel Van den Saffele

DNA and DNA Staining as a Test System for the Development of an Aptamer-based Biosensor for Sensing of Antibiotics **132**
Jacqueline Stamm, Dieter Spiehl, Jeannine Jaeger, Florian Groher, Tobias Meckel, Beatrix Suess and Edgar Dörsam

Session 6B PRINTING IV: Printed Functionality

Overcoming Printing Challenges related to Fabrication of Inkjet-printed Coated Microfluidic Reaction Platforms **142**
Eveliina Jutila, Risto Koivunen, Roger Bollström and Patrick Gane

Surface Energy-guided Patterning for Printed Electronics Applications **152**
Zhiqing Xin, Jianghao Liu, Lingya Gu, Yi Fang, Lixin Mo and Li Yang

About Deinking of Paper-based Printed Electronics **156**
Anne Blayo, Nathalie Marlin and Céline Chrétien

Session 7A PRINTING V: Secure Printing and 3D Printing

Secure Printing for Labels and Packaging using Industrial Digital Printers: authentication of printed matrix codes with smartphone cameras **164**
Slavtcho Bonev and Sviatoslav Voloshynovskiy

Image Watermarking using a Cover Work with Replicated Elements **171**
Elena Yakovleva, Anton Makarov, Valery Gorbachev and Elena Kaynarova

Information Construction of MBD-based 3D Additive Manufacturing Process Model **177**
Linlin Liu, Meng Li, Qiumin Wu, Jie Ma and Xiang Liu

Session 7B PRINTING VI: Printing Processes and Products – industrial processes and product development

Industry 4.0: what does it mean for the graphic arts industry? **185**
Anastasios E. Politis

The modification of a curtain coating Formulation and its effect on Pitting **193**
Samantha L. Schoenfelder, Alexandra Pekarovicova and Paul D. Fleming

Index of authors **202**

Dear 45th iarigai conference participants,

Welcome to Warsaw, Poland, for the annual iarigai conference! This year, the iariagi conference is being held for the first time in Poland. It is a great pleasure to be your host on this occasion in our Department of Printing Technology, Warsaw University of Technology.

2018 is also a special year for us as we celebrate the 50th anniversary of the Printing Technology Department of the Warsaw University of Technology, and, simultaneously, the International Circle of Educational Institutes for Graphic Arts Technology and Management (IC) is holding their 50th annual conference at the same site. Furthermore, apart from celebrating the anniversary of the start of education of printing technology engineers at Warsaw University of Technology, this year Poland celebrates the Centenary of Regaining Independence.

At the beginning, the Institute of Printing was part of the Faculty of Geodesy and Cartography of Warsaw University of Technology and, eventually, as a Department of Printing Technology, became an inseparable part of the Faculty of Production Engineering. Today, our Department is one from two research units, which simultaneously enable the study Printing Technology and to undertake scientific research in the field of printing.

The iarigai conference is one of the top conferences in its field and provides an international forum to present and discuss progress in research and development in the field of printing. The changes of the printing industry both drive and reflect the developments seen amongst the topics of the research papers. Nowadays, the printing industry is focused on digital printing, green printing, packaging and smart printing houses. Furthermore, the printing industry requires more and more innovative equipment, materials and solutions.

It should be highlighted that it is the first time the two biggest Associations, the International Association of Research Organizations for the Printing, Information and Communication Industries (iarigai) and the International Circle of Educational Institutes for Graphic Arts Technology and Management (IC), are holding their annual conferences together at the same time, this October 2018, and it is happening in Warsaw during such an auspicious time of celebration. These events will be historical and memorable!

Summarizing the programme and attendees, the iarigai conference features 24 high-level peer reviewed academic presentations, 3 keynote presentations, and participates in two joint sessions of together with the IC conference. We are happy that our Department is honoured to welcome nearly 100 researchers from over 24 various countries as active participants of the iarigai and IC conferences.

Enjoy the conference and your stay in Warsaw!

With our best regards,

Zuzanna Żołek-Tryznowska, Ph.D., hab. Eng.
Conference Chair

Man-machine Interfaces using Screen Printing

Gunter Hübner, Thomas Fischer and Ricardo Martinez

Institut für Innovative Anwendungen der Drucktechnologien (IAD), Hochschule der Medien, Nobelstr. 10, 70569 Stuttgart, Germany
E-mail: huebner@hdm-stuttgart.de

Short abstract

In a project dealing with Man-Machine-interfaces (MMI) capacitive sensors forming an x-y touchpad have been printed on plastic foils substrates using the screen printing process. On the backside of the foil a corresponding matrix of haptic feedback actuators are printed. The performance of the touchpad has been optimized with respect to the layout and electrical properties of the x-y-crossings and the necessary screen printing parameters. The sensing performance is tested using a commercial application development system.

Keywords: Screen-printing; fine line printing, touchpad; capacitive sensor; haptic feedback.

1. Introduction

Man-machine interfaces (MMI) are very important for the safe and reliable transmission of commands to power driven devices or vehicles. In the investigation presented here the goal is to fabricate a MMI demonstrator that consists of a sensor that detects the touch of a user at a certain point in an area and an active component giving a haptic feedback to the user e.g. by vibration. Thus, the user gets the feedback that a command has been transmitted without looking or waiting for an optical signal.

The novelty is the usage of a flexible substrate on which the touch sensor is placed on the front side and the vibrating device on the backside of the same substrate both using printing technologies, solely. Presently for the reception of a touch of the user capacitive sensors are very common. When arranged in an array it is called a touchpad and, if used in front of a display then it is a touchscreen. Today everybody knows this kind of device and uses it as the intuitive operation to control a smartphone, a tablet or the pointing device in a laptop. Nowadays so called projected capacitive touchpads (PCAP) dominate the market. They need two layers of conductive patterns that are insulated against each other. One layer detects the x- the other the y-direction. The PCAPs either follow the principle of the so called self-capacitance or the mutual capacitance. In this investigation only the mutual capacitance types are used since they make it possible to recognize multi-touches and sliding movements. Touchscreens that are used in smartphones are assembled on a glass substrate (mainly structured ITO) and therefore are satisfactorily transparent. In our case, however, the substrate is a thin, flexible plastic foil on which the touch sensor is printed on which is not fully transparent. It will not have the display function but maybe graphic elements. The plastic foil substrate is needed because the devices that emit a haptic feedback signal (e.g. vibration by a piezo electric effect) are directly printed on the backside of the foil. Whereas for a touchscreen it could be possible to have the x-layer on one side of the glass substrate and the y-layer on the back side in our case the complete capacitive sensors must be placed on the front side of the foil. Figure 1 shows the classical layout of an x-y-touchpad with diamond shaped areas where the x-layer is colored in red, the y-layer in blue and the necessary insulator (dielectric) in green. At the x-y-crossings the insulator has to be introduced to avoid shorts.

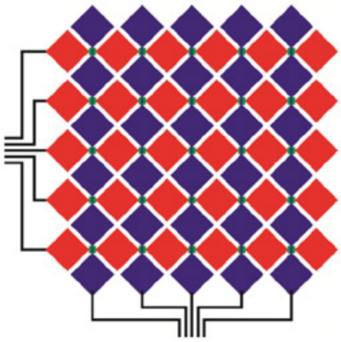

Figure 1: Classical touchpad layout, red: x-layer, blue: y-layer, green: dielectric

Based on previous work from Steiner (2016) and handbooks like Bhowmik (2014) the principle functioning of the printed touchpad according to Figure 1 could be easily proven and it is state of the art for more than 20 years as shown in patents like Seely, et al. (2001).

Now, the first step of this investigation is the optimization of the single touch sensor in the surrounding of an x-y crossing with respect to the layout and electrical properties of the touch areas, the geometry of the x-y-crossings and the necessary screen printing parameters. The sensing performance (reliability, multi-touch, detection of wiping movement) is tested using a commercial application development system specialized for touchpads.

Once the function of the touch-pad side is reliable and the layout fixed, the actuators for the haptic feedback signal will be printed on the backside. For the actuators, a printable piezo-active material is used that is capable of producing a tangible vibration. In the last step it is intended to look for a certain transparency of the whole device by using finer lines and investigate materials like PEDOT and Ag-nanowires.

2. Research methods

The first very important issue to be investigated is the reliable and reproducible printing of the dielectric for the x-y-crossings according to Figure 2.

Figure 2: x-y crossing magnified; red: x-layer, blue: y-layer, green: dielectric

Four different UV-curing dielectric inks were used for the orientating tests conducted by Martinez-Roman (2018). Very quickly it turned out that it is almost impossible to print a pinhole free single layer of dielectric on top of an underlying 2 mm wide silver track. A single pinhole renders the whole touchpad unusable. A double stroke wet-in-wet printing action showed no real improvement. Thus, the only practical and reliable process is to print two layers on top of each other with intermediate drying. The registration is not a big problem if the dielectric patch is significantly larger than the silver track width. Figure 3 shows the results of the different inks.

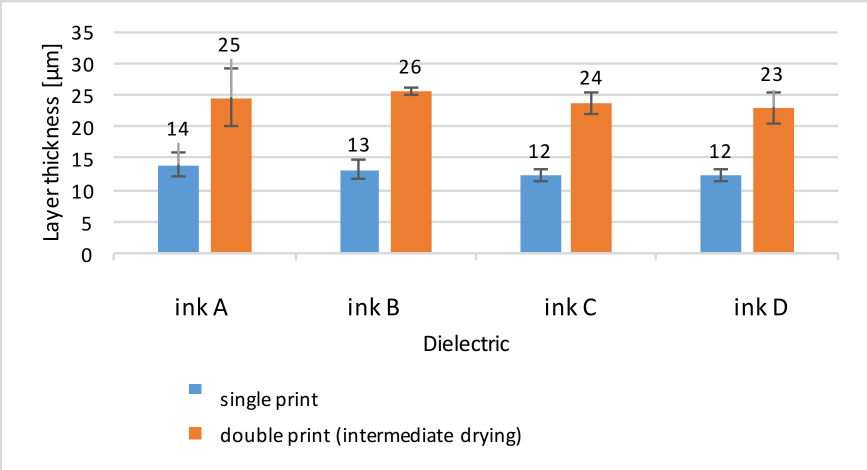

Figure 3: Layer thicknesses of dielectric inks, screen printed with a 120–34 mesh

All four tested inks showed good printing behavior but one ink revealed a poor adherence to the underlying silver track. Ink C was chosen for all following experiments.

For the compatibility with the commercial touch pad application development system, the idle capacitance of a single touch sensor has to be in the range of only a few pF. Since the changes in capacitance caused by a touch of the human finger is detected by a frequency change in appropriate oscillating circuits the corresponding charging and discharging must take place very quickly requiring such low capacitances. Since the measurement of such low capacitances is not possible with simple lab multimeters a microchip circuit according to Figure 4 had to be used.

The setup was used in Seely, et al. (2001) to measure the influences of the touchpad layout.

According to the classic capacitor equation

$$C = \varepsilon_0 \cdot \varepsilon_r \cdot \frac{A}{d} \qquad [1]$$

where
C = capacitance in Farad
ε_0 = dielectric permittivity = 8.85 Farad/m
ε_r = relative permittivity
A = area of opposing plates
d = distance between opposing plates

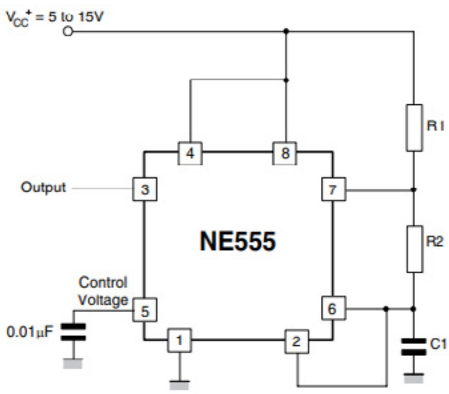

Figure 4: Measurement setup for capacitance C1 using the NE555 microchip from ST microelectronics (2012)

it is clear that the lower the thickness of the printed dielectric layer is the higher the capacitance will be. Therefore, aiming for low single-digit pF capacitance values no more effort has been made to further reduce the layer thickness although sometimes problems occurred when overprinting the edges of the dielectric with the topmost silver tracks. During the duration of the project there will be further investigations towards finer conductive tracks below 100 µm width.

3. Summary of results

3.1 Touch Sensors

The influence of different line widths of the connection lines between the diamond areas of the classic touchpad design were tested, Martinez-Roman (2018). A test pattern according to Figure 5 was printed. The smaller squares are used for contacting purposes.

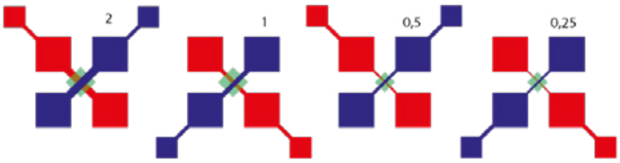

Figure 5: Test pattern with different line width of the connecting lines, Martinez-Roman (2018)

The result is shown in Figure 6. The 0.25 mm line could not be printed defect free. Thus, no capacitance could be detected.

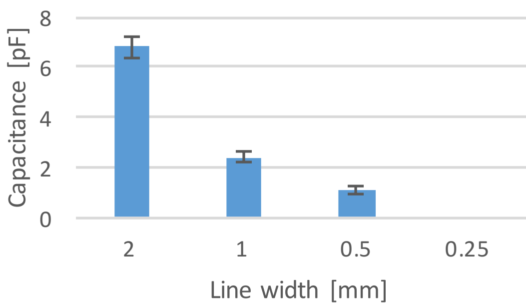

Figure 6: Influence of the connection line width on the idle capacitance of a single sensor, Martinez-Roman (2018)

It seems that the idle capacitance is strongly dependent on the area of the line crossing. Other experiments with varying the distance between the diamonds showed almost no effect on the idle capacitance.

Another important parameter is the actual size of the diamond itself. Figure 7 shows the appropriate test pattern. Again, the patches outside the four diamonds are for contacting purposes, only.

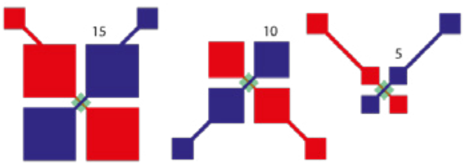

Figure 7: Test pattern with different sizes of the diamond, Martinez-Roman (2018)

As expected, Figure 8 shows that the largest diamond exhibits the largest (but still small) capacitance.

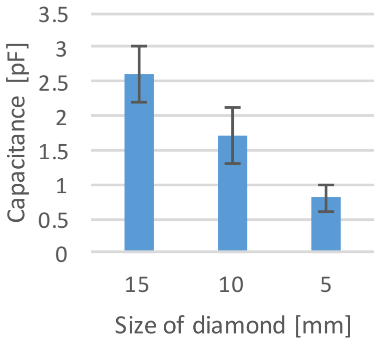

Figure 8: Influence of the size of the diamond on the idle capacitance of a single sensor, Martinez-Roman (2018)

The size of the diamond determines the resolution of the touchpad. A typical value, depending on the size of a human fingertip, is around 10–12 mm.

Whereas the diamond is the classical design, printing technologies offer a wider range of layouts. According to patent literature, e.g. US Patent US7202859, (Speck, McCaughan and Mackey, 2007), there are other possibilities like the intertwined design shown in Figure 9.

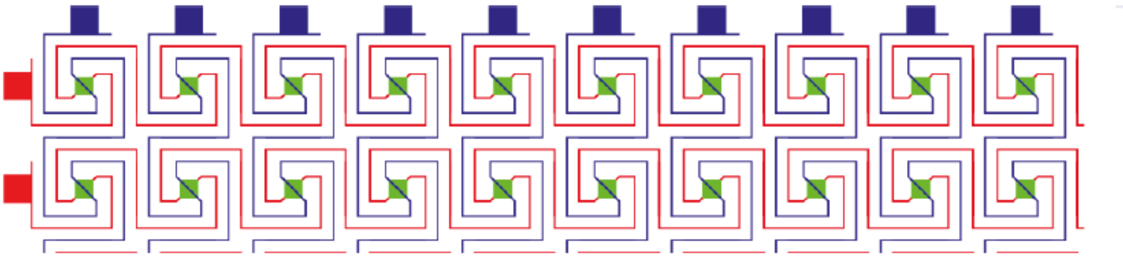

Figure 9: Touchpad design with intertwined design

A test pattern has been created according to Figure 10 with the intertwined design employing three different line width at the x-y-crossings.

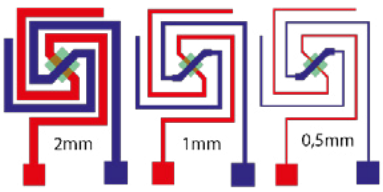

Figure 10: Test print pattern with intertwined design, Martinez-Roman (2018)

The results of the capacitance measurement are depicted in Figure 11.

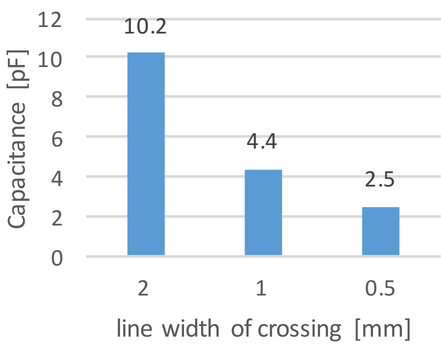

Figure 11: Influence of the line width of the crossings on the idle capacitance of a single sensor, Martinez-Roman (2018)

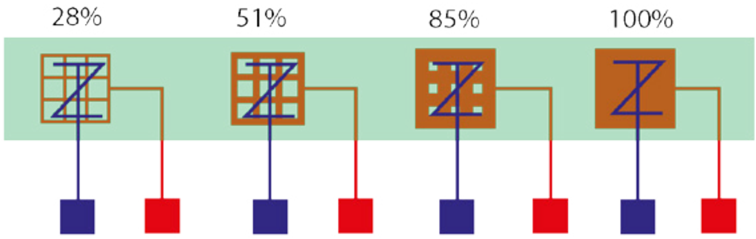

Figure 12: Test print pattern with Z-design and different area coverage of the bottom layer, Martinez-Roman (2018)

Another promising design type is the Z-type patterning according to Figure 12. In this design, the dielectric (green) is printed as a solid tone area above the (red) x-bottom-layer. The y-top-layer is Z-shaped. In order to achieve the desired low idle capacitance of the single sensor a low area coverage is advantageous.

Further testing has been done with the intertwined and the Z-design in the application development system. The most important parameter for the detection of the human interaction is the change in capacitance of the sensor when touched. The tests showed that the reliability of the touch detection (a large or the detection of multi-touches and wiping movements are good with the intertwined design but best with the Z-design. This design also has the potential to move to sufficiently transparent devices by means of fine-line printing and materials like Ag-nanowires which will be investigated in the next steps of the project.

3.1.1 Actuator

The actuator is based on a printed piezo electric active material. In general, the piezo material is sandwiched between a bottom and a top electrode. Electrodes may be printed using various conducting materials like PEDOT:PSS or others. Due to the good transparency of the materials, full assembled devices with sufficient total transparency may be possible. To improve the conductivity of the electrodes, multiple overprints are necessary. Intermediate drying steps further increase the electrical properties. The comparable low roughness of the electrodes is beneficial for the subsequent printing of the piezo active layer. The piezo layer needs to be electrically insulating for successful separation of the adjacent electrodes. Therefore, multiple printing runs are necessary of up to 6–10 repetitions to get a defect free, insulating layer.

3.1.2 Substrates

The materials that are used in our device need comparable high temperatures for annealing of the printed piezo-material film. By using temperatures about 135–140 °C the crystal like structure of the printing film is enhanced, resulting in a more distinct piezo electric effect. PET films have limited temperature stability (Tejin, n.d.). Properties can be optimized up to a certain point by preheating and relaxation processes. However, to reach optimal orientation of the dipoles and a high piezo electric effect, alternatives to PET need to be chosen as a substrate. PEN shows better properties in terms of temperature stability, thermal shrinkage, tensile elongation and was tested as an alternative to PET (Tejin, n.d.).

In order to get a functional device that exhibits a piezo electric effect, the piezo material needs to be polarized. Different procedures can be used to achieve this like it is presented by Setiadi, et al. (1996) or Fedosov, et al. (2007). We currently use a step wise poling method but research of the optimal polarisation parameters is still ongoing. First experiments lead to a successful poling of the device using 0.2 kV, 0.4 kV, 0.6 kV and finally about 0.8 kV poling steps, each applied constantly for few minutes with a relaxation phase of about 1–2 minutes between each step. Figure 13 shows the setup to polarize the piezo-active printable materials under elevated temperatures and high electrical field. The setup is in an enclosure for safety reasons.

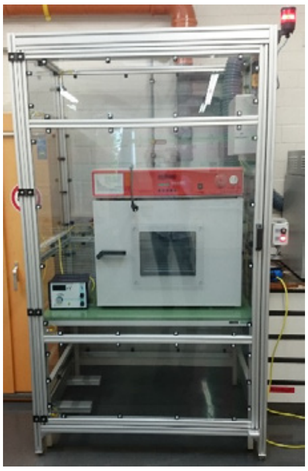

Figure 13: Oven and high voltage power source in a safety housing

When the electrical field is too high, then an electrical breakdown can occur, destroying the whole device. This is shown in Figure 14.

Figure 14: Damaged piezo actuator, because of electrical breakdown of the layers

First results of a functioning piezo actuator device printed on PET film are shown in Figure 15. Crocodile clamps are connected to the device and with the help of a frequency generator a sinus wave is generated, amplified to drive the actuator. Depending on the applied frequency, a hearable noise is generated and the device acts as a printed loudspeaker like it was also shown by other groups like Chemnitz University, Huebler, et al. (2012).

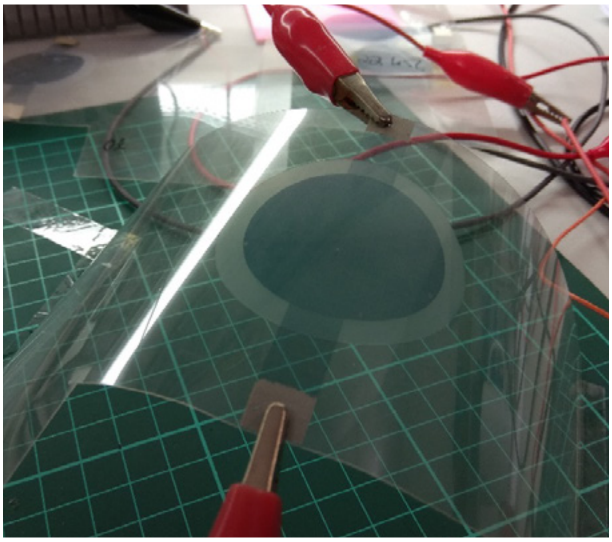

Figure 15: One of the first functioning piezo actuator exhibiting a tangible (haptic) vibration

First results show, that the best haptic feedback is in the frequency range about 130–200 Hz using a sine wave and a high amplification. In future experiments we need to tune the resonance frequency towards the aforementioned frequency range.

On the actuator side the investigations are ongoing and it is expected that good results can be presented at the conference.

4. Conclusion

It could be shown that with the means of the screen printing technologies a reliable and well-functioning touchpad could be designed and optimized. The idle capacitances are in the range that the application development system for touchpads exactly needs. First promising results could be achieved to produce an actuator based on printable piezo active material.

Since the research is ongoing with fine line printing on the touch sensor side and further optimization on the actuator side, more results will be shown at the conference in October 2018.

References

Bhowmik, A.K., 2014. *Interactive displays: natural human-interface technologies*. Chichester: John Wiley & Sons.

Fedosov, S.N., Sergeeva, A.E., Revenyuk, T.A. and Butenko, A.F., 2007. Application of corona discharge for poling ferroelectric and nonlinear optical polymers. *Physics*. http://arxiv.org/abs/0705.0177v1.

Huebler, A.C., Bellmann, M., Schmidt, G.C., Zimmermann, S., Gerlach, A., Haentjes, C., 2012. Fully mass printed loudspeaker on paper, *Organic Electronics,* 13(11), pp. 2290–2295. https://doi.org/10.1016/j.orgel.2012.06.048

Martinez-Roman, R., 2018. *Anpassung und Optimierung des Layouts und der Siebdruckparameter zur Realisierung von kapazitiven Touchsensoren*. Bachelor thesis. HdM, Stuttgart.

Seely, J., Malak, R.L., Allen, T.P., Schediwy, R.R. and Cesarotti, W.A., Synaptics. Inc. 2001. *Two-layer capacitive touchpad and method of making same*. U.S. Pat. 6,188,391.

Setiadi, D., Binnie, T.D., Regtien, P. and Wubbenhorst, M., 1996. Poling of PVDF/TrFE Copolymers using a step-wise method. In: *9th International Symposium on Electrets (ISE 9) Proceedings*. Shanghai, 27 September 1996. IEEE, pp. 831-835. https://doi.org/10.1109/ISE.1996.578215.

Speck, D.A., McCaughan, G.J. and Mackey, B.L., Synaptics Inc. 2007. Capacitive sensing system. U.S. Pat. 7,202,859.

ST microelectronics, 2012. *General-purpose single bipolar timers*. [pdf] Available at: <http://www.st.com/content/ccc/resource/technical/document/datasheet/ba/0a/d7/6e/7c/db/4e/12/CD00000479.pdf/files/CD00000479.pdf/jcr:content/translations/en.CD00000479.pdf> [Accessed 27 February 2018].

Steiner, E., 2016. Fully printed transparent capacitive touchpads from PEDOT:PSS e.g. for touchscreens - a project of the HdM Stuttgart, Germany. *International Circular of Graphic Education and Research*, 9, pp. 18–26.

Tejin, n.d. DuPont Tejin films (DTF) technical data sheets. [online] Available at: <http://www.matweb.com/search/GetMatlsByManufacturer.aspx?manID=819> [Accessed February 2018].

Augmented Print – Cross-media Learning Tools for Primary School Children

Helmut Wittenzellner, Manuela Blass and Eva Paap

Hochschule der Medien, Nobelstraße 10, 70569 Stuttgart, Germany
E-mails: wittenzellner@hdm-stuttgart.de; mr081@hdm-stuttgart.de; paap@hdm-stuttgart.de

Short abstract

Research on the use of augmented print in primary schools was conducted at the Hochschule der Medien (HdM) in Stuttgart. Augmented reality (AR) is a technology that overlays digital imagery onto the real world. It's a vital future technology in education, as it enhances the real world with digital content. Through the use of wearables (head-mounted displays, tablets, smartphones, etc.), AR can be used in education. Augmented print (the next level of print and digital interaction) can be used as a cross-media learning tool to bring textbooks, 4D+ flash cards, etc. to life. These new methods of teaching and learning with AR are increasingly being officially acknowledged by educational researcher's worldwide and leading technology companies worldwide. Research at the HdM examined the possibilities that AR has for creating innovative and novel learning environments. The following questions were researched:

1. What is the general potential of augmented print as a learning tool in the education market for primary school children and how can it be used effectively?
2. How well do parents accept AR and what risks do opponents of digitization see?
3. What possible scenarios are there to increase the motivation and learning performance of the learners, by integrating this supplemental cross-media learning tool into their lessons?

The research, which included primary and field research, concluded with a quantitative and qualitative empirical evaluation on the acceptance of parents as gatekeepers, with regards to the possible use of AR in primary education. The parents are by far open to new technologies and about 75% of the children surveyed use digital media at home. Essentially the parents believe AR offers many positive scenarios and chances, but that this could never replace a dedicated, good teacher. The data content has to be fittingly developed and matched to the age of the target group. The overuse of AR could lead to learning distractions in the classroom up to an internet and games addiction. There are critical factors with respect to digitization in primary schools that need to be researched further. For printing and publishing companies it would be recommended that a long-term research study is conducted using various augmented print products in one study group and comparing the learning results to another study group who abstain from using augmented print products. The results of such a study would not only be of interest to the above mentioned companies but also for teachers, educational institutions and governmental school authorities. Our goal is to gain insight into how German parents view the use of AR in primary schools. What potentials do they see and where are their concerns? This research provides media companies and universities with new insights, encourage publishers to print AR books, and provide teachers and schools with examples of how to improve learning results. Examples of game-based learning through edutainment (a mixture of education and entertainment) will also be included. Another area that is predestined for the use of AR, is teaching deaf children.

Keywords: cross-media learning tools, game-based learning, computer-aided, internet based, wearables

1. Introduction and background

The 1924 saying in Printers' Ink "One picture is worth ten thousand words" (Barnard, 2017) has prevailed nearly a century and affirms the value of an image. In today's 21st century, society is constantly changing because of various technological developments and trends. How we live, how we work and how we learn is strongly impacted by digitization. This change is considered "A cultural revolutionary upheaval comparable to the invention of printing" (Weiner, 2011). With the rapid progress and spread of mobile technologies, users are accustomed to accessing information, at any time and place. This mass use and rapid development of mobile technologies, opens a door to a young but promising technology named: "Augmented Reality", short AR.

AR is a technology that superimposes a computer-generated image on a user's view of the real world, thus providing a composite view. It is an increasingly important future technology in education, as it enhances the real world with digital content. Through the use of "wearables", AR can be used in education. Wearables are now serving as a technological platform that enables computer and internet based augmented reality to be seen, for example via head-mounted displays (Google Glass or Microsoft HoloLens) or via mobile devices (smartphones and tablets), in conjunction with a camera. The ever-improving development of wearables has led to greater interest in integrating the benefits of AR into learning.

Augmented print (the next level of print and digital interaction) can be used as a cross-media learning tool in the areas of language education (national language to English), social studies, math (geometry) and science to bring textbooks or other nonfiction books as well as 4D+ flash cards to life. These new methods of teaching and learning with AR are increasingly being officially acknowledged by educational researchers. AR has the potential to visualize knowledge and enable comprehensive contextual learning.

Today's children are growing up in the digital age and are often referred to as "digital natives" or "Generation Z" (Scholz, 2014). Even the youngest children have access to smartphones, tablets, etc. (Australian Associated Press, 2017). This technological evolution unfortunately has not been evident in many schools. The coexistence of virtual objects and real environments, allows the student to visualize, to hear, and to understand complex spatial relationships and abstract concepts more easily through game-based learning. Hence, allowing for a new era of learning.

Nationally, there is relatively little known about the potential of this technology and how it can support the teaching and learning of primary school children in the classroom. Internationally there has been much more progress. Many of the big tech companies such as Facebook, Google and Apple are setting their focus on AR in conjunction with mobile devices (Vanian, 2017). Combining AR with print as a bridge technology presents new opportunities not only for publishers, but also for print and media service providers.

The goal of this research is to gain insight into how German parents view the use of AR in primary schools. What potentials do they see and where are their concerns? The research results can provide media companies and universities with new insights, encourage publishers to print AR books, and provide teachers and schools with examples of how to improve learning results. Especially on a national basis, more awareness and usage of augmented print in learning environments is a primary objective of this research.

2. Materials and methods

While comprehensive standard research on AR exists, there are hardly any national studies on the use of augmented print products in primary education. Students of the Bergische Universiät Wuppertal, did some research with their Guide for Printing / Media Entrepreneurs by Menne, Strickler, and Zybell (2011): "Augmented Reality: How print media comes to life". Additionally AR print products are often still hard to find in Germany and knowhow in companies is missing (Absatzwirtschaft, 2017). Therefore this research only covers studies of books in the categories children, non-fiction, coloring and school textbooks as well as learning cards. As this research builds a bridge between three areas of knowledge, namely print, education and IT, a comprehensive analysis would be too vast.

According to Azuma (1997) and other scientists, AR systems are defined based on the following characteristics: Reality and virtuality are combined (partially overlaid), interaction occurs in real time and the real and virtual elements are registered in three dimensions. Azuma explains the difference between VR and AR as: "AR allows the user to see the real world, with virtual objects superimposed upon or composited with the real world. Therefore, AR supplements reality, rather than completely replacing it".

The most important components for the implementation of AR are as follows (Schart and Tschanz, 2015):

1. Hardware (one or more cameras as well as sensors such as gyroscope etc. from one mobile terminal or AR/MR glasses)
2. Tracking software and rendering (as a scene generator and for the calculation and correct display of overlays)
3. Display devices (this displays the virtual objects, for example, head-mounted display, monitor or display of a mobile terminal)
4. Server (part of the hardware and software, either a web or cloud server plays a crucial role in storing the database of virtual images. Based at the request of the AR application, virtual images are retrieved from the web or cloud server and sent to the application.

The heart of AR technologies is the tracking software. Important for print media are the image markers which should look good and be inconspicuously integrated into the printed product. However, there are also disadvantages with camera based tracking methods. Markers may not be obscured at any point. Additionally lighting, gloss and substrate unevenness can influence printed markers. For the successful use of augmented print products, these disadvantages must be overcome. This can occur with the use of hybrid tracking or sensor fusion. (Schart and Tschanz, 2015). It has to be fast and stable, especially if the users move with the tablet. If the tracking doesn't work, frustration is great.

Research that was conducted at the HdM included surveys and interviews with parents of primary school children. An online survey (Blas, 2018) was conducted from January 24th through February 10th 2018 for these parents using this link:

https://www.soscisurvey.de/elternbefragung2017/?act=7D8OlxiQnKHqLumfTXIeo7LO.

Here the functionality of AR was demonstrated using a colouring book and learning cards. The survey was slightly changed, after it was evident that parents didn't want to disclose their earnings. In order for parents to fully understand what the different terms mean, a video was placed online as a support for the parents. Here the link:

https://www.youtube.com/watch?v=43DgzMkrsWY

Additionally interviews were conducted and augmented print products available nationally were gathered. In the town of Hassloch, the video was shown and explained at a parent's evening on January 15, 2018. Three towns from different areas of Germany were selected (Hassloch, Ehingen and Stuttgart). Hassloch is known as a first-rate town for research, as it ideally represents the German average (Bluepartner, 2015). The research results (Table 1 and 2) of the three towns were compared, and no significant difference could be documented as the following charts validate:

Table 1: Group statistics

	Postcode starts with 8	**H**	**Mean value**	**Standard variance**	**Standard error mean value**
Risk evaluation	0.00 1.00	39 9	2.7436 3.0556	0.79089 0.45644	0.12664 0.15215
Media ownership of the child (total number)	0.00 1.00	39 9	0.7436 1.4444	0.88013 1.13039	0.14093 0.37680

	Postcode starts with 8	H	Mean value	Standard variance	Standard error mean value
Advantages/Disadvantages AR: total score	0.00 1.00	39 9	1.8359 1.6889	0.68345 0.42850	0.10944 0.14283
Personal setting: total score	0.00 1.00	39 9	2.7664 3.1852	0.77308 0.51819	0.12379 0.17273

Table 2: Test for independent samples

	Equality of variance	F	Sig.	t	df	Sig. (2-sided)	Mean value difference	Standard error difference	Lower	Superior
Risk evaluation	assumed not assumed	2.944	0.90	−1.134 −1.576	46.000 20.822	0.262 0.130	−0.31197 −0.31197	0.27499 0.19796	−0.86549 −0.72385	0.24155 0.09992
Media ownership of the child (total number)	assumed not assumed	0.208	0.651	−2.041 −1.742	46.000 10.352	0.047 0.111	−0.70085 −0.70085	0.34336 0.40229	−1.39201 −1.59310	−0.00970 0.19139
Advantages/Disadvantages AR: total score	assumed not assumed	2.310	0.135	0.615 0.817	46.000 18.787	0.542 0.424	0.14701 0.14701	0.23903 0.17994	−0.33413 −0.22990	0.62815 0.52391
Personal setting: total score	assumed not assumed	2.169	0.148	−1.541 −1.971	46.000 17.364	0.130 0.065	−0.41880 −0.41880	0.27185 0.21251	−0.96601 −0.86644	0.12840 0.02884

Augmented print and publishing will be of growing importance in the future (Carmody, 2018). Areas of application for this are newspapers, magazines, books, commercial printing, etc. As previously explained, the technology works with marker based or image based AR. In this application area there are three main motivating factors for using AR in combination with print products:

1. The attractiveness of the print product using AR applications is increased in order to create additional buying incentive.
2. The reader of the print product is enticed to use the digital products which the publisher offers, and gets to know these.
3. Via cross-media support the consumer can easily purchase products and services directly from the print product to the market.

This provides an added value, which motivates the customer to buy the printed edition. This benefit is also important for publishers and their advertisers who can use ads in newspapers and magazines enriched with AR, to get more attention to their brands and products. A 2013 BVDW study (Bundesverband Digitale Wirtschaft, 2013) found that the effectiveness of a cross-media advertising campaign through the use of conventional advertising channels with online and mobile, can be significantly increased. As a result, brands benefit considerably from digital cross-media.

But not only newspapers and magazines benefit from AR. The emergence of augmented reality in books was clearly seen at the Frankfurt Book Fair in 2017 (Krotki, 2017). In addition to language books, guides and first prototypes of textbook apps, there were also many children's and non-fiction books, many from the Asian market. As mobile media bridges the gap between classical textbooks and digital knowledge content, AR is already being used in textbooks. The Erfurt agency KIDS interactive GmbH is specialized in creating textbooks and they work together with textbook publishers such as Klett, Westermann, Diesterweg, Cornelsen and others. For Westermann, the agency develops the textbook app Zoom (Kidsinteractive, 2018). The textbook is enhanced through interactive content such as explanatory films, knowledge games, three-dimensional representations or audio sequences and thus offers an expanded view of various fields of knowledge. Thanks to the textbook app SchulAR, publishers can add AR content to already printed publications – fast, easy and cost-effective1y!

Thus, textbook publishers have recognized that this technology brings opportunities and that the education market will be correspondingly of interest for publishers. There are new opportunities to be realized in augmented print, and thus to compete with changing media usage behaviour and to find meaningful usage scenarios. With the appropriate digital content, the user can obtain added value and be offered a reading experience that has a lasting effect.

For the investment and marketing costs to be profitable in the long term, augmented print projects must be carefully planned, target groups and feasibility studies conducted and suitable partners for the multimedia and interactive content production to be found. Media companies need to deal with the weaknesses and strengths of AR so that the true potential of AR is utilized and not a one-time wow effect remains.

3. Results and discussion

The three questions which were researched are as follows:

1. What is the general potential of augmented print as a learning tool in the education market for primary school children and how can it be used effectively?
2. How well do parents accept AR and what risks do opponents of digitization see?
3. What possible scenarios are there to increase the motivation and learning performance of the learners, by integrating this supplemental cross-media learning tool into their lessons?

The methodology is both primary and secondary research with parents seen as stakeholders for their children. A total of 49 parents completed the survey (with exactly 49 primary school children), 73 partially participated. The average age of the children was 7.1 years, of the parents 36.9 years. All data (Table 3) was anonymously evaluated. Additional on-site interviews were conducted with two teachers, of which one had reservations regarding the use of AR in primary schools. Potential economic implications for schools (positive and negative) were excluded from the research as this would go beyond the scope of the research and resources available.

Table 3: Data set questionnaire

Questionnaire	Data sets completed /	total /	clicks
Parent questionnaire	49	73	221
Total	**49**	**73**	**221**

Individual statistics on exit pages

Parent questionnaire

Last edited page	Data sets completed /	total	/ **kumulativ**
Page 8	49	49	49
Page 7	0	2	51
Page 6	0	1	52
Page 5	0	3	55
Page 4	0	4	59
Page 3	0	1	60
Page 2	0	12	72
Page 1	0	1	73
Total	**49**	**73**	

A total of 221 clicks were recorded for this questionnaire (including accidental double clicks)

The parent's general attitude towards the use of digital media was researched as well, as seen in Table 4.

Table 4: Positive statements on AR effects

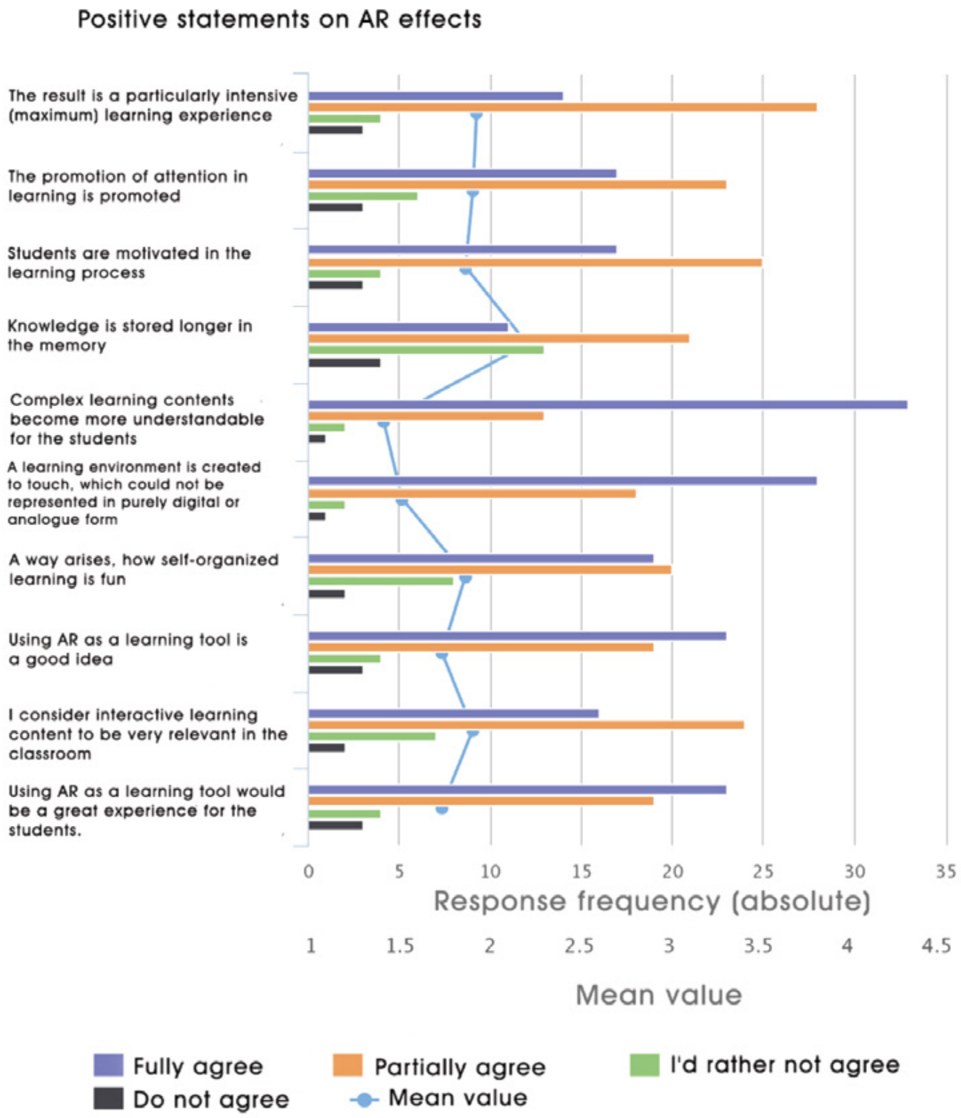

It was surprising in comparison to studies conducted in the past that about 75 % of the children in the survey, currently use one to two forms of digital media (i.e. a tablet or smartphone). Remarkable was however, that only 25 % of the children are using the internet; mostly apps are utilized. Only two of the 49 children surveyed didn't use any kind of digital media.

Despite a general acceptance of 88 % of parents who find that media literacy should be playfully promoted with the help of the teacher (see chart above), nearly half of the parents fully or partially think that it's too early for the usage of digital media in primary schools as seen in Table 5.
Research worldwide has shown that AR and augmented print offer an effective learning tool which motivates students and increases learning levels. Jasmin Bastian and Stefan Aufenanger (2016) documented in their book about the use of tablets in primary schools, how children are intrinsically motivated using tablets to learn:

Based on our research with parents in the form of surveys and interviews, parents regarded the implementation of these new technologies in the learning environment of their children mostly as positive and effective. Many parents however, indicated that these new technologies should be integrated into traditional teaching methods, rather than replace them as seen in Tables 6, 7 and 8.

Table 5: Digital media too early to use in primary school

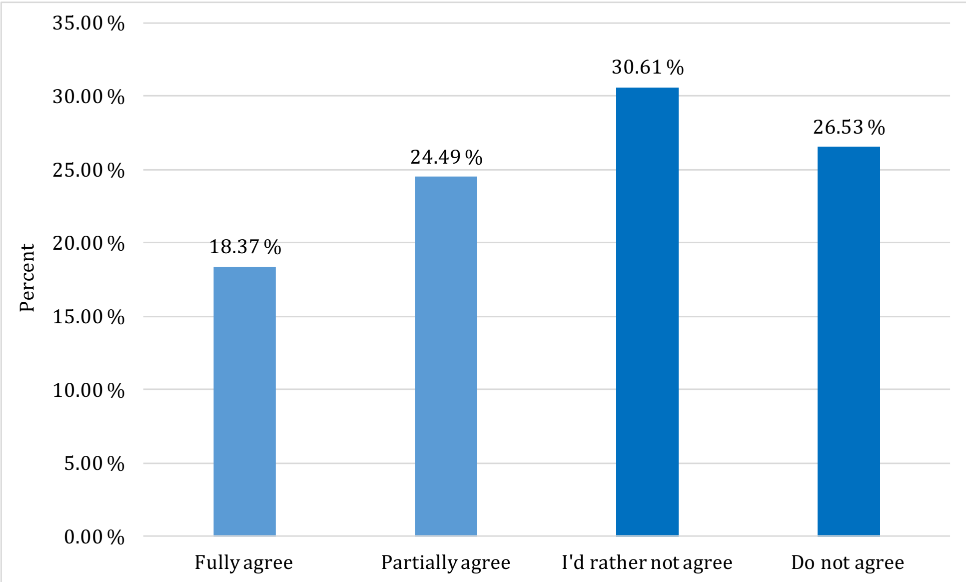

Digital media: I find it too early to use digital media in primary schools

Table 6: General attitude of parents as influencers and financial gatekeepers towards digital media

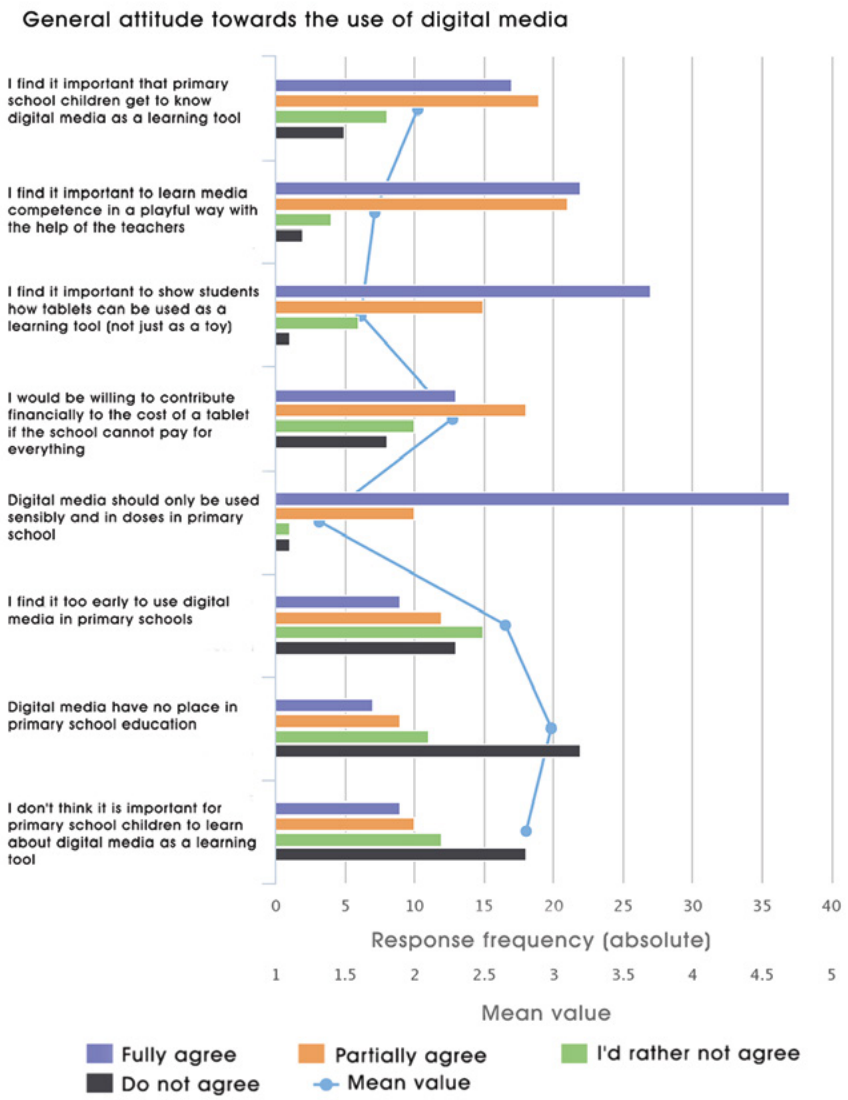

Table 7: Interactive learning content

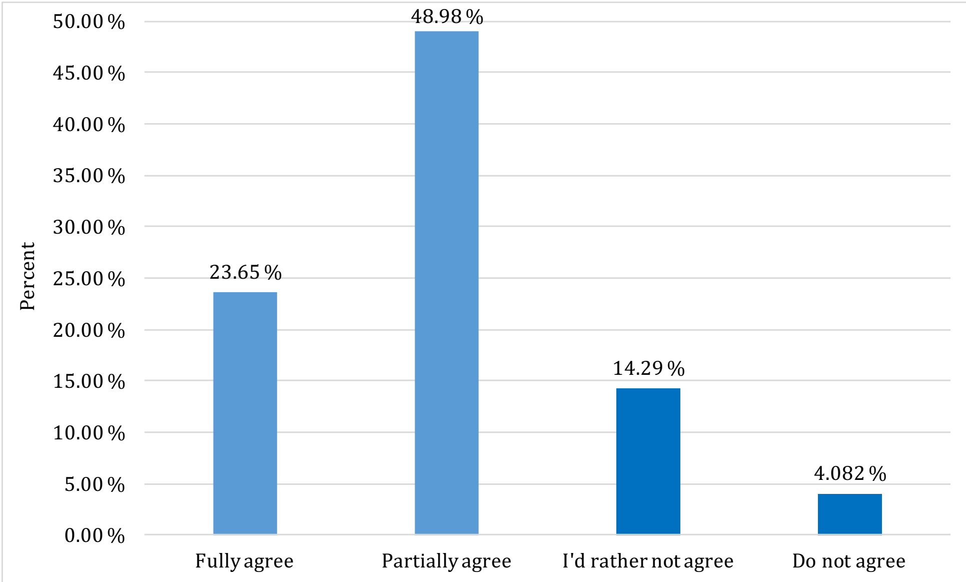

I appreciate interactive learning content (videos, texts, animations, 3D views, sound samples) as very relevant in the classroom

Table 8: AR results in the following for students

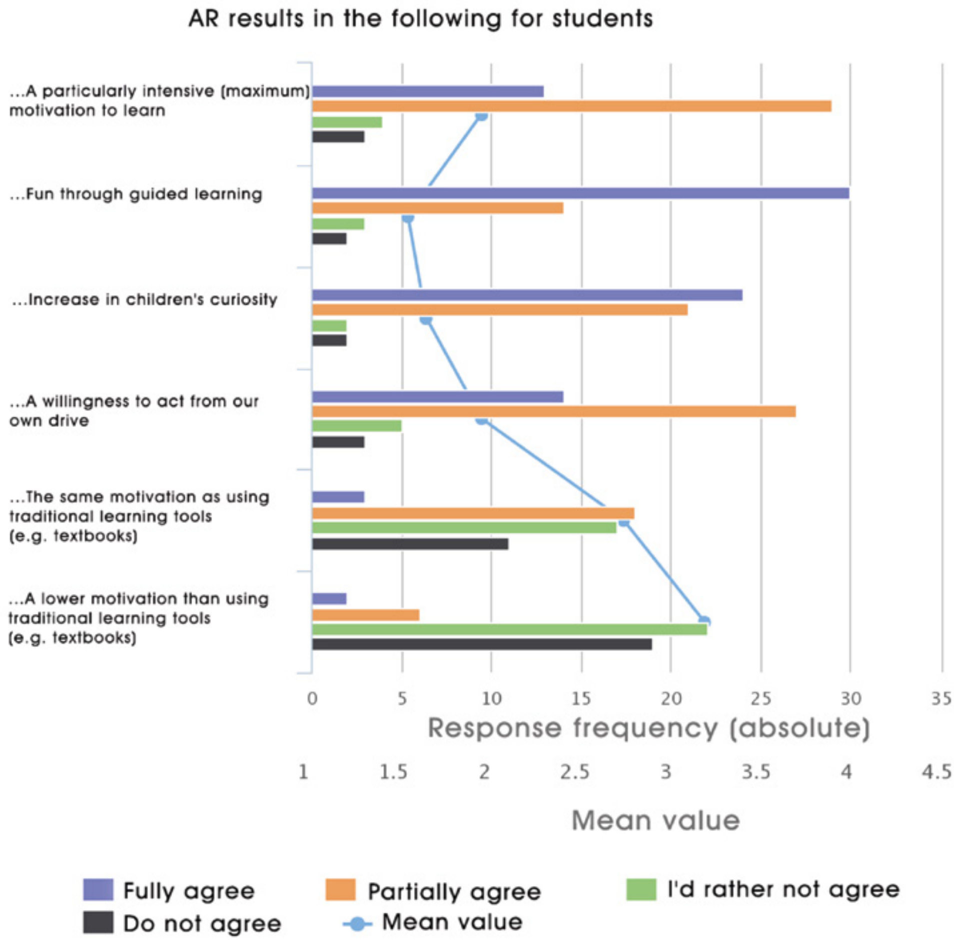

Possible scenarios include training for teachers, increased budgeting of schools for AR based technologies and government activated research on this topic, as well as improved internet systems for fast data transmission. Particularly such school subjects as science, geometry and history greatly profit through the use of augmented print in classrooms. When comparing computer competencies of children worldwide, Germany is only midfield. The Czech Republic, Canada and Australia are currently leading the way with innovative learning tools.

The research concluded with a quantitative and qualitative empirical evaluation on the acceptance of parents as gatekeepers, with regards to the possible use of AR in primary education. Essentially the parents believe AR offers many positive scenarios and chances, but that this could never replace a dedicated, good teacher. The data content has to be fittingly developed and matched to the age of the target group. The overuse of AR could lead to learning distractions in the classroom up to an internet and games addiction.

There are critical factors with respect to digitization in primary schools that need to be researched further. For printing and publishing companies it would be recommended that a long-term research study is conducted using various augmented print products in one study group and comparing the learning results to another study group who abstain from using augmented print products. The results of such a study would not only be of interest to the above mentioned companies but also for teachers, educational institutions and governmental school authorities.

4. Conclusions

The transformation of teaching and learning caused by technologies such as AR, certainly offer exciting opportunities to design modern learning environments that are engaging and fun for school children. Researchers have found that technology has always held a great promise for increasing student engagement and the level of understanding the learning content leading to better academic results. As information technologies transform, educators need to adopt new technologies into their classroom to enhance student learning experience. AR is one the growing technologies that have a great pedagogical potential and this is being increasingly recognized by educational researchers worldwide. With capabilities of merging virtual and real worlds together, new possibilities in improving the quality of teaching and learning are born.

As mobile devices become more advanced, AR apps will vastly improve as well. The usability will be easier, making them more marketable for primary school children. Many successes in educational subjects such as science and math have been tempered by struggles with budgets, technology and educational policies.

Different technologies have been integrated in schools in the past such as computers, multimedia, internet, e-learning, social web, simulations, etc. But the use of mobile devices and immersive environments such as games, virtual worlds and augmented reality presents a huge opportunity not only for learning but also for publishers and print media companies.

When AR is connecting to print, learning based systems offer games, social interactivity, and connectivity. This learning experience is more meaningful and successful. Based on international studies and our research with parents, generally participants feel motivated, have fun and achieve higher levels of engagement in learning performance. However, it is advisable to also focus on pedagogical and learning theory when implementing and developing AR applications. The educational value of AR is not solely based on its features. This technology has vast potential implications and benefits, especially in learning environment and it can be predicted that research will massively surge in this area.

Acknowledgements

A special thanks to the many parents who participated in the surveys and interviews on this subject as well as to Manuela Blass who conducted the research on site.

References

Absatzwirtschaft, 2017. *Deutscher Markenreport 2017: Virtual & Augmented Reality im Marketing – große Erwartungen, aber wenig Know-how*. Meedia GmbH & Co.KG. [online] Available at: <http://www.absatzwirtschaft.de/deutscher-markenreport-2017-virtual-augmented-reality-im-marketing-grosse-erwartungen-aber-wenig-know-how-101341/> [Accessed 17 March 2017].

Australian Associated Press, 2017. *One-third of preschoolers own smartphones or tablets, child health poll finds*. [online] Available at: <https://www.theguardian.com/technology/2017/jun/21/one-third-of-preschoolers-own-smartphones-or-tablets-child-health-poll-finds> [Accessed 20 June 2017].

Azuma, R.T., 1997. A survey of augmented reality. *Presence: Teleoperators and Virtual Environments*, 6(4), pp. 355–385.

Barnard, F.R., 2017. *The history of a picture worth*. [online] Available from: <http://www2.cs.uregina.ca/~hepting/research/web/words/history.html#27ad> [Accessed 18 December 2017].

Bastian, J., Aufenanger, S. eds., 2016. *Tablets in Schule und Unterricht. Forschungsergebnisse zum Einsatz digitaler Medien*. Wiesbaden: Springer VS.

Blass, M., 2018. *Augmentend Print – Ein crossmediales Lernwerkzeug in der Grundschule*. Bachelor Thesis. HdM Stuttgart.

Bluepartner, 2015. Warum Haßloch Testmarkt für Deutschland ist. bluepartner GmbH. [online] Available at: <https://bluepartner.de/blog/testmarkt-hassloch/> [Accessed December 2017].

Bundesverband Digitale Wirtschaft, 2013. *Realtime advertising Kompass 2013/2014*. BVDW [pdf] Available at: <https://www.bvdw.org/presseserver/bvdw_rta_kompass/BVDW_RTA_Kompass20132014.pdf> [Accessed December 2017].

Carmody, T., 2018. *Why print legacies like time are betting big on augmented reality: the latest issue featured 4 AR activations*. Adweek. [online] Available at: <https://www.adweek.com/digital/why-print-legacies-like-time-are-betting-big-on-augmented-reality/> [Accessed 28 February 2018].

Kidsinteractive, 2018. *Schulbuch-App ZOOM mit Augmented Reality von KIDS interactive*. [video online] Available at: <https://www.youtube.com/watch?v=foK0_TyWKT4> [Accessed 8 March 2018].

Krotki, M., 2017. *Augmented Reality eines der Trendthemen auf der Frankfurter Buchmesse 2017*. [online] Available at: <https://www.appear2media.de/augmented-reality-ist-eines-der-trendthemen-auf-der-frankfurter-buchmesse-2017/> [Accessed December 2017].

Menne, K., Strickler, V. and Zybell, C., 2011. *Augmented Reality: Wie Printmedien zum Leben erweckt werden*. Bergische Universität Wuppertal. [online] Available at: <https://www.mediencommunity.de/system/files/Augmented%20Reality-download.pdf> [Accessed May 2011].

Schart, D. and Tschanz, N., 2015. *Praxishandbuch Augmented Reality: für Marketing, Medien und Public Relations*. Konstanz and München: UVK Verlagsgesellschaft.

Scholz, C., 2014. *Generation Z: wie sie tickt, was sie verändert und warum sie uns alle ansteckt*. Weinheim, Germany: Wiley-VCH.

Vanian, J., 2017. *This Is The Next Battleground For Apple, Google, Facebook, and Microsoft*. [online] Available at: <http://fortune.com/2017/06/07/apple-google-facebook-microsoft-are-battling-augmented-reality/> [Accessed 18 December 2017].

Weiner, J., 2011: *„Medienkompetenz" – Chimäre oder Universalkompetenz? – Essay*. Bundeszentrale für politische Bildung. [online] Available at: <http://www.bpb.de/apuz/33557/medienkompetenz-chimaere-oder-universalkompetenz-essay?p=all> [Accessed December 2017].

The Method for Legibility Assessment and its Application for Model Pharmaceutical Leaflets

Petr Roudný and Markéta Držková

Department of Graphic Arts and Photophysics, Faculty of Chemical Technology,
University of Pardubice, Studentská 95, 532 10 Pardubice, Czech Republic
E-mails: petr.roudny@student.upce.cz; marketa.drzkova@upce.cz

Short abstract

Within this paper, different aspects of legibility studies are considered, and a generally applicable method for legibility assessment is presented. The method combines the measurement of the time required to read the text with the subsequent checking of the information understood and remembered by the respondent, complemented by respondent's preferences and comments on various features of the test samples. The test set comprised model pharmaceutical leaflets, differing in selected aspects. The parameters varied were the presence of serifs in the font, the type size, and the paper grammage.

Keywords: legibility assessment method, pharmaceutical leaflet, age dependence

1. Introduction and background

Different definitions of legibility, readability and reading comprehension are in use. Here, the term legibility is used as a measure of people's ability to see, distinguish, and recognize the characters and words in read text (Nielsen, 2015). The history of research on legibility is rather long – not only for prints (Pearson, et al., 1984), but also for presentation on screen (e.g. Bauer and Cavonius, 1980). However, there are still open questions to explore, because the topic is not straightforward, and the new areas or applications to investigate arise. In addition, although the related literature is rich, not all studies consider all aspects that may affect legibility during the experiment, and broader comparison often is not possible due to the absence of a unified approach. There are a number of factors that influence the legibility and reading experience, and this influence is often a result of their interplay, with different significance of individual factors in different situations. For example, if the readers are children (Reynolds and Walker, 2004) or have some kind of reading difficulties, such as dyslexia (Hoffmeister, 2016).

In previous legibility studies, various approaches have been implemented for evaluation, either qualitative or quantitative. The qualitative approach provides valuable insight (Vincent, 2016), which helps also in the interpretation or discussion of the quantitative data (Reynolds and Walker, 2004). In quantitative studies, choosing the optimum length of the examined text and other experimental settings is important, as well as the appropriate statistical treatment. While the approaches utilising advanced methods like eye-tracking (Pušnik, et al., 2014) or even neuroimaging (Barton, et al., 2010) can provide significantly more precise results and in-depth understanding, these methods are not self-sufficient; the quality of the experimental design, chosen measures and data analysis is still essential, because otherwise the gained information is useless. Furthermore, as the legibility results from a combination of objective and subjective factors, too strong generalisation may be inappropriate due to suppressing some factors that may be important for the practical application of the findings, and therefore it should be avoided. Ambiguity or even disagreement among various studies and opinions on the typographic features of text affecting its legibility is shown in the overview given in Lonsdale, Dyson and Reynolds (2006) and recently demonstrated in Tarasov, Sergeev and Filimonov (2015). Similar ambiguity of findings exists also in related research areas, for example in examination of the text highlighting effect on the memory and comprehension of the highlighted and non-highlighted information after reading, as discussed e.g. in Yeari, Oudega and van den Broek (2017).

The objective of this study is to present a generally applicable and simple method for legibility assessment, building on the previous studies and stressing the need for specification of relevant conditions to enable the later use of the results in comparison to other studies. Besides the clear definition of all tested parameters and their settings, this includes the specification of the other parameters that have the influence on legibility.

To verify its usability, it was applied for a model set of pharmaceutical leaflets designed and produced with differences in selected factors. The pharmaceutical leaflets were chosen as a type of product where good legibility is important. Accordingly, easy legibility is explicitly required e.g. by the Directive 2001/83/EC of the European Parliament and of the Council of 6 November 2001 on the Community code relating to medicinal products for human use. The corresponding Guideline on the readability of the labelling and package leaflet of medicinal products for human use (2009) deals e.g. with choosing an easy-to-read font, minimum type size and line spacing, limited use of capitals and italics, avoiding underlining, means for emphasis, contrast between the text and the background, the use of colour, and characteristics of paper. Based on the analysis of a random sample of real pharmaceutical leaflets, the body text of leaflets is mostly justified with multi-column layout; in some samples, the body text is ragged right. The titles are highlighted in bold, in capitals, or graphically, e.g. using background in different colour. Sans serif fonts are more common, and the prevailing body text colour is black. The parameters studied in the model set of pharmaceutical leaflets comprised the presence of serifs in the typeface, the type size with corresponding spacing, and the paper grammage. The experiment included adult respondents, both males and females, representing all age categories. The results are analysed and evaluated with respect to the influence of individual factors as well as their combinations.

2. Materials and methods

The parameters of individual samples were selected on the basis of preliminary qualitative survey asking nine respondents (the age of 19–44) for their opinion on ten randomly selected specimens of real pharmaceutical leaflets in order to identify which features they think contribute to better legibility and which are seen as impairing legibility. Two options were compared for each of the three tested parameters, i.e. the presence of serifs in the typeface, the type size and spacing, and the paper grammage.

2.1 Sample preparation

One pair of serif and sans serif typefaces was chosen, Baskerville 10 Pro and John Sans, respectively. These typefaces have the x-height and width and also the optical weight close to each other. The John Sans Text, Medium and Bold were designed so that their colour is commensurate with their serif counterparts in Baskerville typefaces (Štorm, n.d.). Therefore, both typefaces occupied similar space on the page and had similar coverage.

The typographical parameters common for all samples were the two-column layout with the columns separated using a thin black line, the header of each sample page highlighted as white text on a black background, headings and subheadings highlighted in bold, and justified body text. Two options of type size and spacing were tested, with corresponding page size. The first setting comprised 8/11 pt, with main headings in 9 pt size, on 170 × 272 mm page, while in case of the second one it was 10/13 pt, with main headings in 11 pt size, on 210 × 297 mm page.

With respect to reproduction and substrates, the samples were printed on Océ VarioPrint 2070 using two types of uncoated paper, Xerox Colotech+ and Xerox Premier (Table 1), both having a blue white shade (Novák, 2017). Gloss of both substrates and solid prints on these substrates was characterised using Viptronic VipGloss 1 (illumination angle 45°, detection angles 0° and 45°, providing visual lustre number on scale from 0 to 10, for surfaces from ideally diffusive to highly reflective).

Table 1: Characteristics of papers (CIELAB values for D50/2°) (Novák, 2017)

	Grammage [g/m^2]	CIE whiteness	Opacity [%]	L*	a*	b*
Xerox Colotech+	90	164 ± 3	≥ 92	94.75	2.75	−13.45
Xerox Premier	60	170 ± 3	≥ 87	94.74	4.34	−17.90

The tested content comprised texts from five pharmaceutical leaflets adapted so that the text filled one page with all selected format settings; the average character count was 4 127 ± 10 (maximum difference). One of these five texts was used for the reference sample (see Appendix). Lorem ipsum text was used on the reverse side of prints to test the influence of possible print-through in comparison of paper substrates.

Overall, one reference sample and 12 samples for comparative testing were prepared. The schematic overview of the four tested combinations is given in Figure 1.

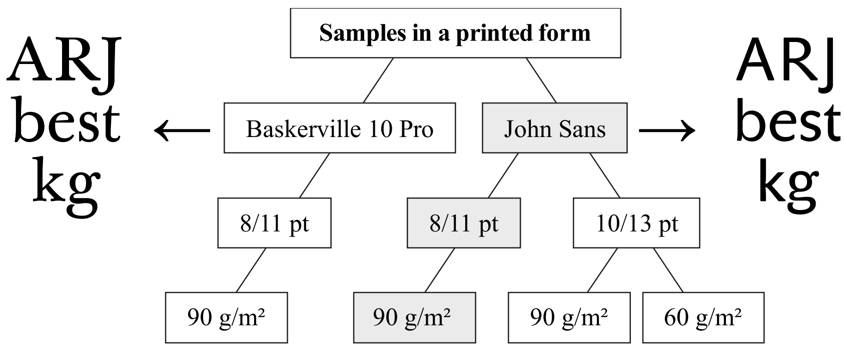

Figure 1: An overview of the tested combinations of the typeface, type size and spacing, and paper grammage for the printed samples; the combination used for the reference sample is marked in grey

2.2 Testing

Within the experiment, three age categories were considered: 26 years old and under, 27–59 years old, and 60 years old and over, representing mainly the student age, the productive age and the age of a retirement period, respectively. The testing was arranged indoors, in the room with natural daylight.

As the first step during testing, the reason and procedure of the test was introduced to each respondent. Second, the time of reading the reference sample by the respondent was measured. Third, the respondent took part in examination of four randomly selected and ordered samples; this enabled to test all three variable parameters. For each sample, the required reading time was measured. Then, the respondent answered five simple questions derived from the sample content (closed questions, each with three choices). The time needed for answering was measured as well. When the respondent was not able to answer all questions, or in case of wrong answer(s), the additional time needed for searching the correct answer(s) by rereading the sample was also measured. Finally, the respondent was asked which features of the sample the respondent likes and sees as improving the legibility, and vice versa.

2.3 Evaluation

The legibility was assessed on the basis of the time required for reading and then for answering the questions related to the given sample leaflet content. In case of the required reading time, both the absolute measured time and the time normalised against the reference reading time for each respondent were considered. For each combination and age category, the average and median reading times were calculated. Further, the percentage of correct answers (based on the first sample reading) was considered.

3. Results and discussion

Overall, 42 adult respondents with normal or corrected-to-normal vision took part in testing (Table 2). The youngest was 19 and the oldest 86 years old. In case of the highest age category, the number of male and female respondents is not balanced; therefore, the influence of gender cannot be discussed.

Table 2: Respondents

Age category	**≤ 26**	**27–59**	**≥ 60**
Female	5	9	12
Male	6	9	1
Total	11	18	13

Table 3: Results obtained within the three age categories for the four tested combinations of the typeface, the type size and spacing, and the paper grammage

Age category	**≤ 26**	**27–59**	**≥ 60**	**≤ 26**	**27–59**	**≥ 60**
	Baskerville 10 Pro, 8/11 pt, 90 g/m^2			John Sans, 8/11 pt, 90 g/m^2		
Average reading time [s]	198	160	204	192	163	209
Reading time standard deviation [s]	43	32	53	35	29	72
Median reading time [s]	206	152	196	194	161.5	196
Average normalised reading time	1.09	1.06	1.00	1.06	1.09	1.02
Percentage of correct answers [%]	93	88	72	90	92	75
Average answering time[1] [s]	42	42	66	41	40	79
Average additional answering time[2] [s]	17	18	20	24	30	33
	John Sans, 10/13 pt, 90 g/m^2			John Sans, 8/11 pt, 60 g/m^2		
Average reading time [s]	182	158	208	191	155	215
Reading time standard deviation [s]	43	35	69	46	37	55
Median reading time [s]	183	151	185	202	146	213
Average normalised reading time	0.99	1.05	1.03	1.04	1.03	1.08
Percentage of correct answers [%]	90	92	75	89	90	79
Average answering time[1] [s]	42	38	61	44	37	54
Average additional answering time[2] [s]	14	30	34	5	17	43

[1] Only for respondents with 100 % of correct answers

[2] Only for respondents who needed rereading to find the correct answers

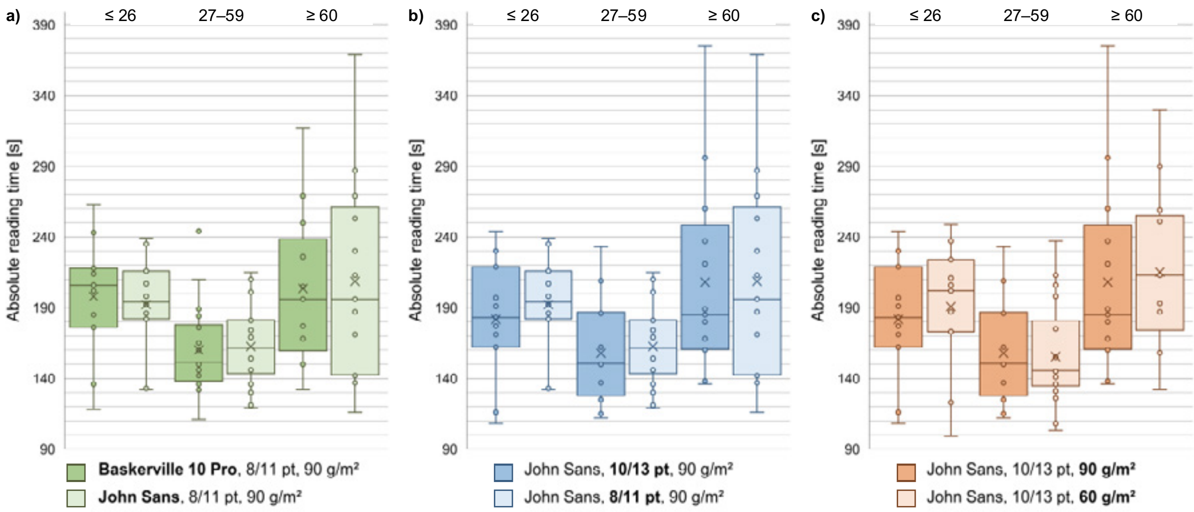

Figure 2: Box plots comparing the absolute reading time measured within the three age categories in dependence on a) the typeface, b) the type size and spacing, and c) the paper grammage

The results for individual tested combinations are summarised in Table 3 and the comparison of the measured absolute reading times in dependence on the tested factors is presented in Figure 2. In most cases, the distribution of the measured reading times is more or less skewed, as illustrated by the differences of average and median values in Table 3 and box plots in Figure 2. This confirms the risk of misinterpretation in legibility studies where the evaluation is based on average values, such as in Pušnik, et al. (2014).

For the age category of 26 and under, the slightly better reading performance in case of the sans serif type is in accordance with the opinions expressed in interviews, where the most of respondents in this age category preferred John Sans. The same applies for the age category of 60 and over in case of the serif type. Among the respondents from 27 to 59 years old, the reading performance was slightly better with the serif type. There were no clear preferences regarding the presence of serifs in the type for this age category. In general, across all age categories, respondents who read mostly on screen more often preferred sans serif type, and respondents who read more books more often preferred serif type. This confirms the conclusion in Tarasov, Sergeev and Filimonov (2015) regarding the importance of reader familiarity with the typefaces.

With respect to the size of type, most respondents preferred the larger type size and spacing, and also the measured reading times were somewhat lower for larger type; the reading performance was similar for both sizes. When comparing the two paper substrates, the median reading times were higher for the paper with the lower grammage in case of the younger and older respondents. The paper with higher grammage was more preferred in all age categories. Some respondents preferred the 60 g/m^2 paper thanks to a better contrast of the printed text, but more respondents expressed negative impression from the sample on 60 g/m^2 paper due to disturbing print-through, especially within the age category of 60 and over. None of the comments was related to gloss, which is in line with the measured lustre having medium values (4.6 for 90 g/m^2 paper, 4.0 for 60 g/m^2 paper, 5.1 and 4.9 for prints on these papers, respectively).

Overall, the best reading performance was obtained for the middle age category. The mean reading times for the other two categories are somewhat higher and similar to each other. However, for the age category of 60 and over, the results show a considerable increase in the variability among the respondents. Within this age group, there are also longer answering times, and the percentage of correct answers is markedly lower as well.

4. Conclusions

More pronounced differences in legibility assessed on the basis of required reading time were obtained across individual age categories. The influence of the tested options differs in each age category. According to the answers in qualitative interviews, the preferences concerning the tested factors also differ in each age category and are mostly connected with reading habits. However, in some cases, the measured performance does not correspond to these preferences.

The method combining the quantitative and qualitative approaches employed in this study enabled to assess the influence and significance of the individual examined factors, as well as to choose the best combination of all tested parameters in respect to the comfort and performance of reading. It helps to identify which settings or conditions can be more easily compromised in dependence on the priorities, which, in general, may be the reading speed, comprehension, etc. The method is versatile in respect to properties possible to test and questions that should be answered. The aspects which should be always considered include the design of experiment, such as the decision regarding the tested parameters and their options, as well as their combinations within individual samples. The attention also should be paid to specification of the other relevant conditions, which are not in focus of the study but have an influence on the legibility, and to keeping these conditions constant during the whole experiment. Finally, due to the nature of this kind of investigation, choosing the appropriate statistical analysis is of great importance.

Acknowledgements

The authors thank all the respondents for their time and willingness to take part in the testing.

References

Barton, J.J.S., Sekunova, A., Sheldon, C., Johnston, S., Iaria, G. and Scheel, M., 2010, Reading words, seeing style: The neuropsychology of word, font and handwriting perception. *Neuropsychologia*, 48(13), pp. 3868–3877.

Bauer, D. and Cavonius, C.R., 1980. Improving the legibility of visual display units through contrast reversal. In: E. Grandjean and E. Vigliani, eds. *Ergonomic aspects of visual display terminals*. London: Taylor & Francis, pp. 137–142.

Directive 2001/83/EC of the European Parliament and of the Council of 6 November 2001 on the Community code relating to medicinal products for human use. [online] Available at: <http://eur-lex.europa.eu/legal-content/EN/TXT/HTML/?uri=CELEX:32001L0083> [Accessed 9 February 2018]

Guideline on the readability of the labelling and package leaflet of medicinal products for human use, Revision 1, 12 January 2009. [pdf] Available at: <https://ec.europa.eu/health/sites/health/files/files/eudralex/vol-2/c/2009_01_12_readability_guideline_final_en.pdf> [Accessed 9 February 2018]

Hoffmeister, S., 2016. *The impact of font type on reading*. Senior Honors Theses. 505. Eastern Michigan University. [online] Available at: <http://commons.emich.edu/honors/505> [Accessed 9 February 2018].

Lonsdale, M.D.S., Dyson, M.C. and Reynolds, L., 2006. Reading in examination-type situations: the effects of text layout on performance. *Journal of Research in Reading*, 29(4), pp. 433–453.

Nielsen, J., 2015. *Legibility, Readability, and Comprehension: Making Users Read Your Words*. [online] Available at: <https://www.nngroup.com/articles/legibility-readability-comprehension/> [Accessed 9 February 2018]

Novák, D., daniel.novak@xerox.com, 2017. *Information on Xerox materials*. [email] Message to P. Roudný (petrroudny@gmail.com). Sent 11 May 2017.

Pearson, P.D., Barr, R., Kamil, M.L. and Mosenthal, P. eds., 1984. *Handbook of Reading Research*, Vol. 1. New York, London: Routledge.

Pušnik, N., Kovačević, D., Brozović, M. and Možina, K., 2014. Is legibility of typefaces designed for screen use the same for different languages? In: *Advances in Printing and Media Technology, Vol. XLI*, Proceedings of the

41st International Research Conference of iarigai, Swansea, United Kingdom, September 2014. International Association of Research Organizations for the Information, Media and Graphic Arts Industries, pp. 117–122.

Reynolds, L. and Walker, S., 2004, ‘You can’t see what the words say’: word spacing and letter spacing in children’s reading books. *Journal of Research in Reading*, 27(1), pp. 87–98.

Štorm, F., n.d. *John Sans*. [online] Available at: <https://www.stormtype.com/families/john-sans/gallery> [Accessed 9 February 2018].

Tarasov, D.A., Sergeev, A.P. and Filimonov, V.V., 2015. Legibility of textbooks: a literature review. *Procedia – Social and Behavioral Sciences*, 174, pp. 1300–1308.

Vincent, J., 2016. Students’ use of paper and pen versus digital media in university environments for writing and reading – a cross-cultural exploration. *Journal of Print and Media Technology Research*, 5(2), pp. 97–106.

Yeari, M., Oudega, M. and van den Broek, P., 2017. The effect of highlighting on processing and memory of central and peripheral text information: evidence from eye movements. *Journal of Research in Reading*, 40(4), pp. 365–383.

Reality Check: What to expect when buying different Print Products for a Campaign – Brand Color Reproduction across Print Substrates and Technologies

Michael Abildgaard Pedersen

The Danish School of Media and Journalism (former Graphic Arts Institute of Denmark),
Department of Media Production and Management, Copenhagen
E-mail: map@dmjx.dk

Short abstract

This study is a continuation of a previous study on why most Brand Manuals fail when it comes to specifying Brand Colors. This present study seeks to examine the practical consequences of the previous study by conducting a spot check of 226 randomly chosen print products from 43 randomly chosen companies. These print products where printed on both paper, foil/film, nylon, polyester, metal, cotton and other substrates. The print products where produced in different print technologies, such as lithographic offset, flexographic print, screen print, gravure and digital print and they were produced both locally in Denmark and from print suppliers around the world. 66 % of the 226 print products where printed in CMYK while 34 % where printed as spot color (one color Pantone). The 226 print products were measured directly on the printed image, where the logo or brand color was located and color differences CIEDE2000 (ΔE_{00}) were calculated in relation to the company's brand color specifications. Only 13.7 % (31) of these 226 print products had a color difference ≤ 3 ΔE_{00} More than 50 % of the 226 print products had a color difference above 6 ΔE_{00} and 19 % (43) had a color difference above 10 ΔE_{00}. Whether the relatively large color differences are due to inappropriate color specification in the Brand Manuals or if there is a general inattention in the printing companies is not to be said. However, it must be presumed that the international process standards in the ISO 12647 series haven't played a significant role in the production of these 43 companies' 226 print products.

Keywords: brand colors, spot colors, color match, print quality, uniformity, consistency, CIEDE2000

1. Introduction and background

In 2016 a study showed that less than 50 % of the current Brand Colors where suitable for reproduction in CMYK print (Pedersen, 2016). It also showed that none of the 156 examined Brand Manuals had any requirements, recommendations or information about any given color deviations that might occur while producing digital or print media (Pedersen, 2016). Thus, it would be interesting to examine what the practical consequences of this actually are.

When a Brand Owner needs to order some print products for e.g. a campaign or an event, the different print products are most likely produced on different substrates, in different print technologies and by different print suppliers from different countries. Thus, one company's campaign can include numerus of print products produced on various substrates in many different print technologies from many suppliers. Nevertheless, it should be possible for the company (the Brand Owner) to expect some reasonable conformance to the company's reference colors (Corporate Brand Colors). That's actually the reason why so many resources are used to produce Brand Manuals, Corporate Design Guides, Corporate Brand Guidelines and Corporate Identity Guidelines. Even though the aforementioned study (Pedersen, 2016) showed that these Brand Manuals were inexpediently produced when it came to specifying Brand Colors it should nevertheless be possible to expect some reasonable conformance between the reference colors and the printed colors.

The process standards in the ISO 12647-serie sets requirements for color deviations for the separate C, M, Y and K ink solids and some of these process standards also have informative recommendations for separate spot color deviations, when measured on the color control bars. However, when a company's logo or Brand Color is printed, it's either printed in some CMYK-combination or it's printed as a single spot color (typical one color Pantone). When logos or brand colors are printed as one color, spot color, issues like color mixing and ink layer thickness are essential. When logos or brand colors are printed in a CMYK-combination, issues like color management, tone value increase, mid tone spread and correction curves play an essential role. Properly more important than the individual CIELAB values for each separate C, M, Y and K ink solid.

In any case, the printed motive that the company pays for, including the corporate colors, brand colors and logos are all placed inside the printed image – not on the color control bar. Thus, in a four-color CMYK-print the printed motive is a result of an overprint of the four-color halftone images. Therefore, it may be argued that it would be a good idea to measure the brand color and logo color where it appears in the printed image – directly on the printed image – where it's seen by the customer.

When measuring on the color control bar the measurements are carried out on one single ink solid and TVI at the time, even though it's carried out fast and automatically. This implies the risk of removing the focus from the printed image, which are what the customer pays for and which is where the logo and brand colors are placed and displayed – to focusing on the color control bar and the single values.

2. Research questions, materials and methods

As a consequence of the above, it would be interesting to examine what the customer actually gets when ordering different print products.

What degree of color match, uniformity and consistency can the customer expect when looking directly at the printed image (instead of the color control bar)?

Six weeks a year from December to January, from 2015 to 2018, students have worked on a case study where they should find a randomly chosen company, collect between 3 to 7 different print products from that company, which have been used in a campaign or an event, use the company's design manual to find the company's Brand Color (reference color) and finally measure the print products to determine if there is consistency between the reference color and the printed color of the printed products. In this way, 226 randomly chosen print products have been collected from 43 randomly selected companies (Brand Owners). Some of the print products have been produced in Denmark and some have been produced in other countries around the world.

All measurements where conducted by using 11 X-rite SpectroEye spectrophotometers (with apertures 3.2 mm (SA) & 4.5 mm) all calibrated before measurements and set (D50, 2°, Absolute white base and no filters) in accordance to ISO 12647-1 (International Organization for Standardization, 2013a). The measurements were made directly on the area of the print product where the company's logo or Brand Color was printed. That is, directly on the print where the company's logo or Brand Color was visible, not on a color bar. The measurements were made immediately after collection of the products.

All reference CIELAB values where found by first consulting the company's Brand Manual where the colors where specified, mostly as Pantone colors, subsequently the CIELAB values for each Pantone Color was found by using the PANTONE COLOR MANAGER Software (version 2.1.0.249 for Windows) that contain the official Pantone CIELAB values for each Pantone Color.

In those few cases where the Brand Color wasn't specified as a Pantone Color but as a CMYK combination or RGB combination, the CIELAB values where found by using Adobe Photoshop where the color settings gradually were changed to relevant RGB and CMYK ICC-profiles using Absolute Colorimetric Rendering Intend and subsequently the CIELAB values for the relevant Brand Color was read out. All calculated ΔH^*, ΔE^*_{ab} and ΔE_{00} values were found by using those official Pantone CIELAB values and the CIELAB values from the measurements.

Since it is the intention of the final print products to show the company's Brand Color including logo colors and since all measurements have been made directly on the print (logo or Brand Color), the ΔE_{00} has been chosen to be the most relevant and fair color difference formula in this case since it was created to display a numeric value for the specific color difference that the human eye perceives.

In the previous study (Pedersen, 2016) it was suggested that the limit for an acceptable color deviation should be 3 ΔE_{00}, when products where produced within the same process (print technology and substrate). This was suggested on the basis of the fact, that

- Fogra suggests that the uniform deviation tolerance for Spot Colors in offset printing should be 2.5 ΔE_{00} (FOGRA, 2010, p. 10)
- ISO 12647-2:2013 (International Organization for Standardization, 2013b) specify informative deviation tolerance of 3.5 ΔE_{00} for the chromatic solid process colors CMY produced in lithographic offset
- ISO 12647-6:2012 (International Organization for Standardization, 2012) specify a variation tolerance of less than 1.5 ΔE_{00} for spot colors produced in flexographic printing.
- A VIGC study that showed that Belgian customers demand a maximum of 2 ΔE^*_{ab} for quality print jobs (VIGC, 2008).

In addition, it was suggested that when products where produced on different substrates and in different print technologies the acceptable color deviation should be 7 ΔE_{00} (Pedersen, 2016).

3. Results and discussions

In the following, the 226 different print products from the 43 different companies will first be systematized and categorized. This will be done by Product types, Substrates, Print Technologies and type of print color systems. After this, an analysis of the color differences will be made and it will be examined how many products that comply to the limits of 3 ΔE_{00} and 7 ΔE_{20}.

3.1 Types of products

When companies and organizations arrange different types of campaigns and events, it is quite normal that many physical products are included in these campaigns and events. It is also typical that these products are printed with the company's brand colors and logos. Therefore, many different product types are included in this study. However, an attempt to form a grouping has resulted in 27 categories and a residual group called "other". In Figure 1 all product types are shown and it's seen that the two largest groups are Bags (including candy bags, shopping bags, fabric bags and sports bags) and "Other" which include lighters, magnets, flags, Access cards, glass and cups.

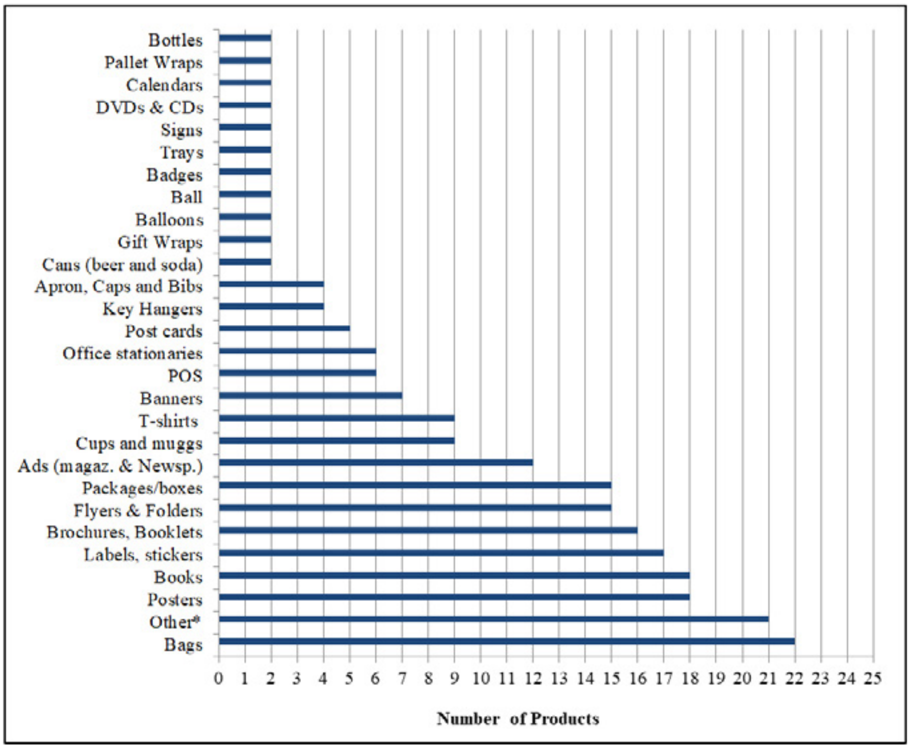

**The 21 other product types include magnets, flags, access cards, lighters, glass and cups*

Figure 1: The 226 print products by product types

3.2 Types of substrates

Among the 226 products, 141 of the products (62 %) was printed on coated and uncoated paper, 41 of the products (18 %) was printed on film/plastic, 4 products was printed on metal, 13 products (5.7 %) was printed on nylon or polyester, 13 products (5.7 %) where printed on cotton and 14 products (6.2 %) was printed on other substrates (glass, porcelain, latex and PVC).

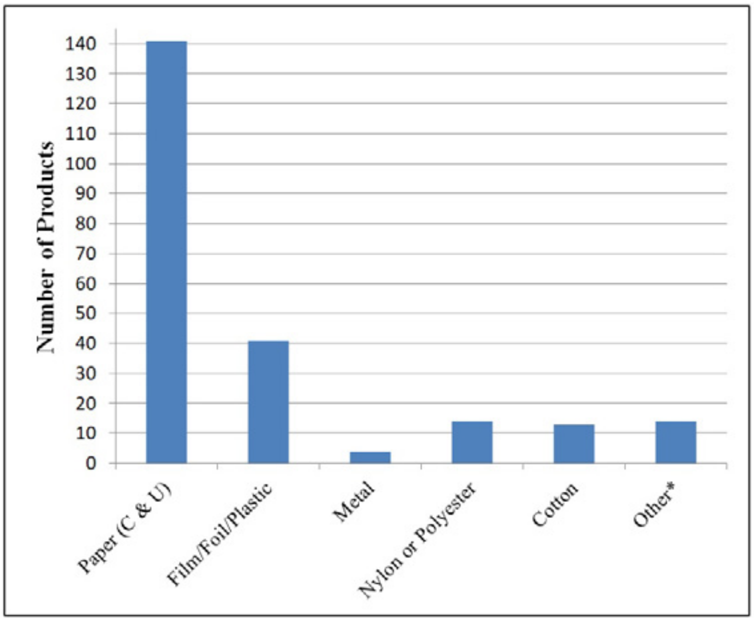

**The other include PVC, porcelain, glass, latex and corrugated board*

Figure 2: The 226 products distributed on type print substrates

3.3 Types of print technologies

Most print technology categories are represented in this study. Among the 226 products, 134 of the products (59.3 %) was printed in Lithographic Offset (including UV offset), 21 products (9.3 %) was printed in flexo, 41 products (18.1 %) was printed in screen printing, 8 products (3.5 %) was printed in gravure, 16 products (7.1 %) was printed in digital inkjet and 6 products (2.6 %) was printed in electrophotographic digital print.

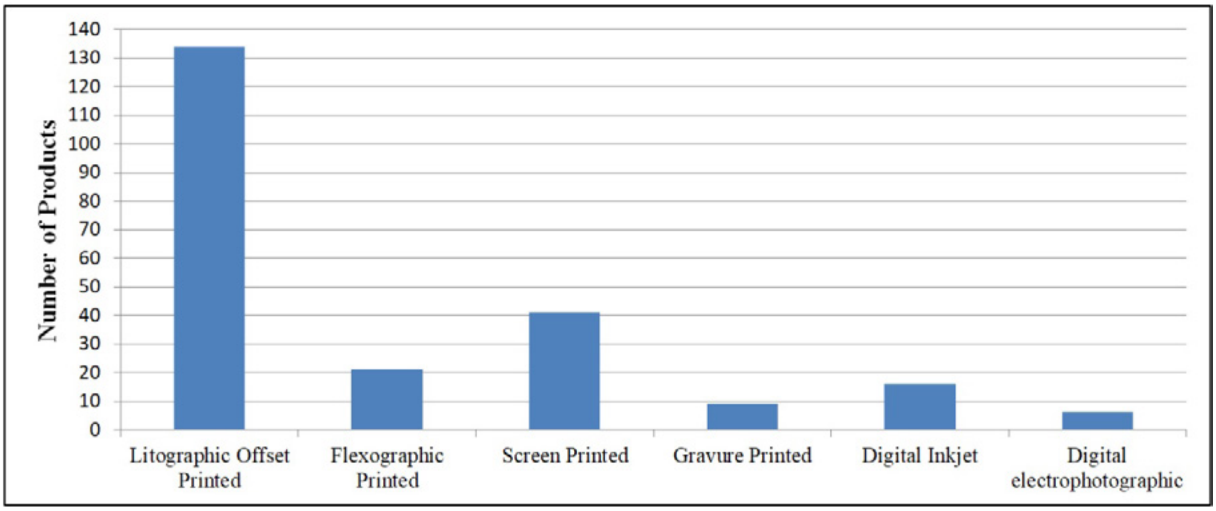

Figure 3: The 226 print products distributed by Print Technology

3.4 Types of color systems

Among the 226 products, 150 of the products (66.4 %) where printed in CMYK process colors while 76 of the products (33.6 %) was printed as a 1-color, spot color.

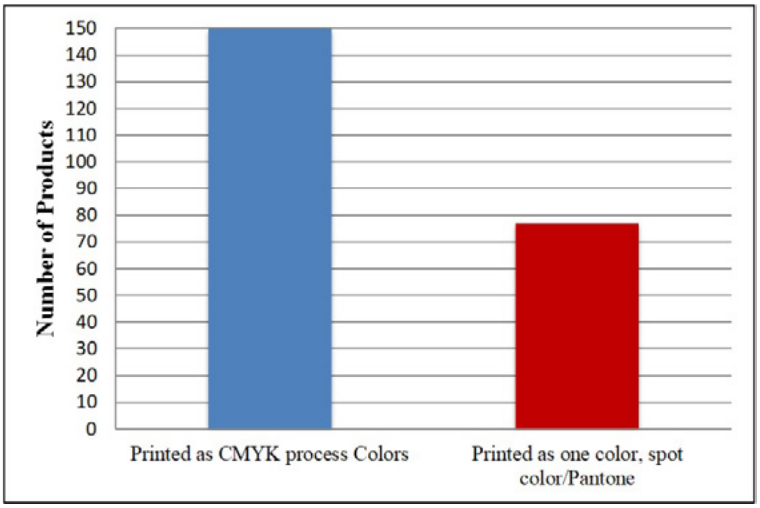

Figure 4: The 226 print products distributed by print color system

A review of the 43 company's reference colors (the companies brand colors) showed that 11 of the companies (25.6%) had a brand color that wasn't achievable in CMYK-print. However, 9 of those 11 companies produced 39 of their products in CMYK. When looking at the total number of products, 169 of the print products (74.8 %) had a reference color within the relevant CMYK-gamut while 57 of the print products (25.2 %) had a reference color outside the relevant CMYK-gamut.

3.5 Color deviations CIEDE2000

When examining the 226 product's color difference (ΔE_{00}) in relation to the desired reference color, it appears that less than 15 % of the products can comply with the requirement for a difference ≤ 3 ΔE_{00}. If the acceptance limit is raised to ≤ 7 ΔE_{00} only a little more than half of the products can meet this requirement.

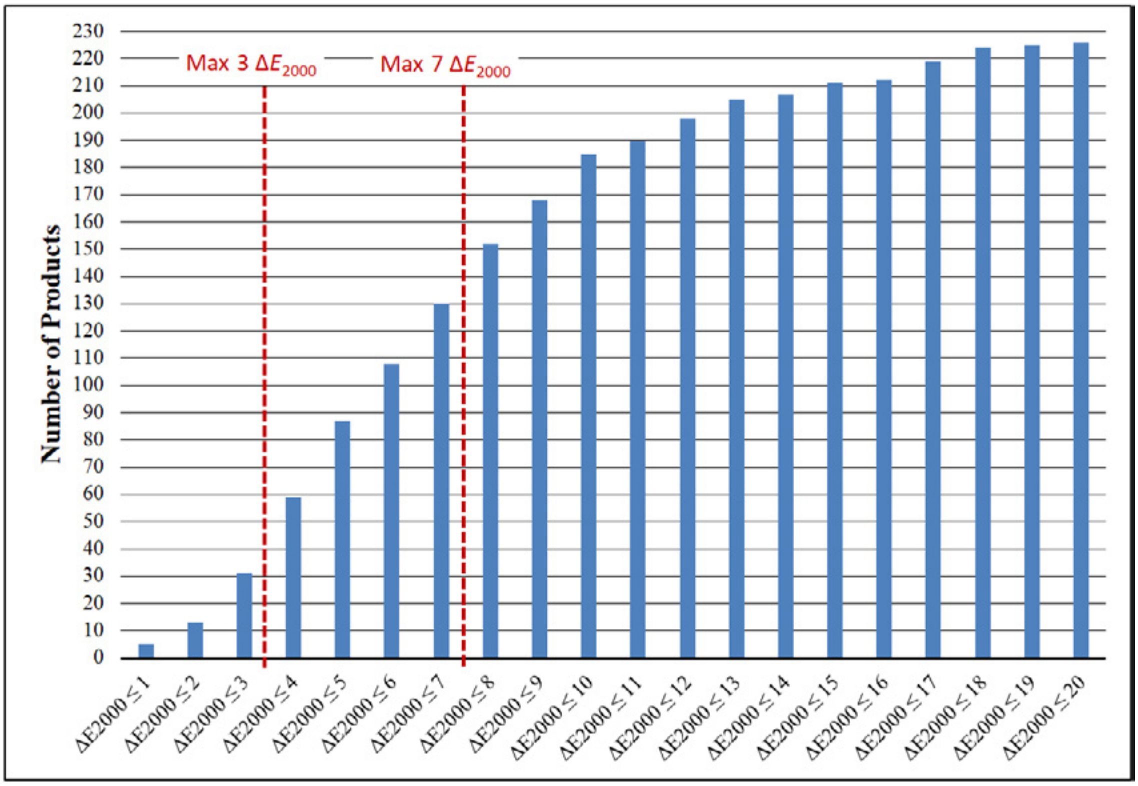

Figure 5: The 226 print products distributed by different limit values

Among the 226 products, only 31 of the product had a color difference ≤ 3 ΔE_{00}. That account for 13.7 % of all the products. 22 of those products where printed in CMYK while 9 of the products were printed as spot color / 1-color Pantone. Among those 31 products, 21 of the products where printed in lithographic offset, 2 products were printed in flexographic print, 2 where printed in gravure, 4 in screen printing and 2 in digital print. Among those 31 products, 21 where printed on paper, 7 products were printed on film/ plastic, 1 product was printed on metal, 1 was printed on nylon and 1 was printed on cotton.

When raising the acceptance limit to a higher ΔE_{00}, it will of course result in more products falling within the acceptable limit. But where should the limit be set?

- 31 of the products (13.7 %) had ΔE_{00} ≤ 3
- 130 of the products (57.3 %) had a ΔE_{00} ≤ 7
- 151 of the products (67 %) had a ΔE_{00} ≤ 8

This means, that 42.5 % of all products have a ΔE_{00} above 7 which, according to the previous study, is above acceptance (Pedersen, 2016).

The average of all the 226 product's ΔE_{00} is the mean 7.3 ΔE_{00} However if this is set to be an acceptance limit, only 134 of the products (59.3 %) can comply, although it might have been expected that 155 of the products (68,6 %) should fall within this limit. The limit should be raised to 8.2 ΔE_{00} for this study's products if 68% of the products should fall within an acceptance limit.

In Figures 6 and 7 the distribution of the color differences shows that most products had a color difference between 2 and 10 ΔE_{00}. Approximately half of the products had a color difference above 6 ΔE_{00} and 6 products had a ΔE_{00} between 21 and 34 (these might be considered as outliers and are removed in Figure 7). In the positive end of the scale 5 products had a $\Delta E_{00} \leq 1$.

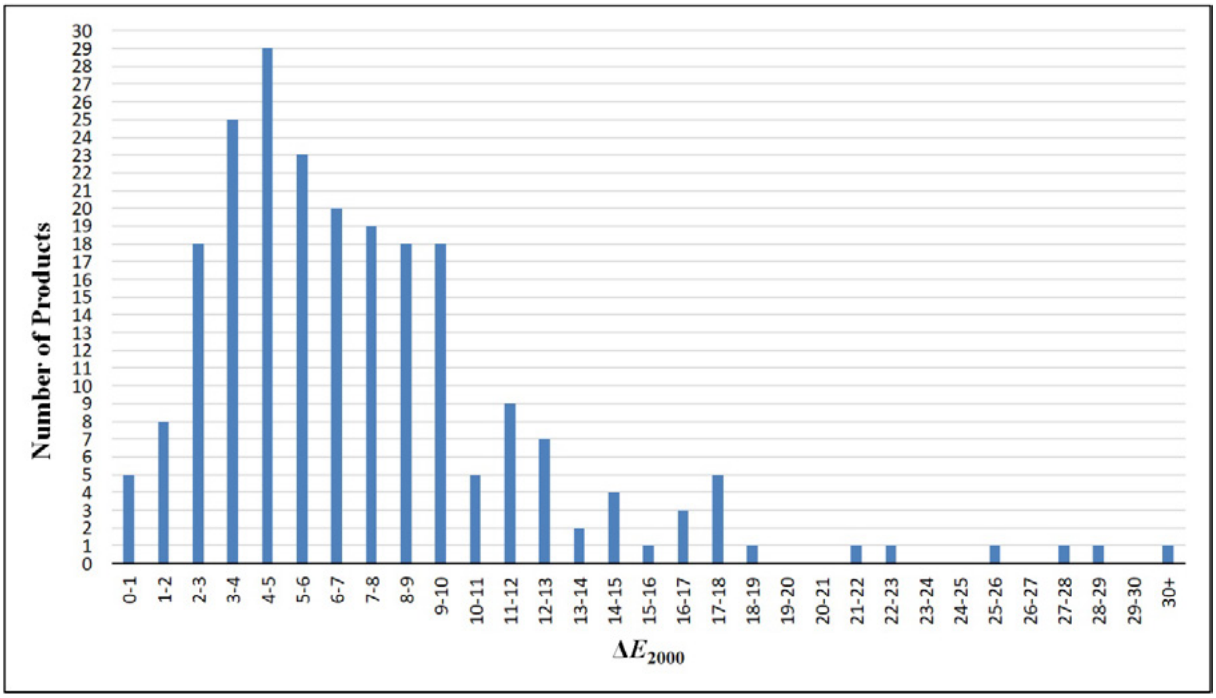

Figure 6: The 226 print products distributed as color difference intervals; the mean is 7.3 CIEDE2000

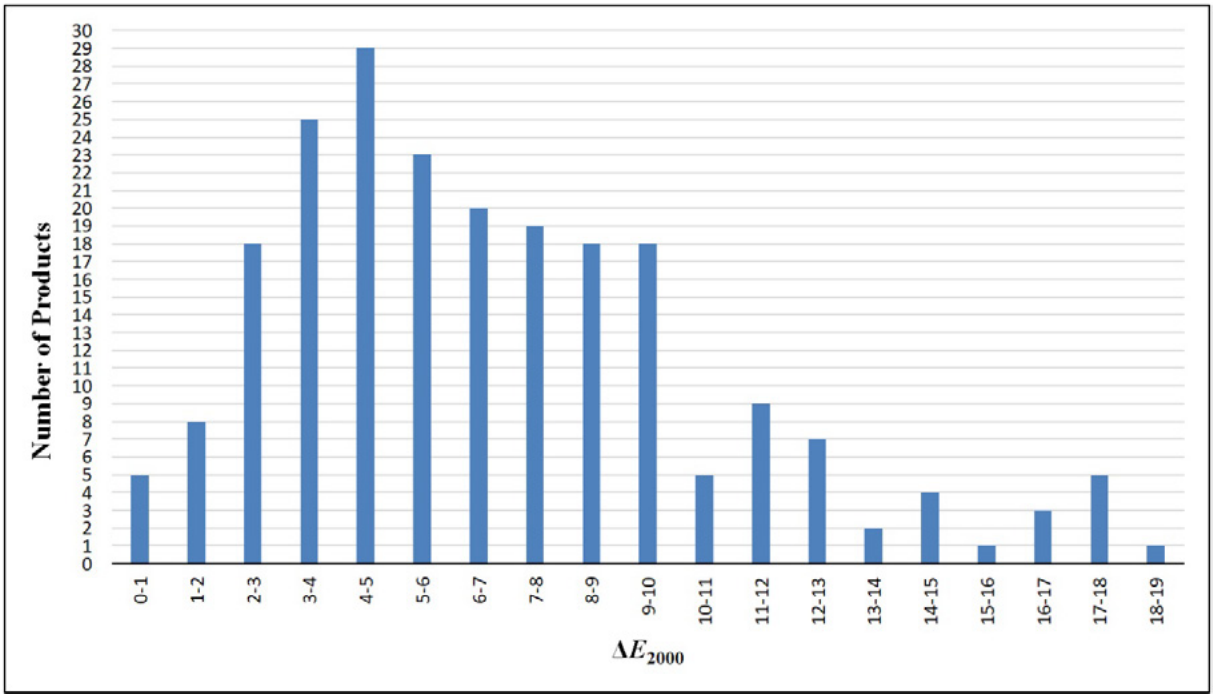

Figure 7: After removal of 6 outliers aboveCIEDE2000 20, the remaining 220 print products distributed as color difference intervals; the new mean is now 6.3 CIEDE2000

3.6 Comparison of color differences across substrates, technologies and color systems

It might be interesting to see if there is a correlation between a large color difference and the used substrate type, print technology or color system. This is shown in Figures 8–10. It will of course be difficult to compare these means because some are calculated on the basis of few data points (products) and others are calculated based on many data points.

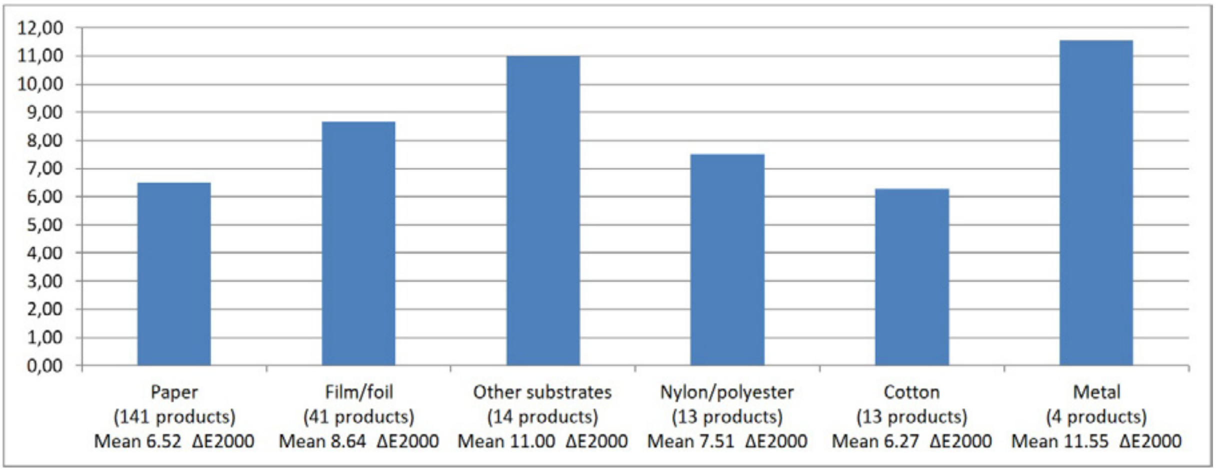

Figure 8: Comparison of color difference means across substrates, distributed by number of products

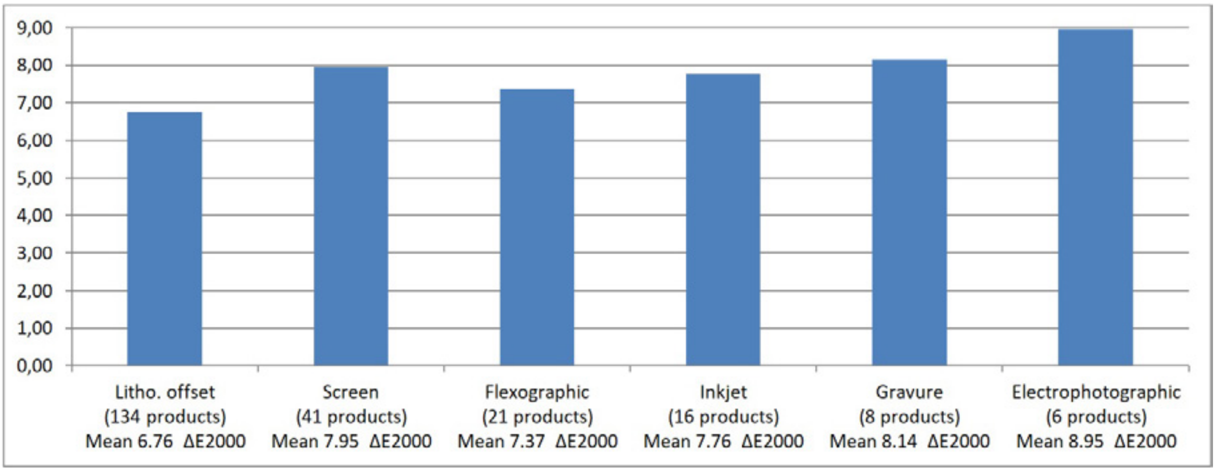

Figure 9: Comparison of color difference means across technologies, distributed by number of products

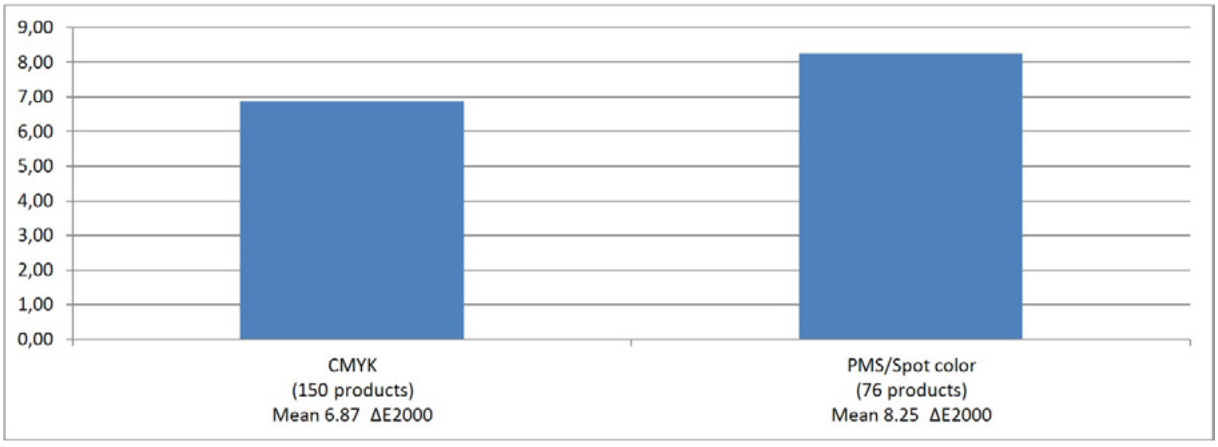

Figure 10: Comparison of color difference means across color systems, distributed by number of products

3.7 Other color deviations

For the sake of completeness, it should briefly be mentioned which other color differences these print products had. Among the 226 print products only 20 of the products had a $\Delta E^*_{ab} \leq 5$ and 162 of the products had a $\Delta E^*_{ab} \geq 10$ while the highest color difference was 67.8 ΔE^*_{ab}. When evaluating ΔH^*, 75 of the products had a $\Delta H^* \leq 2.5$ and 32 of the products had a $\Delta H^* \geq 10$, while the highest ΔH^* was 46.6.

4. Conclusions

Apparently this variety of color conformance is what to expect when buying different print products for a campaign or an event. Even though 86.3 % of the 226 products had a color deviation above 3 ΔE_{00} and almost half of the products had a color difference above 7 ΔE_{00}, these 226 print products have obviously been approved and paid for and must therefore be useful to the companies (customers).

Whether the relatively large color differences are due to inappropriate color specification in the Brand Manuals or if there is a general inattention in the printing companies is not to be said. However, it seems that standardized color management, quality control and process standardization haven't played a key role in these productions. Or, put in another way, the focus has apparently not been on the color rendering in the printed images. There is apparently no significant correlation between a large color difference and a particular print technology, substrate or color system. It can of course be discussed whether it makes sense to compare print products that are manufactured on different print substrates and in different print technologies. But for the customer, there is probably an expectation that all their print products look alike no matter how and where they are produced.

References

FOGRA, 2010. *Fundamantals for the standardization of spot colours in offset printing: Uwe Bertholdt Fogra Research report no. 32.158*. Fogra.

International Organization for Standardization, 2013a. ISO 12647-1:2013 *Graphic technology - Process control for the production of half-tone colour separations, proof and production prints - Part 1: Parameters and measurement methods.* Geneva: ISO.

International Organization for Standardization, 2013b. ISO 12647-2:2013 *Graphic technology - Process control for the production of half-tone colour separations, proof and production prints - Part 2: Offset lithographic processes.* Geneva: ISO.

International Organization for Standardization, 2012. ISO 12647-6:2012 *Graphic technology - Process control for the production of half-tone colour separations, proofs and production prints - Part 6: Flexographic printing.* Geneva: ISO.

Pedersen, M.A., 2016. Why most Brand Manuals fail when it comes to defining Brand Colors and how to determine acceptable Color Deviations for specific Brand Colors. In: P. Gane and C. Ridgway, eds. *Advances in Print and Media Technology: Proceedings of the 43rd International Research Conference of iarigai*. Toronto, Canada, 24–27 August 2016. Darmstadt: iarigai.

VIGC, 2008. *VIGC study on spectrophotometers reveals: instrument accuracy can be a nightmare.* Turnhout, Belgium: Vlaams Innovatiecentrum voor Grafische Communicatie.

Key Elements of Developing a Customized Web-to-Print Platform

Yung-Cheng Hsieh[1], *Cheng-Cheng Jiang*[1], *Xin-Yi Wong*[2]

[1] School of Digital Media and Art Design, Hangzhou Dianzi University. Xiasha Higher Education Zone, Hangzhou, 310018, Zhejiang Province, People's Republic of China

[2] Department of Graphic Communication Arts, National Taiwan University of Arts. No.59, Sec. 1, Daguan Rd. Banqiao Dist., New Taipei City. 22058, Taiwan (R.O.C.)

E-mails: yunghsieh@gmail.com; c.jiang@hdu.edu.cn

Short abstract

"Web-to-Print (W2P)" has become a new trend of printing industry all over the world since 2007. A widely definition of Web-to-Print is commercial activities for trading of printing products/services through the internet. Most of Asian printers still use traditional processes to print orders. Comparing to the printers in the U.S. or European countries, these printers in Asia seem not so active in the development of Web-to-Print. Under the influence of digitalization, it will be very important for them to consider how to provide "Web-to-Print" services. Not until four years ago, printers in Taiwan, Hong Kong, and China started to pay much attention to the investment into W2P. However, the development of W2P in Asia reminds on the stage of cloud printing for paper-related product with standardized and mass production workflow. In the meantime, printers in North America and Europe have elevated their services from W2P to customized W2P due to the great need of personalization and sharing of the young generation. To understand the needs, key elements, criteria, and necessity of a profitable customized W2P platform, this research conducted content analyses on major successful W2P service websites in North America, China, and Taiwan. To explore how Taiwanese printers view the must-have requirements and might-have obstacles, to understand the bottlenecks and difficulties encountered, and to comprehend the web structure and important functional items in the process of establishing, implementing, and maintaining a customized W2P platform, the study carried out thirteen in-depth interviews of experienced printers and educators in Taiwan. The qualitative research approach constructed interview agendas based on four dimensions, namely, information, capital, business, and logistics. This study disclosed the essential functionalities and obstacles of a successful me-commerce web-to-print platform. It presents the synergistic combination of traditional printing, web printing, and digital imagery to achieve the goal of yielding maximal utility for creative design resources, while providing an interactive internet-plus model for B2C (Business to Consumers), B2B (Business to Business), B2B2C, C2B (Consumers to Business), C2F (Consumers to Factory) or C2M (Consumers to Manufacturers) trade transactions empowering renewed competitiveness for the future of the printing industry. We hope that this study will elevate competitiveness of traditional printing enterprise and create a new blue ocean for the conventional printers.

Keywords: Customization, Web-to-Print, Me-commerce, E-commerce, Printing Industry

1. Introduction and background

The combination of Web to Print (W2P) and me-commerce (custom-made e-commerce), so called customized W2P, is the key trend of the digital printing industry worldwide. Customized W2P has been well established in the US and is developing rapidly in Taiwan and China, especially under the pressure of paperless and green policy. Compared with the W2P market in the US and Western Europe, the market in Taiwan and China is facing a stage of transformation from traditional business model to so called me-commerce model. The printers have heavily relied on the internet and web platform to maintain the business, reduce cost, increase productivity, and enhance competeiveness no matter what printing processes they use. The customized W2P has brought a new business opportunity and challenge for conventional printers.

In Taiwan, although many printers have introduced some kind of W2P into their workflow, only a few of them offer custom-made services in terms of custom-made online design (Yao, 2015). The demand of personalized merchandises has been increased and its market competition has been intensified. Consumers' need for diverse printing products with high quality and personalized creativity from customers or their favor designers. The request of custom-made or unique design of images of text has become the main stream of W2P. Moreover, some of advanced W2P printers have even provided smart phone applications (Apps) for users to do the online estimation, order, design, editing, and job tracking anytime and anywhere. In Taiwan, most of conventional printers own high quality facility and equipment with capability of performing W2P, but it is a pity that not many of them invest on customized W2P due to the lack of strong online service. To understand the needs, key elements, criteria, and necessity of a cost-effective customized W2P platform, this study conducted content analyses on major successful W2P service websites in Europe, North America, China, and Taiwan. To explore how Taiwanese printers view the must-have requirements and might-have obstacles, to understand the bottlenecks and difficulties encountered, and to comprehend the web structure and important functional items in the process of establishing, implementing, and maintaining a customized W2P platform, the study carried out thirteen in-depth interviews of experienced top managers and educators in Taiwan. The qualitative research approach constructed interview agendas based on four dimensions, namely, information, capital, business, and logistics. The study were to:

1. explore the current content and service items of domestic and foreign customized W2P platform,
2. understand the current W2P development and personalized online services of Taiwanese printers,
3. realize the requests of functional items and internal/external obstacles while developing a cost-effective customized W2P platform,
4. provide suggestions to maintain a successful customized W2P business for current W2P owners and concerns for conventional printers when leading into customized W2P business.

Web to Print service is the core business of the cloud printing. It can be separated into seven parts (Liu and Cao, 2016):

1. Product type: Description of the available printing products on the website
2. Online editing: A technical platform for product design. Consumers can customize their products online or do so with the help of a designer. The online editing system includes online templates and specifies the print area.
3. Online preview: It can be used to preview the result of the product after a customer or a designer finishes the design.
4. Order service: To record the ordering process such as online orders, purchase history and tracking, etc.
5. Quotation: To provide diversified options to customers. Services include independent quotations, online inquiries, information for customers and past quotations, etc.
6. Transaction management: To ensure the safety of the transactions between customers and businesses such as online payment, payment reminders and payment history.
7. Shipping method: Self collection or delivery

Currently in other countries the technology of W2P is mainly focusing on the short-run and on-demand markets. It is mostly used to develop commercial marketing in combination of digital content as it can maximize the scale and value of the application. The initial development of variable data printing focused on the printing of textual variations. To date, textual content remains the mainstream in variable data printing. However, as the requirement of customized content becomes more complex, variable data printing is transitioning to image printing, or sometimes even to basic security printing and other special effects. It can allow customers to change the content of any page and is flexible. Research expert Romano at Graphic Arts Technical Foundation (GATF) even defined the process of variable data printing as non-analog printing, i.e.

without the use of films, printing plates or other image generators. Instead, the output combines different content from the database. The advantage of variable data printing is to provide suitable information to the targets by maximizing the use of limited resources. It has become valuable thanks to the prevalence of customized or tailor-made printing which is the core of me-commerce web to print.

Me-commerce targets individual customers and is an extension of e-commerce. Its only difference from e-commerce is that me-commerce focuses on individual needs of customers and emphasizes on the individual target marketing. The new habits of new customers “4Ps” include Pervasive, Participatory, Personalized, Prescriptive. They are the following (Radice, 2014).

- Pervasive: prevalent and available for purchase anywhere
- Participatory: Sharing with one another instantly
- Personalized: Customization. Customers can win coupons by providing personal information
- Prescriptive: Specific. Customers should have access to purchase deals on their mobile devices before shopping.

In an era where mobile devices are so prevalent, the relationship between me-commerce and W2P is closer than ever. The printing industry will experience drastic changes in the coming ten years and will embrace Customized Web to Print or so-called Me-commerce Web to Print under the trend of SMAC (Social, Mobile, Analytics and Cloud). This will maximize the use of conventional printing facility in combination with me-commerce that provides customization to meet unique needs of consumers (Boone, 2015).

2. Materials and methods

This research employed the content analysis method to examine the internationally known web-to-print platforms and their related web structure. The study aims to identify the trend of customized web-to-print printing and to provide suggestions to conventional printers that wish to develop online custom printing platforms in the future. This research analyzed 59 websites involved in W2P transactions and services, including 22 US companies, 22 Taiwanese companies, 4 UK companies, and one Hong Kong company. All of the companies provide both conventional mass-production printing and customized printing services. Customers can select their favorite photos from Facebook or Instagram for design and then print. Photos and designs can be stored in the cloud. Among the 22 US companies, five of them, such as “Shutterfly” and “CafePress” allow customers to buy products made by designers and even encourage customers to shop, create and sell their own design. Their platforms provide a variety of customized products and gifting services. In addition, those platforms cooperate with a multitude of brands and provide high quality licensed photos. The rest of companies specialize a certain type of printing services such as book/paper printing, T-shirt printing, fabric printing, wedding material printing, and so on. The 22 web-to-print companies in Taiwan are still at a budding stage; currently only 11 of them provide online design/editing tools to allow customers design their own products and sell their own design. The content analysis result indicates that the number of website providing web-to-print services is increasing.

In addition, the research conducted in-depth individual interviews of 13 experts including experienced high level printing management, stakeholders, and educators. The interviews discussed the requirements of leading into customized W2P service from a conventional printing business or establishing a new customized W2P platform, as well as the bottlenecks faced by the businesses. All interviews were conducted between March 29 to May 25, 2017. The agendas of the interviews are as follows.

1. Understanding online printing services in Taiwan: Does your company provide customized W2P services? If yes, can you share with us the bottlenecks or dilemmas that your companies have faced? If not, please explain why the company decides not to provide such services.

2. Currently most traditional printers are faced with difficulties caused by business transformation and customized W2P services.
3. The prerequisites of developing customized W2P platforms in Taiwan
4. Requirements of internal development: Evaluate and align company's capabilities such as logistics, cash flow, information flow and online editing functions with the requirements of the customized W2P platforms.
5. The considerations of traditional printers investing customized W2P platforms and suggestions about website structures

The summary of the opinions collected from the expert interviews is as follows.

Change conventional mindset and learn new concepts
Most traditional printers and employees still adopt a traditional mindset towards printing when it comes to business operation. A customized W2P system should include cloud platforms, information systems, online marketing, website design and more. What these provide customers with are less expensive, more convenient, more time saving, and highly custom-made online shopping experiences. Traditional printers are encouraged to learn new mindsets through participation in seminars and classes, and exchange ideas with industry professionals. This helps make customized W2P more prevalent and services will therefore improve.

Improve the UI and UX of online editing tools
The interview results show that there are existing sets of software available on the market that printers can either rent or buy. However, there is a lack of creativity in these templates. One way to improve this is to differentiate the platform by designing the functions based on the custom-made features for customers to use on line freely. In addition to improving the editing tools and uniquely design the company website, the UI should also look modern and sleek while the UX should be easy enough to use. Adjustments to computer and mobile versions are to be made. Only if the aesthetic value of the website and editing tools increases will they attract more users.

Use big data to analyze the customers' preferences
Businesses can maximize the use of big data collected from their platforms to explore customers' shopping habits and to predict their shopping behaviors in the future; moreover, do target marketing accordingly. The personalized marketing tactic of announcing discount codes and sales can boost customer spending. In addition to attract new customers, businesses should understand current consumers' buying behaviors, changes in preferences, changes in transaction processes to increase their loyalty. While boosting sales, companies should also pay attention to their cash flow. This can be achieved by evaluating the credit score of customers using big data analyses, which avoids unnecessary labor costs.

Tap into overseas markets and improve quality and services
Since Taiwan's print market is limited, most business owners believe the W2P industry should also tap into overseas markets, especially Southeast Asia. Nonetheless, customized W2P is not the ultimate goal of business transformation. The key is to become specialized in a particular field and continously strengthen the quality of its products.

Cooperate with IT specialists to construct a better customized W2P system
Most successful W2P platforms are partner with business owners with IT background. The key for online printing is to keep the communication between customers and the printing house. Although "Content is the King", a successful customized W2P platform should have an operating system that runs smoothly in the backend. IT specialists are necessary to maximize the readability and user friendliness of customized W2P platforms.

Online marketing and offline promotion
In addition to a good platform, personalized marketing also plays a vital role. Businesses can draw attention from the target audience by using keyword ads, social media, hot searches and starting conversations. Big data analyses reports can be very useful in personalized marketing, specifically for festive and special event products. As to offline promotion, word-of-mouth is very critical tool for marketing. Consumers nowadays see the CP value of a product as an important influence of purchase. They evaluate products and services online as well as offline. Therefore, products and services should be reasonably priced and should continue to improve customer purchase experience. Businesses should pursue continual improvement in pre-sale and post-sale activities, as well as in the product itself, which translates into word-of-mouth marketing in the long term.

Collaborate with cloud and platform economy
The biggest feature of e-commerce is that it allows users to look for business partners in the cloud. Printing companies can outsource different tasks such as designing, printing, finishing, binding, packaging, and delivering to other business partners and share the profits. Especially in a me-commerce W2P, it requires diverse creativity for personalized design, communication, custom service, and marketing. Companies can make the best use of the platform to learn about users' preferences and improve their services accordingly (Cheng, Hsieh and Wei, 2017).

Adopt a customer-oriented approach to sell a lifestyle to consumers
Nowadays most consumers pay more attention to the personalized quality of a product used in daily life than price itself. It is suggested that companies should put more efforts in developing DIY (Design It Yourself) gifts for consumers to buy for their family members, friends, and even pets. The design and packaging of these custom-made products should be heavily emphasized so that products look presentable to customers. Custom-made gifts are not only a good way to surprise a loved one, they can also be an effective way to promote a brand especially when these products are offered during new year/ year-end celebrations or other festive occasions and special events.

3. Results and discussion

This research takes reference from the Top Ten Reviews in the United States that rate the performance of different web-to-print services in 2016 and evaluate the top ten service providers based on their overall performance. The rating criteria are as follows.

1. Price Competiveness
2. Product Choices
3. Users Create online/ Degree of Customization
4. User Interface
5. Trading mode
6. Shipping
7. Customer Service; Help & Support

The business flow refers to the pricing and trading modes while the information flow refers to printing product options and customer services. Online editing functions include the evaluation of online design tools available to creators, customization availability and user interface while logistics refers to shipping methods. The research has concluded the results in Table 1 below. Figure 1 shows the functions of the web-to-print websites outside of Taiwan as well as their focus and service trends.

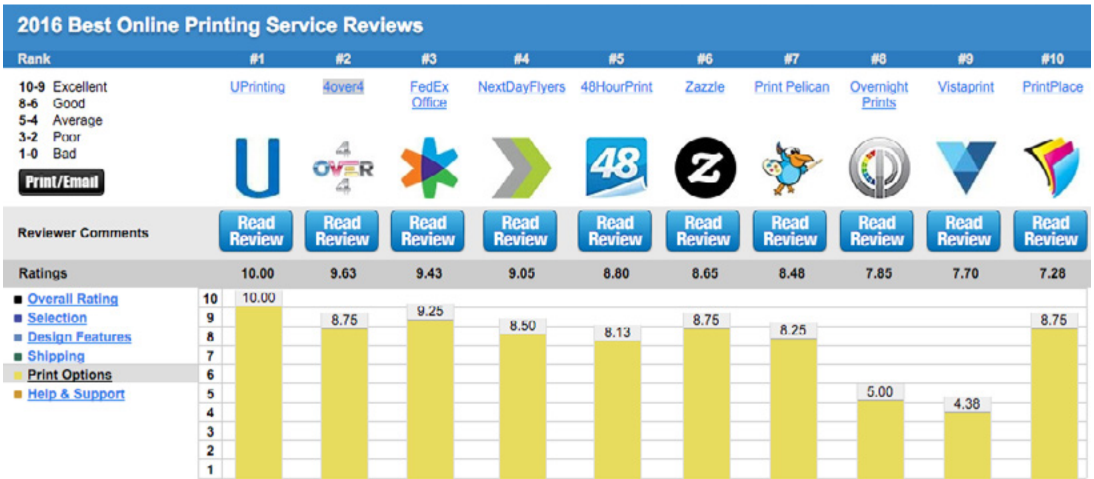

Figure 1: 2016 top ten web-to-print service platforms (TopTenReviews, 2016)

Table 1: 2016 US top ten online printing service platforms, compiled by authors

Platform/Items	1	2	3	4	5	6	7	8	9	10
Price (US Dollars)										
Business Cards (500 sheets)	$21	$33	$40	$24	$55	$54	$25	$23	$19	$18
DM (500 sheets)	$113	$99	$325	$96	$91	$95	$211	-	$58	$170
Postcards (500 sheets)	$65	$47	–	$46	$129	$300	$284	$43	$58	$63
Product Category										
Quality Score	95	90	85	80	60	80	65	70	70	65
Brochures & Business Cards	●	●	●	●	●	●	●	●	●	●
Event Cards & Postcard	●	●	●	●	●	●	●	●	●	●
Flyers & Banners/Poster	●	●	●	●	●	●	●	–	●	●
Stickers/Labels	●	●	●	–	–	●	–	–	●	●
Magnets	●	●	●	–	–	●	●	●	●	●
Menus/Table Tents	●	●	–	●	●	●	●	–	●	●
Booklets/Bookmarks	●	●	–	●	●	●	●	●	–	●
Hang Tags	●	●	–	●	●	●	●	–	–	●
Calendars	●	●	●	–	–	●	●	●	●	●
Mugs	–	●	–	–	–	●	–	–	●	–
Phone Case	–	–	–	–	–	●	–	–	●	–
T-shirt and Fabric	–	●	–	–	–	●	–	–	●	–
Stationary	–	–	–	–	–	●	–	–	●	–
Puzzle	–	●	–	–	–	●	–	–	–	–
Electronic-USB/ Speakers	–	–	–	–	–	●	–	–	–	–
Food Package	–	–	–	–	–	●	–	–	–	–
Online Design Service and Customization										
Many choices of size/page/color etc.	●	●	●	●	●	●	●	●	●	●
Upload design/photos	●	●	●	●	●	●	●	●	●	●
Select Template and Online Editing	●	–	●	–	●	●	●	●	●	–
Download template	–	●	–	●	●	–	–	●	–	●
Many choices of images	–	–	–	–	●	●	–	●	●	–
Online file saving space	●	–	–	–	●	●	●	●	●	–
Online preview and editing	●	–	–	–	●	●	●	●	●	–

Platform/Items	1	2	3	4	5	6	7	8	9	10
User Interface Design (Information Flow)										
Product search	●	●	●	●	●	●	●	●	●	●
List of price and Quantity	●	●	●	●	●	●	●	●	●	●
Simplicity of site operation	●	●	–	●	●	●	●	●	●	●
Q&As	●	●	●	●	●	●	●	●	●	●
Online estimation	●	●	●	●	●	●	●	●	●	●
App for download	–	–	●	–	–	●	–	–	–	–
Trade model (Capital/Cash Flow)										
Visa	●	●	●	●	●	●	●	●	●	●
MasterCard	●	●	●	●	●	●	●	●	●	●
PayPal	●	●	●	–	●	●	●	●	●	–
American Express	●	●	●	●	●	●	●	●	●	●
Discover/Others	●	●	●	●	–	–	–	–	–	–
Online order tracking	●	●	●	●	●	●	●	●	●	●
Shipping (Logistics)										
Post mail	●	●	●	●	●	●	●	●	●	●
Rush delivery	●	●	●	●	●	●	●	●	●	●
Ship to Customer	●	●	●	●	●	●	●	●	●	●
Shipping within 24 hrs.	●	●	●	●	●	●	●	●	–	●
Shipping tracking	●	●	●	●	●	●	●	–	–	–
Refund/reprint	●	●	●	●	●	●	●	●	●	–
Customer Service / Help & Support										
Overall Rating	100	85	85	70	85	60	90	75	70	90
Email inquiry	●	●	●	●	●	●	●	●	–	●
Phone inquiry	●	●	●	●	●	●	●	●	●	●
Live Chat	●	●	–	●	●	●	●	–	–	●

Table 1 shows that the top performing W2P platforms that provide digital content added-value applications on their websites generally put great emphases on five areas. These include online editing functions, free online digital content sharing, unlimited online storage, customized products and 100% customer happiness service. In addition to online editing functions, some international companies also provide a variety of customizable products (including phone cases, T-shirts, stationery, interior decoration or even pet products). As a result, products that used to be restricted to mass printing can now be available through Print on Demand. Consumers can create customized products and gifts. Some international companies provide trading services to creators, designers, and artists which allow them to sell their creativity on the platforms. Taiwanese W2P platforms, on the other hand, rarely provide the five aforementioned services. In regard to product customization, the Taiwan market is still in the process of development. Generally, the product types are not as varied as those of international companies. Regarding the content editing process, consumers generally design their files offline before uploading them to a W2P platform. Few provide personalized content editing software to consumers on line or free download services. To date, this research has yet to find any Taiwanese customized W2P platform that offers consignment services for designers and/or artists.

Web to print services has become increasingly popular in China. Chen Yan published the Top 20 digital printing companies in China in the "Analysis and forecast of the online printing market in China 2017" in March 2017. The report showed that the number of online printing platforms has increased from 80 in 2014 to more than 400 in 2016, at least 280 of which are in good operation.

Chinese enterprises invest heavily in e-commerce and digital content industry. These financial figures are massive. In the publication of the top 20 W2P companies in 2017, the concept of "brand" is emphasized. PEK (Printing Industry E-commerce Data Key Indicators) created by keyin.cn is a ranking mechanism which evaluates the overall performance of the W2P service in China (excluding Hong Kong, Macau and Taiwan) using criteria such as content quality, volumes and website security, etc. 20 companies have been selected on the basis of PEK index as shown in Table 2.

Table 2: Top 20 web-to-print companies in China in 2017 (Keyin.cn, 2017)

Company name	**Web Site**
36588.com	http://www.36588.com.cn/
Easy Print	http://www.98ep.com/
EP365.com	http://www.ep365.com/
Namex	http://www.namex.cn/
Yifutu	http://www.yifutu.com/
Yofus	http://www.yofus.com/
Hucais	http://www.hucais.com/
kaixinyin.com	http://www.kaixinyin.com/
FastPrint	http://www.92mp.com/
wdxc.cn	http://www.wodexiangce.cn/
ininin.com	http://www.ininin.com/
pptake.com	http://www.pptake.com/
CYT sq.kiy.cn	https://www.0757p.com/sq.kiy.cn/
Yi Si De	http://www.yiside.com/
Zhi Xiang Ge	http://www.zhixiangge.com/
eheyin.com	http://www.eheyin.com/
Zhonghao Ziyun Technology Co.,Ltd	http://www.11ziyun.com/
Xuan Cai	http://www.xuancai2008.com/
duoduoyin.com	http://www.duoduoyin.com/
Xiangin	http://www.xiangin.cn/
Boxdiy	https://www.boxdiy.cn/
art2print.cn	http://www.art2print.cn/scene
LVAI	https://lvaifood.1688.com/
Xiao Mei Ji	http://www.xiaomeij.com/Index/Packing.html
huluwa360.com	https://www.huluwa360.com/
suyinw.cn	http://www.cailuan.cc/

The development of customized W2P in China is being popular as companies learn from overseas counterparts to provide uniqueness and value in their services. In addition to the common customization printing services, five of the companies target the massive packaging market by providing customized packaging design and printing services to small- to medium- sized enterprises. "Zhi Xiang Ge" has integrated advertising into its package printing business, taking advantage of the advertising influence. Some W2P platforms, from reading to usage, are user-friendly and simple. Few of them even provide online editing tools, which makes online ordering, automatic quotation, order allocation, production plans and seamless online payments possible. Customers can easily place orders online, receive quotations, conduct file transfers, complete online payments and have products delivered to a designated address. They can even track their order online.

To understand the platform requirement for customization services of traditional printing, this research selected and compared 10 outstanding customized W2P websites from eight regions. The result is shown in Table 3.

Table 3: Ten selected successful W2P platform worldwide, on 10 May 2017

Company name	**URL**
Vistaprint (USA)	http://www.vistaprint.com/
Shutterfly (USA)	https://www.shutterfly.com/
36588.com (China)	http://www.36588.com.cn
ininin.com (China)	http://www.ininin.com/
Gain How (Taiwan)	https://gainhow.tw/
Eprint (Hong Kong)	https://www.e-print.com.hk/
CEWE (France)	https://cewe-photoworld.com/
Pixartprinting (Italy)	https://www.pixartprinting.it/
Printpac (Japan)	http://www.printpac.net/
Printi (Brazil)	www.printi.com.br

The evaluation results are shown in Table 4 and are used as a reference for the research. The table analyzes the major functions and services of the top 10 companies that provide customized W2P services.

Table 4: Evaluation and comparison of the platform functions and services offered by companies that customize traditional printing

Platform/Items	1	2	3	4	5	6	7	8	9	10
A: Main Page										
Search	●	●	●	●	●	●	●	●	●	●
Language	●	–	–	–	–	●	●	●	–	–
Free shipping on order	–	●	●	–	–	–	●	–	●	–
Live chat	●	●	●	●	–	●	●	–	–	●
Email inquiry	●	●	–	●	–	●	●	●	●	●
Customer hotline	●	●	●	●	●	●	●	●	●	●
Consignment	–	–	–	●	–	–	–	–	–	–
Shopping cart	●	●	●	●	●	–	●	●	–	●
Promote code	●	●	–	–	●	–	●	–	–	–
News	●	●	●	●	●	●	●	●	●	●
Best seller	–	●	●	●	●	–	–	–	●	●
Season promotion	●	●	●	–	–	●	–	●	●	●
Feature product	●	●	●	●	●	●	●	–	●	●
Customized products for event	●	●	–	●	●	–	●	–	–	–
Office supplies /Clothing/Bags etc.	●	●	●	●	●	–	●	–	–	●
Upload your design	●	●	●	●	●	●	●	●	●	●
Design Service	●	–	●	●	–	–	–	–	–	●
Customer reviews	●	●	●	–	–	–	–	–	●	●
Contact us	●	●	●	–	●	–	●	●	–	●
Artist/celebrity endorsement	–	●	–	–	–	–	–	–	–	–
Refer a friend	●	●	–	–	–	–	–	–	–	–

Platform/Items	1	2	3	4	5	6	7	8	9	10
Mobile App	–	•	–	•	•	•	•	–	–	–
Average customer ratings	•	•	•	–	–	–	–	–	–	•
Customer product photos	•	•	•	–	•	–	•	•	–	–
B: Member Account/Services										
Account tools	•	•	•	•	•	•	•	•	•	•
View order history	•	•	•	•	•	•	•	•	•	•
Reorder	•	–	–	–	–	–	–	–	–	–
Update account settings	•	•	•	•	•	•	•	•	•	•
Stored payments	•	–	–	–	•	–	–	–	–	–
View recent communications	•	–	–	–	–	–	–	–	–	–
My images and logos	•	•	–	•	•	•	•	•	–	•
My favorites	•	•	•	•	–	–	–	–	–	–
Business e-mail	•	–	–	–	–	–	–	–	–	–
Domain names	•	•	–	–	–	–	–	–	–	–
C: Products/Services										
Postcard mailing	•	•	–	–	–	–	–	–	–	–
Design Re-creation Service	•	–	–	•	–	–	–	–	–	–
Graphic design services for customers (e.g. logo, cards, DM…)	•	–	•	•	–	–	–	–	–	•
Product & Package design service (food package, phone cases…)	•	–	•	•	–	–	–	–	–	–
Email marketing	•	–	–	–	–	–	–	–	–	–
Local listing	•	–	•	•	–	–	–	–	–	–
Social media marketing	•	–	–	–	–	–	–	–	–	–
Browse our designs	•	•	•	•	•	–	•	–	–	•
Upload your own complete design	•	•	•	•	•	•	•	•	•	•
Design yourself	•	•	•	•	•	–	•	–	–	•
Gift certificates	•	–	–	–	–	–	–	–	•	–
Personalized mugs	•	•	•	•	•	–	•	–	–	•
Holiday cards	•	•	•	•	•	•	•	•	•	•
Canvas prints	•	•	–	•	•	–	•	•	–	•
Phone cases	•	•	•	–	•	–	•	–	–	–
Clothes (e.g. T-shirt)	•	–	•	–	•	–	–	•	–	•
Puzzles	•	•	•	–	–	–	•	–	–	–
Labels & gift tags	•	•	–	•	•	–	–	•	–	–
Home decor	•	•	–	–	•	–	•	•	–	–
D: Tutorial										
Getting started	•	•	•	•	•	–	–	–	•	•
How-to-video	–	•	–	–	–	–	–	–	–	–
Help center	•	•	•	•	•	•	•	•	•	•
Contact us	•	•	•	•	•	•	•	•	•	–
Shipping & delivery	•	•	•	•	•	•	•	•	•	–
Request samples	•	–	–	–	•	–	–	•	•	–
E: Partner with us										
Upload designs	•	•	–	•	•	•	•	•	–	•
Our partners	•	•	•	•	–	•	–	–	–	•

Platform/Items	1	2	3	4	5	6	7	8	9	10
Contributing Photographer/designer	●	●	●	●	–	–	–	–	–	●
Advertising with us	●	●	●	–	–	–	–	–	–	–
Reseller program	●	–	●	●	●	●	–	–	–	●
Popular searches	●	●	–	●	●	●	●	–	●	–
F: Our Company										
About us	●	●	●	●	●	●	●	●	●	●
Careers	●	●	●	●	–	–	●	●	–	●
For media	●	●	●	●	●	●	–	●	–	–
For investors	●	●	–	–	–	–	–	–	–	–
G: Our Policies										
Copyright matters	●	–	●	–	–	●	●	●	●	●
Trademark matters	●	–	–	–	–	–	–	–	–	–
Patents	●	–	–	–	–	–	–	–	–	–
Terms & conditions	●	●	●	●	●	●	●	●	●	●
Privacy policy	●	●	●	●	●	●	●	●	●	●
Absolutely guaranteed	●	●	●	–	–	–	–	●	–	–
H: Connect with us										
Facebook	●	●	–	–	●	–	●	●	–	●
Instagram	●	●	–	–	–	–	●	●	–	–
Twitter	●	●	–	–	–	–	●	●	–	●
Pinterest	●	●	–	–	–	–	●	–	–	–
Google+	–	●	–	–	–	–	●	–	–	●
WeChat	–	–	●	–	–	–	–	–	–	–
Line@	–	–	–	–	–	–	–	–	–	–
Weibo	–	–	●	●	–	–	–	–	–	–
QQ	–	–	–	–	–	–	–	–	–	–

The evaluation shows the focus of the services provided by the 10 platforms concerning customized W2P service includes homepage, search function, customer hotline, latest news and hot selling products, followed by instant customer service, promotion codes and seasonal discounts. Many platforms are now available in smart phone applications due to the growing popularity of mobile devices such as smart phones and tablets in recent years. In addition, multilingual websites also bring convenience to users around the world. Conditional free shipping, promotion codes and "share with friends to enjoy discounts" can also stimulate customers' buying desire. In regard to memberships, besides the essential account information, purchase history, updates for members, the "my favorite" function (save button in the website) can be a very useful to users. It will be even better if the website provides free storage space for members. From the analyses, only some of the platforms provide print and packaging design service and online marketing services. An increasing number of platforms are developing "online templates and editing tools" for users. This will not only result in labor cost and time savings, but also increase efficiency.

Finally yet importantly, each company shares content on their social media platform based on the region in which it is located. Apart from China-based companies, most printing platforms have their only Facebook fan page. Companies that operate in Europe and Americas share the work of their customers on Instagram while those in China promote their brand on WeChat.

4. Conclusions

The combination of web to print and me-commerce has become the mainstream trend in the digital printing industry. The customized W2P market will be more and more prevalent around the world, especially under the pressure of paper-less and green policy. Traditional printing business must undergo transformations or make appropriate changes in their operations. In Taiwan, many printers still adopt a conventional production operation and business model, while many W2P business in the United States and Europe do not only provide trading platforms for customers, but also advertising and marketing services. In light of this, Taiwanese printers should devise better strategies to accommodate this trend.

The data analyses showed that customized W2P became a hotly debated topic in the industry as early as 10 years ago. Nevertheless, only about 11 printing companies in Taiwan that started to provide W2P services; the market share is relatively low. The expert interviews revealed that many print business owners hold a pessimistic view toward customized W2P services. The research has therefore summarized the challenges faced by traditional printing companies during their transformations and the corresponding suggestions to Taiwanese printers proposed by the experts interviewed as shown in Table 5.

Table 5: Common challenges faced by traditional printing companies during transformations and the corresponding suggestions proposed by the interview experts

Problems faced by traditional printers	**The expert suggestions**
Different business models between traditional printing and me-commerce.	Relearn and change conventional mindset
High cost in building creative editing tools. Poor performance of the current tools.	Improve front-end design. Focus on improving UI (User Interface) and UX (User Experience), as well as differentiate the platform from competitors.
Low Internet bandwidth. Unable to handle the number of files and cope with the huge "online" demand.	Suggest Internet providers (telecom. providers) to increase Internet bandwidth and provide faster Internet speeds to its users.
Lack of human resources such as web engineers, data analysts. Unable to quickly resolve problems of customers and product.	Partner with IT specialists and develop a win-win partnership that is sustainable.
Second generation of business owners unwilling to take over traditional businesses.	Participate in the "Digital service plan for SMEs" implemented by the government. Attract talents to join the industry by reforming traditional businesses.
Saturated market in Taiwan. Fear low investment return due to limited development.	Follow the New South Bound Policy of Taiwan (Bureau of Foreign Trade, 2017). Set long-term plan to develop overseas markets.

The results of the content analysis and interviews showed that the technologies of traditional plate-making and ink-paper printing are highly mature among traditional printing companies while information flow, human resources, marketing and management, and software and hardware are relatively lacking. However, it is important to note that the integration of the front-end information flow design and the back-end database are inextricably intertwined to me-commerce in W2P platforms. Companies interested in developing s services can focus on improving the three aspects: information flow, human resources and marketing management. Figure 2 provides suggestions to printing businesses.

Figure 2 shows that it is possible for traditional printing businesses, front-end designers, IT specialists to cooperate and share a business model. During the interviews, it was found that there is an absence of IT engineers and data analysts in the majority of W2P businesses. Training and recruiting these quality professional are not easy. The study suggests that printers cooperate with IT specialists and designers/artists to develop a partnership model that is beneficial to all and makes resource and profit sharing possible. It is also important to conduct big data analyses to evaluate the current positioning of the company and make predictions about future market trends based on customers' buying preferences and behaviors.

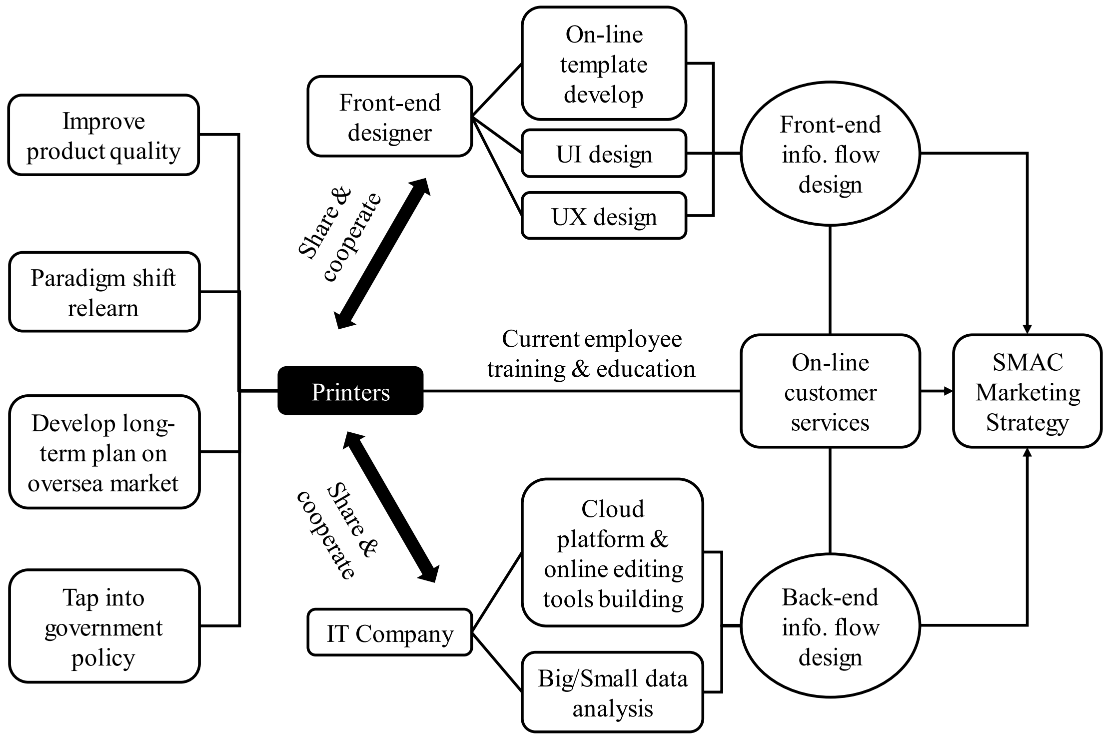

Figure 2: Suggestions to printing businesses (by authors)

Acknowledgements

The study wishes to express a great amount of gratitude to the printing experts and educators who participated in the study and provided valuable opinions and suggestions.

References

Boone, C., 2015. How print-on-demand is leading the Me-Commerce revolution. *The Magazine: Forecast Part 1, The Year Ahead*. 1.2015. [online] Available at: < https://www.coveroo.com/docs/Coveroo-Printing-Industries-of-America-Clip.pdf> [Accessed January 2018].

Cheng, C.-F., Hsieh Y.-C. and Wei, M.-C., 2017. Printing media's new blue ocean – from customized Web-to Print to Me-Commerce cloud printing. In: P. Zhao, Y. Ouyang, M. Xu, L. Yang and Y. Ren, eds. *Applied Sciences in Graphic Communication and Packaging: Proceedings of 2017 49th Conference of the International Circle of Educational Institutes for Graphic Arts Technology and Management & 8th China Academic Conference on Printing and Packaging*. Beijing, China, 14–16 May 2017. Switzerland: Springer Nature, pp. 361–368.

Keyin.cn, 2017. *2017 Top 20 e-commerce printing companies in China* (in Chinese). [online] Available at: <http://www.keyin.cn/special/spcexp/201703/07-1103050.html> [Accessed 07 March 2017].

Liu, N. and Cao, C., 2016. The design of network printing function model. In: Y. Ouyang, M. Xu, L. Yang and Y. Ouyang, eds. *Advanced graphic communications, packaging technology and materials*. 369. Singapore: Springer Science+Business Media, pp. 423–431.

Radice, R., 2014. *The four Ps of customer behavior*. [online] Available at: <http://www.imaginewow.com/social-media-marketing/customer-behavior/Rebekah> [Accessed 2014].

TopTenReviews, 2016. *TopTenReviews*. [online] Available at: <https://www.toptenreviews.com> [Accessed 2016].

Yao, S., 2015. *How digitalization changes the DNA of printing* (in Chinese). [online] Available at: <http://www.niia.tw/share_detail.aspx?NO=122> [Accessed 3 November 2015].

The Influence of Nanocellulose Addition on Printing Properties of Recycled Paper

Gregor Lavrič and Igor Karlovits

Pulp and Paper Institute, Ljubljana, Slovenia
E-mails: gregor.lavric@icp-lj.si; igor.karlovits@icp-lj.si

Short abstract

Nanocrystalline (NCC), nanofibrillated (NFC), microfibrilated (MFC) and bacterial (BC) cellulose is more and more used for different applications not in just paper industry, but also in other industries (construction, ink manufacturing, cosmetics, etc..). In papermaking, there are numerous ongoing researches regarding adding this type of materials in coatings and base papers for different mechanical and optical enhancement. In this paper, we have studied the influence of adding different types of nanocellulose into the recycled paper on printability with water-based flexo printing. We have measured the surface roughness, GLCM values of the print unevenness and dynamic contact angle of flexo prints. Results indicate that different kind of nanocellulose influence mottling differently. While the NCC enhanced paper had different contact angle curves the main differences were in the surface roughness values measured with different measurement techniques.

Keywords: nanocellulose, wettability, surface roughness, GLCM, mottling

1. Introduction and background

Sustainable development and recycling are at most importance in many industries in recent years. They also play a significant role in the pulp and paper industry, where recycled waste paper represents an important source of fibers all over the world. According to Cepi (2018), 72.5 % of all paper consumed in Europe was recycled in 2016.

High-quality requirements require manufacturers to use various new materials and approaches in their production. One of these is the use of different types of nanocellulose in order to improve mechanical, physical and barrier properties of paper.

Nanocellulose is contemporary nanomaterial that can be obtained in many different ways. With chemical procedures (Saito et al., 2006; 2009), mechanical procedures (Correia, et al., 2016) or with the use of appropriate microorganisms. (Jozala, et al., 2016) According to the method of production, nanocellulose is roughly divided into nanocrystalline, nanofibrilated and bacterial nanocellulose. The use of nanocellulose in papermaking has been the subject of numerous researches in last few years. Majority of them were carried out in the field of nanocellulose usage in virgin fiber based papers. Some authors (Balea, et al., 2016; Merayo, et al., 2017) also included nanocellulose in recycled papers. In the research of Balea, et al. (2016) corn stalk, an agricultural waste was valorized by the production of cellulose nanofibers (CNF), which were tested for improving recycled paper properties. Addition a mass fraction of 0.5 % CNF produced from corn organosolv (C-CNF) pulp to recycled paper increased the tensile index by 20 %, whereas the same improvement with CNF from eucalyptus kraft pulp (E-CNF) was achieved at mass fraction of 1.5 %. Tensile index was further enhanced by increasing the E-CNF, whereas C-CNF achieved its maximum effect at this dose. C-CNF improved tensile strength in all the different recycled furnishes studied. The tensile index improvement caused by C-CNF did not depend on the proportions of old newspaper and old magazine paper used. Addition of C-CNF to recycled corrugated board fluting increased the tensile strength, but to a slightly lower extent than in the case of recycled newsprint paper. Balea, et al. (2017) also studied the influence of cellulose nanofibers from residues on linting and mechanical properties of recycled paper. Addition of a mass fraction of 3 % CNFs from pine residues into the recycled paper with a mass fraction of 15.7 % of total filler reduced linting by 40 % and increased tensile strength by 15.1 %; further improvements on linting and mechanical properties were achieved at a mass fraction of 5 %. Paper containing 1.5 % of CNF presented a higher tensile strength and stiffness than paper from beaten pulp with similar freeness and water retention values in research of Delgado-Aguilar, et al. (2015). A higher amount of CNF further improved the mechanical properties. Based on these studies, it can be concluded that nanocellulose can have a positive effect on the mechanical properties of recycled paper. In our study, however, we examined the effect of different nanocellulose additions on printing properties of recycled paper, which are just as important. In a previous study no larger differences in optical properties of flexo prints were observed on prints made from virgin fibres and different kinds of MFC and NFC.

Flexo print quality depends mainly on the dynamic penetration of the liquids, dynamic wettability and dynamic topography. Print unevenness, mottling, and uncovered areas are typical print defects which can hamper good optical print quality. At the surface interaction, different kind of nanocellulose materials influence the availability of –OH groups which induce the reactivity of surface. High specific surface area of the nano fibers and crystals result in a large number of available hydroxyl groups located on the fibril/crystal interface which induces different wetting behaviors. Also, a review by Yamane (2015) indicates good correlation with the orientation of crystal planes. One important effect is that the nanocellulosic materials have different surface energy and wetting behaviors regarding if the film is wet or dry. As water-based flexo inks have a high amount of water this could be also an influencing factor.

Barros (2006) indicated that the topographic characteristics of the uncovered areas clearly indicate that surface depression are the primary cause of uncovered areas in flexographic printing. He identified two typical flexography patterns: sub-millimeter elongated structures and millimeter-scale blotches and used several methods to calculate their respective influence. In her dissertation, Johnson (2008) found that the substrates with the fastest wetting had a decrease in print mottle and Olsson (2007) in his Ph.D. pointed out that ink setting, ink vehicle removal and dynamic surface tension and polarity of the surface influences the final flexo print quality. Mottling in full-tone areas decreased with increased water and the influence of surfactant was also positive. The effects were explained by the softening effect of water or by the influence of surfactant on wetting and spreading. Both surface properties and absorption of ink into the substrate affect mottling and average reflectance. The results did not unambiguously show that it was increased penetration, decreased spreading or decreased transferred of ink that has caused the variations in mottling.

2. Materials and methods

To evaluate the print quality of the recycled papers with differently modified nanocellulose added, we have made laboratory sheets with a basis weight of 45 g/m^2. Recycled fibers suspension was refined to 78 °SR. Dual retention system containing polymer (cationic hybrid polymer) and starch was used. To the basic suspension of a mass fraction of 3% of differently obtained MFC, NFC and NCC were added which resulted in 75 g/m^2 laboratory sheets in the end. Commercially available Exilva MFC series P were used with 10 % paste and 2 % dispersion of dry matter and two solutions produced by the Biotechnology Faculty in Ljubljana. NCC was produced by the National Institute of Chemistry also from Ljubljana Slovenia. The reference sample was the laboratory sheet with no added MFC, NFC or NCC.

The prints were printed with IGT F1 flexo printability tester using 180 L/cm anilox roller, the water-based Doneck flexo ink viscosity (flow time) was 20–21 s and the following printing parameters were used: printing speed of 0.6 m/s, 100 N printing force, and 60 N anilox force. The printing plate was a 1.7 mm thick photopolymer plate imaged in HD flexo technology. The paper samples were measured before printing regarding surface roughness, then we evaluated the print unevenness and uncovered areas with the GLCM (Gray Level Co-Occurrence Matrix). We have used the standard 4 angles (0^0, 45^0, 90^0, 135^0) with an offset angle of 1 pixel. All printed samples were scanned at 600 spi with no alteration. The surface roughness was evaluated with air leak methods (Bekk, Bendsten) and stylus profilometry which can give more useful data for the evaluation of uncovered areas. The wettability of the samples was measured with Fibrodat 1100 dynamic contact angle measurement device. We have measured the contact angles and the drop volume change as it can also influence mottling.

3. Results and discussion

The results of the surface roughness parameters are presented in Table 1.

Table 1: Surface roughness parameters

Sample/parameter	**Reference**	**Exilva 10 %**	**Exilva 2 %**	**NFC BTF***	**NCC NIC****
Bekk (s)	9	14	11	10	21.5
Bendsten (ml/min)	315	266	355	489	371
Average surface roughness Ra (µm)	2.96	2.92	3.08	2.84	2.88

*BTF – Biotechnical Faculty of the University of Ljubljana

**National Institute of Chemistry

As we can observe from Table 1, the surface roughness ratio and values are very dependent on the used measurement method and there is no in-between correlation between the samples. With Bekk smoothness tester, the least smooth was the reference sample and the smoothest sample measured with this method was the NCC sample. With Bendsten low values would preferably equal higher Bekk values which was not observable for all samples. Correlation between stylus profilometry and air leak methods has a nonlinear correlation.

As delayed or inhibited surface wetting can cause also mottling contact angle was checked and the results are presented in Figure 1 and Figure 2.

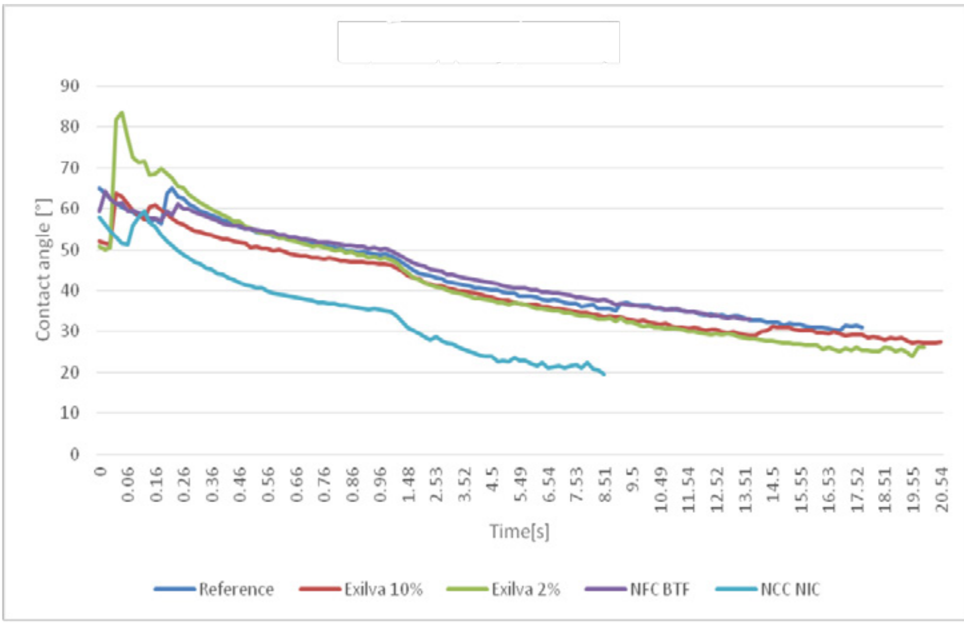

Figure 1: Dynamic contact angle

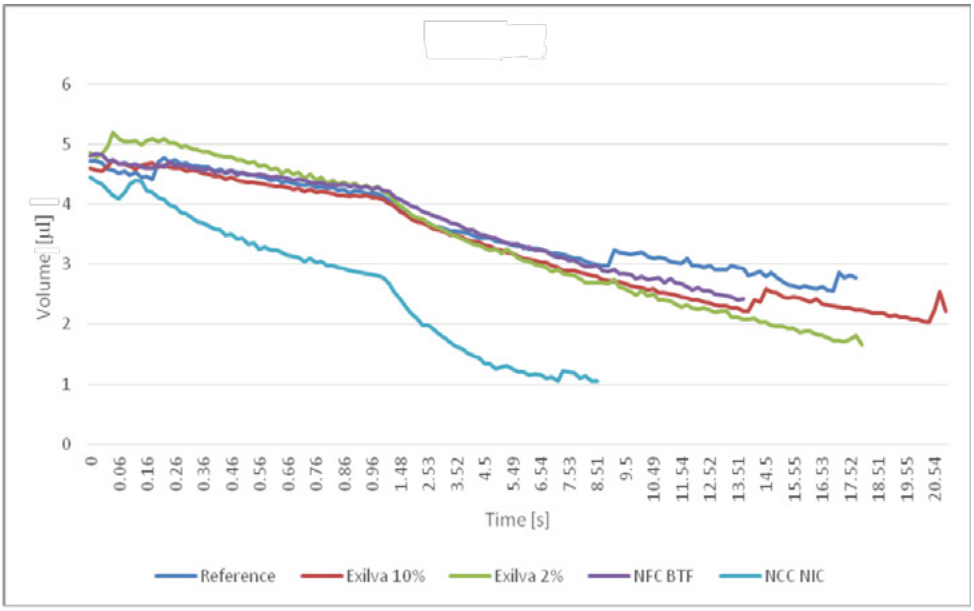

Figure 2: Volume of drop

As we can observe all samples had similar contact angles beside sample with added NCC which had lower contact angle and more rapid drop volume decrease as can be observed which indicate larger porosity than for other samples. The largest differences occurred in the first half of the second when the water drop came in contact with the surface and quickly after the majority of the samples had very similar results.

The print unevenness was tested with GLCM algorithm in R programming language ("radiomics") package which has previously shown good results in evaluating mottling by Jurič, et al. (2016) and Karlovits, et al. (2017). We have calculated the GLCM energy, entropy and correlation values which are presented in Table 2.

Table 2: GLCM values of the tested samples

Sample	GLCM energy	GLCM correlation	GLCM entropy
Reference	0.0007386662	0.8301965	7.770987
Exilva 10 %	0.0006589189	0.8546802	7.907238
Exilva 2 %	0.0005208555	0.8462686	8.141362
NFC BTC	0.0005148561	0.5013072	8.140765
NCC KI	0.0004715338	0.6585847	8.257591

From Table 2 we can see that the energy value is decreasing from Reference sample which has the highest value to the NCC KI sample which has the smallest value. For entropy, the NCC KI sample had the highest value (most non-uniform) as higher value indicate a higher disorder and also low energy and low value for correlation. Regarding correlation, the NFC BTC and NCC KI had the smallest values which indicate there is a weak linear correlation between pixel intensities and indicate also larger non-uniformity while the reference sample and Exilva 10 % and Exilva 2 % indicate the higher value of print uniformness. The NCC KI samples had the highest Bekk smoothness value and the quickest drop volume.

4. Conclusions

As the potential use of NFC and MFC as an enhancing additive is gaining more attention with a different type of produced MFC and NFC materials, their enhancement of mechanical properties as not only ones which has to be checked. Currently, there is not a lot of references regarding the influence of MFC and NFC on the optical print quality and printability parameters. In our work, we tested the mottling print non-uniformity appearance regarding from the type and form of added MFC and NFCs. There were some differences regarding surface roughness on different measurement scales mainly in the air leak methods (the stylus profilometer had no big differences in the range of application) and as expected no in between correlations were found. The contact angle of the samples was very similar and only the samples with the added NCC showed a significant difference. From this, we can conclude that further research is needed regarding surface characterization (nano or micron scale are surface characterization) and surface chemistry of the enhanced print samples regarding flexo print quality. Also, the added concentration and the retention value of the added nanocellulose is still a challenge to be determined to better correlate the measured values.

Acknowledgements

The work was carried out within the RDI project Cel.Cycle: »Potential of biomass for development of advanced materials and bio-based products« (contract number: OP20.00365), co-financed by the Republic of Slovenia, Ministry of Education, Science and Sport and European Union under the European Regional Development Fund, 2016–2020.

References

Balea, A., Merayo, N., Fuente, E., Delgado-Aguilar, M., Mutje, P., Blanco, A., and Negro, C., 2016. Valorization of Corn Stalk by the Production of Cellulose Nanofibers to Improve Recycled Paper Properties. *BioResources,* 11(2), pp. 3416–3431.

Balea, A., Merayo, N., Fuente, E., Negro, C., Delgado-Aguilar, M., Mutje, P. and Blanco, A., 2017. Cellulose nanofibers from residues to improve linting and mechanical properties of recycled paper. *Cellulose*, 25(2), pp. 1339–1351.

Barros, G.G., 2006. *Influence of substrate topography on ink distribution in flexography*. Doctoral thesis. Karlstad University.

Cepi.org, 2018. *Recycling. CEPI: Confederation of European Industries*. [online] Available at: <http://www.cepi.org/taxonomy/term/14> [Accessed 15 February 2018].

Correia, V.daC., dos Santos, V., Sain, M., Santos, S.F., Leão, A.L. and Savastano Junior, H., 2016. Grinding process for the production of nanofibrillated cellulose based on unbleached and bleached bamboo organosolv pulp. *Cellulose*, 23(5), pp. 2971–2987.

Delgado-Aguilar, M., González, I., Pèlach, M.A., De La Fuente, E., Negro, C. and Mutjé, P., 2015. Improvement of deinked old newspaper/old magazine pulp suspensions by means of nanofibrillated cellulose addition. *Cellulose*, 22(1), pp. 789–802.

Jurič, I., Karlović, I., Novaković, D. and Tomić, I., 2016, Comparative study of different methods for the assessment of print mottle. *Color Research and Application*, 41(5), pp. 493–499.

Johnson, J., 2008. Aspects of flexographic print quality and relationship to some printing parameters. Doctoral thesis. Karlstad University.

Jozala, A.F., de Lencastre-Novaes, L.C., Lopes, A.M., de Carvalho Santos-Ebinuma, V., Mazzola, P.G., Pessoa-Jr, A., Grotto, D., Gerenutti, M. and Chaud, M.V., 2016. Bacterial nanocellulose production and application: a 10-year overview. *Applied Microbiology and Biotechnology*, 100(5), pp. 2063–2072.

Karlovits, I., Grkman, J.J., Ravnjak, D. and Lavrič, G., 2017. The evaluation of bio-based binders influence on offset print mottle using GLCM. In: P. Gane and C. Ridgway, eds. *Advances in Printing and Media Technology: Proceedings of the 44th International Research Conference of iarigai*. Fribourg, September 2017. Darmstadt: iarigai, pp. 187–192.

Merayo, N., Balea, A., de la Fuente, E., Blanco, Á. and Negro, C., 2017. Synergies between cellulose nanofibers and retention additives to improve recycled paper properties and the drainage process. *Cellulose*, 24(7), pp. 2987–3000.

Saito, T., Nishiyama, Y., Putaux, J.-L., Vignon, M. and Isogai, A., 2006. Homogeneous suspensions of individualized microfibrils from TEMPO-catalyzed oxidation of native cellulose. *Biomacromolecules*, 7(6), pp. 1687–1691.

Saito, T., Hirota, M., Tamura, N., Kimura, S., Fukuzumi, H., Heux, L. and Isogai, A., 2009. Individualization of nano-sized plant cellulose fibrils by direct surface carboxylation using TEMPO catalyst under neutral conditions. *Biomacromolecules*, 10(7), pp. 1992–1996.

Yamane, C., 2015. Structure formation of regenerated cellulose from its solutions and resultant featured of high wettability: a review. *Nordic Pulp and Paper Research Journal*, 30(1), pp. 78–91.

Development of a unidirectional Switchable Photochromic Ink for Smart Packaging

Mustafa Bilgin and Johannes Backhaus

Bergische University of Wuppertal, Rainer-Gruenter-Straße 21, 42119 Wuppertal, Germany
E-mails: bilgin@uni-wuppertal.de; jbackhaus@uni-wuppertal.de

Short abstract

Switchable materials or also named as smart materials are common at several applications, e.g. time-/ temperature indicating labels, smart packaging and more. Switchable materials can impart binary information in form of a one binary digit, which can take two possible values (0 or 1). These two values in a binary variable are represented by a colour switching functionality of smart materials, which can switch reversibly or irreversibly from one colour-state (0) to another colour-state (1). Smart materials, e.g. photochromic compounds, have a light detecting behaviour. Thus, its irreversible behaviour can be used to realize cheap printable light sensors, e.g. a light dependent resistor (LDR), without a build-in energy supply. In form of an array with several printed sensitive dots inside a matrix code, different deviations can be displayed and readout by a common smart device. Many photochromic compounds base on reversible spiropyran or spirooxazine. The aim of this study will be the usage of alternative materials like Prussian blue (iron ferrocyanide), to develop an irreversible unidirectional switchable photochromic compound for piezoelectric inkjet. Its development process, characteristic behaviour, printability and functionality was analysed and a prototyped material was tested at a lab scale.

Keywords: irreversible, photochromic, smart packaging, intelligent code, piezoelectric inkjet

1. Introduction and background

Smart Materials like hydrochromic, photochromic and thermochromic inks can switch between minimum two states – by changing their colour – depending on environmental influences, e.g. temperature, humidity, water, UV/Vis light, pressure and acids. This colour changing behaviour can be used to develop printable sensors. Smart materials can impart binary information in form of a binary digit (1-Bit), which can take two possible values (0 or 1). Many photochromic compounds base on the reversible compound spiropyran or spirooxazine. Spiropyran was first examined in 1952 (Hirshberg and Fischer, 1954). Today, there are many researches about molecular switches and 3-D optical memories, which base one of the mentioned photochromic compounds, because data is writable, erasable and rewritable with a laser in three dimensions (Patel, Cao and Lippert, 2017). Nevertheless, the idea is not new; already Hirshberg (1956) formulated the usability as a kind of photochemical memory.

Smart materials will be differentiate between two switching mechanisms: Reversible materials can switch back to their initial state, due to heat or light with a particular wavelength. Irreversible materials remain in their actual state after activation (unidirectional colour switching) and cannot switch back. Thus, irreversible smart materials can be used against counterfeit. Therefore, information about critical environmental influences during the entire transport can be detected and stored. Additionally, a kind of unique fingerprint is given due to its multi component composition of different smart materials inside one code (smart code). Especially smart materials could be printed at low cost in form of a dot array – with different sensitivities – inside a matrix code. Irreversibly stored information about critical deviations can be readout due the CCD-camera of a smart device (e.g. a smartphone) which then can send the included data inside the intelligent code bi-directionally via browser to a secure web-server. The combination of smart materials, smart devices and intelligent codes allows to create an Internet of Things (IoT), where all components communicate in an autonomous network to accomplish preassigned tasks, give consumers information, collect feedback about their products and give information about critical environmental influences during the entire transport (Ashton, 2009).

1.1 Chemical process

Prussian blue (ferric (III) hexacyanoferrate (II), $Fe_4^{III} [Fe^{II}(CN)_6]_3 \cdot x\,H_2O$), also known as Berlin blue, was the first modern synthetic pigment. Prussian blue was less expensive and easily produced and it was used for the uniform of the royal Prussian army and is used today as a pigment in the application fields of electrochromics, sensors and medicine. Its discovery was due to a mistake – a chemist was trying to produce red colour, but an additive was contaminated with ferric hexacyanoferrate (Kraft, 2008) – so that he got an irreversible and lightfast blue colour. The Prussian blue colour is due to a process, which is called intervalence charge transfer (IVCT). The light irradiation initiates an active electron exchange of two metal ions in different chemical environments. They are spatially close to each other so that they interact with each other. The iron (II) ion forms a low-spin complex and is surrounded in a six-fold carbon environment (cyanide). While the iron (III) ion forms a high-spin-complex and is surrounded in an environment of nitrogen (cyanide) and oxygen (water of crystallization). The light irradiation initiates a transfer of a low-spin electron into the high-spin state and weak-field ligands. The transition causes an intensive blue colour (Klöckl, 2015).

1.2 Photochemical process

Another variant of a photochromic smart material is the photosensitive Prussian blue (irreversible and unidirectional switchable), which bases on a light-induced redox reaction. UV light activates a redox reaction at exposed areas, oxidizes the citrate anion, and turns the trivalent (ferric) iron into divalent (ferrous) iron. As a result, a blue compound is formed, which bases on different oxidation states of iron – Prussian blue (Figure 1). It is compounded by adding ammonium ferric citrate and potassium ferrocyanide and dissolving them in an aqueous solution. The resulting yellow-green solution is photosensitive. After exposure, the citrate reduces to potassium ferrocyanide and reacts with iron (III) gradually to a dark blue precipitate (Figure 4), the Prussian blue (Roesky and Möckel, 1994).

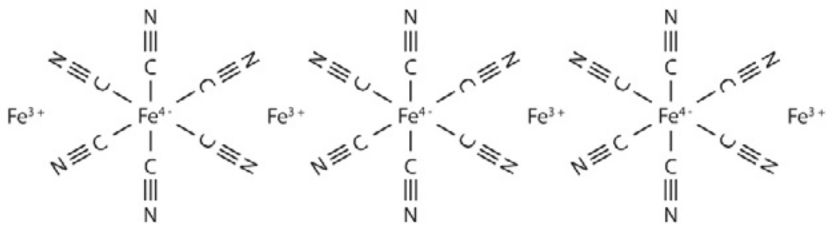

Figure 1: Structural formula of iron (III) hexacyanoferrate (II)

The aim of this study is to analyse alternative smart materials such the photosensitive Prussian blue (iron ferrocyanide) to develop a water based photochromic ink for piezoelectric inkjet. Until today, there are very limited irreversible smart inks available, which are printable in an inkjet printer. Various smart materials should be integrated in a smart code, which can indicate whether e.g. a package has been contaminated (e.g. exposure by light). The prototyped ink was tested at a lab scale. Specimens were printed with a piezoelectric inkjet printer. The developed ink was examined in order to analyse its colour changing behaviour under different light sources (especially its sensitivity to UV light), characteristic wavelengths and viscosity flow behaviour.

2. Materials and methods

2.1 Instruments

A piezoelectric inkjet printer (Epson WorkForce WF-3620) was used to print samples with the prototyped photosensitive ink. Technical parameters: Print Head: PrecisionCore; Thin Film Piezo element: 1/1 000mm; Droplet Size: 2.8 pl (range of 1.5–32.5 picoliters); Nozzle Configuration: 800 Nozzles Black (K), 256 Nozzles per Colour (CMY); Printing Resolution: 4 800 × 2 400 DPI.

Measurements of the colour changing functionality of the photochromic compound were realised through a spectral-densitometer (TECHKON SpectroDens), to analyse their characteristic remission curves, RGB and CIELAB values. Technical parameters: polarising filter: off; type of light: D50, 2° standard observer; diameter of measuring orifice: 3 mm.

Rheological properties (viscous flow behaviour) were analysed by a rotational rheometer (Physica MCR 101) through a corresponding cone and plate measurement system (CP50-1); diameter: 49.966 mm; cone angle: 1°.

2.2 Standardization

All experiments were conducted under controlled laboratory surroundings – the reproducibility was ensured through an air-condition system and deviations were recorded inside logs. Temperature: 20° C (± 1 ° C); relative humidity: 55 % (± 1 %) were continuously audited.

2.3 Materials

In Table 1 are all materials listed, which were used for this research work. To ensure the reproducibility, all experiments are based on standardised substrates Multicolor Mirabell and Inapa tecno. Adverse particles of the photosensitive Prussian blue were filtered (Millex-SV), to get particle size less than 5.0 µm – which is recommended for inkjet printing. Additives e.g. humectants, surface tension regulator and an antifoaming agent were added to control adverse factors.

Table 1: Materials

Substrates for printing	Multicolor Mirabell, Chromo-duplex-carton with white and double-faced front and a grey pigmented back, Papyrus Deutschland GmbH & Co. KG. Thickness: 0.340 mm, Grammage: 250 g/m^2 Inapa tecno, oxygen pure high-white recycled paper, Format: 210 × 297 mm (A4), Grammage: 80 g/m^2
Dye	Photosensitive Prussian blue, CAS Number: 14038-43-8, Chemical formula: $C_{18}Fe_7N_{18}$, Molar mass: 859.24 g·mol^{-1}
Water-based base ink	E24, Octopus Fluids GmbH & Co KG, Colour: colourless, pH: 7,86, Conductivity: (mS/cm): <5, Viscosity (mPa·s): 3,00
Additives of the ink	Humectants: Glycerine ($C_3H_8O_3$), Urea (CH_4N_2O) Surface tension regulator: Alkyl sulfonate, Alkyl polyglycoside Antifoaming agent: Polydimethylsiloxane (C_2H_6OSi)
Equipment (Filtration)	Millex-SV (SLSV025LS) • Pore Size: 5.0 µm • Maximum Inlet Pressure: 5.2 bar (75 psi) • Hold-up Volume: < 0.1 mL • Filtration Area: 3.9 cm^2 • Material: Hydrophilic Polyvinylidene Fluoride (PVDF)

2.4 Test chart

The test chart (Figure 2) is divided in three sections. The first section contains formal test information (e.g. temperatures, date, time, additives); the second bases on three printed squares (grid, QR code, and full tone area). The third (lower) section contains a large full tone area with an unprinted (white) symbol.

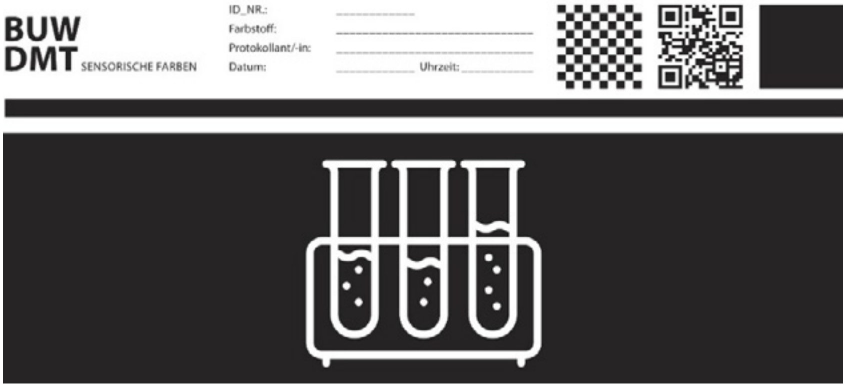

Figure 2: Simplified test chart for piezoelectric inkjet

3. Results and discussion

3.1 Manufacture of a prototypical Ink

A photosensitive Prussian blue was manufactured in a lab scale. The photosensitive compound was embedded in a water-based ink system, which was adjusted by additives. The base-ink is a particularly composed base ink for Epson inkjet printers from Octopus Fluids. The additives (Table 1) were used to control the performance of the developed ink, in order to prevent nozzle drying and clogging (humectants), an antifoaming agent (prevent formation of foam) and a surface tension regulator (droplet performance). 0.25 g of ammonium ferric citrate, 0.2 g of potassium ferrocyanide, additives and 5 ml of water-based ink (E24) were filled into an amber glass (protect light-sensitive applications) and mixed for about 5 minutes. The resulting yellow-green irreversible photochromic solution was applied to a substrate and it was exposed to UV light, to test its functionality. 5 mL with E24 prepared solution were filled into an opaque inkjet cartridge to print samples.

3.2 Rheological properties

The rheological properties – more the viscous flow behaviour of the photosensitive Prussian blue was analysed by a rotational rheometer Physica MCR 101, through a corresponding cone and plate measurement system CP50-1; diameter of 49,966 mm; cone angle of 1°. Each of the three concentrations 0.45 g (0.25g ammonium ferric citrate and 0.2 g potassium ferrocyanide), 0.9 g (0.5 g ammonium ferric citrate and 0.4 g potassium ferrocyanide) and 1.35 g (0.75 g ammonium ferric citrate and 0.6 g potassium ferrocyanide) were embedded in a 5 mL E24 base ink. Next, the concentrations were measured in an exposed (with UV-light) and unexposed form to analyse its viscous flow behaviour as to be expected for inkjet inks. The (water based) photosensitive inkjet ink shows pure Newtonian flow behaviour and very low shear viscosity around 0.0030 to 0.0050 Pa·s (Figure 3). After contamination with UV-light, the viscosity of all concentrations decreases a little at 0.45 g from 0.0036 to 0.0037 Pa·s, 0.9 g from 0.0041 to 0.0042 Pa·s and with a concentration of 1.35 g from 0.0047 to 0.0050 Pa·s. The viscosity behaves in a printable range of 0.001 to 0.05 Pa·s (Zapka, 2018).

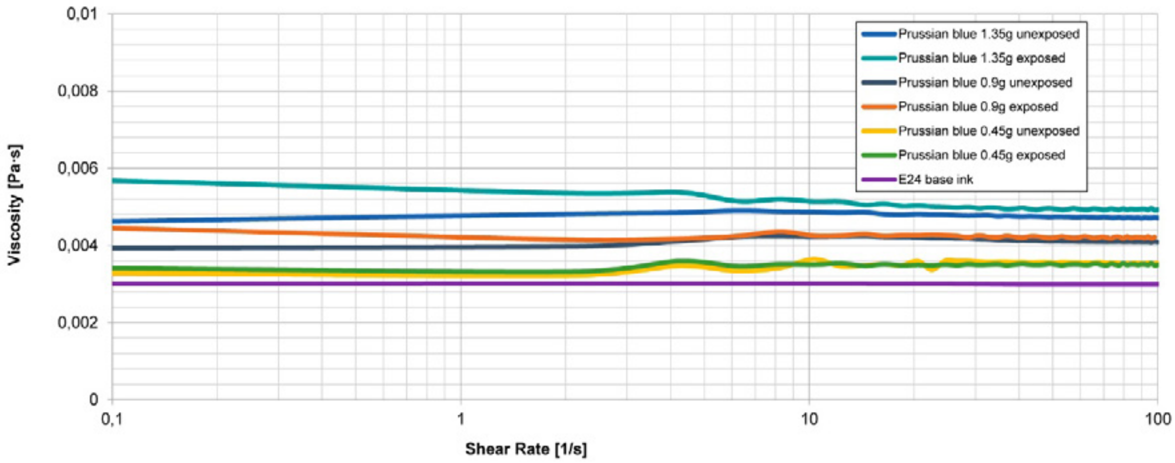

Figure 3: Flow behaviour in comparison to various concentrations and exposure

An additional effect could be observed after exposing the photosensitive Prussian blue. Here, its photosensitive activation process (reduction of Fe^{3+} to Fe^{2+}) includes a precipitation – this accompanies a change of the particle size. This observation requires further investigation. The contamination of the inkjet cartridge due to light may lead to adverse effects e.g. clogging of the nozzle.

3.3 Colour switching behaviour and binarisation

First results were realised with a piezoelectric inkjet printer from Epson (WorkForce WF-3620). The samples were prepared as a basis for following experiments. In this experiment, the behaviour of the developed photochromic ink was analysed under the influence of three different types of light sources (exposure to light) to simulate different environmental conditions (Figure 4). The sensitivity of the photochromic compound has been adjusted to show a gradual colour changing in a range of minutes. Every 5 minutes in a range of maximum 60 minutes, 12 squares of 1 cm^2 were activated by three different light sources TL84, D65 and UV (Figure 4).

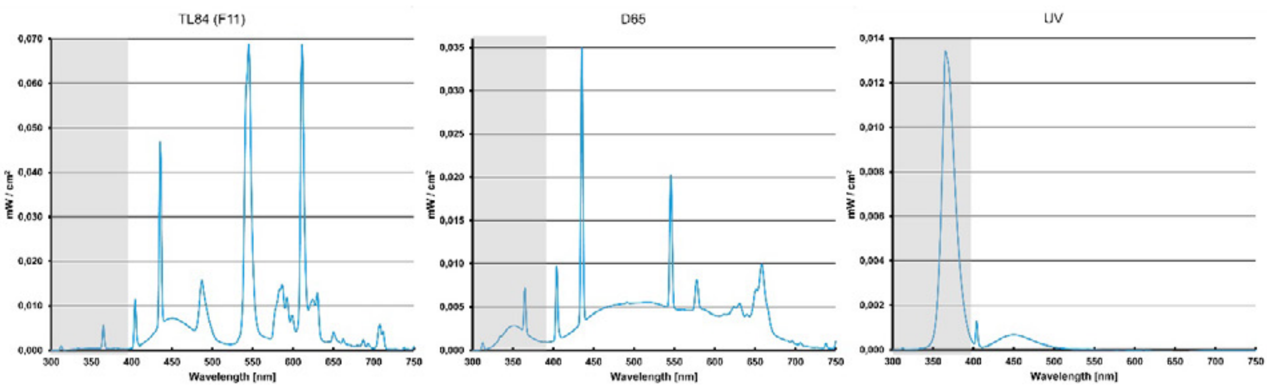

Figure 4: Light sources TL84, D65 and UV

The light source TL84 (F11) – often used in retail and supermarkets – has a wavelength range from λ = 380 nm to 750 nm with a small UV peak at around 370 nm and a colour temperature of about 4 100 K. The CIE Standard Illuminant D65 is in accordance to the DIN EN ISO 11664. It bases on experimental measurements of daylight in a wavelength range from λ = 300 nm to 750 nm (UV-Vis to near-IR) with a UV-A component at around 370 nm and a colour temperature about 6 500 K. The ultraviolet light source shows a high peak at a wavelength about 365 nm.

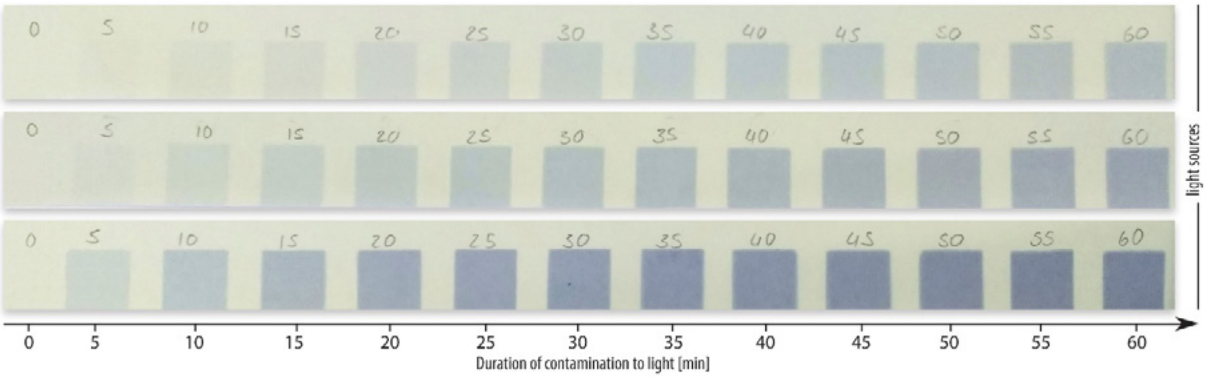

Figure 5: Photosensitive Prussian blue exposed through different types of light

The photochromic compound shows different intensities of reaction depending on the type of light source and the duration of exposure (Figure 5). The TL84 exposed surface needs more time for its activation process than the D65 and UV light (Figure 6). After 60 minutes, the TL84 exposed surface becomes nearly the same intensity such the UV light after 10 minutes (similarities). The D65 exposed surface becomes after 60 minutes, nearly same intensity such UV light after 25 minutes. The activation process of the UV light is faster than D65. The gap between TL84 and D65 is small. The contrast difference between D65 and UV light is large, which indicates the required minimum amount of photon energy (UV-light), which is required for the activation of the photochromic reaction (the amount of photon energy will be determined in a further investigation). The amount of energy is in coherence with the luminance and saturation of the photosensitive Prussian blue.

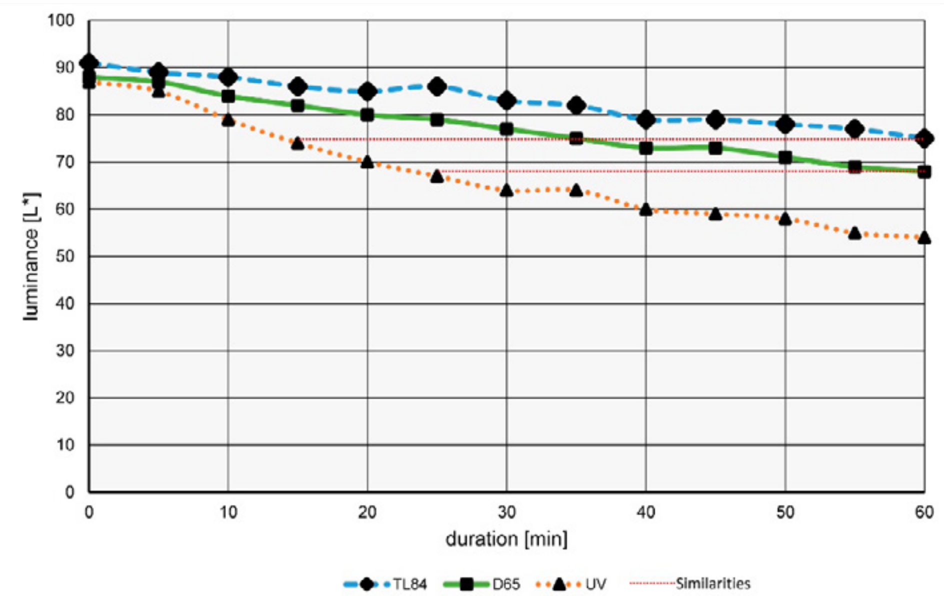

Figure 6: Luminance in comparison to duration of contamination

Additionally, the unidirectional colour switching behaviour of the photosensitive Prussian blue will be analysed to detect differences between its binary states under the exposure of different light influences. Inactive surfaces are yellow (0 min). After exposure, the yellow colour switches gradually to a blue colour - into an active (1) state. The colour values (Figure 5) were measured according to CIELAB and RGB (Adobe RGB, 1998) and transformed (Adobe Photoshop) into a greyscale mode. It is possible to convert CIELAB data into different standards and colour spaces to transform the respective colour value into information about the intensity of an environmental contamination. This is necessary for the detection of different environmental influences by different smart materials, which change their colour between more than two colour states.

The L^* value can be used to determine adverse lighting conditions as a measuring error and store them in variables inside control-patterns of an intelligent code. This error-variable can be used to eliminate deviations (adverse light conditions) from captured images of a smart device. Captured images of an intelligent code – with a loss of quality – can be automatically corrected by the system through comparison of the nominal and actual position in a colour space. Required patterns for position, alignment and timing are included inside the intelligent code to encode information about different environmental states. Each dot of the intelligent code can contain different smart materials, to show different environmental influences.
The twelve activated squares (Figure 5) can be analysed by the measurement of the RGB and CIELAB values or alternative by the RGB greyscale and L^* values. Therefore it is possible to store information about critical deviations in a range from 0 (white) to 255 (black) in RGB or 0 (black) to 100 (white) in L^*. A smart device can identify the L^* intensities of the different colour shades (intelligent dots) and compare them with the initiate L^* intensity and set the colour difference (ΔE) into correlation with duration and intensity of exposition by light.

Table 2: Measurement of the photosensitive Prussian blue, CIELAB, ΔE and RGB (Adobe RGB, 1998) in grayscale mode

	[min]	**0**	**5**	**10**	**15**	**20**	**25**	**30**	**35**	**40**	**45**	**50**	**55**	**60**
TL84	RGB grayscale	229	223	219	215	211	208	205	198	196	193	191	187	184
	L^* a^* b^*	91 −4 9	89 −4 9	88 −5 8	86 −5 6	85 −5 2	86 −6 4	83 −6 4	82 −6 −1	79 −7 −2	79 −7 −2	78 −6 −2	77 −4 −1	75 −7 −3
	ΔE	7.35	82.40	2.80	4.10	2.40	3.60	3.10	3.30	0.00	1.00	3.00	4.10	
D65	RGB grayscale	218	216	210	203	188	184	187	183	179	175	172	168	164
	L^* a^* b^*	88 −4 10	87 −6 6	84 −7 5	82 −8 2	80 −8 0	78 −8 −1	77 −7 −3	75 −8 −3	73 −7 −4	73 −7 −4	71 −5 −5	69 −6 −7	68 −5 −8
	ΔE	4.58	3.30	3.70	2.80	2.20	2.40	2.20	2.40	0.00	3.00	3.00	1.70	
UV	RGB grayscale	212	211	194	181	170	162	154	155	149	140	137	132	128
	L^* a^* b^*	87 −4 8	85 −8 3	79 −7 −3	74 −6 −6	70 −7 −10	67 −5 12	64 −5 −14	64 −5 −12	60 −5 −14	59 −5 −14	58 −4 −13	55 −5 −14	54 −5 −15
	ΔE	12.80	6.00	5.90	5.70	22.30	26.10	2.00	4.40	1.00	1.70	3.30	1.40	

By means of the measured values in Table 2, a lower limit (0 = inactive) and upper limit (1 = active) can be determined. The measured values could be translated into 1-bit binary information. For example the D65 light source is based on experimental measurements of daylight. In the following the L^* values of the D65 light source will be used to simulate environmental influences through natural light conditions and give an output in form of information about the duration of the exposure by light. For example, two conditions can be determined: $L^* < 77$ could be defined as a lower limit and $L^* > 77$ could be defined as an upper limit. Therefore, a kind of photosensitive switch could be realised, which displays a single on / off functionality after an exposure duration of 30 minutes. It is also possible to divide the data values into four equal groups (quartiles): If ($L^* < 87$) then display 5 minutes exposure; If ($L^* < 82$) display 15 minutes; If ($L^* < 77$) then display 30 minutes and if ($L^* < 68$) display 60 minutes exposure. Therefore, a kind of spectrum could be realised, which can display information about exposure of light in four categories.

3.4 Spectrophotometric analysis

The colour switching functionality of the photosensitive Prussian blue ink was measured through a spectral-densitometer (TECHKON SpectroDens). In Figure 5, the differently exposed characteristic parts of wavelength are shown. The light sources TL84, UV and D65, which were discussed in chapter 3.3, were also used in these measurements. Light intensity and wavelength distribution affect properties of photosensitive Prussian blue. The three samples were measured every 5 minutes in a maximum range of 60 minutes. All exposed samples are independent from exposure at 400–450 nm (blue) and show distinct differences across the entire range of 500–700 nm – where the colour switching process is localised. The more intense the colour, the greater the proportion of absorbed light. In this range, the remission decreases continuously with the duration of exposure, while the blue part remains in a stable state. The gaps between the exposure-phases of TL84 are consistent, which adverts to a low UV component (Figure 6).

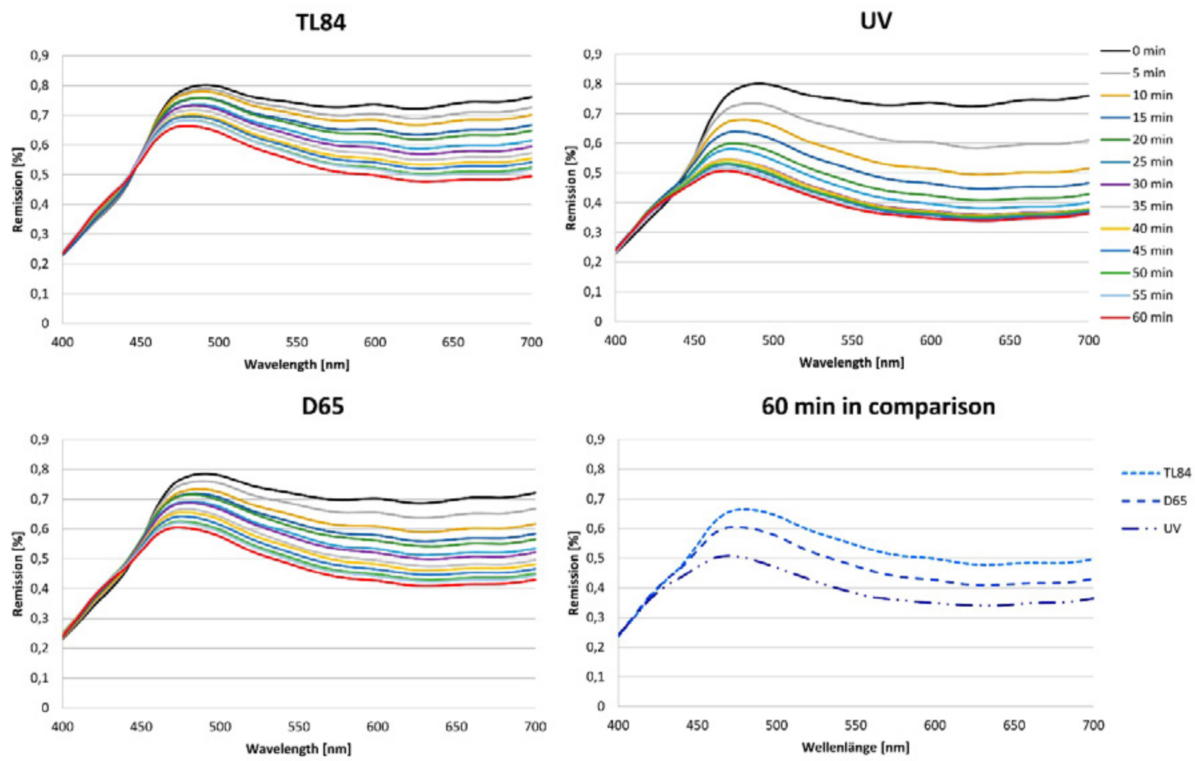

Figure 7: TL84, D65 and UV light in comparison

In comparison, the distances of the gaps of D65 and UV are inconsistent and decrease with the duration of exposure. After 60 minutes, the comparison of the three differently exposed samples illustrates that the energy difference of the UV part has an influence on the intensity of the blue colour. A minimum amount of energy (UV-light) is needed to excite the electrons, which explains the marginal colour intensity of TL84. As a result, the photosensitive Prussian blue responds to UV light and switches its colour gradually to the duration and intensity of UV light.

4. Conclusions

This research demonstrated, that a prototypically developed unidirectional switchable photosensitive Prussian blue (photochromic ink) is suitable to detect UV-light and to display the duration of exposure in form of different colour shades. It was also possible to transform the RGB greyscale and L^* values of the different colour shades into binary information. Irreversible unidirectional switchable smart materials can store and provide dynamic information about environmental influences. It is possible to store dynamic information (switchable dots) about possible deviations and static consumer or product information inside an intelligent code. Therefore, various printable sensors (sensitive dots) can detect different grades of temperature, UV exposure and humidity without a build-in energy supply. In form of an array with several printed sensitive dots inside a matrix, different deviations can be displayed and readout via IoT by a common smart device. The intelligent code is customizable, can be printed cost efficiently and can be used for the purpose of anti-counterfeit. The next step will be the development of an intelligent code with a corresponding code generator and code reader.

Acknowledgements

Many thanks to Octopus Fluids GmbH & Co KG for their base ink and many thanks to Kristin Wörpel and Thomas Dridiger for their technical assistance in the laboratory.

References

Ashton, K., 2009. *That 'Internet of Things' thing: in the real world, things matter more than ideas*. Hauppauge, New York, USA: RFID JOURNAL LLC. [online] Available at: <www.rfidjournal.com/articles/view?4986> [Accessed 2 May 2017].

Hirshberg, Y. and Fischer, E., 1954. Photochromism and reversible multiple internal transitions in some spiropyrans at low temperatures. Part I. *Journal of Chemical Society*, 0, pp. 297–303.

Hirshberg, Y., 1956. Reversible formation and eradication of colors by irradiation at low temperatures. A photochemical memory model. *Journal of the American Chemical Society*, 78(10), pp. 2304–2312.

Kraft, A., 2008. On the discovery and history of Prussian blue. *Bulletin for the History of Chemistry*, 33(2), pp. 61–67.

Klöckl, I., 2015. *Chemie der Farbmittel in der Malerei*. Berlin, Germany: Walter de Gruyter, p. 123.

Patel, S.K., Cao, J. and Lippert, A.R., 2017. A volumetric three-dimensional digital light photoactivatable dye display. *Nature Communications*, 8, article number: 15239. https://doi.org/10.1038/ncomms15239.

Roesky, H.W. and Möckel K., 1994. *Chemische Kabinettstücke: Spektakuläre Experimente und geistreiche Zitate*. Weinheim, Germany: VCH Verlagsgesellschaft, p. 57.

Zapka, W. ed., 2018. *Handbook of industrial inkjet printing: a full system approach*. Weinheim, Germany: Wiley-VCH Verlag. p. 12.

Interpretation of Ink Tack Stability Testing Results for Improved Offset Printability

Dominik Kapović[1]*, Branka Lozo*[1] *and Wilco De Groot*[2]

[1] University of Zagreb, Faculty of Graphic Art

[2] GT Testing Systems, Almere, The Netherlands

E-mails: dkapovic@grf.hr; blozo@grf.hr; degroot@igt.nl

Short abstract

One of the key requirements for offset ink is for it to remain fluid while in the offset machine, whilst it must also dry sufficiently once on the printing substrate. Too fast or too slow drying of ink on a substrate can cause its own variety of printing problems such as mottle, set-off failure, gloss reduction. Thus, the appropriate ink transfer through the rollers as well as to the printing substrate is of great importance. Ink tack is considered responsible for ink transfer, insufficient ink tack results in poor ink transport, high tack may influence the surface causing damage to the printing paper. Ink tack should not be considered as a static value due to the numerous factors influencing it; in addition, these factors are not constant during the printing process. The presented study aims to observe the dynamic ink tack readings from the printers' perspective. As a function of distribution and splitting time, readings serve to determine the ink stability on the printing press. The impact that prolonged film splitting has on the printability is evaluated in the laboratory conditions. The ink tack results are taken as an ink tack curve, formed from readings taken as a function of time and should be explained as such. The experiment was performed on an IGT Tackoscope, a tack measuring device, IGT inking unit and IGT Amsterdam, a printability tester. The IGT Tackoscope operates by sensors to define and calculate the force required to separate the ink layers in the contact zone between two rollers fed initially by a distribution system. Two different inks were tested, one ink being a faster drying ink than the other. By setting different distribution times on the high-speed inking unit, the strips of a laboratory reference paper were subsequently printed under laboratory conditions. The evaluation of the laboratory prints showed a good correlation between the ink tack readings and printability results. The presented method of evaluating dynamic tack test results can help in preventing a variety of printing problems by providing a more precise prediction of offset ink stability during the printing process.

Keywords: tack stability test, printability, ink splitting, tack curve

1. Introduction and background

Ink tack, also called ink stickiness, is a rheological property of an ink used to describe the ink movement and transfer response through the printing sequence. In offset printing, the intrinsic ink tack can be defined as the resistance to the rapid splitting of a thin film of ink between two rollers. It is also a major factor influencing the ink transfer to the paper. General relationships between tack and plastic viscosity suggest that extremes of high and low plastic viscosity are usually related to high and low tack values. The suggestion is that tack embodies both the viscous behaviour of liquids and the elastic rapture properties associated with solids (Thompson, 2004.).

Insufficient ink tack results in poor ink transport and uneven ink distribution between the rollers. This is why the consistency of an offset ink has to be sufficient for ink not to flow away between the ductor blade and the roller while under the stress applied by gravity. It also has to allow the ink to break its static structure and flow onto the ductor roller and from there to continuously flow through the inking roller system (Thompson, 2004.). In the case of too high tack there is a risk of surface damage of paper, like picking or delamination of coated paper and linting of uncoated paper. There is thus a critical value for tack that interrelates type of process, number of printing stations, printing speed and surface strength of paper.

Ink tack is important to minimize the problem of ink re-splitting (back-trapping) from the previous inking unit application to the subsequent inking unit by adapting the rheological properties of the ink or to graduate the tack of the inks accordingly (Kipphan, 2001).

It is important to recognize that on a running offset press, that has reached equilibrium, the ink retained on subsequent colour blankets is aged both over time and in respect to tack. The blanket-retained tack has been built-up during multiple contacts with progressively setting ink as the blanket makes contacts with the paper. Therefore, tack must be studied over long timescales if the equilibrium press conditions are to be simulated realistically. This is important when considering the dynamic absorption by the contact of coatings and such aged ink (Gane, Matthews and Schoelkopf, 2003).

Measurement of tack is related only to offset and some letterpress inks and vehicles, it is a key quality control parameter (NAPIM, 2017.). Ink tack readings are used for quality control so they can provide a helpful way of ascribing numbers to an ink whose working properties are known to be commercially satisfactory on the press, so that later batches can be supplied to a similar quality.

Commercially available tack measuring devices measure the tack under dynamic conditions at known ink film thickness, temperature and speed. Tack devices in combination with a printability tester, such as an IGT Amsterdam, can help to prevent some problems that can happen on the press. They can give an indication concerning the safe machine speed for any paper and ink combination. It is important to recognize that under press printing conditions there is a steady flow of ink from the ink doctor roll to the blanket and so to the substrate. This substrate removes in a steady way an amount of ink from the system. So recognizing this it is clear that the results of off-line tack measurement are only comparative.

In a view of the various construction geometries and the choice of various physical quantities measured in the tack devices, one cannot determine a single value for the given ink tack. It can be suggested that under certain conditions like controlled temperature and roller speed there is a reproducible correlation between the results achieved using a variety of devices (Hamerliński and Pyr'yev, 2013).

Ink tack is influenced by a number of factors such as temperature, composition of the ink, the age of the ink, speed of the measurement or printing. By running the ink tack measurements for a set period and noting the change of ink tack in time, some conclusions can be drawn on the press stability of the ink. However, press stability evaluations are only relative to known samples and, unless a series of tack standards is available for which values have been obtained on a suitable tackmeter, it is not possible to ascribe numerical values to unknown samples (Leach, et al., 2007).

Offset inks are highly viscous dispersions in which the solid pigment particles are dispersed in an oil based varnish consisting of dissolved resins and miscellaneous additives. Properties like ink tack, setting, final gloss and colour fastness are principally attained by the proper selection and combination of pigment, resins and oils. An offset ink common formulation is: pigments (mass fraction of 10–20 %), resins (mass fraction of 20–40 %), oil based varnish (mass fraction of 30–50 %) and a variety of additives (mass fraction of 0–10 %) (Leach, et al., 2007).

When applied to a porous substrate, such as coated paper, an offset ink changes its tack from the well-defined film split value to a complex ink-on-paper tack behaviour. In contrast to the intrinsic tack, ink-on-paper tack behaviour includes the fluid loss, roughness and absorptive properties between ink and paper (Rousu, et al., 2000a; Ridgway and Gane, 2004), where fluid loss is due to evaporation, setting, oxidation and/or polymerisation. Ink-coating interactions have significance both in the initial ink transfer from the printing plate and in the first stages of ink drying as well as later in the polymerisation phase for smear and rub resistance (Gane and Seyler, 1994). Regardless of the primary drying mechanism of ink on paper, absorption is an important stage of drying in all cases as it results in the initial setting and enables the subsequent colours to be printed. Optimally, only a certain fraction of the ink, namely the low viscous vehicle, absorbs into the paper while pigments and resins remain on the surface. The concentrating ink resins which are filtered out on the surface of the paper begin to polymerise and adhere to the surface. Initial separation of ink components is largely determined by the ink component compatibility whereas coating structure and chemistry are responsible for further separation phenomena during absorption (Rousu, et al., 2000b; Ridgway and Gane, 2004).

The presented study aims to observe the dynamic ink tack readings from the printers' perspective. As a function of distribution and splitting time, readings serve to determine the ink stability on the printing press. The impact that prolonged film splitting has on the printability is evaluated in the laboratory using test equipment. Although the laboratory conditions are much different from those on an offset press this type of evaluation can serve as a helpful way to prevent some printing problems. The presented results focus on the intrinsic ink tack measurements only and they do not cover all the aspects of ink tack and printability (ink-on-paper tack behaviour).

2. Materials and methods

Measuring equipment and printing materials were conditioned during 24 h in the standard atmosphere, 23 ± 1.0 °C and 50 ± 2.0 % rh, prior to testing and printing.

2.1 Materials

The inks used in this study are both sheet-fed offset inks produced by Huber group, as follows:

Inkredible Rapida magenta 42RP250, the quick-setting sheet-fed offset process ink. Designed for printing on absorbent substrates, capable for high-speed printing on straight presses. It contains mineral oil and is not recommended to be used in packaging printing. Additional information about the ink is provided in Figure 1. Ink information is taken from Huber group technical information (Huber group, 2017a).

Figure 1: Rapida Ink properties

Inkredible Reflecta magenta 42RL250, the high-gloss sheet-fed offset process ink. Suitable for exceedingly high-gloss print jobs on coated and on other absorbent substrates. Formulated as mineral oil free but it is not the low-migration type so is not recommended for the manufacture of food packaging. Additional ink information is in Figure 2 (Huber group, 2017b).

Figure 2: Reflecta ink properties

2.1.1. Printing substrates used in the ink transfer method
Prints produced on the IGT Amsterdam printability device were printed on specified IGT art paper code Ka, 340 mm × 55 mm, APCO II/II.

2.2 Methods

2.2.1 Ink tack testing
The method was implemented according to the IGT operating manual version July 2015 for IGT Tackoscope 3LC all in conformance with the requirements of ISO 12634:2018. Before the start of the test an operating profile was made. Settings were set to a fixed temperature of 30 °C and fixed speed of the rollers of 50 m/min for the distribution and 100 m/min during the measurement. The ink was then applied in an amount of 0.40 cm^3 with the IGT ink pipette on the Tackoscope rubber-covered distribution roller which was brought in contact with the metal centre roller. The distribution roller then gave an even distribution of the ink. After 30 s of ink distribution the measuring top roller was automatically brought into contact with the centre roller. The tack was measured by the mechanism between the two inked rollers on the top. More precisely, the measuring roller provides the calculated force required to split the ink film from the central roller. The signal output depends on the displacement of the measuring roller and is expressed in tack units and shown on the touch-screen of the built-in computer. These calculations are then obtained as comma separated files which were transferred on to a computer and transformed into tack graphs. The measurements were done three times for each of the inks and average values are shown on the graphs.

2.2.2 Ink distribution and ink transfer
Methods are implemented according to the IGT information leaflet W81. Ink was applied in a volume of 0.4 cm^3 with IGT ink pipette on to the IGT high speed inking unit. The inking unit was connected to a water bath which was set to a controlled temperature of 30 °C. It is important that this temperature is the same as it set on the Tackoscope since the temperature has a large impact on the tack measurement. The speed of the rollers was set to 1.2 m/s. After the ink on the inking unit was evenly distributed for 15 s, the 50 mm wide aluminium printing disc was inked for the desired time. For the experiment the printing disc inking times were set to 30, 60, 300 and additionally 420, 600 and 720 s.

An IGT Amsterdam 2 device was used as a printability tester. Printing force was adjusted to 1 000 N with a constant speed of 0.2 m/s. The substrate was mounted on the sector of the device and the printing disc was mounted on the printing disc shaft. The print was made for every measurement after 20 s between the steps. Before and after the printing, the printing disc was weighed on a precision scale with a reading accuracy of 0.1 mg. From these weights and the sizes of the print the ink transfer was calculated by using the formula:

$$\text{Ink transfer} = [10\,000 / (L \times W)] \times (G_1 - G_2) \qquad [1]$$

where L is the length of the print in cm, W is the width of the print in cm, G_1 is weight in g of printing disc with ink before printing, and G_2 is weight in g of printing disc with ink after printing.

After the prints were dry, the substrates were measured for dry print properties. 5 spots across the length of each print were collected with an IGT Gloss Meter G60 (60°) for print gloss and Techkon Spectrodens for print density.

3. Results and discussion

Figure 3 shows the stability of the ink tack in time, it is performed as a standard test for sheetfed inks; using 0.4 cm^3 of the ink, regulated temperature of 30 °C, distribution time 30 s, distribution rollers speed 50 m/min, measuring time 600 s and measuring rollers speed of 100 m/min.

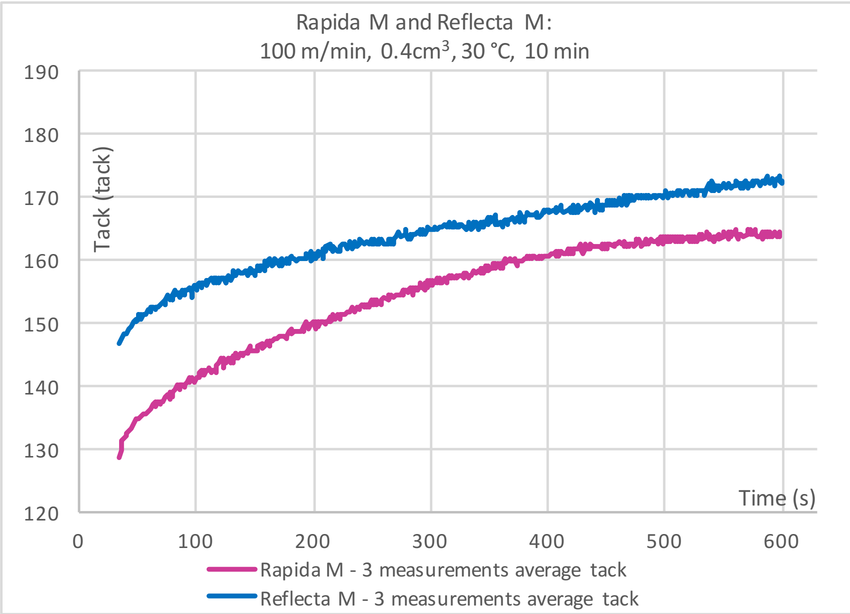

Figure 3: Tack curves of both inks as a function of time

Differences in tack increase between the two inks are noted. To get more information on the behaviour of the tack stability of both inks, the same test was performed for a prolonged time.

Figure 4 shows the Rapida magenta ink tested for approx. 1 400 s showing a maximum tack value at approx. 700 s. After the peak, the tack value of the ink decreased. It can be assumed that after the peak, the ink starts to degrade and will not make a good print – which will later be proven to be the case.

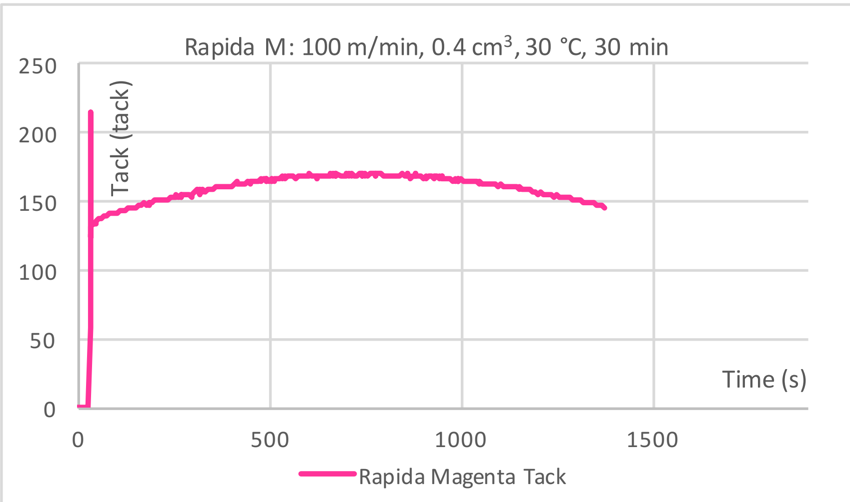

Figure 4: Rapida magenta ink tack curve as a function of time

Figure 5 shows the Reflecta magenta ink, tested for 1 800 s and it does not show a maximum tack value (yet). Comparing to the Rapida ink, we see that the Rapida tack is lower than that of the Reflecta ink. The ink tack curve continued to increase not reaching the peak during the test time. It can be assumed that this ink can tolerate longer distribution times – which is later proven to be correct.

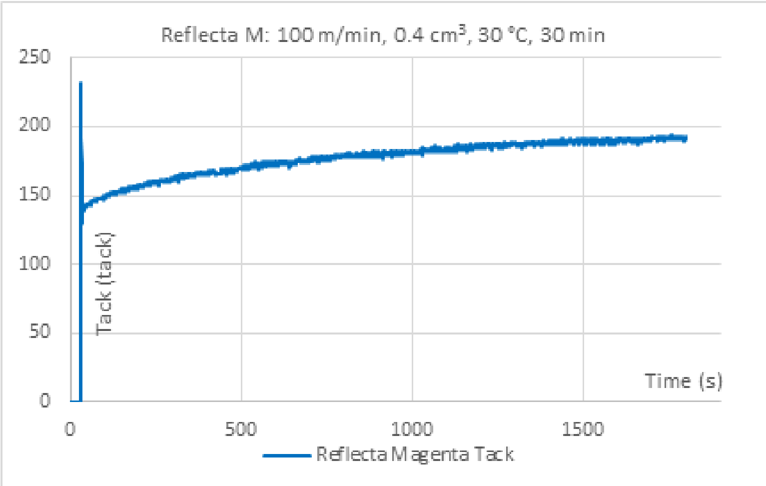

Figure 5: Reflecta Magenta ink tack curve as a function of time

The Reflecta magenta ink tack was then also measured at a higher speed of 200 m/min for over 2 500 s and its tack value increased getting to a maximum tack value at approx. 1 370 s. To some extent, the rise in ink film separation velocity can lead to the increase of ink tack value (Yang, 2015).

In Table 1 is shown how different lengths of time for the ink distribution on the IGT high speed inking unit affect the print made with the Rapida magenta ink. Each strip of the printed reference paper was measured for the dry ink properties of the print; ink transfer, print density, print gloss and by a visual assessment.

Table 1: Dry properties of the print printed with Huber Rapida Magenta Ink

Distribution time / s	Ink transfer / g/m²	Average print density	Standard deviation, print density, σ_d	Average gloss at 60° / GU	Standard deviation, gloss, σ_g / GU	Visual print quality
30	1.19	1.40	0.04	40.0	0.8	Good
60	1.22	1.37	0.02	38.0	0.8	Good
300	0.98	1.26	0.03	37.4	1.6	Good
420	0.58	0.55	0.02	25.8	0.8	Bad
600	0.32	0.36	0.01	38.8	0.3	Bad

In Table 2 are shown the ink distribution time, ink transfer, print density and gloss results of the Reflecta Magenta ink.

Table 2: Dry properties of the print printed with Huber Reflecta Magenta Ink

Distribution time / s	Ink transfer / g/m²	Average print density	Standard deviation, print density, σ_d	Average gloss at 60° / GU	Standard deviation, gloss, σ_g / GU	Visual print quality
30	1.05	1.48	0.00	59.1	1.4	Good
60	1.02	1.63	0.01	65.1	1.1	Good
300	1.03	1.71	0.01	72.8	1.1	Good
720	1.20	1.73	0.01	69.4	0.6	Good

Figures 6 and 7 show a scanned image of printed and dry paper substrates. All the prints were made under the same conditions; printing speed and pressure. The only variable parameter was the printing disc inking time.

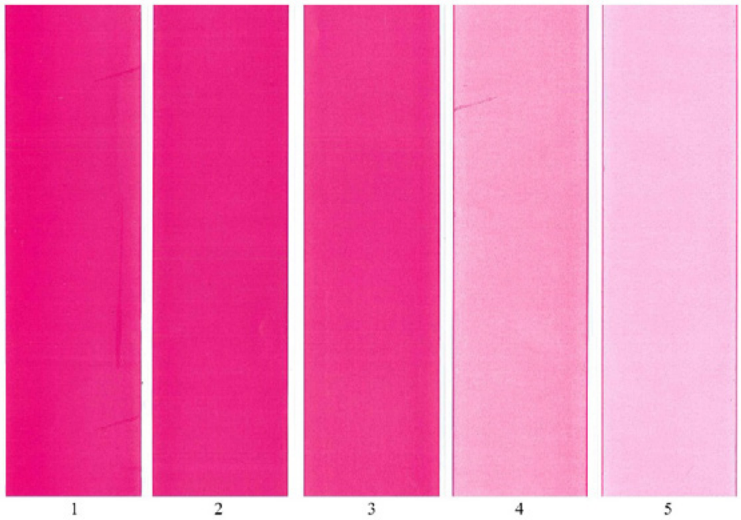

Figure 6: Scan of substrates printed with Rapida Magenta Ink; (1) 30 s, (2) 60 s, (3) 300 s, (4) 420 s, (5) 600 s

The inking of a printing disc with the Rapida ink for longer than 5 min results in a bad print.

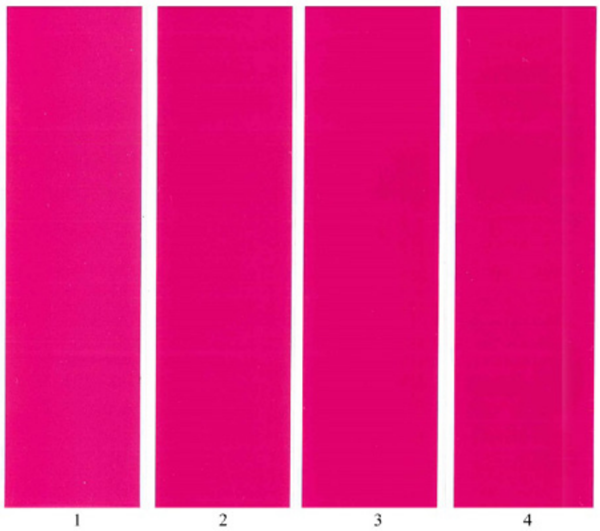

Figure 7: Scan of substrates printed with Rapida Magenta Ink; (1) 30 s, (2) 60 s, (3) 300 s, (4) 720 s

The inking of a printing disc with the Reflecta ink results in a good print even after it was inked (distributed) for 12 min.

From the printer's perspective, the combination of laboratory testers presented in this study gives a good indication on ink stability on the printing press and how prolonged film splitting affects the printability. More detailed analysis which includes characterization of the ink components would provide a better understanding of ink setting on paper.

4. Conclusions

The ink tack is a major factor influencing ink transfer to the substrate. The ink manufacturers usually assign a tack value in the ink technical information as a single number aiming to serve to graduate the inks on the printing units by the tack to avoid difficulties in multicolour printing. Besides the tack value, modern tack devices can also measure the dynamic stability of the ink tack in time under controlled settings, such as temperature. The information can be used to predict the print stability of the ink and to prevent problems in printing. Under laboratory conditions, it was demonstrated that with a combination of laboratory testers it is possible to find a relation between the ink tack stability under distribution over time and the print characteristics. The inks were let to run under distribution and film split for a set period and the change in the ink tack over that time was recorded. The ink with the more stable tack measurement curve over time showed better durability in printing. The number of revolutions between the inked rollers on the ink distribution tester was affecting the properties of the ink. For ink distribution not longer than 5 min, the ink for fast printing showed lower tack with satisfactory printability.

Acknowledgements

The authors would like to thank IGT Testing Systems, Almere, the Netherlands for placing at our disposal the laboratory equipment used in this paper.

References

Gane, P.A.C., Matthews, G.P. and Schoelkopf, J., 2003. Offset ink tack and rheology correlation part 1: ink rheology as a function of concentration. *Tappi Journal*, 2(6).

Gane, P.A.C. and Seyler, E.N., 1994. Tack Development: an analysis of ink/paper interaction in offset printing. In: *1994 TAPPI Coating Conference* Proceeding. San Diego, California, 1-5 May 1994. Atlanta: Tappi Press, p. 243.

Hamerliński, J. and Pyr'yev, Y.., 2013. Modelling of ink tack property in offset printing. *Acta Poligraphica*. 1, pp. 31–40.

Huber group, 2017a. *Technical information: Rapida Cofree, 10.P.002.* [online] Available at: <http://www.hubergroup.de/en/information/ti-finder/> [Accessed 15 January 2018].

Huber group, 2017b. *Technical Information; Reflecta Cofree, 10.P.003.* [online] Available at: <http://www.hubergroup.de/en/information/ti-finder/> [Accessed 15 January 2018].

Kipphan, H., 2001. *Handbook of print media: technologies and production methods.* Berlin, Heidelberg, Springer.

Leach, R.H., Pierce, R.J., Hickman, E.P., Mackenzie, M.J. and Smith, H.G. eds., 2007. *The printing ink manual*. 5^{th} ed. Dordrecht, The Netherlands: Springer, pp. 786–801.

NAPIM, 2017. *Printing ink handbook*. 7^{th} ed. Peachtree Corners, GA: National Association of Printing Ink Manufacturers.

Ridgway, C.J. and Gane, P.A.C., 2004. Ink-coating adhesion: the importance of pore size and pigment surface chemistry. *Journal of Dispersion Science and Technology*, 25(4), pp. 469–480.

Rousu, S.M., Gane, P.A.C., Eklund, D.E. and Spielmann, D.C., 2000a. Differential absorption of offset ink components on coated paper. In: *Proceedings of the 2000 TAPPI International Conference on Printing and Graphic Arts*. Savannah, Georgia, 1–4 October 2000. Atlanta: Tappi Press.

Rousu, S., Gane, P., Spielmann, D. and Eklund, D., 2000b. Separation of off-set ink components during absorption into pigment coating structures. *Nordic Pulp and Paper Research Journal,* 15(5), pp. 527–535.

Thompson, B., 2004. *Printing materials: science and technology, a Pira International printing guide*. 2^{nd} ed. Leatherhead, UK, Pira International, pp. 356–370.

Yang, Y.G., 2015. Study on the relationships between plastic viscosity and tack value of offset printing ink. *Applied Mechanics and Materials,* 723, pp. 814–818.

Direct Observation of High-speed Fluid Transfer Phenomena in the Nip of a Gravure Printing Machine

Julian Schäfer, Hans Martin Sauer and Edgar Dörsam

Institute of Printing Science and Technology, Darmstadt University of Technology, Magdalenenstr. 2, 64289 Darmstadt
E-mails: schaefer@idd.tu-darmstadt.de; sauer@idd.tu-darmstadt.de; doersam@idd.tu-darmstadt.de

Short abstract

A measurement technique for high-speed video observations of fluid splitting phenomena in the nip of a gravure printing unit is presented. Video frame rates of 10 kfps at a resolution of 768 × 512 pixels with 45 μm per pixel were achieved at printing velocities up to 3 m/s (180 m/min). The ink meniscus of a lamella splitting process was studied directly in the narrow wedge between printing cylinder and the rigid, non-porous transparent substrate. Highly dynamic wetting phenomena, viscous fingering and filament formation were observed. The investigation of the filling and emptying process of individual gravure cells should be feasible in this way as well.

Keywords: gravure printing, fluid transfer phenomena, wetting, high-speed imaging

1. Introduction and background

1.1 Gravure printing and recent studies

Printing accuracy and quality as well as the chemical resistance of machinery parts to volatile and aggressive solvents make gravure printing one of the promising techniques for fast and cost-efficient production of functional printing devices. Specifically, this applies to e.g. printed organic thin film transistors (Ganz, 2017) and organic light emitting diodes (OLED) (Bornemann and Dörsam, 2013). Being well-established and controllable in graphical applications, gravure printing faces significant demands for enlargements of the established process window when functional fluids with polymer semiconductors or OLED materials are used (Bornemann, Sauer and Dörsam, 2011). New ink splitting and defect formation phenomena are observed, with apparently complex two-phase flows in the nip. Analyzing the physics of fluid transfer in gravure printing it is our aim to make transport and fluid splitting phenomena directly visible in the printing nip, using high-speed video technology. Thinking about gravure as a sequence of distinct physical regimes has recently motivated new activity to this field of research. Figure 1, displaying the principal design of a gravure unit, also illustrates this concept by displaying these substeps. Fernandes, Campanelli and Dörsam (2017) use fluorescence to measure the cell pick-up volume of anilox rollers in the field of ink acquisition.

Hoang and Ko (2015) study the doctor blading process and the resulting fluid menisci in the cells. Simulations often take place in the field of high shear fluid dynamics at the doctor blade (Hariprasad, et al., 2016; Schmidt, Schloßer and Schollmeyer, 2009; Kuhlmann, Nienhüser and Rath, 1999), the fluid transfer process (Hoda and Kumar, 2008; Huang, et al., 2008) and the filament building and break-up (Khandavalli, et al., 2015). Experimental studies on this topic can also be found (see e.g. Miura and Yamamura, 2015). On fluid transfer from the gravure cells experiments are rare. Most studies here restrict on simulation (Lee, et al., 2012; Lee and Sung, 2013). Experimental studies then cover the last regime as they are the building of fluid filaments (Griesheimer, 2014; Sauer, et al., 2017), the drying of printed layers (Stamm, 2017) and the inspection of the resulting layers (Bornemann and Dörsam, 2013). Due to difficult optical access to the nip, fluid transfer and splitting has remained a black box, and only very limited efforts on simulations and models are available.

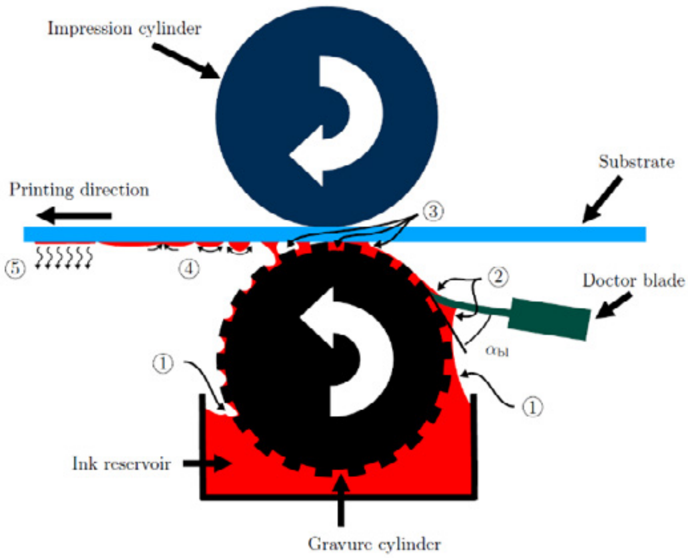

Figure 1: Sketch of the gravure printing process with separation into five regimes: 1) Ink acquisition from ink reservoir, 2) Doctor blade process, 3) Ink transfer, 4) Fluid dynamics on the substrate, 5) Solidification of the ink (adapted from Bornemann and Dörsam, 2013)

In this paper, we present a technique that we specifically developed for high-speed fluid transfer observations in the nip. A lab-scale sheet fed gravure printing machine was used. An optical light deflection prism was integrated into the substrate carrier. This enabled the direct optical observation of the fluid transfer using a high-speed camera at 10 000 frames per second.

1.2 Aim of research

The aim of our study is the detailed, time-resolved observation of substrate wetting and fluid transfer in a gravure printing machine. In this way, we want to understand the complex interrelation of printing velocity, gravure parameters, hydrodynamical transport and wetting phenomena. In this paper we introduce the experimental setup, the modifications to the substrate carrier (section 2.1), and high-speed imaging setup (section 2.2). We then describe preliminary experiments in section 2.3. After discussing the results of our research in section 3, we provide an outlook in section 4.

2. Materials and methods

2.1 Experimental gravure printing machine

In this study the laboratory gravure printing machine Superproofer made by GT&W, Rödermark, Germany, was used (GT&W, n.d.). Cylinder width and diameter are 100 mm and 200 mm, respectively. The machine provides a one-sided bearing for easy optical access to the nip from the side. The sheet fed printing machine has a linear drive with a substrate carrier system. Substrates with 100 mm × 50 mm in length and width are mounted here. The velocity of the linear drive is electronically synchronized to the circumferential speed of the printing form cylinder, as well as to the belt-driven impression roller. Figure 2 shows the arrangement, with a standard carrier mounted. Substrate sheets can be taped to the surface marked with a circle.

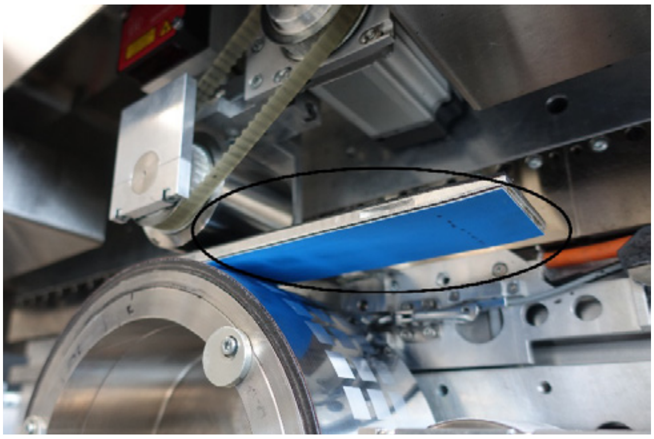

Figure 2: Close-up view of the printing form cylinder, the impression roller and the substrate carrier

Our printing sleeve contained ten sections with raster widths in the range from 40 l/cm to 140 l/cm. Each section consisted of 12 squares of 13 mm × 13 mm in size, with tonal values from 5 % to 100 % (see Figure 3). With this pattern a relevant range of printing form parameters is covered. Fluid transfer phenomena can be studied as a function of raster width and tonal value. The stylus angle was 120°, allowing the use of standard gravure inks with common solvents as ethanol, isopropanol and toluene, including the pure solvents as well.

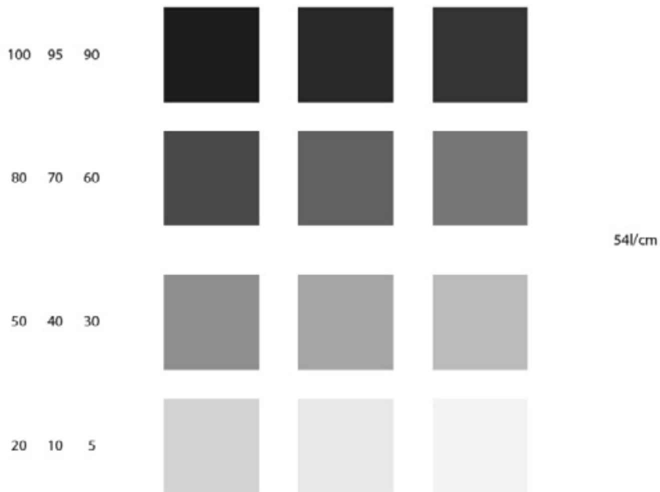

Figure 3: One section on the printing form layout with a screen width of 54 l/cm, containing 12 test squares with tonal values between 5 % and 100 %

Further technical data of the experimental gravure printing machine are summarized in Table 1.

Table 1: Technical data of the experimental gravure printing machine

Indication	**Value**
Printing speed	0.5 m/s–5.0 m/s (30 m/min–300 m/min)
Printing form cylinder	Diameter: 220 mm, Width: 100 mm,
Substrate size	150 mm × 50 mm
Substrate thickness	0.05 mm–1.00 mm
Fluid volume per print	1.5 ml
Nip pressure	4 N/mm–16 N/mm
Doctor blade angle	30°–90°
Doctor blade pressure	0.2 N/mm–1.8 N/mm

2.2 Modification of the substrate carrier

An essential feature of our experimental setup was the optical access to the nip. As printing cylinder and impression roller were made from steel and intransparent, we utilized the gap between the printing form cylinder and the impression roller for optical access. An extended substrate carrier containing an optical reflection prism was designed, fitting into the gap of 20 mm in height. This enabled the perpendicular view on the printing form. Concerning the wetting of the substrate the focal plane is aligned with the surface of the substrate. We took this as the reference plane for x-y-coordinates. A schematic sketch of the printing machine is shown in Figure 4.

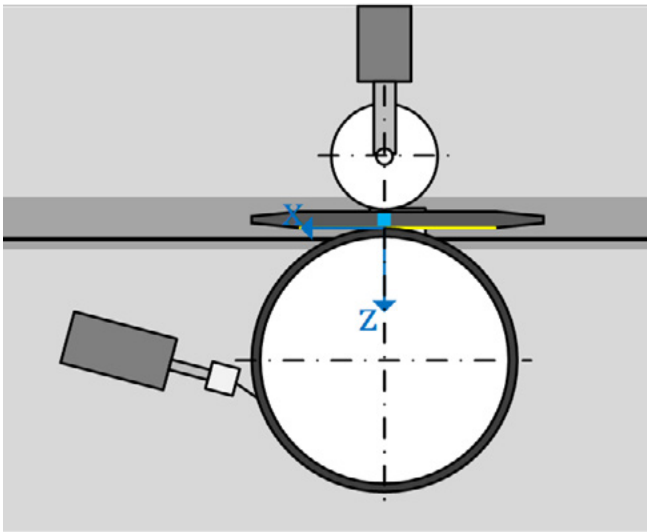

Figure 4: Schematic sketch of the printing form cylinder, impression roller and substrate carrier with definition of a coordinate system

The camera was installed in front of the Superproofer and oriented parallel to the cylinder axis as shown in Figure 4. The camera was mounted to an optical lab jack with a linear stage in order to provide adjustments in camera height (z-axis) and in printing direction (x-axis) as shown in Figure 5.

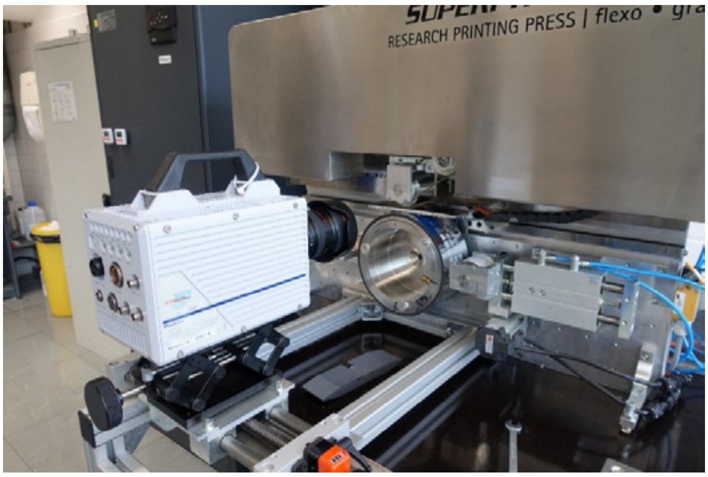

Figure 5: Camera mounted to a lab jack and linear stage to align the optical axis and the y-axis of the working coordinate system

The prism in the substrate carrier rotated the viewing direction by 90°. The camera was focused on the nip, i.e. on the substrate surface respectively a test square of the printing form. In this way wetting and fluid transfer could be observed as is shown in Figure 6. Simultaneously the distance between the imaging plane and the imaging sensor is kept constant as the substrate carrier only moves in the x-direction.

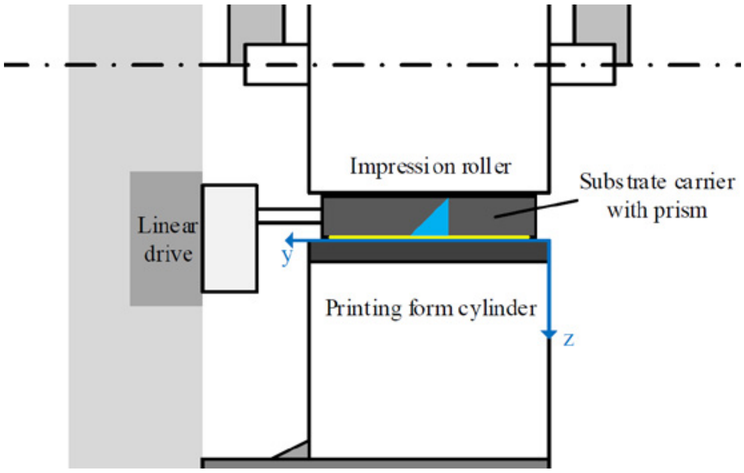

Figure 6: Sectional view of the y-z-plane of the gravure printing machine with the modified substrate carrier in the nip; the optical axis of the camera is redirected onto the wetting plane (x-y-plane) by the inserted prism

A first prototype of this substrate carrier was made from PLA, using an Ultimaker 2+ 3D-printer (Ultimaker, 2018). The result is shown in Figure 7. A 15 mm × 15 mm aluminum and VIS 0° coated glass prism (Edmund Optics, 2018) was inserted into the plastic body. With a wall thickness of 4 mm the stack height of the carrier is 19 mm, i.e. smaller than the available gap height and suitable for substrates of up to 1 mm in thickness.

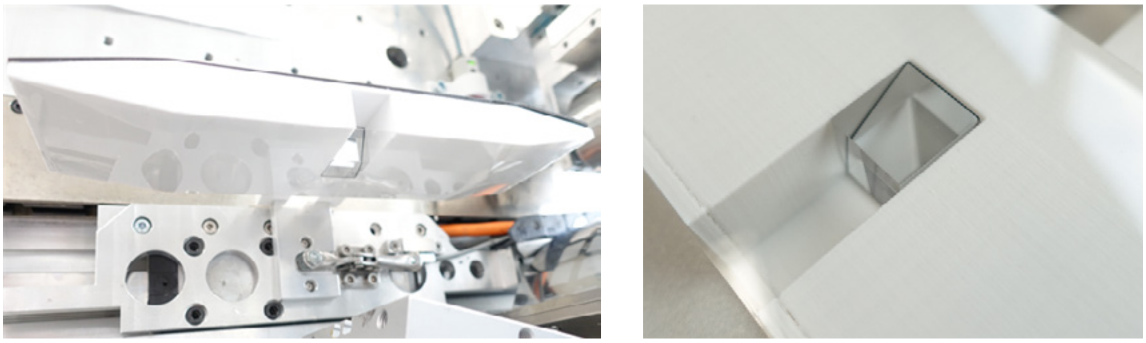

Figure 7: Prototype of the investigational substrate carrier with an inserted prism for directly observing fluid transfer phenomena in the nip of a gravure printing machine

This modified carrier enables observation of fluid transfer phenomena to the substrate or, in case that the substrate is omitted, to the the prism itself. The prism is held in the center of the prototype carrier allowing the observation of the midst test squares with tonal values of 10 %, 40 %, 70 % and 95 % (see Fig. 3). The time span of observation, when the carrier passes through the nip at 5 m/s (300 m/min) is 42 ms.

2.3 High-Speed imaging and lighting setup

We used a Photron Fastcam SA-4 Highspeed Camera (Photron, 2013). This device can take 3 600 frames per second (fps) at full resolution of 1 024 × 1 024 pixels, in combination with a Canon 100 mm f/2.8 Macro lens. The size of the monochrome sensor is 20 mm × 20 mm. Each pixel has a size of 20 µm. Due to the maximum data output of the sensor, maximum frame rate and resolution are interdependent. By reducing the resolution, the frame rate can be increased to a maximum of 500 kfps as it is shown in Figure 8. Previous works at our institute show that a good compromise between framerate and resolution is of significant importance for investigating fluid splitting phenomena (Griesheimer, 2014). Regarding to Griesheimer's results a framerate of 10 000 fps with a resolution of 768 × 512 pixel was considered as sufficient.

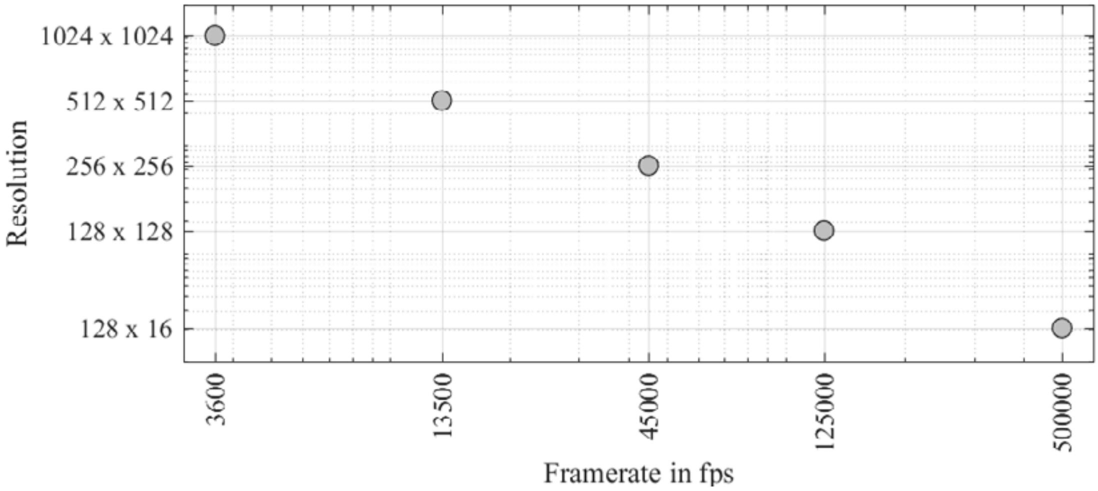

Figure 8: Relation between resolution and framerate of the Photron Fastcam SA-4 used in the experiments

For nip illumination an additional beam splitter with a transmission ratio of 0.5 was inserted into the optical path of the camera. A high-speed imaging LED light source (Veritas, 2015) was attached to the optical assembly in order to keep the optical imaging path length to the moving substrate carrier strictly constant. The light source is used in pulsed mode and is synced with the cameras frame rate. The whole high-speed imaging setup was attached to the printing machine as is shown in Figure 9.

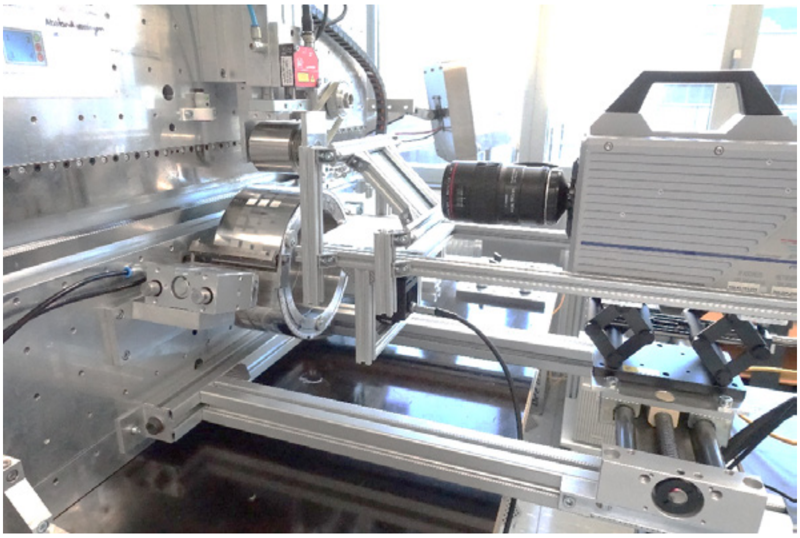

Figure 9: In front of the camera lens a beam splitter and a high-speed imaging led light source is installed for illuminating the fluid transfer phenomena in the nip

2.4 Preparation of the fluid transfer acquisition

Starting the experiment, the respective fluid was dosed onto the rotating printing form cylinder directly in front of the doctor blade. As the doctor blade fills the gravure cells and removes abundant fluid from the cylinder no further care for precise fluid dosing had to be taken. The doctor blade pressure was 0.2 N/mm, and the nip pressure was 12 N/mm for all the experiments. As optical interferences between the prism and transparent substrate foils were noted in preliminary experiments the substrate was abandoned and we printed the fluid directly onto the rigid, non-porous glass prism. A light barrier mounted behind the nip triggers the high-speed camera when the carrier passes through the nip and provides precise timing of video acquisition.

3. Results and discussion

The analysis of the video data from the previously described experiments shows that the modified substrate carrier and the optical acquisition assembly are suited for direct observation of high-speed fluid transfer phenomena in the nip. Due to the motion of the carrier and the prism the field of observation moves from the right to the left side in the video and the images shown, whereas the nip position is fixed (see Figure 10).

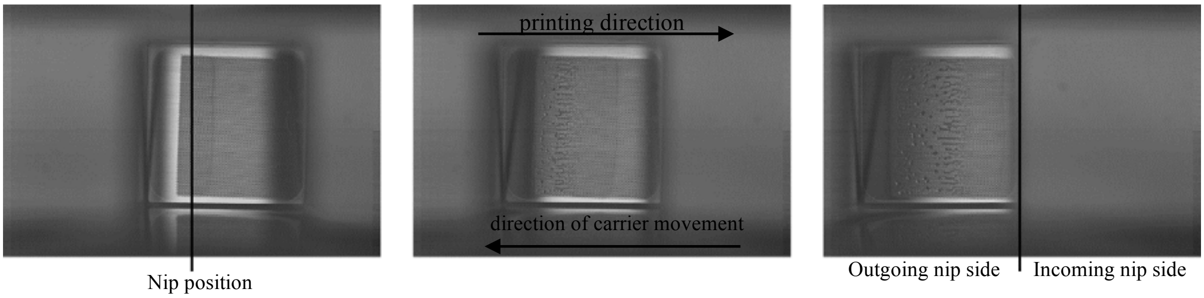

Figure 10: Three full image frames of an experiment with ethanol and a printing speed of 1000 mm/s (60 m/min), time difference between the images is 5 ms; the nip position is marked with a black line, which divides the frame into the incoming and outgoing nip side

The observations essentially show the fluid transfer phenomena known or suggested from earlier studies. Three different phenomena can be simultaneously observed and separated as shown in Figure 11, which held for all of the used fluids (ethanol, toluene, isopropanol) for tonal values larger than 40 %:
Development of an almost straight contact line and a completely wetting at the incoming nip side.
Fluid splitting at the outgoing nip side, with fluid finger formation.
Separation and decay of the fluid fingers into separated droplets.

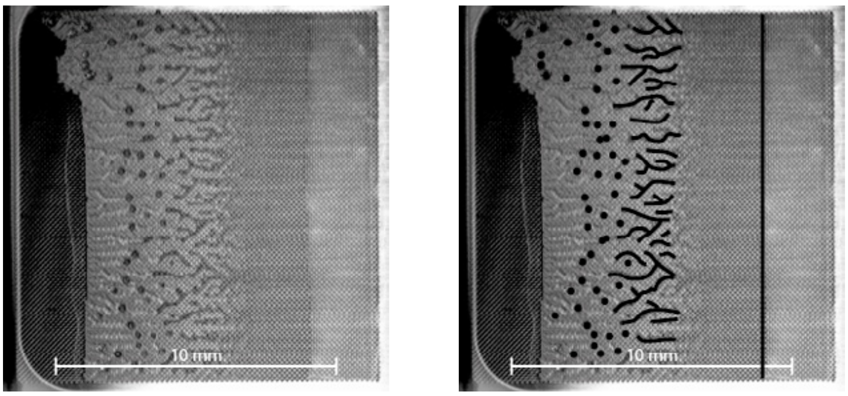

Figure 11: Fluid transfer from the cells of a test square with 80 l/cm and a tonal value of 95 % with toluene as fluid; on the left side, the raw image frame is shown, on the right side the phenomena are highlighted in black and numbered in white referring to the list of phenomena

Viscous fingering could be confirmed to be the most important instability at the outgoing nip side. It was verified that in case of lamella splitting the finger width scaled with printing velocity as $v^{-1/2}$, as is proposed by the analogy to the Saffman-Taylor cuvette experiment (Saffman and Taylor 1958). This also agrees well with the findings of Bornemann (2014) and Kitsomboonloha and Subramanian (2014). However, we also observed evidence for a deviation from this simple law in case that finger width and raster width of the gravure pattern may be in the same range. Further, we could confirm that the meniscus at the incoming nip side, in spite of being highly volatile as well, is remarkably stable against such phenomena. The slight curvature of the ends of the meniscus is presumably caused by the air flow induced by the rapidly moving cylinder. We can exclude a mechanical deformation of printing cylinder or substrate as a possible origin here. This may be a hint that not only the flow of the printing fluid but also the adjacent air flow should be considered closer in future research on fluid splitting.

For tonal values equal or smaller than 40 %, the fluid transfer showed deviations from the previously described behavior. A meniscus at the incoming nip side cannot be observed any more. Further, the substrate surface is not completely wetted any more, and the viscous finger instability at the outgoing side disappears. The fluid is transferred in separated drops as is shown in Figure 12. This result indicates that the fluid volumes of the cells form liquid bridges on the walls for larger tonal values, which underlines former results regarding lamella or film splitting in gravure printing. For smaller cells, such an interaction does not appear because the distance of the single fluid volumes is too large.

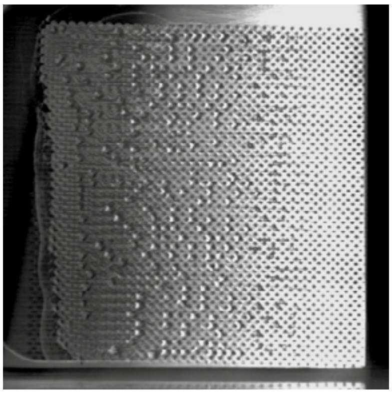

Figure 12: Dropwise fluid transfer from a test square with 40 l/cm and a tonal value of 40 %

In comparison to the larger tonal values, the image frames appear to be much brighter. This effect is related to the decreased ratio of cell to wall area. Therefore, more light is directly reflected by the cylinder, which propagates using a brightness adjustment algorithm with intensity correction dependent to the tonal value.

A qualitative influence of the printing speed on the lengths of the fluid fingers can be observed as well for tonal values larger 40 %. In Figure 13, two image frames are shown of experiments with printing speeds of 1 000 mm/s (60 m/min) on the left and 3 000 mm/s (180 m/min) on the right.

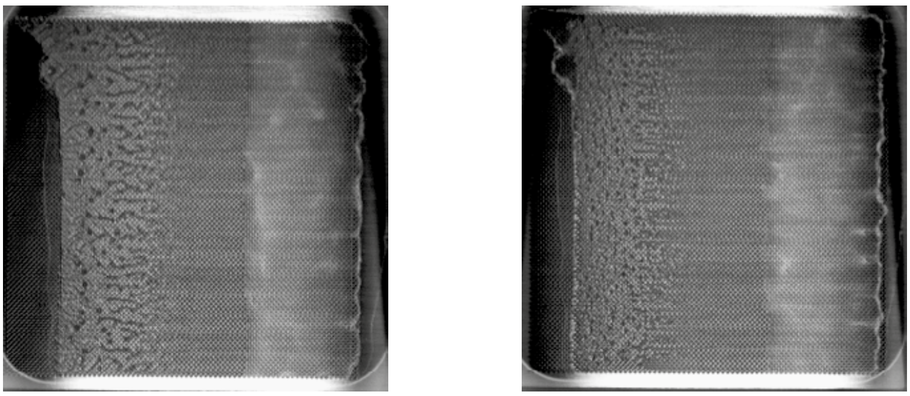

Figure 13: Fluid transfer for a test square with 80 l/cm and a tonal value of 95 % with printing speeds of 1 000 mm/s (60 m/min) on the left and 3 000 mm/s (180 m/min) on the right; the fluid was ethanol

We observed that with rising printing speed the length and width of the fluid fingers decrease, whereas the length of the completely wetted area even increases. A possible explanation is that the time scale at larger printing speeds might be too short for certain instabilities to develop. Further experiments with even larger printing speeds (up to 5 000 mm/s resp. 300 m/min) have to be done to quantify and verify these results.

Note that fluid filament splitting and fluid transfer depend on the surface characteristics of the substrate e.g. porosity, roughness and surface chemistry (Sauer, Daume and Dürsam, 2015; Ridgway and Gane, 2002; Yang, 2013). Thereby the observed fluid transfer phenomena may only be applicable for non-porous and rigid substrates.

4. Conclusions

In this work, an experimental setup is shown which allows the direct observation of high-speed fluid transfer phenomena in the nip of a gravure printing machine. Preliminary tests confirmed an influence of printing speed and tonal value on the fluid transfer behavior to a non-porous substrate in gravure printing. We could directly observe the transition between point and lamella splitting to occur as a function of cell volume, as claimed in Bornemann, Sauer and Dörsam (2011). An influence of the engraved cells on the fluid movement along the fingers at printing speeds up to approximately 3 000 mm/s (180 m/min) is observed. This could give a first hint that the formation of fluid fingers at the outgoing nip side deviates from the Saffman-Taylor instability. In near future, more experiments are planned to investigate the influences of the mentioned parameters in this work and to quantify them in form of a model for fluid transfer processes. Additional investigations on size and time scales of the observed instabilities in the second region of the fluid transfer process should yield new insight into the complex fluid dynamics of ink splitting.

Acknowledgments

We kindly acknowledge the financial support by the German Research Foundation (DFG) within the Collaborative Research Centre 1194 “Interaction between Transport and Wetting Processes”, Project C01.

References

Bornemann, N., Sauer, H. and Dörsam, E., 2011. Gravure printed ultrathin layers of small-molecule semiconductors on glass. *Journal of Imaging Science and Technology*, 55(4), pp. 40201-1-40208-8.

Bornemann, N. and Dörsam, E., 2013. A flatbed scanner for large-area thickness determination of ultra-thin layers in printed electronics. *Optics Express*, 21(19), pp. 21897–21911.

Bornemann, N., 2014. *Characterization and investigation of large-area, ultra-thin gravure printed layers*. Dr.-Ing. Dissertation. Technische Universität Darmstadt.

Edmund Optics, 2018. *TechSpec: 15mm, Aluminum & VIS 0° Coated, N-BK7 Right Angle Prism*. [online] Available at: <https://www.edmundoptics.com/optics/prisms/right-angle-image-reflection-prisms/15mm-aluminum-amp-vis-0deg-coated-n-bk7-right-angle-prism/?site=EN&countryid=232> [Accessed 22 February 2018].

Photron, 2013. *Fastcam SA4 high-speed imaging system*. [online] Available at: <https://photron.com/wp-content/uploads/2014/07/FASTCAM_SA4.pdf> [Accessed 14 February 2018].

Fernandes, F., Campanelli, F. and Dörsam, E., 2017. On the measurement of the pick-up volume of anilox rollers by fluorescence. In: G. Patrick and C. Ridgway, eds. *Advances in Printing and Media Technology: Proceedings of the 44th International Research Conference of iarigai*. Darmstadt, Germany: International Association of Research Organizations for the Information, Media and Graphic Arts Industries.

Ganz, S., 2017. *Drucken organischer Feldeffekttransistoren: Prozessbezogene Analyse des ladungsträgertransports*. Dr.-Ing. Dissertation. Technische Universität Darmstadt.

Griesheimer, S., 2014. *Farbspaltungsphänomene von Druckfarben an strukturierten Oberflächen am Beispiel des Flexodrucks*. Dr-Ing. Dissertation. Technische Universität Darmstadt.

GT&W, n.d. *Superproofer 220: research printing press*. [online] Available at: <http://www.gtandw.com/superproofer/datasheet> [Accessed 09 February 2018].

Hariprasad, D.S., Grau, G., Schunk, P.R., and Tjiptowidjojo, K., 2016. A computational model for doctoring fluid films in gravure printing. *Journal of Applied Physics*, 119(13), article id. 135503.

Hoang, H.P. and Ko, S.L., 2015. Effect of doctoring on the performance of direct gravure printing for conductive microfine lines. *Journal of Micromechanics and Microengineering*, 25(11), article id. 115018.

Hoda, N. and Kumar, S., 2008. Boundary integral simulations of liquid emptying from a model gravure cell. *Physics of Fluids*, 20(9). article id. 092106.

Huang, W.-X., Lee, S.-H., Sung, H.J., Lee, T.-M. and Kim, D.-S., 2008. Simulation of liquid transfer between separating walls for modeling micro-gravure-offset printing. *International Journal of Heat and Fluid Flow*, 29(5), pp. 1436–1446.

Khandavalli, S., Lee, J.A., Pasquali, M. and Rothstein, J.P., 2015. The effect of shear-thickening on liquid transfer from an idealized gravure cell. *Journal of non-Newtonian Fluid Mechanics,* 221, pp. 55–65.

Kitsomboonloha, R. and Subramanian, V., 2014. Lubrication-related residue as a fundamental process scaling limit to gravure printed electronics. *Langmuir*, 30(12), pp. 3612–3624.

Kuhlmann, H. C., Nienhüser, C. and Rath, H.J., 1999. The local flow in a wedge between a rigid wall and a surface of constant shear stress. *Journal of Engineering Mathematics*, 36(3), pp. 207–218.

Lee, J.H., Seena, A., Lee, S.-h. and Sung, H.J., 2012. Turbulent boundary layers over rod-and cube-roughened walls. *Journal of Turbulence*, 13(1), p. N40.

Lee, J.H. and Sung, H.J., 2013. Comparison on very-large-scale motions of turbulent pipe and boundary layer simulations. *Physics of Fluids*, 25(4), document id. 0452103.

Miura, H. and Yamamura, M, 2015. Direct thickness measurement of doctor-bladed liquid film on gravure roll surface. *Journal of Coatings Technology and Research*, 12(5), pp. 827–833.

Ridgway, C.J. and Gane, P.A.C., 2002. Controlling the absorption dynamics of water-based ink into porous pigmented coating structures to enhance print performance. *Nordic Pulp & Paper Research Journal*, 17(2), pp. 119–129.

Saffman, P.G. and Taylor, G., 1958. The Penetration of a Fluid into a Porous Medium or Hele-Shaw Cell Containing a More Viscous Liquid. *Proceedings of the Royal Society of London: Series A: Mathematical and Physical Sciences*, 245(1242), pp. 312–329.

Sauer, H.M., Daume, D. and Dörsam, E., 2015. Lubrication theory of ink hydrodynamics in the flexographic printing nip. *Journal of Print and Media Technology Research,* 4(3), pp. 163–172.

Sauer, H.M., Schäfer, J., Brulin, S. and Roisman, I.V., 2017. Fast liquid sheet and filament dynamics in the fluid splitting process. In: *ECIS 2017 31st Conference of the European Colloid and Interface Society*. Madrid, Spain, 3–8 September 2017.

Schmidt, M., Schloßer, U. and Schollmeyer, E., 2009. Computational Fluid Dynamics Investigation of the Static Pressure at the Blade in a Blade Coating Process. *Textile Research Journal*, 79(7), pp. 579–584.

Stamm, J., 2017. *Modellbildung zur Schichtdickenmessung an dünnen gedruckten Filmen*. Master thesis. Darmstadt University of Technology, Institute of Printing Science and Technology.

Ultimaker, 2018. *Ultimaker 2+ specifications*. [online] Available at: <https://d3v5bfco3dani2.cloudfront.net/file/download/productgroup/Ultimaker%202+%20specification%20sheet%20v2.pdf/59918f37b6b13.pdf> [Accessed 14 February 2018].

Veritas, 2015. *Veritas: miniConstellation: specification sheet Model 120*. [online] Available at: <http://veritaslight.com/docs/mini_constellation_120_spec_sheet.pdf> [Accessed 9 February 2018].

Yang, L., 2013. A physical model for liquid movement into a porous substrate under the action of a pressure pulse. *Nordic Pulp & Paper Research Journal*, 28(1), pp. 94–100.

Study of the Effect of the Adhesion Promoter on the Coefficient of Friction, COF, of OPP Film

Małgorzata Zakrzewska[1] *and Halina Podsiadło*[2]

[1] hubergroup Polska Ul. Nowa 21, Nowa Wieś Wrocławska, 55-080 Kąty Wrocławskie

[2] Department of Printing Technologies, Institute of Mechanics and Printing, Faculty of Production Engineering, Warsaw University of Technology Ul. Narbutta 85, 02-524 Warszawa.

E-mails: malgorzata.zakrzewska@hubergroup.pl; h.podsiadlo5@onet.pl

Short Abstract

Coefficient of Friction, COF, is a very important parameter in the process of flexographic printing. For film substrates are particularly important to determine the static and dynamic coefficient of friction. Research has therefore been undertaken to determine the effect of the adhesion promoter on the coefficient of friction for OPP film. It should be stressed that low value is required due to the fast-working packaging machines. The test of COF were made for OPP film, which is a printing substrate before printing, substrate OPP, immediately after printing and after 20 minutes and after drying at 50° C. The printing sample were made using Labratester-automatic machine. Dried in a laboratory oven, SML. The coefficient of friction, COF, was measured by using a Zwick / Roell. The adhesion promoter reference No. 70GH278345 does not contain acetylacetone. It is used in flexo printing in order to improve adhesion and temperature resistance in following Gecko based. series: Gecko Frontal Eco, GFE, Gecko Frontal Uni, GFU, Gecko Frontal Shrink, GFS, Gecko Bond Top, GBT, Gecko Bond Star, GBS. Coefficient of Friction for printing substrate, OPP film and Gecko Frontal Eco CMYK printing inks, surface printing.

Keywords: Coefficient of Friction, adhesion promoter, printing ink.

1. Introduction and background

Coefficient of Friction (COF) is a very important parameter (Holm, 1938; Blau, 1995) in the process of flexographic printing. For film substrates are particularly important to determine the static and the dynamic coefficient of friction. Influence on the COF gives packaging manufacturers the opportunity to optimize productivity and avoid problems during the printing and packaging process, transport and storage of packaging. It should be stressed that low value is required due to the fast-working packaging machines (Meyer, et. al., 1999).

Research has therefore been undertaken to determine the effect of the adhesion promoter on the coefficient of friction for OPP film.

2. Materials and methods

The test of COF were made for OPP film, which is a printing substrate:

- before printing, transparent substrate OPP,
- immediately after printing,
- after 20 minutes and after drying at 50 °C.

The printing sample were made using Labratester-automatic machine. The machine used to transfer inks to the substrate. Printed samples dried in a laboratory oven, SML. The coefficient of friction, COF, was measured by using a Zwick / Roell testing machine. The COF measured in accordance with the PN-EN ISO 8295 NORM (International Organization for Standardization, 1995). The research focused on kinetic coefficient of friction.

2.1 Inks from hubergroup Polska company

In test used flexographic inks (Jakucewicz, 2001; Leach and Pierce, 1993) standard process CMYK to frontal printing series Gecko Frontal Eco. Gecko Frontal Eco solvent-based ink is designed as good value series for a variety of substrates, ideal for surface printing standard applications. The series is recommended for shopping bags or basic applications on OPP where specific fastnesses (e.g. deep freeze resistance) are not required, delivering an excellent overall full and halftone printability in flexo and gravure.

Special Properties (Huber, 2018):

- Excellent half- and fulltone printability
- Low solvent retention
- Good blocking resistance
- Good heat resistance (up to 160 °C)

May require adhesion promoter or adhesion enhancer on OPP only very occasionally addition of special additives is needed.

2.2 The additive adhesion promoter from hubergroup company

The adhesion promoter reference No. 70GH278345 does not contain acetylacetone. It is used in flexo printing in order to improve adhesion and temperature resistance in following Gecko based series:

- Gecko Frontal Eco, GFE,
- Gecko Frontal Uni, GFU,
- Gecko Frontal Shrink, GFS,
- Gecko Bond Top, GBT,
- Gecko Bond Star, GBS.

The mentioned additive can be added to flexographic inks and varnishes in amount to 6 % (maximum). The additive adhesion promoter was added into inks with following amount:

- 1 %, 2 %, 3 % and max. 6 % (according Technical information No. 11400).

2.3 Substrate OPP film

BOPP, thickness 20 µm, transparent biaxially oriented polypropylene film, both side heat sealable, for general purpose. Low water vapour content, odour permeability, slip and antiblock, facilitate its processing on packaging machines.

3. Results

The presentation focus on the results of the impact of the adhesion promoter No. 70GH278345, on COF, for OPP film printing substrate, and Gecko Frontal Eco CMYK printing inks, surface printing. The research focused on kinetic COF, and the effect of additive No. 70GH278345 on the COF. All results are presented in Tables 1 to 12.

3.1 Process Yellow No. 61GE02606; substrate: OPP film

Table 1: The impact of additive No. 70GH278345 on COF OPP film before drying, for Process Yellow ink No. 61GE02606

Additive quantity [%]	COF before drying Process Yellow + additive	COF before drying Process Yellow (without additive)	COF OPP film
1	0.19	0.18	0.17
2	0.21	0.18	0.17
3	0.20	0.18	0.17
6	0.15	0.18	0.17

Table 2: The impact of additive No. 70GH278345 on COF OPP film after drying, for Process Yellow ink No. 61GE02606

Additive quantity [%]	COF after drying Process Yellow + additive	COF after drying Process Yellow (without additive)	COF OPP film
1	0.17	0.15	0.17
2	0.24	0.15	0.17
3	0.19	0.15	0.17
6	0.16	0.15	0.17

Table 3: The impact of additive No. 70GH278345 on COF OPP film before and after drying; comparison, for Process Yellow ink No. 61GE02606

Additive quantity [%]	COF before drying Process Yellow + Additive	COF after drying Process Yellow + additive
1	0.19	0.17
2	0.21	0.24
3	0.20	0.19
6	0.15	0.16

3.2 Process Magenta No. 62GE820606; substrate: OPP film

Table 4: The impact of additive No. 70GH278345 on COF OPP film before drying, for Process Magenta ink No. 62GE820606

Additive quantity [%]	COF before drying Process Magenta + additive	COF before drying Process Magenta (without additive)	COF OPP film
1	0.22	0.16	0.17
2	0.19	0.16	0.17
3	0.18	0.16	0.17
6	0.16	0.16	0.17

Table 5: The impact of additive No. 70GH278345 on COF OPP film after drying, for Process Magenta ink No. 62GE820606

Additive quantity [%]	COF after drying Process Magenta+ additive	COF after drying Process Magenta (without additive)	COF OPP film
1	0.18	0.16	0.17
2	0.18	0.16	0.17
3	0.18	0.16	0.17
6	0.16	0.16	0.17

Table 6: The impact an additive No. 70GH278345 on COF OPP film before and after drying; comparison, for Process Magenta ink No. 62GE820606

Additive quantity [%]	**COF before drying Process Magenta + additive**	**COF after drying Process Magenta + additive**
1	0.22	0.18
2	0.19	0.18
3	0.18	0.18
6	0.16	0.16

3.3 Process Cyan No. 63GE820106; substrate: OPP film

Table 7: The impact of additive No. 70GH278345 on COF OPP film before drying, for Process Cyan ink No. 63GE820106

Additive quantity [%]	**COF before drying Process Cyan + additive**	**COF before drying Process Cyan (without additive)**	**COF OPP film**
1	0.20	0.19	0.17
2	0.18	0.19	0.17
3	0.17	0.19	0.17
6	0.17	0.19	0.17

Table 8: The impact of additive No. 70GH278345 on COF OPP film after drying, for Process Cyan ink No. 63GE820106

Additive quantity [%]	**COF after drying Process Cyan + additive**	**COF after drying Process Cyan (without additive)**	**COF OPP film**
1	0.19	0.16	0.17
2	0.20	0.16	0.17
3	0.20	0.16	0.17
6	0.18	0.16	0.17

Table 9: The impact of additive No. 70GH278345 on COF OPP film before and after drying; comparison, for Process Cyan ink No. 63GE820106

Additive quantity [%]	**COF before drying Process Cyan + additive**	**COF after drying Process Cyan + additive**
1	0.20	0.19
2	0.18	0.20
3	0.17	0.20
6	0.17	0.18

3.4 Process Black No. 69GE800506; substrate:OPP film

Table 10: The impact of additive No. 70GH278345 on COF OPP film before drying, for Process Black ink No. 69GE800506

Additive quantity [%]	**COF before drying Process Black + additive**	**COF before drying Process Black (without additive)**	**COF OPP film**
1	0.19	0.16	0.17
2	0.22	0.16	0.17
3	0.17	0.16	0.17
6	0.17	0.16	0.17

Table 11: The impact of additive No. 70GH278345 on COF OPP film after drying, for Process Black ink No. 69GE800506

Additive quantity [%]	COF after drying Process Black+ additive	COF after drying Process Black (without additive)	COF OPP film
1	0.17	0.16	0.17
2	0.21	0.16	0.17
3	0.18	0.16	0.17
6	0.18	0.16	0.17

Table 12: The impact of additive No. 70GH278345 on COF OPP film before and after drying; comparison, for Process Black ink No. 69GE800506

Additive quantity [%]	COF before drying Process Black + additive	COF after drying Process Black + additive
1	0.19	0.17
2	0.22	0.21
3	0.17	0.18
6	0.17	0.18

4. Conclusion

It can be noticed that the flexographic ink used in test - even without special additives affects the coefficient of friction of the tested film. It can be assumed that the ready ink changes the coefficient of friction. It can depend on solvents inside. It is the reason the difference mentioned parameter before and after drying printed sample.

Moreover, the main component in the formulation of each ink is system additive Gecko Eco. The additive Gecko Eco is responsible for printing properties. The additive GE has oleamide inside, responsible for decrease slip between surface in directly contact.

The additive adhesion promoter has influence on COF film in different ways. The higher COF is after drying, by amount 2 % added into Process Yellow , the result: 0.24, the lower is at a higher percentage 6 %, result: 0.15. It can be assumed that the higher influence has at a small percentage 1 % and 2 % added into each inks. The lower at the higher percentage promoter adhesion added into inks.

The COF film changed after drying, is more stable to COF printed samples each inks without additive and transparent OPP.

Summarizing results, tested additive added in the ready ink has a different effect on the coefficient of friction, depending on:

- the quantity of the additive,
- the type of film,
- the type of ink,
- drying time the printed samples.

References

Blau, P.J., 1995. *Friction science and technology*. Boca Raton: CRC Press.

Holm, R., 1938. The friction force over the real area of contact. *Wiss. Veroff. Siemens-Werk*, 17(4), pp. 38–42.

Huber, 2018. Specjaliści farb drukarskich. [online] Available at: <www.hubergroup.pl> [Accessed 1 January 2018].

International Organization for Standardization, 1995. *ISO 8295:1995 Plastics - Film and sheeting - Determination of the coefficients of friction*. Geneva: ISO.

Jakucewicz, S., 2001. *Farby drukowe*. Wrocław: Michael Huber Polska.

Leach, R.H. and Pierce, R.J. eds., 1993. *The printing ink manual*. 5th ed. Dordrecht, the Nederlands: Kluwer Academic Publishers.

Meyer, K.H., Herzau-Gergardt, U., Hars, C. and Kurz, R., 1999. *Technik des Flexodrucks*. 4th ed. St. Gallen: Rek & Thomas Medien.

Evaluating Contact Angle on Complex Surfaces to obtain a meaningful Surface Energy for Print Adhesion

Patrick Gane[1,2], *Cathy Ridgway*[1] *and Dirk Kisters*[1]

[1] Omya International AG, CH-4665 Oftringen, Switzerland

[2] School of Chemical Engineering, Department of Bioproducts and Biosystems, Aalto University, 00076 Aalto, Helsinki, Finland

E-mails: patrick.gane@omya.com; cathy.ridgway@omya.com; dirk.kisters@omya.com

Short abstract

Wettability of surfaces is a key factor in many industrial printing, converting and finishing processes. Surface energy balance between the surface and the liquid is the determining factor defining wet print adhesion. The sessile drop method is used to determine the contact angle at the circumference wetting front between a droplet of liquid and the surface. However, on highly complex surfaces, being designed to absorb, for example, inkjet ink vehicle, or displaying reactive properties with solvents and interaction with surface roughness or patterning on non-absorbent surfaces, measuring he contact angle using relevant liquid involves many uncertainties if limited to the accepted analysis of a state of equilibrium. We propose an analysis which accounts for a realistic estimate of the surface free energy at the instance of liquid-surface contact to assist in the design of desirable ink/varnish-surface interaction properties.

Keywords: contact angle, porous coating, inkjet printing, surface free energy, complex surface, absorbing surface, reactive surface

1. Introduction and background

Wettability of surfaces plays a major role in many industrial processes, ranging from coating, gluing and printing to plant protection and the application in medicine of pharmaceutical active agents. Surface free energy balance between the surface and the liquid is the determining factor defining either phobicity or philicity (wettability) of the surface toward a specific liquid. In the case of requiring adhesion of wet ink or varnish to the surface during application it is necessary to satisfy the positive work of adhesion between the liquid and the solid, W_{ls}, in respect to the balance of surface free energy and liquid surface tension such that

$$W_{1s} = \gamma_1 + \gamma_s - \gamma_{s1} \qquad [1]$$

where γ_1 and γ_s are the surface tension of liquid and the surface free energy of the solid surface phase, respectively.

Usually, a sessile drop method is used to determine the contact angle, θ, at the circumference wetting front between a droplet of liquid and the surface. Equation [1] can be restated in terms of the contact angle using the Young-Dupré equation

$$W_{1s} = \gamma_1 (1 + \cos\theta) \qquad [2]$$

However, on highly micro and nanoporous surfaces, being designed to absorb, for example, inkjet ink vehicle, or on surfaces that display chemical reactivity with the liquid or complex roughness/patterning, measuring the contact angle involves many uncertainties as the Wenzel model for considering surface roughness or voids is neither relevant for a continuously absorbing surface, nor for a description of a reactive surface or one that shows complex roughness. For phobic surfaces, nonetheless, the Cassie-Baxter model naturally remains valid even though the surface may be porous due to the lack of absorption.

2. Stages of wetting on a complex surface

Figure 1 shows a schematic of the stages of wetting in the case of an absorbing surface. When applying the sessile liquid droplet to the surface there is some initial inertia retained in the liquid mass as the droplet-forming needle in a typical experimental apparatus is moved away and disjoined from the droplet, whilst simultaneously, if the liquid wets the surface, the droplet interfaces with the solid and the air becoming further extended and, as a result, the bulk liquid is accelerated inducing a further inertial component. These inertial kinetic effects distort the observed contact angle over short times. In addition, as soon as the droplet contacts the wetting surface the fluid starts to absorb into the porous network structure of the sample. Since this network structure is 3-dimensional, not only does the liquid absorb into the bulk pore volume (*z*-direction) but it traverses beneath the surface laterally in the *xy*-plane, and necessarily re-emerges at the surface at a position that may be ahead of the contact wetting line between the droplet and *xy*-plane. This results in the contact line at the interface consisting of solid, liquid in the surface pores and the liquid of the droplet itself, such that the interface surface energy balance is not solely between liquid and the desired measurable surface but is modified by the liquid already migrated into the neighbouring surface pores. As time progresses this ratio of filled pores to virgin surface increases, resulting in an equilibrium contact angle reflecting this ratio of surface void and surface solid.

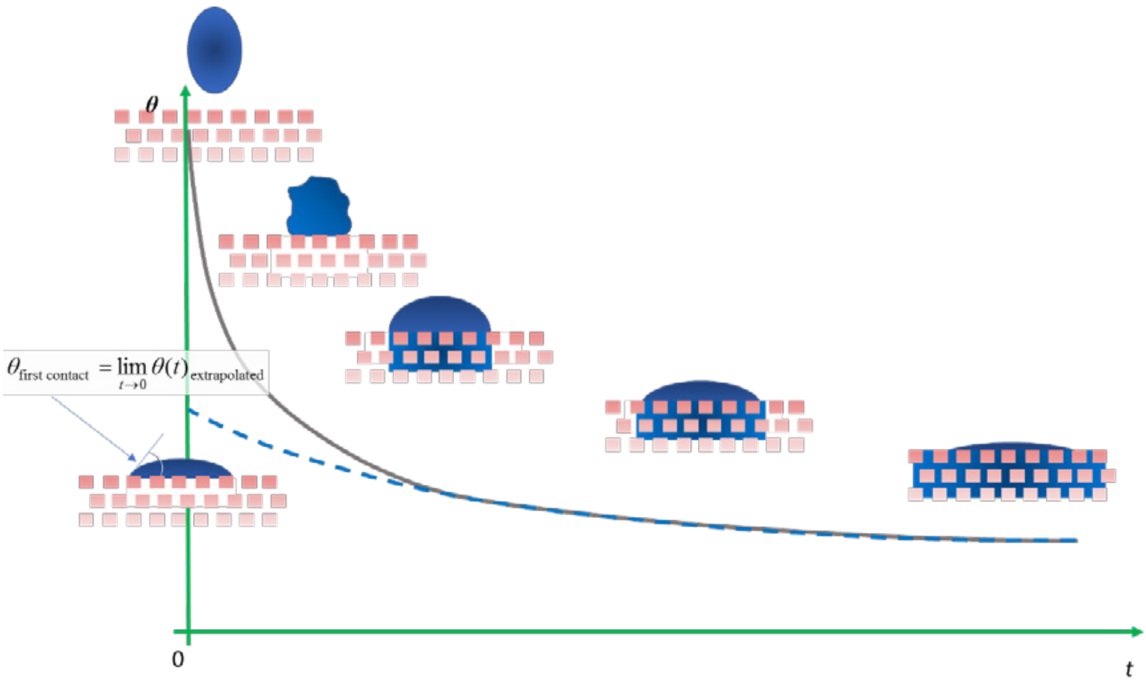

Figure 1: Schematic diagram showing stages wetting of a drop during contact angle measurement: the proposed extrapolation to zero time is shown as the dashed curve

There may also be surface roughness on the scale of the micro-solid regions or larger scale roughness spanning both the solid and liquid filled surface, as well as possible material inhomogeneities in the surface itself, e.g. regions of binder, added polymeric water retention aid(s), dispersants and pigment particles of present. The contact angle is, thus, constantly changing with time, firstly discontinuously in the advancing state and secondly discontinuously in the retreating state if evaporation is occurring and/or continued absorption. These factors raise significant doubt in the meaning and reliability of the apparent surface free energy result at any stage of the droplet evolution on the surface.

Other classes of materials may themselves not necessarily be absorbent. The sample may perhaps be slightly soluble in the contacting liquid, which can also manifest itself in a change in contact angle after in addition to or after the inertial contact period. Measuring the contact angle on a changing surface using an interacting liquid becomes hugely complex, especially of the interaction yields reaction products, maybe even including a gaseous phase. In either case, this results in the contact line consisting of solid, liquid and solubilised material and the liquid itself, such that the interface surface energy balance is not solely between liquid and the desired measurable surface but is modified by the liquid already having migrated amongst the molecular structure. There may also be surface roughness on the scale of the micro-solid regions or larger scale roughness spanning both the solid and interacted surface, as well as further possible material inhomogeneities in the sample, e.g. regions of polymer and filler in the case of plastics. The contact angle is, thus, constantly changing with time.

The factors discussed above raise significant doubt in the meaning and reliability of the apparent surface free energy result at any stage of the droplet evolution on the surface.

3. Method proposal

We newly propose a method to derive a relevant initial contact angle based on the supposition of the ever-increasing ratio of liquid-filled pores/modified surface to that of the virgin surface as a function of time until equilibrium is reached. Thus, by fitting the observed contact angle development with time from the point where it is judged the inertial factor has dissipated until the equilibrium plateau value is reached it is suggested that an extrapolation back to zero time delivers a more relevant contact angle of the droplet liquid related to the surface as if it consisted totally of original surface material or the structure that is relevant. Following this procedure, we can report the initial advancing contact angle value, $\theta_{\text{first contact}}$, derived as

$$\theta_{\text{first contact}} = \lim_{t \to 0} \theta(t)_{\text{extrapolated}} \qquad [3]$$

as exemplified in Figure 1 (shown schematically).

Experience shows that a polynomial of order ≤ 4 generally captures the nature of the curve reasonably well without introducing non-physical results. In addition, we undertake to make the fit with the lowest order possible whilst remaining coincident with the experimental data. What is more, the higher the order of polynomial the more rapidly the function oscillates and so this precludes high orders as being non-physical *per se*. The problem here is that the underlying physics, or more exactly the order in which the many factors at play manifest themselves, cannot be precisely defined in each case. This is because all the mechanisms acting depend on the surface energy, and that, unfortunately, is unknown as it is the parameter trying to be measured. This unknown parameter leads, therefore, to a vicious circle in that it is impossible to provide an overarching combination of mechanisms even though each mechanism in principle might be assumed to be known, but the magnitude and rate related through the surface free energy remains unknown. Possibly an iterative method could be used in some cases where the surface is non-complex, i.e. make a measurement, then model all the factors with that resulting surface energy and see how it fits, then remeasure and so on until convergence is found. However, if the surface is so simple that this could be applied then it is likely an equilibrium contact angle can be measured anyway. The drawback in proposing such a procedure for more complex surfaces is that one must know *a priori* all the mechanisms occurring and the interactions under which they act. This is not easy, and we give the example of modelling absorption into complex porous media – the best is an approximation based on a model structure, as real structures cannot be fully exploited as the computational complexity is intractable.

In the same way, the time considered for the curve fitting is defined (a) by being post inertial oscillation of the droplet, and (b) before any discontinuities occur in the contact angle, related, for example, to Haines' jumps, chemical reaction with the surface or excessive evaporation. The extrapolation is applied to data obtained from a Dataphysics OCA 50 sessile drop device, capable of delivering drop volumes down to 30 pL, with options to reduce even further to the nL range. A high-speed microscope camera captures the evolution of the droplet configuration over time after it is deposited on the surface. Image analysis and chosen curvature fitting software can be applied in relation to a user-defined linear continuous liquid-solid interface to determine the droplet meniscus shape, droplet volume and contact angle with the surface. The surface free energy may be calculated using the Owen, Wendt, Rabel and Kälble (OWRK) calculation (Kaelble, 1970; Owens and Wendt, 1969; Rabel, 1971) with the database liquids water (Ström, Frederiksson and Stenius, 1987), diiodomethane (Ström, Frederiksson and Stenius, 1987) and ethylene glycol (Gebhardt, 1982).

4. Example studies

4.1 Porous surface

For this study, the initial advancing contact angle value thus derived, $\theta_{\text{first contact}}$, has been used (taken as the average of 3 measurements) to determine the effective surface energy for liquid contact on two representative pigmented paper coatings, A and B (Figure 2). The procedure is applied to example data fitting using a suitable polynomial for three liquids used to determine effective surface energy.

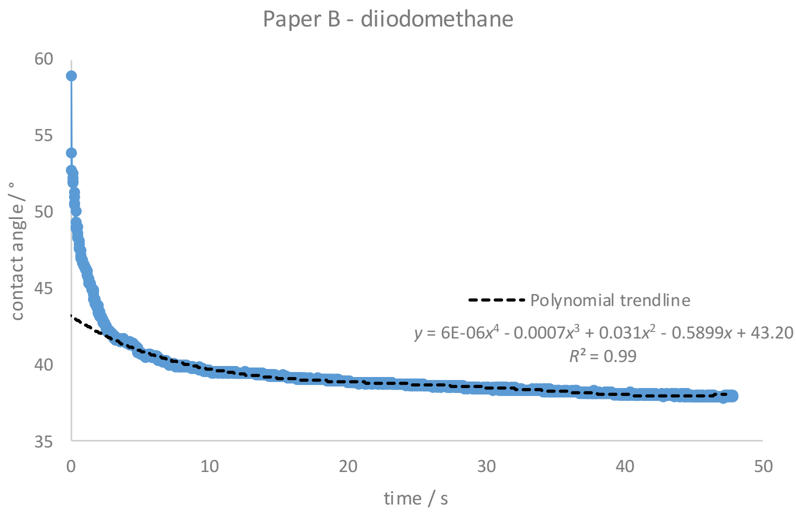

Figure 2: Example fitting to determine the initial advancing contact angle $\theta_{\text{first contact}}$ of diiodomethane on the absorbing coated sample Paper B

Table 1 shows the extrapolated initial advancing contact angle values $\theta_{\text{first contact}}$ as shown in Figure 3 for the three fluids on the paper samples.

Table 1: Values of initial contact angle $\theta_{\text{first contact}}$ of three fluids on the two coated paper samples

Sample	Average initial extrapolated contact angle ± standard deviation / °
Paper A water	52.78 ± 2.94
Paper B water	44.43 ± 1.53
Paper A diiodomethane	37.20 ± 3.50
Paper B diiodomethane	44.11 ± 1.85

Paper A ethylene glycol	48.44 ± 0.90
Paper B ethylene glycol	48.74 ± 2.08

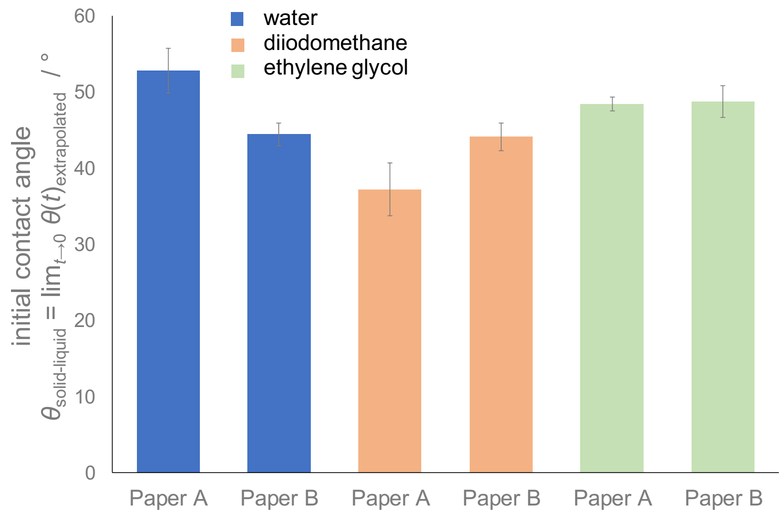

Figure 3: Initial advancing contact angle $\theta_{first\ contact}$ of the three test fluids on the two paper samples

Table 2 and Figure 4 show the surface free energy values calculated for the paper samples using the novel extrapolated value of initial advancing contact angle.

Table 2: Values of surface energy of the three fluids on the samples

Sample	**Total surface energy ± standard deviation / mN·m^{-1}**	**Dispersive ± standard deviation / mN·m^{-1}**	**Polar ± standard deviation / mN·m^{-1}**
Paper A	48.08 ± 1.76	33.46 ± 0.93	14.62 ± 0.83
Paper B	49.65 ± 1.28	29.10 ± 0.89	20.55 ± 0.40

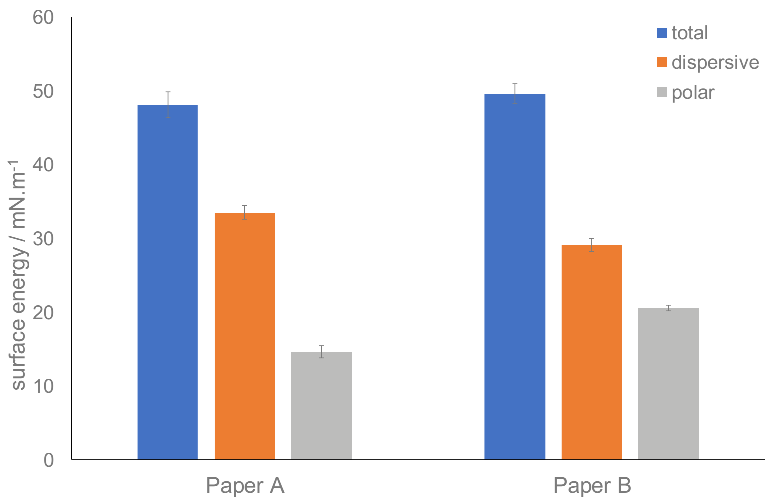

Figure 4: Surface free energy derived from the three fluids on the two paper samples

The total surface free energy of the Paper B sample is seen here to be slightly higher than that for the Paper A sample. The Paper B sample has a higher polar surface energy value based on the extrapolated initial advancing contact angle value, and exemplifies the potential of the method to deliver a meaningful surface interaction energy for an absorbent porous medium.

4.2 Non-porous surfaces

4.2.1 Reactive/inhomogeneous surface

Figure 5: Pigment filled polymer (dog-bone shaped) sample
(14.7 cm long, 2.0 cm wide at ends, 1.0 cm wide in the middle, 0.4 cm thick)

Here we take the example (Figure 5) of recycled polymer filled with a suitably surface treated alkali metal carbonate filler, designed typically to deliver enhance stiffness and impact resistance to a native polymer matrix.

In Figure 6 we see the behaviour recorded for the droplet contact angle of the various liquids as a function of time used to determine surface free energy. Clearly, the initial contact period for water is not only displaying the inertial region, but also a significant step function as time proceeds. Given the unknown nature of the contact behaviour during this step function, extrapolation is used once the first monotonic behaviour is reached. Diiodomethane, is behaving classically – if only all such measurements were so! – and an equilibrium contact angle can easily be determined. The picture is different, however, for ethylene glycol, where we see several subsequent steps in the contact angle as a function of time, indicating a likely interaction with the surface or the jump effect of the liquid in contact with surface inhomogeneities, in which case an extrapolation is used from the first section of this behaviour to represent the most likely initial state of contact between the liquid and the surface.

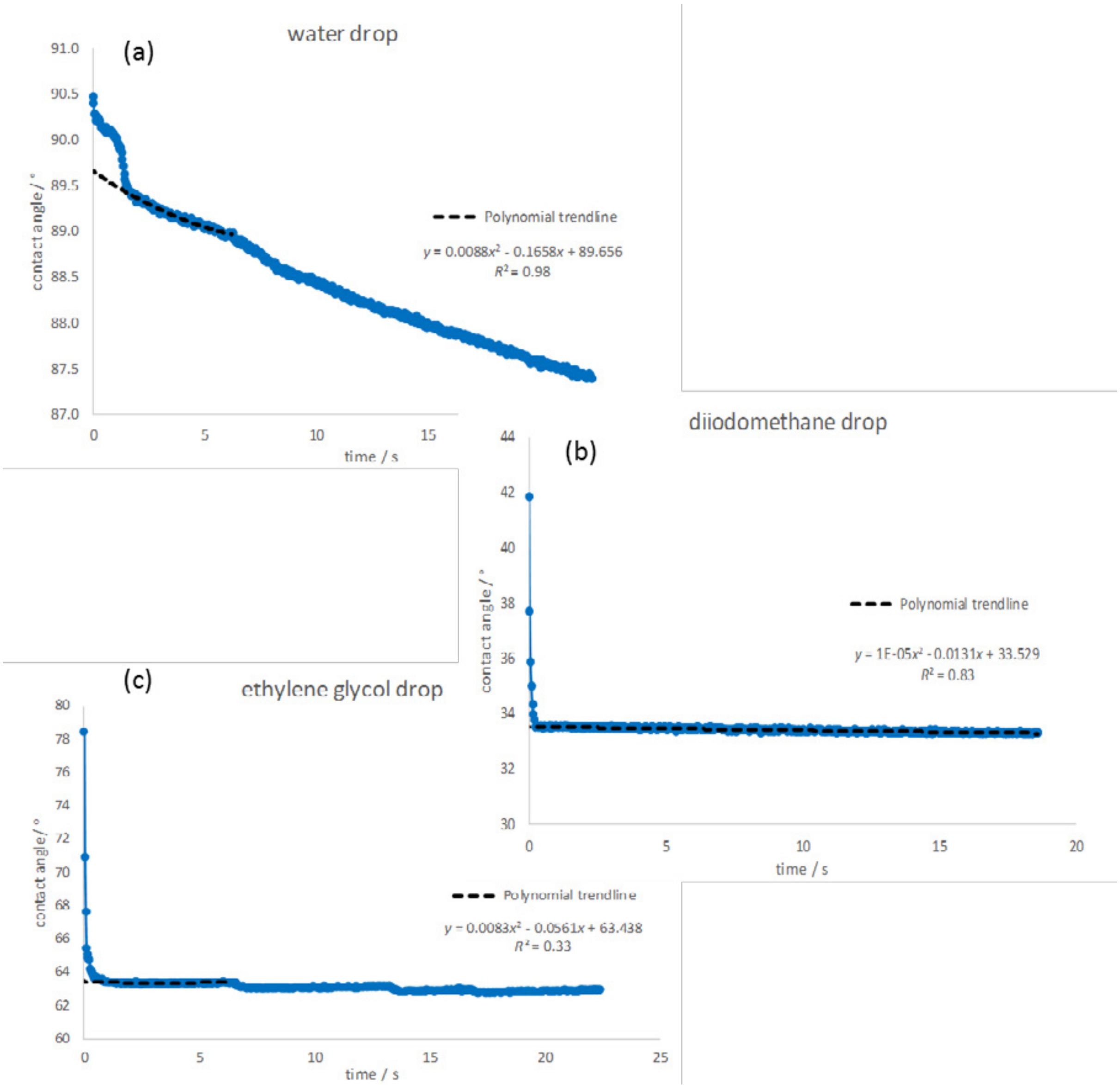

Figure 6: The contact angle development as a function of time for (a) water, (b) diiodomethane, and (c) ethylene glycol

The resulting surface free energy values are displayed in the chart in Figure 7.

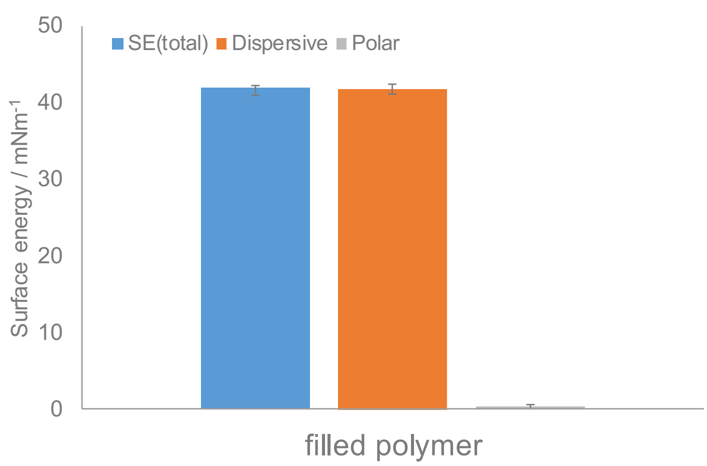

Figure 7: Surface free energy – polar and dispersive components

4.2.2 Complex roughness

As a liquid wetting front approaches a discontinuity in the form of a step or sharply defined feature on the sample surface the contact angle abruptly changes. It can be that the angle momentarily exceeds 90°. Under this condition the wetting becomes terminated and the liquid meniscus front halts in a pinned position. Eventually, due to molecular diffusion, surface and/or pore condensation, the liquid continuity is re-established on a molecular or thin film level, such that the front can jump forward and return to its previous wetting progress. Such a sudden change is termed a Haines' jump (Zacharoudiou and Boek, 2016), and is often associated with an equilibrium change in contact angle.

Figure 8: Water on PET – example of surface roughness (area 10 mm × 13 mm)

In Figure 8 we observe a complex surface microroughness under grazing angle illumination in the form of a polyethylene terephthalate (PET) surface. Studying the wetting property for water, in terms of contact angle as a function of time, Figure 9, the Haines jump phenomenon is seen occurring on a timescale of between 1 s and 2 s, preventing an equilibrium being reached monotonically.

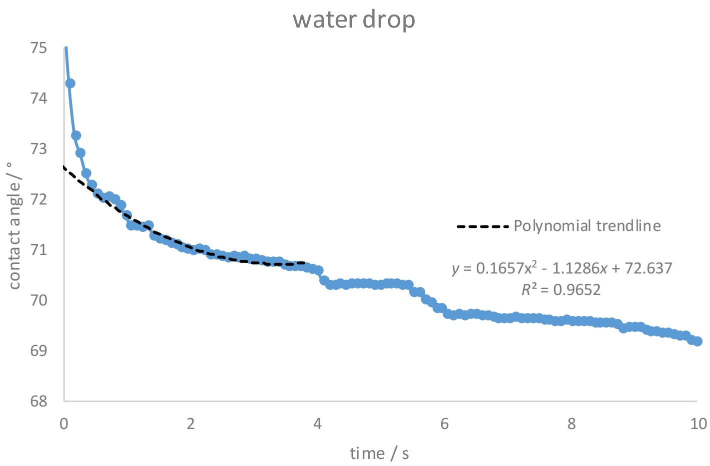

Figure 9: Evolution of contact angle as droplet spreads over surface roughness – $\theta_{first\ contact}$ = 72.6°

5. Conclusions

Surfaces used for printing are becoming ever more complex, especially when considering new materials in packaging and for functional printed designs. Costly time and materials can be wasted seeking to print on a surface that is unsuitable in respect to surface energy balance with that of the ink or varnish to be printed or coated. To ensure adhesion in the wet state during transfer it is essential to be able to have a realistic measure of the surface wetting property and effective surface energy. Surfaces that are designed to be porous, liquid reactive or have a complexity of surface roughness patterning can be particularly difficult to characterise using the traditional sessile drop method. To overcome the shortcomings of the measurement under non-equilibrium conditions, the authors propose a method of extrapolation of the contact angle using the first period of monotonic behaviour after the inertial region to establish and effective advancing contact angle representing the first moment of contact.

The method is exemplified, and the experience of the authors working in an industrial testing laboratory is that enquiries from the printing industry, coatings and metals industry and polymer materials industry, food and personal care, to name but a few, are steadily increasing as practitioners find the results bring an extra security to their operations and support successful developments.

References

Gebhardt, K.F., 1982. *Grundlagen der physikalischen Chemie von Grenzflächen und Methoden zur Bestimmung grenzflächenenergetischer Probleme*. Stuttgart: IGB.

Kaelble, D.H., 1970. Dispersion-polar surface tension properties of organic solids. *The Journal of Adhesion* 2(2), pp. 66–81.

Owens, D.K. and Wendt, R.C, 1969. Estimation of the surface free energy of polymers. *Journal of Applied Polymer Science,* 13(8), pp. 1741–1747.

Rabel, W., 1971. Einige Aspekte der Benetzungstheorie und ihre Anwendung auf die Untersuchung und Veränderung der Oberflächeneigenschaften von Polymeren. *Farbe und Lacke* 77(10), pp. 997–1005.

Ström, G. Frederiksson, M. and Stenius, P., 1987. Contact angles, work of adhesion and interfacial tensions at a dissolving hydrocarbon surface. *Journal of Colloid and Interfacial Science*, 119(2), pp. 352–361.

Zacharoudiou, I. and Boek, E.S., 2016. Capillary filling and Haines jump dynamics using free energy Lattice Boltzmann simulations. *Advances in Water Resources*, 92, pp. 43-56. https://doi.org/10.1016/j.advwatres.2016.03.013.

Assessing the Quality of Pad-printed Images by evaluating Edge Sharpness

Christina Bodenstein[1], *Hans Martin Sauer*[1], *Felipe Fernandes*[1], *Edgar Dörsam*[1] *and Elisabeth Warsitz*[2]

[1] Technische Universität Darmstadt, Institute of Printing Science and Technology
[2] Franz Binder GmbH & Co. Elektrische Bauelemente KG, Neckarsulm
E-mail: bodenstein@idd.tu-darmstadt.de

Short abstract

We analyzed the edge sharpness and edge defects of pad-printed patterns and developed an image-based method to quantitatively assess the quality of edge patterns. We traced the two types of observed defects, filament formation and stamp effects, to the printing parameters, and the gravure features of the printing form, respectively. By optimizing the printing velocity, printing pressure and gravure, we were able to reproduce patterns with an edge roughness of less than 2 µm. With this process optimization, it seems feasible to use pad printing for source and drain contact manufacturing on printed thin film transistors. Thus, the reproduction of electrically conductive, interdigital patterns for sources and drains having an electrode distance of less than 10 µm appears possible.

Keywords: pad printing, printed electronics, edge sharpness and roughness, quality control, evaluation method

1. Introduction and background

Pad-printing is often used to print small, high-resolution patterns on curved surfaces. This technology is also known as indirect gravure printing technology since the printing pattern is engraved and the ink in it is picked up by a flexible subcarrier, the pad. The pad is made of elastic, compressible silicone and can thus adapt to curved surfaces. This makes it feasible to print on dye-cast plastic bodies, pre-structured PCB boards, 3D-printed rapid prototypes and individually-shaped surfaces in a most cost-efficient manner. Moreover, the low-energy silicone surface permits complete transfer of ink from pad to substrate, leaving a perfectly clean pad for the next transfer sequence.

In recent years, new technologies for producing printing forms such as direct laser engraving, have become available. Alternative gravure patterns beyond the classical gravure cell raster are now possible, tailored to specific applications and printing inks, and this promise substantial progress in printing resolution and quality.

Particularly for printed electronics, pad-printing is becoming more widely used, with successful applications in solar cells (Hahne, et al., 2001; Krebs, 2009), microwave antennas (Xiong and Qu, 2011), sensor structures (Leppävuori, et al., 1994), UHF RFID (Merilampi, et al., 2011), electrodes (Mooring, et al., 2005), electroluminescence (Lee, et al., 2010) and source-drain structures (Willfahrt, 2007).

Especially in fields of printed electronics it is important to evaluate the printed patterns, since in this area functional materials with electrical properties are used. Instead of pigments or dye, that are responsible for colouring in a common printing ink, particles with electrical properties are used. When printing microstructures the edges play a significant role. Typical appearing defects in pad-printing have to be avoided, without changing the electrical properties of the ink to guarantee stable conditions of the printed component. These defects, which will be discussed in detail later, lead to a dysfunction of the component. Up to now evaluating printed edges was empiric in pad-printing. In this study, we introduce and demonstrate a method that systematically reduces printing defects by evaluating and controlling the edge roughness of pad-printed images.

In indirect gravure printing technology, the printing pattern is engraved as a raster of microscopic cells on a planar printing form. The size of these cells, usually a few tens of microns in width and depth, determines the amount of ink transferred to the surface of the substrate. The pad printing process is shown in Figure 1. After the engraved cells are filled with ink and excess material is removed from the walls by blading (a), a soft silicone pad is pressed against the printing form (b). When the pad is lifted from the printing form (c), it takes the ink out of the cells (d) and subsequently deposits it on the surface of the substrate (e, f).

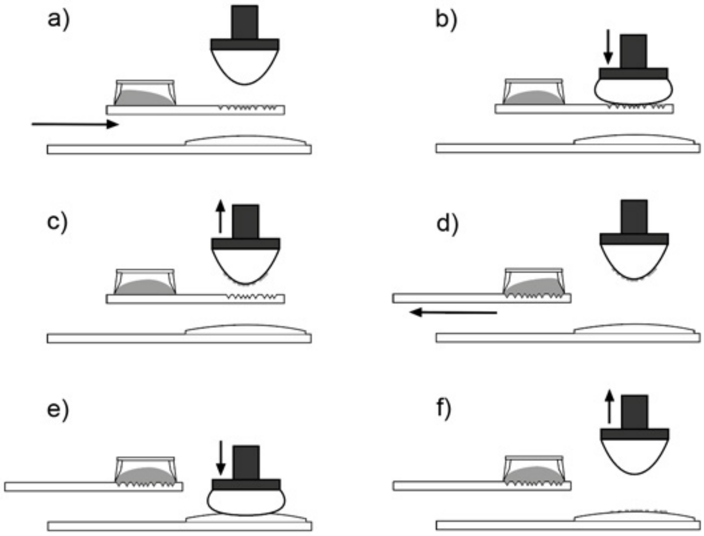

Figure 1: Schematic of pad printing process

2. Materials and methods

The pad printing machine used in the experiments is based on the machine described by Hakimi Tehrani and Dörsam (2016). We modified it, by replacing the pneumatic drives of the gravure plate and pad holder by linear stepper drives. These drives were controlled via a National Instruments LabVIEW programme. This allows to independently control each motion of the printing process in distance and velocity, thus making this machine a unique research platform for process evaluation. To increase the versatility of our setup, we also installed force sensors. This enables independent control of each motion by setting forces instead of positions.

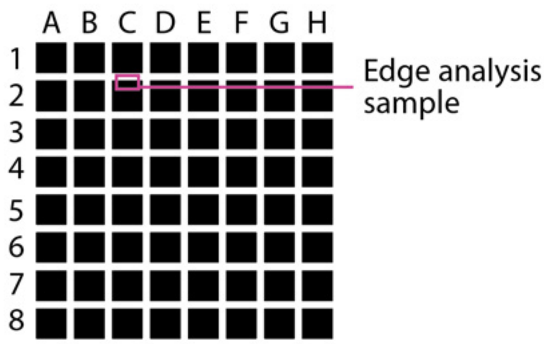

Figure 2: Printing layout and field C2 as edge analysis sample

We used a chessboard printing pattern with 64 squares, each with an area of 4 mm × 4 mm. Each square is assigned a column (A – H) and row (1 – 8) identifier, as shown in Figure 2, where the upper edge of field C2 is verified. We used printing forms made of polymer or steel with raster widths of 80, 100, and 120 L/cm (lines per centimeter) and area coverage of 86 %. The printing forms are from ITW Morlock GmbH, Dornstetten, Germany. We chose the solvent-based printing ink from Marabu GmbH & Co. KG, Tamm, Germany, type TPL 489 (black) due to its universal applicability on a big variety of materials. The ink is blended with a suggested amount of 20 vol % of solvent (TPV) to adjust the viscosity. The antistatic pad (TP082 (blue) 12 Shore A with the dimensions 67 mm height, 84 mm × 74 mm ground plate) is from Tampoprint AG, Korntal-Münchingen, Germany; and the substrate is a 125 µm PET Hostaphan GN 4600 foil from Pütz GmbH + Co. Folien KG, Taunusstein, Germany. Printing velocities were initially set to 200 mm/s in each process step. The velocity of the pad lift-off motion (Figure 1, (c)) was reduced to 50 mm/s for reasons that will be discussed in detail later.

To use an automatic edge-recognition software tool on printed patterns, one must precisely map a three-dimensional feature onto a continuous line, as shown in Figure 3. This results in a printed three-dimensional layer, with edges on top or in direct contact with the substrate. The critical edge which is used for edge evaluation in this work is specified in Figure 3.

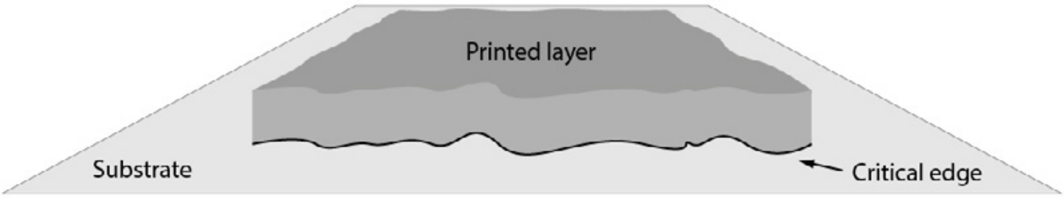

Figure 3: The three dimensions of a printed layer

After the printing process, it is likely that the edges are not perfectly even (Figure 3). On top of that printing defects are occurring. The most critical of these defects are those found at the edges: thin ink bridges that extend beyond the desired border. Without controlling these defects on conductive patterns, that lead to a short circuit between adjacent electrodes. Thus, in printed electronics, it is especially important to precisely evaluate the resolution of printed microstructures.

To evaluate this critical edge, we take microscope images from the top view of the printed samples to map the three-dimensions onto a plane to detect the edge. To characterize height profiles, we adapted the roughness measures used in surface technology, as illustrated in Figure 4. Here, L_m is the centre line and di is the distance from a peak to the centre line. We applied this procedure to the top view of the border lines of the printed samples, which were measured by optical microscopy. By applying digital contrast amplification, thin ink bridges and residuals can be observed, regardless of the printed layer's local thickness.

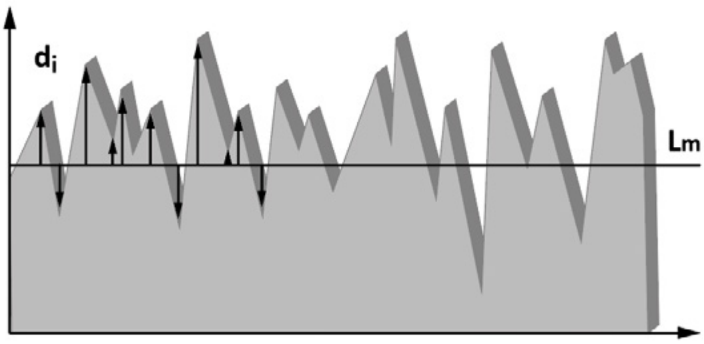

Figure 4: Roughness measure for height profiles

In this work, the edge roughness is defined as R_m, the average absolute distance between the desired border line and the actual border line. This is calculated via equations [1] and [2] and is used as an edge roughness and blurring measure.

$$L_{\mathrm{m}} = \frac{1}{n}\sum_{i=1}^{n} d_{\mathrm{i}} \qquad [1]$$

$$R_{\mathrm{m}} = \frac{1}{n-1}\sum_{i=1}^{n} |d_{\mathrm{i}} - L_{\mathrm{m}}| \qquad [2]$$

With n we denote the number of measuring points from L_m to each d_i. Using digital contrast amplification, regardless of the local thickness of the printed layer. A perfect edge sharpness is R_m = 0 µm. For R_m > 0 µm we talk about edge roughness.

For the digitalized measurement analysis, we implemented a tool using Matlab software. The initial aim of the tool is to detect the straight center line L_m and the actual printed critical edge, for purposes of calculating R_m as described above. Printed patterns were determined using a digital Leica microscope DM4000M camera image with a tenfold magnification objective lens. In our validation experiments, we took images from the upper edge of field C2 in the layout (Figure 2) of the printed samples.

The tool we developed to analyze printed edges works as follows. As shown in Figure 5, the acquired RGB image (1.) is converted to an 8bit grayscale (2.) image, with gray levels between 0 (black) and 255 (white). The image contrast is adjusted such that 1 % of the data has a gray value of 0, whereas the top 1 % of the data has a gray value of 255. This yields a more robust edge distinction (3.). The edge of the printed image is detected using a Canny edge algorithm (Canny, 1986). Because the edge points obtained are not continuous, dilatation and erosion processes are performed (4.) to reconstruct a continuous edge between the left and the right image border (5.). The end points of the reconstructed edge are then connected by a straight line L_m (6.). The average absolute distance R_m between L_m and the detected edge is calculated with pixel-to-pixel resolution and a pixel distance of 0.5 µm.

Note that this algorithm is well-defined even when there is a non-unique mapping of the center line to the border curve (e.g., for tilted or curved ink filaments) or when isolated ink residuals are situated close to the rim.

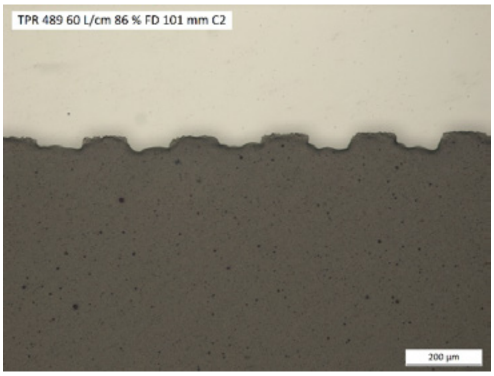

1.: Original image

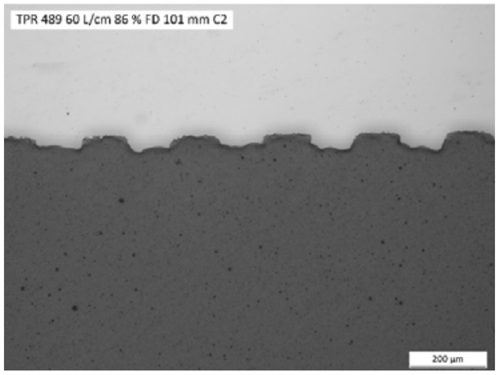

2.: Grayscale image

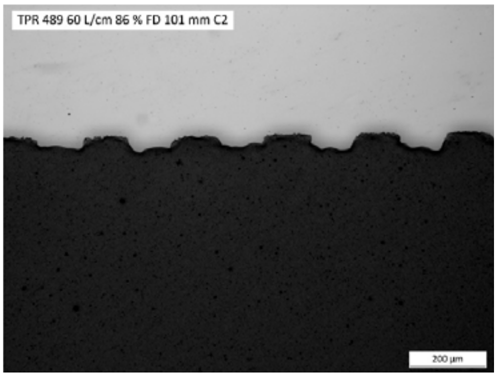

3.: Adjusting contrast

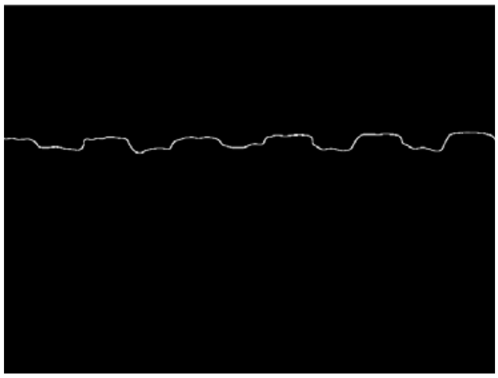

4.: Reconstruction of the printed edge based on Canny edge detection

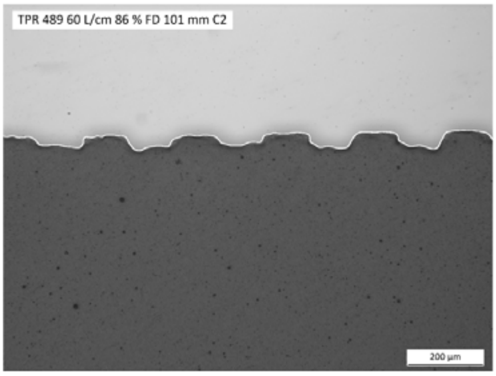

5.: Overlay of grayscale image and reconstructed edge

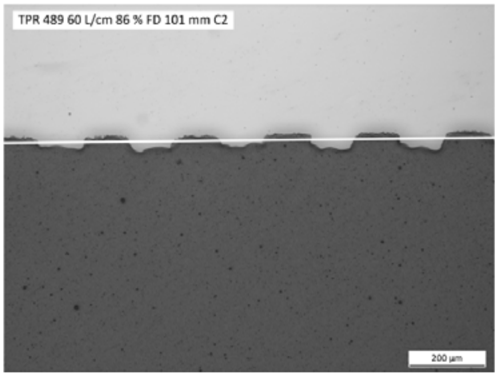

6.: Determining straight edge line L_m

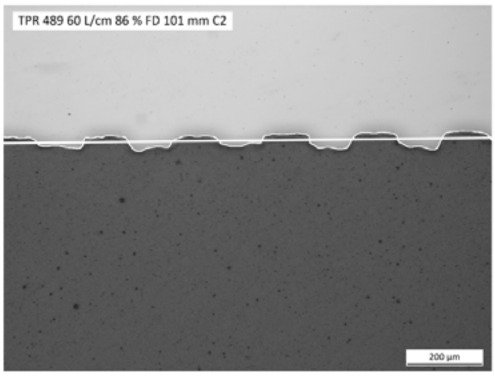

7.: Grayscale image with detected edge and L_m

Figure 5: Steps of image processing for determining straight edge line L_m and average roughness R_m at field C2

3. Results and discussion

We have identified two major classes of edge defects, a "stamp" defect and an ink filament defect, and offer systematic strategies to treat them.

As clearly seen in Figure 6, the stamp defect is related to the raster dots at the border of the ink transfer areas on the printing form's surface. The sharpness measured on the printed patterns (Figure 7) is quite variable in the individual fields and ranges from 10 µm to 35 µm. A closer comparison with the gravure patterns of the printing form reveals that this type of defect is related to the relative gravure cells' row distance to the geometric border of the respective field on the printing form.

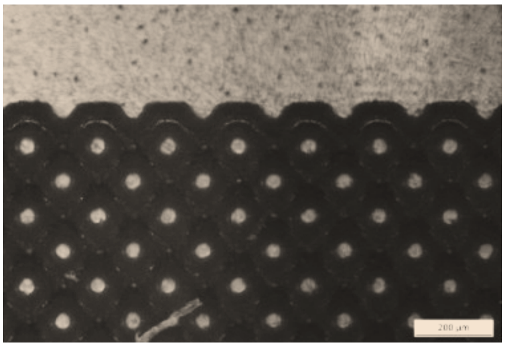

Figure 6: Image of a conventional produced printing form

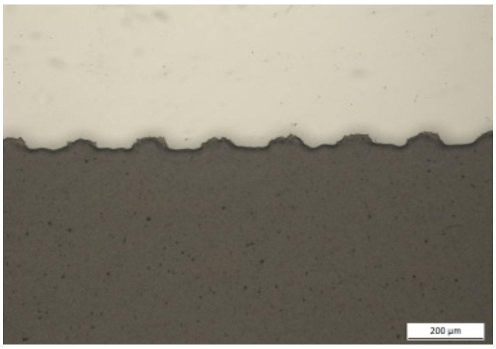

Figure 7: Image of printed result with transferred stamp defect

The raster in pad-printing forms are necessary when printing large-scale areas to prevent tilting of the blade in the blading process (Figure 1, a) and displacing the ink by the pad when pressing against the printing form (Figure 1, b). The printing layout is designed with a software, for example Adobe Illustrator. In the conventional pad-printing form production the process is divided into two exposure steps. In the first step the light-sensitive plate material is exposed with a film of the printing layout. The second exposure step is placing a film that is fully covered with the desired raster width onto the printing plate. In this step the raster dots are developed and thus the shape of the raster dots also occur at the edges of the printing image in the form of a wavy contour, the so called "stamp effect" (Figure 6) and will be transferred to the printed image (Figure 7).

If rastered printing images with straight edges and without these defects are desired so-called outlines should be used (Hahne, 2001). These outlines must be implemented in the digital layout design by aligning a contour inward around the layout with a width of 50 µm. Thus, in the printing form production (exposure or etching), outlines eliminate the raster dots at the edges (Figure 8) and reveal in a printed result as shown in Figure 9 with a straight edge.

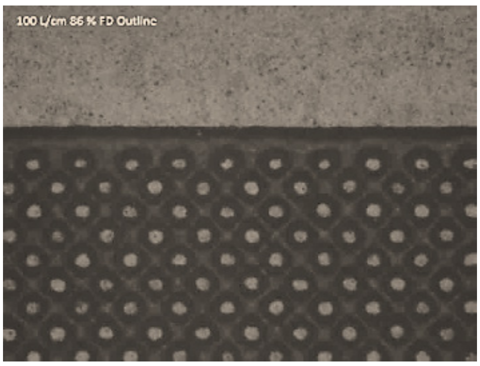

Figure 8: Image of a printing form with outlines

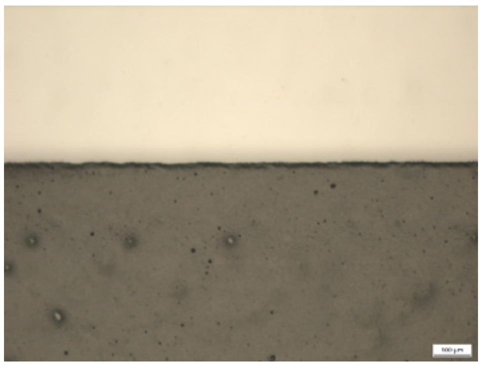

Figure 9: Image of printed result with a straight edge

The second defect type, thin ink filaments emanating from the borders, is illustrated in Figure 10. These filaments are roughly 1 µm thick and can be as long as 200 µm. Since they are usually invisible to the naked eye, they clearly represent a major issue for printed electronic components.

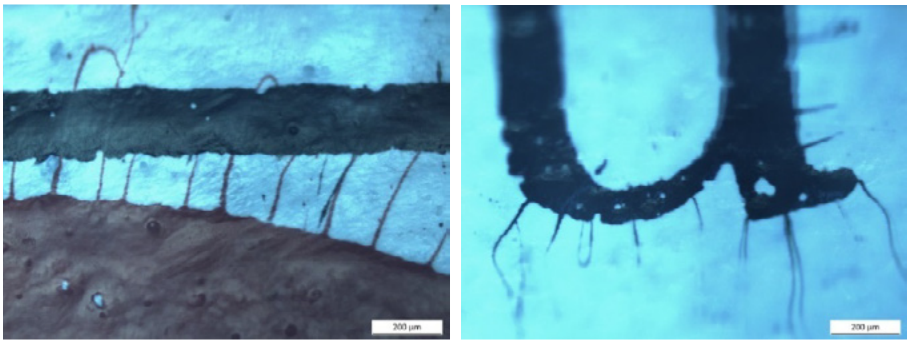

Figure 10: Images of ink filaments at the borders (tenfold magnification) in graphical applications

As long as filaments are 1 µm or less in thickness, they are usually not considered critical for graphical applications. Figure 11, however, shows an image in which conductive silver ink is used. Here, the filaments lead to electrical short circuits - clearly a critical defect.

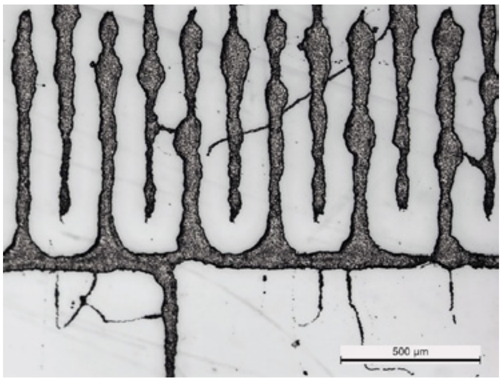

Figure 11: Image with ink filaments at borders short circuiting the conductive patterns

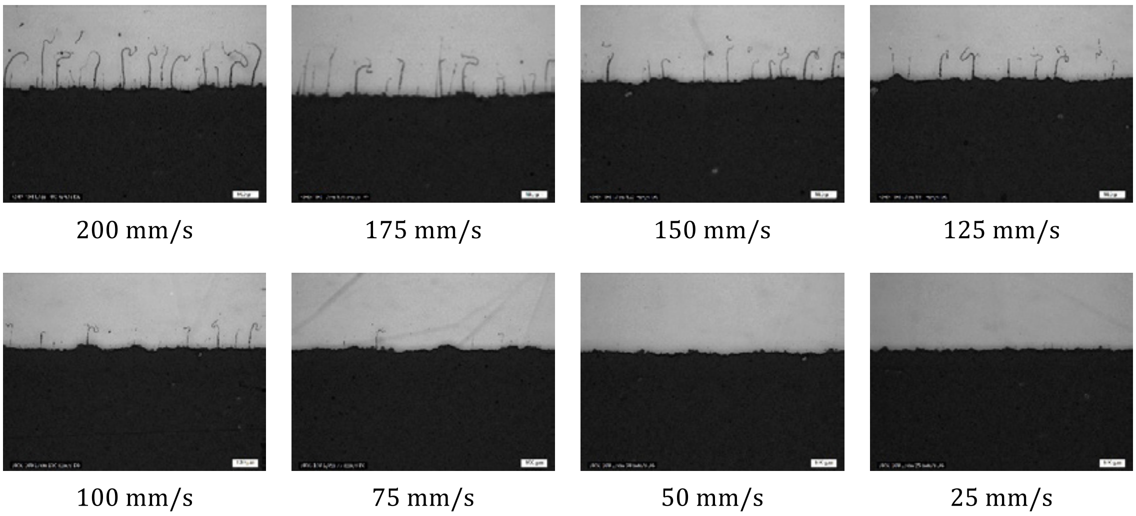

Figure 12: Influence of lift-off velocity of pad from printing form on ink filament formation (fivefold magnification)

We studied the effect on filament formation of pad deposition and retraction velocities from the printing form and substrate. Filament formation was more pronounced when the pad was more rapidly lifted-off the printing form. In the instant the pad separates from the form, it takes up ink from the gravure cell and splits the ink. We tentatively identify this (Figure 1, (c)) as the origin of filament formation. Ink drops from the gravure cells are elongated at lift-off, forming liquid filaments. At some point, these spontaneously break and the ends are drawn back either to the pad or the printing form by capillary forces. A fast lift-off creates more and longer filaments than a slow lift-off. This could explain the relationship between lift-off velocity and the frequency of filament defects. In contrast, no significant relationship between filament formation and pad lift-off velocity was observed during the printing step (Figure 1 (f)). Figure 12 shows the influence of reducing the pad lift-off velocity from 200 mm/s to 25 mm/s.

We counted the number of filaments and calculated the edge sharpness for various lift-off velocities. The results are shown in Table 1 and Figure 13. Decreasing lift-off velocity reduces filament formation and edge roughness.

Table 1: Influence of pad lift-off velocity on the number of filaments and edge roughness

Pad lift-off velocity (mm/s)	Number of filaments	Edge roughness (µm)
200	24	64.13 (± 1.7)
175	20	49.85 (± 3.1)
150	12	47.13 (± 7.0)
125	10	39.74 (± 6.4)
100	10	38.80 (± 2.9)
75	3	11.38 (± 1.2)
50	0	4.85 (± 0.8)
25	0	3.93 (± 0.2)
10	0	3.70 (± 0.6)

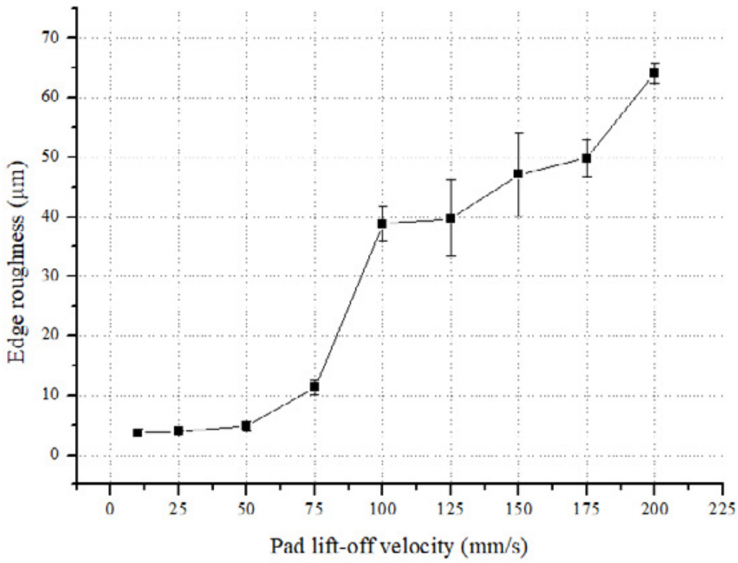

Figure 13: Edge roughness as a function of pad lift-off velocity from printing form

When we replaced conventional printing forms with those having outlines and reduced the velocity of pad lift-off from the printing form from 200 mm/s to 50 mm/s in our printing trials, we achieved an average edge roughness R_m of 1.80 ± 0.31 µm. This represents an enormous improvement in edge quality (Table 2).

Table 2: Edge roughness R_m results of the printing experiments

Printing form material	**Resolution (L/cm)**	**R_m (µm)**
Polymer	80	2.44 (± 1.02)
	100	1.76 (± 0.95)
	120	1.50 (± 0.28)
Steel	80	1.74 (± 0.38)
	100	1.83 (± 0.48)
	120	1.55 (± 0.27)
		Average
		1.80 (± 0.31)

4. Conclusion

In this work, we consider the edge quality of pad-printed structures. We identify two classes of printing defects, stamp defects and filament formation defects, and optimize the process parameters so as to improve edge quality. Stamp defects are related to the structure of the printing area of the gravure plate. By providing an outline feature, stamp defects can be avoided. Filament formation defects appears to be the result of an ink splitting effect that is correlated to the lift-off velocity of the printing pad from the gravure plate. Although filament formation also occurs in offset-, flexo-, and direct gravure printing, it does not usually cause such defects. Thus, the question arises as to what is different with pad printing in this respect. Inappropriate ink viscosity due to low humidity, high ambient temperature or extensive solvent evaporation might affect printing quality. This, however, does not explain why the filaments are ejected across the printing border. The formation of static electric charges on the pad might explain this phenomenon. This, however, does not conform with the observation that filaments frequently appear on just one side of a printed line. In any case, antistatic additives, which could almost completely eliminate static electricity, are not an option in the field of printed electronics, since they might spoil some functional features of the printed pattern.

Another possible origin of filament defects is the pad material itself. It is a blend of silicone and silicone oil, which are reliable electrical insulators. Using an antistatic pad or applying an ionized gas flow on top of its surface to neutralize free electrical charge carriers would therefore seem to be plausible countermeasures. However, when we tried these strategies in our investigations, neither led to significant improvement. Although closer examination of this phenomenon is recommended for future work, a tentative explanation can be offered already, based on recent studies of ink splitting phenomena.

According to Lindner and Wagner (2009), Griesheimer (2014) and Weickgenannt, et al. (2015), filaments form when a liquid film is split between two parallel plates that are rapidly separated. These filaments can be very thin and quite long. When the filaments break, capillary forces draw them back to the plate surfaces. In the experiments of these researchers, the motion of the retracting filament is directed perpendicular to the filament base and the liquid carried by the filament is gathered there. No filament residuals form at the printing edges. In pad printing, however, the kinematic situation is different. Because the pad is elastically deformed at the moment of lift-off, the velocity vector at the pad surface has a small component parallel to the surface of the printing form. Therefore, ink filaments breaking off the printing form have an angular velocity with respect to their base point on the pad. In contrast to offset or direct gravure printing, the filaments are tilted when they deposit on the pad. Those filaments at or near the border of the printing area may thus fall outside the desired zone during in the ink deposition step. This could explain the effect of reducing the lift-off velocity of the pad from the gravure plates: the filaments get shorter and their tilting becomes less pronounced.

The tool developed here allows the user to quantitatively evaluate the quality of a printed edge using the metric of edge roughness. An average edge roughness of less than 2 µm was achieved with pad printing technology when pad lift-off velocity was reduced to prevent filament formation. With the help of the tool more parameters can be investigated in future to understand the influence to the edge roughness. With implementation of this tool into a manufacturing process of printed electronic components, printing defects can be detected and sorted out at early stage.

Acknowledgments

The authors would like to acknowledge the support by Stefan Ernst from Franz Binder GmbH & Co. They are thankful for many helpful hints by Jürgen Veser from Flint Group Germany GmbH and the working group Innovation Tampondruck. Our studies on pad printing technology were achieved within the BMBF Project ELSE under grant no. 13N13079.

References

Canny, J., 1986. A Computational approach to edge detection. *IEEE Transactions on Pattern Analysis and Machine Intelligence*, PAMI-8(6), pp. 679–698.

Griesheimer, S., 2014. *Farbspaltungsphänomene von Druckfarben an strukturierten Oberflächen am Beispiel des Flexodrucks*. Dr.-Ing. Dissertation. Technische Universität Darmstadt.

Hahne, P., 2001. *Innovative Drucktechnologien: Siebdruck - Tampondruck*. Lübeck: Verlag der Siebdruck, p. 94.

Hahne, P., Hirth, E., Reis, I. E., Schwichtenberg, K., Richtering, W., Horn, F. M. and Eggenweiler, U., 2001. Progress in thick-film pad printing technique for solar cells. *Solar Energy Materials and Solar Cells*, 65(1), pp. 399–407.

Hakimi Tehrani, A. and Dörsam, E., 2016. Improving automation and process control of an indirect gravure (pad) printing machine. *Acta Polytechnica Hungarica,* 13(4), pp. 221–240.

Krebs, F.C, 2009. Pad printing as a film forming technique for polymer solar cells. *Solar Energy Materials and Solar Cells,* 93(4), pp. 484–490.

Lee, T.M., Hur S., Kim, J.H. and Choi, H.C., 2010. EL device pad-printed on a curved surface. *Journal of Micromechanics and Microengineering,* 20(1), article id. 015016.

Leppävuori, S., Väänänen, J., Lahti, M., Remes, J. and Uusimäki, A., 1994. A novel thick-film technique, gravure offset printing, for the realization of fine-line sensor structures. *Sensors and Actuators A: Physical*, 42(1-3), pp. 593–596.

Lindner, A. and Wagner, C., 2009. Viscoelastic surface instabilities / Instabilités interfaciales dans les liquides visco-élastiques. *Comptes Rendus Physique*, 10(8), pp. 712–727.

Merilampi, S.L.; Björninen, T., Ukkonen, L., Ruuskanen, P. and Sydänheimo, L., 2011. Characterization of UHF RFID tags fabricated directly on convex surfaces by pad printing. In: *The International Journal of Advanced Manufacturing Technology*, 53(5-8), pp. 577–591.

Mooring, L., Karousos N.G., Livingstone, C., Davis, J., Wildgoose, G.G., Wilkins, S.J. and Compton R.G., 2005. Evaluation of a novel pad printing technique for the fabrication of disposable electrode assemblies. *Sensors and Actuators B: Chemical*, 107(2), pp. 491–496.

Weickgenannt, C.M., Griesheimer, S., Sauer, H.M., Roisman, I.V., Dörsam, E. and Tropea C., 2015. Atomization of a stretched Newtonian liquid bridge. In: *Proceedings of ICLASS 2015, 13th Triennial International Conference of Liquid Atomization and Spray Systems*. Tainan, Taiwan, 23–27 August 2015.

Willfahrt, A., 2007. Examination of the printability of microstructures by means of pad printing for the realization of minimal structures for the use of conductive inks on PET-Substrate. In: *Proceedings of the Printing Future Days: 2nd International Student Conference on Print and Media Technology*. Chemnitz, Germany, 5-8 November 2007. Berlin, Germany: Verlag für Wissenschaft und Forschung.

Xiong, Y. and Qu, Z., 2011. Antenna 3D pad printing solution evaluation. In: *Proceedings of the 2011 IEEE International Symposium on Antennas and Propagation (APSURSI)*. Spokane, WA, USA: IEEE, pp. 2773–2776.

Using FEM Simulation as a Tool to develop Pad Printing

Ahmad Al Aboud, Edgar Dörsam, Arash Hakimi Tehrani and Dieter Spiehl

Technische Universität Darmstadt, Institute of Printing Science and Technology, Magdalenenstr. 2, 4289 Darmstadt, Germany
E-mails:aboud@idd.tu-darmstadt.de;doersam@idd.tu-darmstadt.de;hakimi_a@idd.tu-darmstadt.de;spiehl@idd.tu-darmstadt.de

Short abstract

Pad printing is a method to print on objects with complicated geometries or rough surfaces. Although pad printing is widely used in advertising and industrial printing, there are few scientific studies. The process parameters are therefore still determined today by experience. This applies in particular to the selection of the pads. Experienced experts select a suitable pad shape from the wide range of sizes and geometries. The finite element method (FEM) could be a method to support the selection of pad shapes. The FEM software requires various input parameters such as material model, material parameters and mesh types and sizes for simulation. For many FEM applications, the material parameters as well as the type and size of the mesh have a large influence on the quality of the simulation result. There is therefore a great uncertainty as to which parameters should be used. Therefore, this paper first examines the determination of material parameters using tensile tests and then the influence of different mesh types and sizes. The results are shown here as examples for a medium pad size with a hardness of 6 Shore A. It turns out that simple FEM tools are suitable for rough estimation of the forces in a pad during the printing process.

Keywords: pad printing, pad geometry, FEM simulation, silicone rubber, mesh

1. Introduction and background

Pad printing is an indirect gravure printing process. It can be used to print on a wide variety of materials almost independently of shape and surface structure in contrast to with existing printing systems such as screen and embossing printing. Therefore, pad printing is very well suited for printing on three-dimensional objects. Figure 1 shows examples of using pad printing technology.

Figure 1: Examples of products printed with pad printing and (on the left side) the used pad to print on a pacifier; all products are objects with curved and partly rough surfaces, photos from Tampo-Technik (2018), Binder (2018) and Wilson (2018)

The printing pads are made of silicone rubber and are available in various qualities, shapes and hardnesses. The shape of the printing pad is adapted to the geometry of the substrate to be printed. This is why there are countless different sizes and shapes of printing pads on the market. The mixing ratio of silicone rubber and silicone oil determines the hardness of the printing pad, measured in Shore A. Hardnesses from 2 (soft) to 18 (very hard) Shore A are common. Depending on the combination of the parameters geometry and hardness, the printing result of the pad varies. For almost every special printing task it is possible to produce a suitable printing pad to optimize the printing result. Therefore, every manufacturer of printing pads should have several hundred different printing pads on offer (Kipphan, 2001).

This research focuses on the silicone rubber with 6 Shore A hardness. This hardness is selected because it is located in the medium range of pad hardnesses which are used in pad printing. In order to get test specimens with the same specifications of pad materials, the Tampo-Technik GmbH was selected to mold the test specimens. This company is a pad manufacturer and it produced the test specimens exactly with the same material and the same process as used in pad production.

The finite element method (FEM) could be a method to support the selection of pad shapes.

Finite element method is a numerical method for solving technical problems by simulating a real technical operation on the computer. Typical problems solved by FEM are structural analysis, heat transfer, fluid flow and acoustics (Shih, 2014). There are two types of softwares, which can solve the numeric equations, CAD software such as SolidWorks and FEM software such as Abaqus.

SolidWorks is a CAD software with integrated packages for FEM simulations, is developed by Dassault Systemes (Shih, 2014). It is an inexpensive and easy-to-use software that is used by many small and medium-sized companies. Abaqus is a very comprehensive FEM program, which has already been used in some previous studies and simulations (Jungh, et al., 2017). It is a very powerful, but also complex software that requires experienced engineers for modeling. Because of the high licensing costs, it is usually used in large companies or specialized engineering offices.

In this study we will investigate whether simple FEM software (such as SolidWorks) can be used to model pads. The method is to use Abaqus to study the influence of mesh types and sizes on the reaction forces. For the investigation we use a pad with a simple rectangular shape on a flat surface that makes the validation very easy. For the evaluation we compare the reaction force on this flat surface of the pad from the experiment with that from the simulation. With regard to simulation of the printing pads, mechanical properties of the pad material are needed to be implemented in the simulation tools such as Abaqus.

2. Determination of mechanical proterties

Pads are made of a mixture of silicone oil and silicone rubber, that mixture is a kind of an elastomer. The mechanical properties of this pad material should be determined by mechanical tests and the poission test. The results of these tests are input parameters to the simulation of the silicone rubber material 6 Shore A hardness. Therefore, we have characterized the material in a Zwick Z050 test machine to obtain the following results.

Poisson's ratio is defined by the negative ratio of strain in "passive" direction (normal to load) to the "active" strain in length direction by ASTM D638 (American National Standards Institute, 2014). The Poisson's ratio is achieved with Equation 1. In this equation the strain in transverse direction is devided by strain in axial direction and its absolute value is calculated (American National Standards Institute, 2014). The strain in transverse and axial directions is measured with a video extensometer system during the tensile test execution at the same time. Then, Poisson's ratio is calculated according to ASTM D638. The value of 0.49 was calculated for silicone rubber test specimens with hardness of 6 Shore A.

$$\text{Poisson's ratio} = \left|\frac{\text{Strain in transverse}}{\text{Strain in axial}}\right| \qquad [1]$$

The uniaxial tensile, compression and planar tests should be executed to get the material specifications. Here, the Zwick Z050 test machine with ±2 µm position repetition and 27 nm travel resolution accuracy was used to execute the tests.

The uniaxial tensile test was performed according to ASTM 412 and ISO 37 standard test methods (American National Standards Institute, 1998; International Organization for Standardization, 2005). In this case, the dumb-bell shape test specimen type 1 was selected and the test length of 25 mm on test specimens was marked accordng ISO 37, and ASTM D412 (International Organization for Standardization, 2005; American National Standards Institute, 1998). A video extensometer system measured the marked area length changes to calculate the strain values in the test process. Force values were measured during the test execution to calculate the stress. Figure 2 shows the specimen.

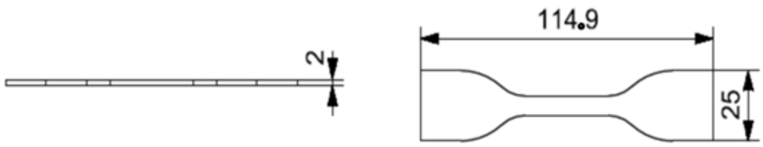

Figure 2: Uniaxial tensile test probe in accordance to ISO 37

The planar tensile test was applied in the same method till the maximum strain of 55 % with a rectangular test specimen. In this case, the test specimen is a silicone rubber plane with the test length of 8 mm and width of 60 mm.

The compression test method is defined in ISO 7743 standard (International Organization for Standardization, 2011). The test type B was performed on a cylindrical test specimen with diameter 17.8 ±0.15 mm and height 25 ±0.25 mm according to this standard ISO 7743.

The experimental results of tensile, planar and compression tests with 6 Shore A are presented in Figures 3 to 5. The strain and stress loading-unloading behavior of silicone rubber with 6 Shore A hardness are clarified here.

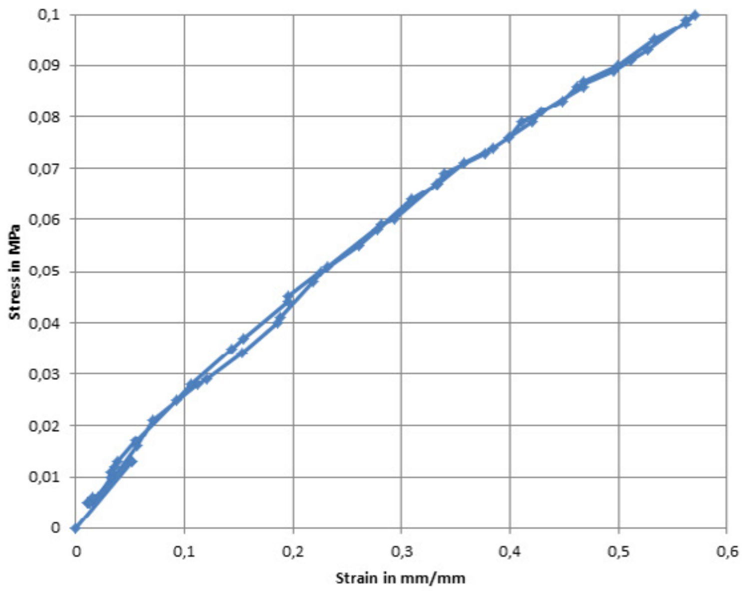

Figure 3: The tensile stress-strain curve for 6 Shore A silicone rubber

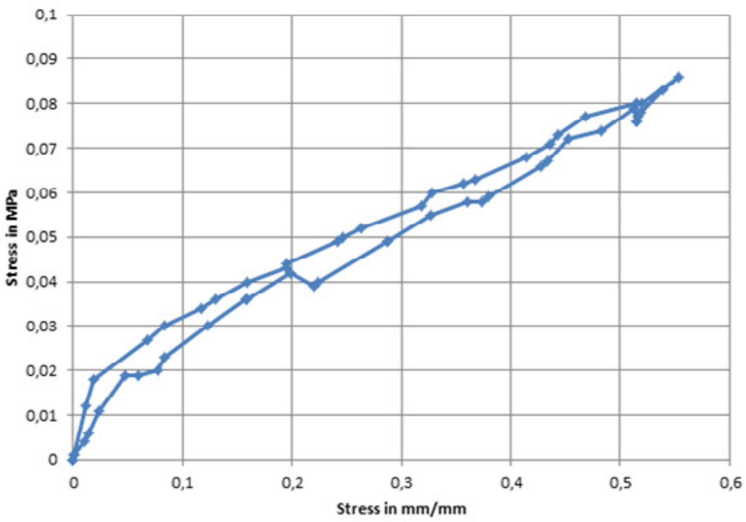

Figure 4: The planar stress-strain curve for 6 Shore A silicone rubber

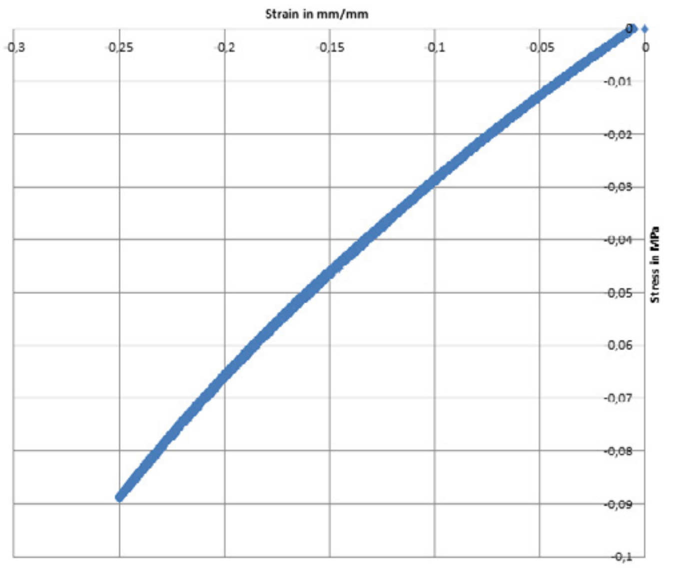

Figure 5: The compression stress-strain curve for 6 Shore A silicone rubber

These data were entered into the FEM software as parameters for the pad material. Thus, all requirements for a simulation are met.

3. FEM simulations

For FEM simulations, Abaqus is used to obtain accurate results. To approximate the pad geometry a three-dimensional mesh is generated by the FEM Software. The mesh element type and mesh element size play important roles in simulation results (Tadepalli, Erdemir and Cavanagh, 2011). In general, three-dimensional meshes for finite element analysis must consist of tetrahedra, pyramids, prisms or hexahedra. Figure 6 shows the shapes of the possible mash types with their nodes. Only three-dimensional element types can be used to approximate the pad geometry.

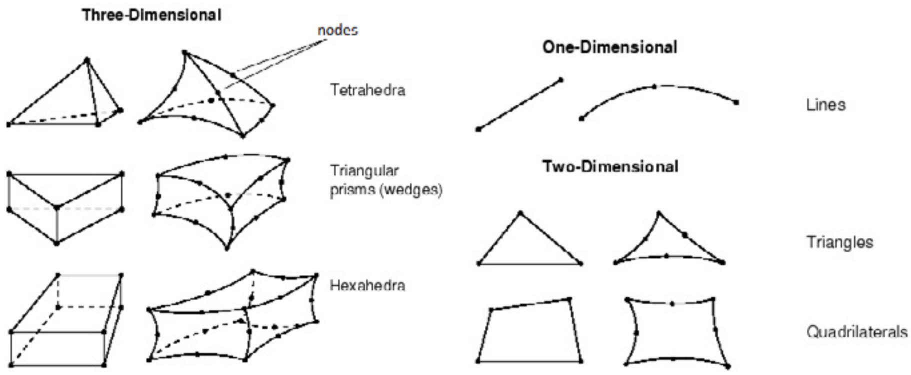

Figure 6: Mesh element types in Abaqus with their nodes (Simulia-Dassault-Systemes, 2011); only three-dimensional element types can be used to approximate the pad geometry

For the given pad geometry, only two of the three-dimensional mesh types are possible. These are the two basic types Tetrahedra (C3D10) und Hexahedra (C3D20). A hybrid mesh element type is proposed for the mechanical response of two-dimensional heterogeneous materials (Zhang and Katsube, 1995). They are in this simulation silicone rubber (pad) against steel (substrate table). For the geometry of the silicone rubber pads, the mesh element type C3D10MH and C3D10H are used in this simulation. In literature (Tadepalli, Erdemir and Cavanagh, 2011) the mesh element type C3D10MH has been used for the simulation of incompressible neo-Hookean material and it has given very good results (Guo, et al., 2016). Reduced integration and modified mesh element types are used in this simulation (Brown, 1997). This causes buckling of the mesh element with one node. This problem is called hourglassing. In these places of the geometry the mesh density must be increased (Brown, 1997). Table 1 shows the used element types.

Table 1: The used mesh element types

Mesh element type	Description
C3D10MH	10 nodes modified tetrahedron, with hourglass control, hybrid
C3D10H	10 nodes tetrahedron, with hourglass control, hybrid
C3D20H	20 nodes quadratic brick, hybrid

The Mesh element size is the maximum length of mesh element in mm. This parameter determine the density of the mesh of the geometry. The mesh element size in this simulation is chosen between two and eight mm. Figure 7 shows an example of the simulation of the pad with the mesh type C3D10MH and the flat steel surface with the mesh type C3D20H.

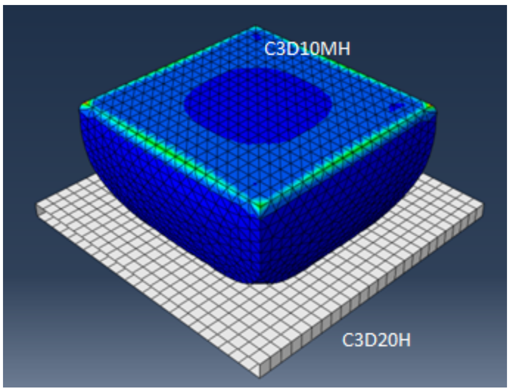

Figure 7: Mesh of the 6 Shore A silicone rubber pad (74 mm ×72 mm × 52 mm) on a flat steel surface, mesh element size is 5 mm, the initial velocity of the silicone rubber pad is 8.5 mm/s; a polynomial of order 2 for the strain energy equation is chosen

4. Results of the simulation

The FEM simulation results were validated by means of experimental investigations. An improved pad printing machine (Hakimi Tehrani and Dörsam, 2016) is used to monitor the pad displacement and reaction force during printing by the use of sensors and it stores the data for analysis. Afterwards, the measured parameters are compared with the simulation results.

Figure 8 shows the reaction forces during printing. At the zero point, the tip of the pad just touches the flat steel surface. With increasing vertical movement, the reaction forces increase. They do not increase linearly. The simulation results of three different mesh element sizes compared to the real measured data are shown in Figure 8. A small deviation between the experimental data and the simulation results could be recognized. This deviation is acceptable because the simulation results usually are not fitted exactly on the experimental results (Tadepalli, Erdemir and Cavanagh, 2011). The simulation results of three different meshes clarify the effect of a mesh element on the simulation results. The mesh with 2 mm element size is a very fine mesh type that is possible to use. The calculation of the simulation takes a very long time (12 hours) in comparison with other mesh element sizes 4 mm and 8 mm while their results are nearly the same. So, it can be concluded that the mesh element size in this range doesn't have an effective role in the simulation results accuracy, in this case.

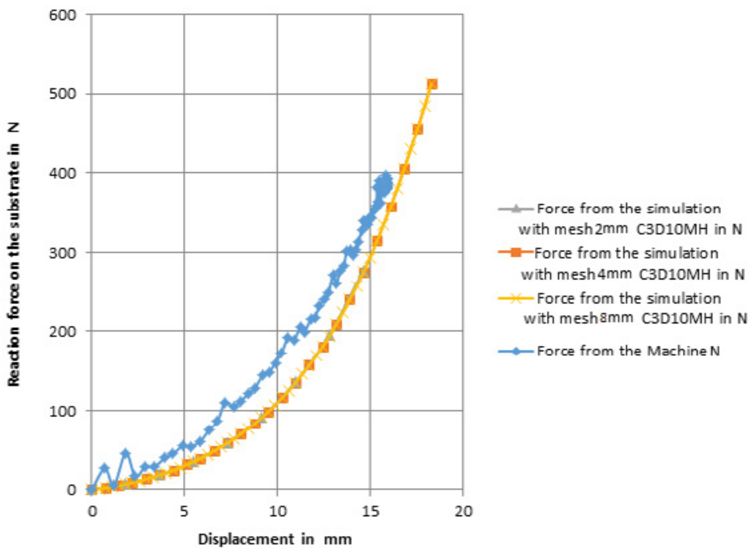

Figure 8: Comparison of the force displacement diagram from experimental data and the simulation results with three different mesh element sizes

Figure 9 shows the simulation results of different mesh element types with the element size of 2 mm. The mesh type of 3D10MH is compared with 3D10H. The mesh element type 3D10MH is a modified formulated meshing method which is compared with normal mesh type and the experimental result.

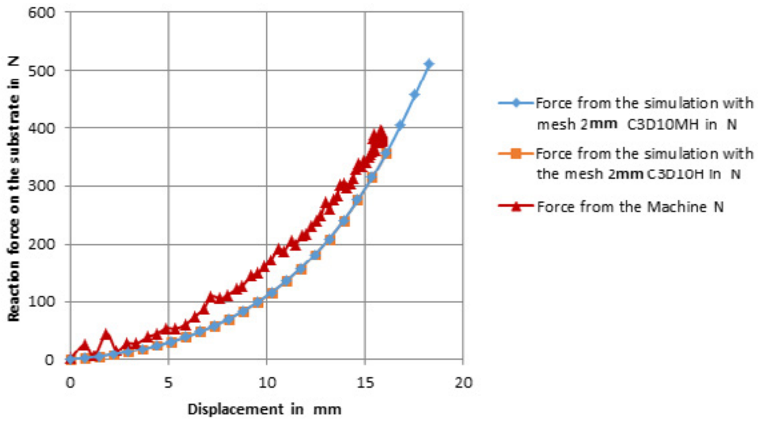

Figure 9: Comparison of the force displacement diagram from the machine and the simulation results with two different mesh element types

It can be concluded that the mesh element type in this range doesn't have an effective role in the simulation results accuracy.

5. Conclusion

For the design of pads in pad printing today, the mostly small to medium sized manufacturers of pads still proceed very empirically. FEM tools in CAD software could support the design. But how can the quality of the FEM software be assessed in view of the complex material behavior of pads? For a typical pad of medium size and a Shore A hardness of 6, experimental data of the occurring reaction forces were measured in printing tests and compared with FEM simulations. The silicone pads show a strong non-linear behaviour during printing. Therefore it is very important to determine the characteristic material properties. FEM simulations carried out with these material properties show that mesh type C3D10MH generally suitable for pad materials with standard mesh sizes (2 mm to 8 mm) then leads to useful results. C3D10MH as a representative for Tetrahedra mesh element types is also a standard element type in simple FEM tools. Therefore, simple FEM tools implemented in CAD softwares are also suitable for a rough estimation of the deformation behavior. The most important is the knowledge of the material parameters. Manufacturers of pads are therefore recommended to have the material parameters determined for each Shore A hardness. Then they will find a first good support in today's usual FEM tools. Scientific research will be continued to develop methods and tools for designing pads.

Acknowledgement

The authors gratefully acknowledge the support of Tampo-Technik GmbH for pad and test material manufacturing. We thank for the support of the "Dr. Ing. Wilhelm und Maria Kirmser" – scientific scholarship.

References

American National Standards Institute, 1998. *ASTM D412-98a Standard test methods for vulcanized rubber and thermoplastic rubbers and thermoplastic elastomers-tension*. West Conshohocken, PA, USA: ASTM.

American National Standards Institute, 2014. *ASTM D638-14. Standard test method for tensile properties of plastics*. West Conshohocken, PA, USA: ASTM.

Binder, 2018. *Elektrische Bauelemente KG*. [online] Available at: <www.binder-connector.de> [Accessed January 2018].

Brown, J., 1997. Characterization of MSC/NASTRAN & MSC/ABAQUS elements for turbine engine blade frequency analysis. In: *Proceedings of MSC Aerospace Users' Conference*. Newport Beach, California, USA, 17–20 November 1997.

Guo, Z., Chen, Y., Peng, X., Shi, X., Li, H. and Chen, Y. 2016. Shear stiffness of neo-Hookean materials with spherical voids. *Composite Structures,* 150, pp. 21–27.

Hakimi Tehrani, A. and Dörsam, E., 2016. Improving automation and process control of an indirect gravure (pad) printing machine. *Acta Polytechnica Hungarica,* 13(4), pp. 221–240.

International Organization for Standardization, 2005. *ISO 37:2005 Rubber, vulcanized or thermoplastic - Determination of tensile stress-strain properties*. Geneva: ISO.

International Organization for Standardization, 2011. *ISO 7743:2011 Rubber, vulcanized or thermoplastic - Determination of compression stress-strain properties*. Geneva: ISO.

Jungh, T., Glasenapp, T., Fraas, M., Schulz, A. and Bauer, H.-J., 2017. Durchführung von FEM Simulationen zur Anwendung des Superpositionsprinzips der Filmkühlung. In: *Deutscher Luft- und Raumfahrtkongress 2017 (DLRK)*. München, Germany, 5–7 September 2017. Lilienthal-Oberth, Germany: Deutsche Gesellschaft für Luft- und Raumfahrt.

Kipphan, H., 2001. *Handbook of Print Media*. Berlin, Heidelberg: Springer.

Shih, R., 2014. *Introduction to finite element analysis using SolidWorks simulation 2014*. Mission, KS, USA: SDC Publications.

Simulia-Dassault-Systemes. 2011. Abaqus 6.11: theory manual. Providence, RI, USA: DS SIMULIA Corp. [pdf] Available at: < http://130.149.89.49:2080/v6.11/pdf_books/THEORY.pdf> [Accessed January 2018].

Tadepalli, S.C., Erdemir, A. and Cavanagh, P.R., 2011. Comparison of hexahedral and tetrahedral elements in finite element analysis of the foot and footwear. *Journal of Biomechanics*, 44(12), pp. 2337–2343.

Tampo-Technik, 2018. *Tampo-Technik Lück*. [online] Available at: <http://www.tampotechnik.de/de/> [Accessed January 2018].

Wilson, 2018. *40 years. 1 ball*. [Online]. [online] Available at: <http://www.wilson.com/en-us> [Accessed January 2018].

Zhang, J. and Katsube, N., 1995. A hybrid finite element method for heterogeneous materials with randomly dispersed rigid inclusions. *International Journal for Numerical Methods in Engineering*, 38(10), pp. 1635–1653.

Cardboards printed with Water-based Inkjet Inks

Sandra Rosalen and Johannes Backhaus

Bergische Universität Wuppertal, Rainer-Gruenter-Straße 21, 42119 Wuppertal, Germany
E-mails: srosalen@uni-wuppertal.de; jbackhaus@uni-wuppertal.de

Short abstract

Water based inkjet printing inks are still rarely used in cardboards printing. They show poor adhesion and too slow drying behavior for industrial manufacturing processes. This paper shows how to improve the adhesion and to reduce the drying duration of dye and pigment water based inkjet inks on customary market cardboards. The basis for this is a pretreatment of the cardboards, here exemplarily with a polyvinyl alcohol based primer, as well as a drying assistance by means of infra-red. These simple applicable procedures allow acceptable processing speed for industrial packages production without ink set-off by pile stacking or ink smudge it in subsequent post-printing steps. Macro roughness, micro roughness and contact angle measurements are also presented in order to explain specific variations in the results.

Keywords: water based inkjet inks, polyvinyl alcohol, primer, drying assistance

1. Introduction

The production of a secondary packages as folding boxes is carried out through the following processes: printing, coating or laminating, dye-cutting and gluing. Among these steps there are intermediary processes as stacking, pile loading and unloading.

To ensure the quality of the final products it is mandatory that the inks are sufficiently dry when the printed sheets are stacked at the delivery of the press. Otherwise set-off can take place. Drying depends on several physicochemical properties of the ink, the substrate and their interaction as: viscosity, surface tension, porosity, roughness, binding forces, capillarity and hydrophobic/hydrophilic nature. As these properties are interconnected, it is recommended to choose consumables considering the type of application performance, compatibility with printing and finishing systems, drying duration, adequate quality and regulatory issues (Magdassi, 2010, p. 16).

Substrates compatible with inkjet printing can be divided in two main groups depending on the type of coating: nonporous (swellable IRL) and porous (microporous IRL). A polymer is the main component of swellable IRL's. Microporous IRL is a blend of a binder and inorganic minerals. An IRL is applied as the top layer on a coating-free basepaper.

Considering the type of application, as folding boxes or boxes with fold-up lids, a cardboard with a coating suitable for WB inkjet ink is unknown until this moment. The current surface of cardboards is not enough absorbent and the chemistry used in coated boards is not compatible with, for example, anionic inkjet inks (Svanholm, 2007, p. 10). Therefore, cardboards are commonly printed in inkjet with UV or solvent based inks. Although these inks provide an efficient production process, there are some drawbacks. Set-off or diffusion migration caused by incomplete polymerization or residual amounts of retarders/solvents can be a risk for health and environment. A production process with WB primers and inks can reduce these disadvantages.

2. Concept

As explained, cardboards hardly can be printed with WB inkjet inks. The ink has no rub resistance and/or take days to dry. To improve the adhesion of inks, a primer can be applied.

As a starting point to define the application parameters for a primer, a virtual printing line with WB inkjet inks for cardboards is drafted (Figure 1). As already mentioned, it is essential that the ink dries when the sheet arrives the delivery pile stacking. The ink does not need to be completely *finger dry*, but dry enough (*pile dry*) to avoid ink set-off. Based on the speed of current inkjet presses for B1 and B2 format, printing itself takes about 2 seconds. As both the primer and the ink should have an aqueous base, a drying assistance is placed subsequently the printing. Considering a production of 200 sheets the total printing duration is approximately 6.6 minutes. A five minutes interval is supposed pile removal after the job finishing.

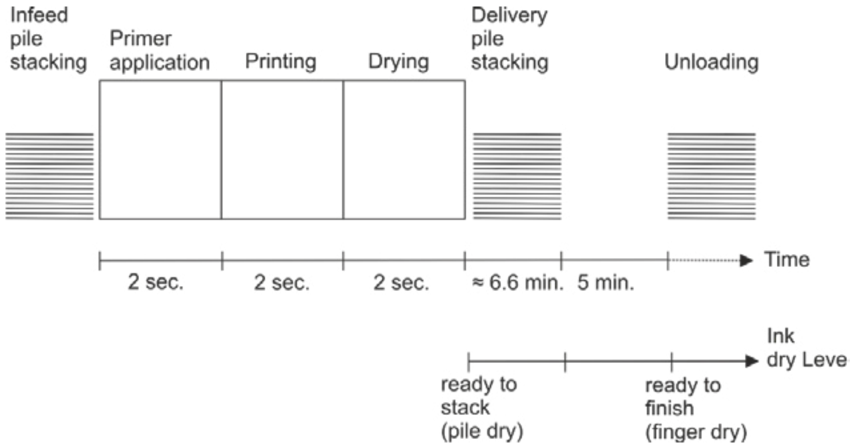

Figure 1: Printing line with WB inkjet inks for cardboards

3. Materials

3.1 Cardboards

Seven cardboards with similar grammage and thickness were selected for the tests (Table 1).

Table 1: Properties of the cardboards (data sheets – Paper mills)

	Property [Unit]				
Cardboard [ID]	Grammage [g/m²]	Thickness [µm]	Moisture [%]	Roughness (Top) [µm]	Coating Layers (Top)
B-01	300 ± 5 %	365 ± 5 %	5.5 ± 1 %	1.8 ± 6 %	2
B-02	300 ± 4 %	474 ± 5 %	8.2 ± 1 %	< 1.3	2
B-03	295 ± 2 %	505 ± 3%	8.1 ± 1 %	1.0 max. 1.3	1
B-04	300	345 ± 3%		1.0	1
B-05	300 ± 4 %	365 ± 4%	6.5	0.9 max. 1.4	2
B-06	300 ± 4 %	395 ± 4%	6.0 ± 1	0.9 ≤ 1.4	3
B-07	295 +3 % / -5%	505 ± 5%	8.2 ± 1	1.0 max. 1.7	3

3.2 Printer and inks

The inkjet printer used for tests is a Canon PIXMA iX6850. This printer can print dye inks (CMYK – Canon CLI-551) and in addition one so called PBK black pigment ink (PBK – Canon PGI-550).

3.3 Primers

The use of polyvinyl alcohol (PVOH) in pigment coatings is well documented (Onishi, Iida and Owatari, 1997; Kettle, Lamminmäki and Gane, 2010; Lamminmäki, Kettle and Gane, 2011;Ridgway, Kukkamo and Gane, 2011; Sousa, et al., 2014; Chang, et al., 2018), albeit applied always on top of basepapers and usually only as a binder for other components.

For these experiments it was pre-established that the primer should be printed on an inkjet system, whose ink viscosity and surface energy parameters are defined, for example, surface tension 25–50 mN/m and viscosity 1–25 mPa·s (Magdassi, 2010, p. 35), surface tension 20–50 mN/m (Hoath, 2016, p. 127) and viscosity 1–20 mPa·s (Hoath, 2016, p. 143). The addition of minerals to produce a microporous IRL increases the viscosity that a drop formation cannot take a place. Besides, the minerals in microporous coatings have a particle size about 0.1–1 µm (Klöckl, 2015, pp. 604–605; Diamond and Weiss, 2002, pp. 611–612), i.e. around 10 times bigger than pigment particles (~0.01–0.1 µm) (Hoath, 2016, p. 9). As the diameter from the printhead nozzles is ~10–50 µm (Hoath, 2016, pp. 43, 143, 159), the printheads clog.

Thereupon, for this research, the development of a primer to be applied on top of the pigment coating of cardboards as an IRL, follows two criteria: use of a hydrophilic polymer and without any addition of minerals or industrial standard stabilizers. Four different PVOH (6–88, 23–88, 4–98 and 20–98) are tested in twelve different concentrations.

4. Methods

4.1 Preliminary tests

Twelve recipes, PVOH mixed with distilled water are prepared by means of magnetic stirrer with temperature control until the mixtures become homogenous. The primers are applied by means of a Mayer rod. The transferred weight is ~0.6 g/m^2.

A test chart with C, M, Y, K, PBK, C+M, C+Y and M+Y charts in gradients from 20, 50 and 100 % ink coverage is printed with 300 dpi on 5 samples from each cardboard to investigate which colors, gradients and cardboards show inefficient adhesion or inappropriate drying duration.

The initial results show that C, M and Y as well as their combinations (red, green and blue) do not present significant drawbacks (good adhesion and immediate drying), except for B-04, a cast coated board. In contrast, the K and PBK patches did not show improvements from adhesion and drying duration by 100 % ink coverage. Two repetitions of this test printing confirm the results. In these two following test sets, only the four recipes that obtained the best results on most cardboards are tested again (Table 2). In addition the samples are conditioned at 50 ± 2 °C for 30, 60 and 120 seconds, one with ventilation and one without ventilation. Drying duration of both dye and pigment inks were reduced, but none of them dries (*finger dry*) in less than 1 minute.

Table 2: Primer recipes with the good results

Recipes [ID]	PVOH	PVOH [wt%]	Water [wt%]
P-03	PVOH 6-88	3	97
P-04	PVOH 23-88	10	90
P-07	PVOH 20-98	4	96
P-08	PVOH 20-98	2	98

4.2 Main tests

Among the four best primers of the preliminary tests the P-07 presented best results (improvement of adhesion and reduction of drying duration) and therefore selected for the following main tests. P-07 is applied by means of a Mayer rod with 3 different transferred amount of coating: rod-W: ~0.6 g/m^2, rod-G: ~1.2 g/m^2 and rod-R: ~1.8 g/m^2. A test chart only with K and PBK patches (100 % ink coverage) is designed to test the drying duration and adhesion (Figure 2).

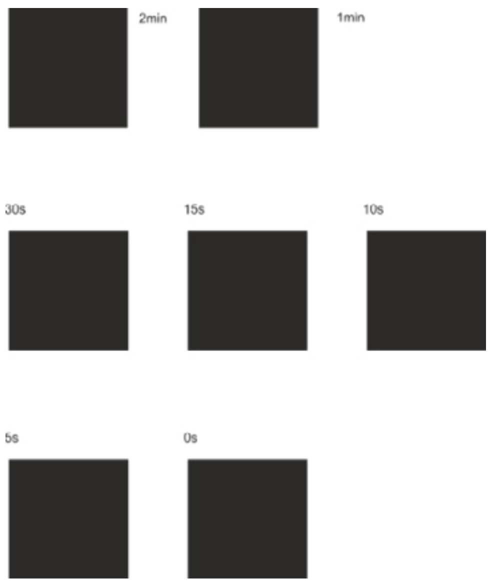

Figure 2: Test chart – Main tests

After printing, the first patch (zero seconds) is rubbed and the test chart is placed under a ceramic infrared (IR) panel radiators (wavelength 2–10 µm, panel temperature 200 ± 5 °C, distance 38 mm) and promptly removed for followings rub tests in the intervals of time defined for each patch (5, 10, 15, 30, 90 and 120 seconds).

The main tests were divided into four groups (Table 3) in order to eliminate possible distortions in the analysis.

Table 3: Description of test groups

Group	Primer P-07	IR-Drying
A	no	no
B	yes, with 3 rods	no
C	no	yes
D	yes, with 3 rods	yes

4.3 Line concept test

During the preliminary and main tests the adhesion test is conducted by "*finger dry*" method, this means that the results presented in section 5.1 and 5.2 represent the maximum time necessary for the ink to be completely dried (ready to finish).

To ascertain if the line concept (Figure 1) is feasible, a stacking test is conducted (Figure 3). The cardboards primed with P-07 (rod-G) and printed are placed under the IR-dryer for 2 seconds and stacked then. In the following the next sheets are stacked each after 2 seconds. After stacking 200 sheets the bottom of the first sheet but one (control board 1) was controlled. If no set-off was observed, the board is categorized as ready to stack (enough ink adhesion). After 300 seconds the last stacked board (control board 2) was also controlled by means of rub test. If the ink did not smudge the board is categorize as ready to finish (ink dried sufficiently).

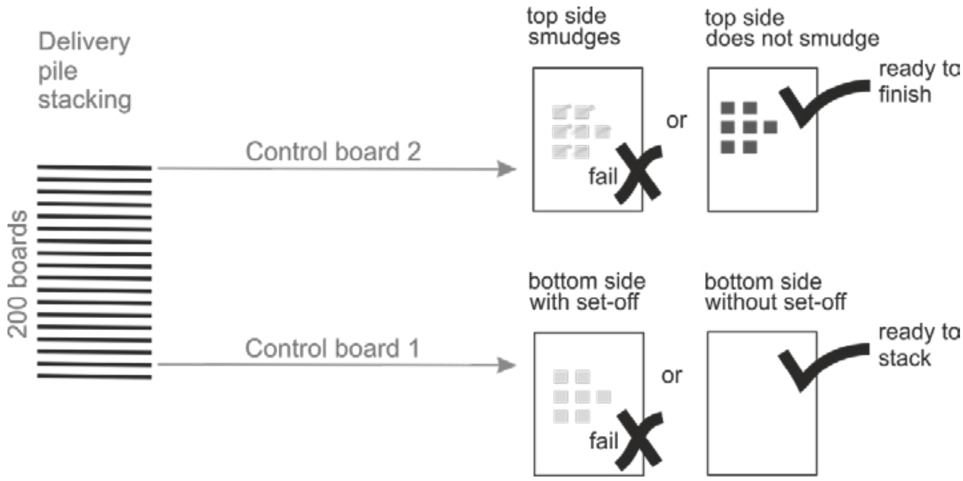

Figure 3: Scheme for the Line concept test

4.4 Surface analysis

Some surface analysis of the cardboards are carried out with following equipment and methods:

- Roughness measurement with L&W PPS Tester, 10 measurements, 1.0 MPa
- Roughness measurement with a Keyence Confocal 3D Laser Microscope, 10 measurements, total area: 14 mm^2
- Surface free energy measurement with a Data Physics OCA 30, fluids: Water, Diiodomethane and Ethylene Glycol (15 measurements each fluid), calculations by means of OWKR (Deutsche Institut für Normung, 2011) with three fluids.

5. Results

The preliminary tests show that a single component PVOH based primer can improve the adhesion of the ink. However, the drying duration is not compatible with industrial inkjet presses. The main tests with IR-drying assistance showed better results in relation to drying duration. The data are summarized in Table 4. A resume of the results is presented below:

5.1 Dye ink – ready to finish test

Test D – The drying duration for 5 of 7 cardboards was reduced with the P-07 pretreatment and additional IR-drying assistance. The maximum drying duration is 5 seconds depending of the rod.

Test C – Not primed cardboards do not show IR influences on drying.
Test B – On primed sheets the ink dries within from 10 seconds to 120 seconds.

5.2 Pigment ink – ready to finish test

Test D – The drying duration of all prints with primer and with IR-drying was reduced. The maximum drying duration is 15 seconds. Missing both, the inks were not dry even after 24 hours. The most consistent results are achieved using rod-G.
Test C – Not primed cardboards do not show IR influences on drying.
Test B – On primed sheets the ink dries in about 120 seconds.

Table 4: Drying duration – ready to finish tests

Test Group	Cardbaord [ID]	Drying duration [sec]							
		Pigment ink				Dye ink			
		N/A	rod-W	rod-G	rod-R	N/A	rod-W	rod-G	rod-R
A	B-01	-				30			
	B-02	-				5			
	B-03	-				60			
	B-04	-				5			
	B-05	-				60			
	B-06	-				120			
	B-07	-				120			
B	B-01		-	120	120		60	15	15
	B-02		-	120	120		120	15	15
	B-03		120	120	120		30	60	60
	B-04		-	120	-		30	60	120
	B-05		120	120	120		120	30	10
	B-06		120	120	120		30	15	10
	B-07		-	120	120		120	30	10
C	B-01	-				10			
	B-02	-				5			
	B-03	-				60			
	B-04	-				5			
	B-05	-				120			
	B-06	-				-			
	B-07	-				60			
D	B-01		15	10	10		5	5	5
	B-02		10	15	10		5	5	5
	B-03		30	15	30		5	10	10
	B-04		30	15	-		5	5	10
	B-05		15	15	15		5	10	5
	B-06		15	15	15		10	5	5
	B-07		15	15	15		10	5	5

- = Ink was not dry after 24 hours

5.3 Line concept test – ready to stack and ready to finish tests

The line concept tests show that WB inkjet printed cardboards will be stackable when the substrate is PVOH primed before. As well cardboards will be ready for further finishing when the ink will be IR-dried, in addition. However, B-04 printed with dye ink and also with pigment and B-02 printed with pigment ink are not ready to finish after 5 minutes at the delivery of the press. Due to the reduction of the drying duration, the temperature of the IR-dryer must be highly increased from 200 °C to 500 ± 5 °C. Deformations on the cardboards were not observed. Figure 4 and 5 show a comparison of the 100 % K and PBK patches without primer and IR-drying with the same patches with both primer P-07 (rod-G) and IR-drying assistance.

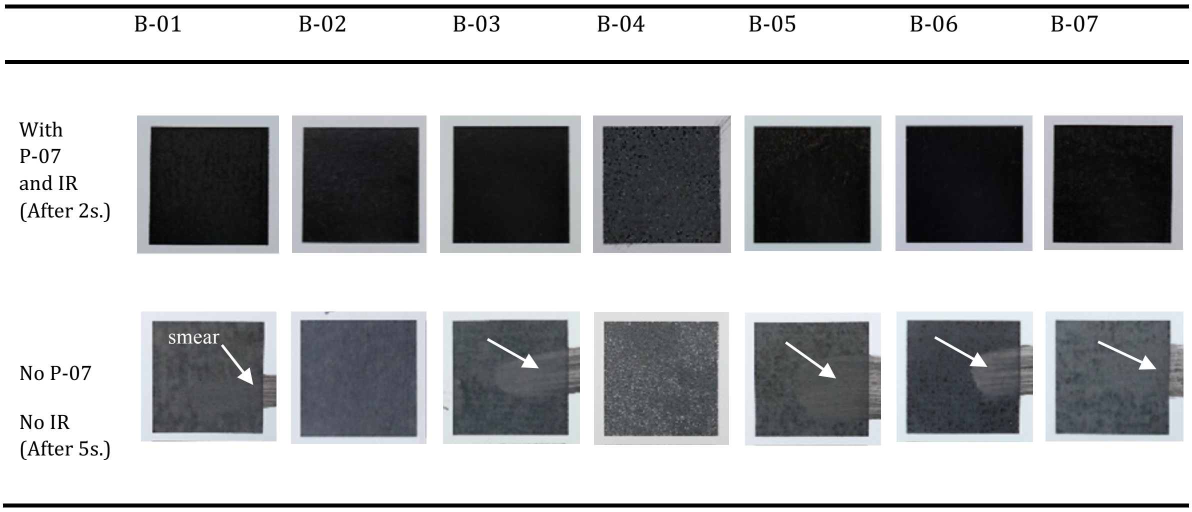

Figure 4: Results – Dye based K-Ink (K)

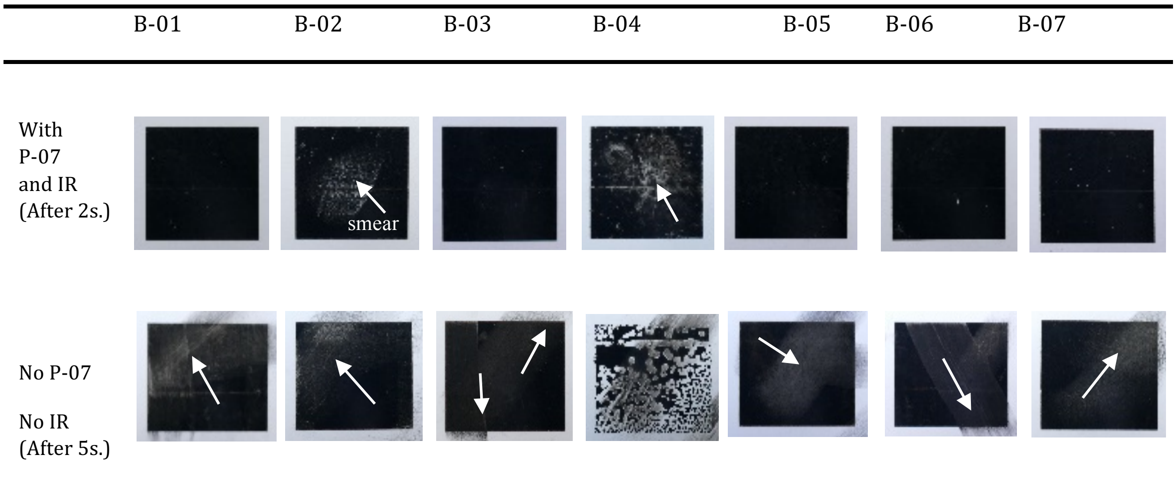

Figure 5: Results – Pigment based K-Ink (PBK)

6. Discussion

6.1 Influence the macro roughness

The PPS measurements show that the macro roughness of the cardboard decrease by application of primer (Table 5).

Table 5: Roughness measurements – PPS

	B-01	B-02	B-03	B-04	B-05	B-06	B-07
Without primer	1.70	1.33	1.02	0.94	1.36	1.20	1.30
With P-07	1.52	1.23	0.83	0.64	1.25	1.01	0.90

B-04 is an extremely smooth cast coated board. Primer application reduces even more its macro roughness, which may be an explanation for the inefficient ink adhesion both for pigments and dyes.

6.2 Influence of micro roughness

As the PPS test provides a partial characterization of the surface, further surface roughness measurements were conducted with a confocal 3D Laser Microscope. The results are presented in Table 6.

Table 6: Roughness measurements – Confocal 3D Laser Microscope

Cardboard [ID]	Sa [µm]	Str	Sdr [%]	Sku	Vvv [ml/m²]
B-01	0.971	0.85	202 %	3.27	0.150
B-01 - with primer	0.736	0.66	87 %	3.04	0.101
B-02	0.972	0.54	227 %	3.31	0.151
B-02 - with primer	0.800	0.68	133 %	3.28	0.122
B-03	0.870	0.87	219 %	3.47	0.136
B-03 - with primer	0.666	0.80	117 %	3.11	0.095
B-04	0.363	0.63	54 %	3.77	0.053
B-04 - with primer	0.357	0.63	51 %	4.05	0.052
B-05	0.921	0.73	188 %	3.31	0.145
B-05 - with primer	0.793	0.66	120 %	3.32	0.117
B-06	0.828	0.73	212 %	3.42	0.129
B-06 - with primer	0.588	0.75	83 %	3.18	0.086
B-07	0.925	0.54	224 %	3.42	0.140
B-07 - with primer	0.742	0.59	130 %	3.24	0.110

The Sa and Sdr measurements support the PPS measurements, i.e., the use of primer reduces both the surface roughness of all cardboards and the differences between the real and ideal area surface. The Str measurements not only evidences the difference between peaks and valleys, but also that these difference is very variable in all samples (a value close to 0 means that the surface is uniform and close to 1 not uniform).

The Sku measurements show that the form of the peaks of all samples tending to sharp (Sku > 3, Figure 6) but also show a reduction after priming. The fact that B-04 obtain higher sharpness after the primer application is unexpected and cannot be explained yet. Maybe the primer concentrated on certain areas. Since the amount of primer applied can vary inside a particular range, it is not possible to affirm that the small reduction of the volume of the valleys (Vvv) could be an argument against the accumulation of the primer on specific areas. De facto, the primer application over B-04 is inhomogeneous, the primer pearls, impairing the uniform transfer of the primer.

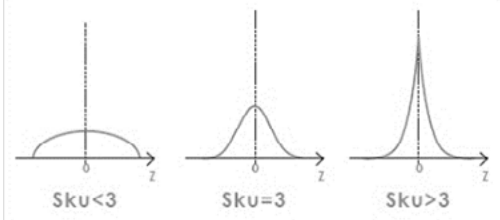

Figure 6: Peak forms – Sku (Keyence Corporation, 2015, pp. 9–15)

6.3 Influence of surface free energy

In comparison, the results obtained from contact angle measurements (Table 7) show that the application of P-07 reduced the contact angle and, as expected, increased the surface energy in all samples as a consequence of polar component increase.

Even though the test results show a relative uniformity, the repeatability of the tests is questionable. The measurement of the contact angle on each cardboard sample depends on the point of stability of the fluid on the cardboard's surface.

The dwell until each fluid takes to reach total repose takes between 3 seconds and 15 seconds. During this period the volume of the fluid's drop reduces due to absorption and the contact angle changes. Furthermore, it is not possible to identify on cardboard accurately the exact moment that the fluid stops to spread.

Though this test does not present any indication that explains the variation of results of B-02, it is possible to identify a trend. The polar component of all samples increased after the primer application what in general, improve the adhesion. B-04 shows an extremely low polar component with or without primer. However, as explained above, this test could not provide precise results with this type of porous and heterogenic surface.

Table 7: Contact angle and surface free energy (total, dispersion and polar components)

	B-01	B-02	B-03	B-04	B-05	B-06	B-97
				Without Primer			
Total [mJ/m²]	42.67	39.60	35.33	27.97	32.99	38.84	35.65
Disp. [mJ/m²]	27.89	32.50	28.52	23.43	24.81	23.61	29.93
Polar [mJ/m²]	14.78	7.10	6.81	4.54	8.17	15.22	5.71
CA - Diiodomethan [°]	50.56	50.04	51.64	55.38	52.72	57.16	49.76
CA - Water [°]	62.66	74.90	77.42	87.24	77.36	65.32	79.08
CA - Ethylene glycol [°]	44.46	56.04	56.34	72.34	63.58	52.98	56.04
				With P- 07			
Total [mJ/m²]	56.52	42.43	49.67	28.04	41.47	54.92	44.30
Disp. [mJ/m²]	31.90	23.56	29.80	22.94	30.98	27.68	30.62
Polar [mJ/m²]	24.62	18.87	20.18	5.10	10.48	27.24	13.68
CA - Diiodomethan [°]	40.56	51.98	54.90	51.68	58.70	50.76	54.86
CA - Water [°]	42.92	63.68	53.56	83.40	71.24	42.62	63.68
CA - Ethylene glycol [°]	15.96	23.88	15.02	71.52	20.02	17.08	26.52

7. Conclusions

The experiments demonstrate that PVOH can improve the adhesion of both pigment and dye WB inkjet inks. Considering the compatibility with the speed of current printing presses the ink drying process can be accelerate be means of IR radiation. Nevertheless, these effect do not base on priming and IR-drying only. As well these effects occur depending on the paper coating in addition. The B-02 and B-04 cardboards did not show the desired behavior.

Since the surface energy tests as well as roughness measurements did not provide a clear explanation, in particular for the B-02 (pigment) variation, future tests need to be performed as porosity measurement and chemical interactions between cardboard pigment coating and primer.

The visual appearance of all samples improved, but further tests will be conducted to investigate the print quality, as well as finishing tests in order to verify the influence of the primer on the adhesion of varnishes and laminations.

References

Chang, J., Gong, X., Pang, J., Wang, Y., Tu, J., Wu , H., & Liu, Z., 2018. Experimental Study on the Ink Jet Printing Quality Improvement of Ordinary Printing Paper with Polyvinyl Alcohol. In: P. Zhao, Y. Ouyang, M. Xu, L. Yang and Y Ren, eds. *Applied Sciences in Graphic Communication and Packaging: Proceedings of 2017 49th Conference of the International Circle of Educational Institutes for Graphic Arts Technology and Management & 8th China Academic Conference on Printing and Packaging. Lecture Notes in Electrical Engineering,* 477. Singapore Springer Nature, pp. 629–634.

Diamond, A.S. and Weiss, D.S. eds., 2002. *Handbook of Imaging Materials - Second Edition Revised and Expanded.* Basel: Marcel Dekker Inc.

Deutsche Institut für Normung, 2011. *DIN 55660-2:2011-12 - Paints and varnishes – Wettability – Part 2: Determination of the free surface energy of solid surfaces by measuring the contact angle*. Berlin: DIN, Beuth Verlag GmbH.

Hoath, S.D. ed., 2016. *Fundamentals of Inkjet Printing.* Weinheim: Wiley-VCH Verlag.

Kettle, J., Lamminmäki, T. and Gane, P., 2010. A review of modified surfaces for high speed inkjet coating. *Surface and Coatings Technology*, 204(12-13), pp. 2103–2109.

Keyence Corporation, 2015. *Referenzhandbuch - Laserscanningmikroskop für die Oberflächenanalyse*. Keyence.

Klöckl, I. 2015. *Chemie der Farbmittel: In der Malerei.* Berlin: De Gruyter.

Lamminmäki, T.T., Kettle, J.P., & Gane, P.A.C., 2011. Absorption and adsorption of dye-based inkjet inks by coating layer components and the implications for print quality. *Colloids and Surfaces A: Physicochemical and Engineering Aspects*, 380(1-3), pp. 79–88.

Magdassi, S., 2010. *The chemistry of inkjet inks.* Singapore: World Scientific Publishing.

Onishi, H., Iida , J. and Owatari, A., Seiko Epson Corp. 1997. *Ink jet recording film comprising cation-modified polyvinyl alcohol and recording method using the same*. U.S. Pat. 5,662,997.

Ridgway, C.J., Kukkamo, V. and Gane, P.A.C., 2011. Effect of binders and additives on inkjet coating pigment pore structure. In: *Proceedings Paper Conference and Trade Show 2011 (PaperCon 2011)*. Covington, Kentucky, USA, 1–4 May 2011. Tappi Press GA, pp. 1305–1319.

Sousa, S., Sousa, A.M., Reis, B. and Ramos, A., 2014. Influence of binders on inkjet print quality. *Materials Science*, 20(1), pp. 55–60.

Svanholm, E., 2007. *Printability and ink-coating interactions in inkjet printing.* Ph.D. Thesis. Karlstad University.

List of acronyms

IRL	Inkjet Receiving Layer
WB	Water Based
PVOH	Polyvinyl Alcohol
PBK	Pigment Black Ink
IR	Infrared
Sa	roughness average
Str	texture aspect ratio
Sdr	difference between real and ideal surface
Sku	sharpness of the roughness profile
Vvv	volume of the valleys
CA	Contact Angle

Design of a Lightfastness Calculator for Printed Materials

Fons Put[1] *and Michiel Van den Saffele*[2]

[1] Flemish Innovation Center for Graphic Communication, Campus Blairon 5, 2300 Turnhout, Belgium
[2] Arteveldehogeschool, Department Graphic and Digital Media, Industrieweg 232, 9030 Gent-Mariakerke, Belgium
E-mail: fons.put@vigc.be

Short abstract

Print for outdoor applications has gained popularity, as shown for example by the further growth of large format printing. Specific point of attention for outdoor applications is the lightfastness of the printed matter. Exposure to light will degrade substrate and color pigments or dyes with unacceptable color changes as a consequence. Specific developed toners and inks for digital printing equipment have targeted the market with enhanced outdoor performance. The challenge for printing companies lies in selecting the right printing materials for the job. Over dimensioning means extra costs, inadequate performance causes claims. The lightfastness properties of a number of offset and digital printing materials were analyzed. With the results a calculator is designed to support printing companies in selecting the proper printing materials and methods.

Keywords: accelerated weathering tests, lightfastness, digital printing

1. Introduction and background

In 2008 we received the first signal that printing for outdoor applications demands a minimal knowledge of the lightfastness of printed materials. A producer of digital printing equipment started printing labels for selling flowers in garden centers. The labels were exposed in direct sunlight during spring – see Figure 1. Already within 2 weeks the labels lost their color properties with customer claims as a consequence. Since then lightfastness properties of conventional and digital printed matter were tested for a number of clients. During this period, we used identical testing methods, but improved our reporting towards our clients. ISO 12040, “Graphic technology - Prints and printing inks - Assessment of light fastness using filtered xenon arc light” (International Organization for Standardization, 1997), gives already a rough indication of lightfastness quality by defining a wool scale category. This is a good start but lacks accuracy for the different outdoor conditions. Our goal was to develop a reporting method that enables our clients to compare materials and processes and make reliable simulations for specific outdoor conditions.

Research in this area was conducted in previous years by Fogra (Rosenberg, Pertler and Steger, 2002; Kraushaar, et al., 2008) and by Koltai, Horváth and Bartha (2017).

Figure 1: Color degradation of offset printed packaging in outdoor conditions

2. Materials and methods

2.1 Equipment

An Atlas Suntest CPS+ weathering unit is used to carry out accelerated weathering tests, Figure 2a. The unit consist of a powerful Xenon lamp with services to control the temperature and radiation in the exposure chamber.

Configuration:

- Light source: filtered Xenon (coated quartz filter)
- Irradiance: 765 W/m^2
- Temperature: 35 °C (Black Panel Temperature)

The X-rite i1PRO2 spectrophotometer enabled us to quantify the color changes, Figure 2b. Spectral measurements were made with instrumentation "D50, 2-degree, geometry 45/0, no polarization filter, white backing, M1 mode according to ISO 13655:2009" (International Organization for Standardization, 2009). Note that the D50-like illuminant of this instrumentation characterize optical brighteners in papier coatings accurately. This is of importance because optical brighteners were found to be very sensitive to degradation by outdoor exposure.

a) b)

Figure 2: a) Exposure chamber of the Atlas Suntest CPS+ weathering unit;
b) the X-rite i1Pro2 spectrophotometer in practice

2.1 Exposure procedures

To further improve the number of tested materials, suppliers of printing equipment were asked to print a test form on uncoated/coated paper substrates and a plastic substrate, Figure 3. The print results were first measured unexposed and later on exposed in the Suntest CPS+ unit. The strips were daily measured during a 3-week total exposure time. Important to note that the position of the different printed strips in the exposure chamber is changed after every measurement. This to level out exposure variations in the chamber.

Figure 3: Printing form to characterize digital print output

Following patches are used for lightfastness analysis:

- Process colors: cyan, magenta, yellow, black
- Overprint colors: red, green, blue
- Grey halftones: composed by black only and a cyan, magenta, yellow mixture.

2.2 Color measurement procedures

The CIELab coordinates of the patches during exposure are the result of averaging 4 measured patches, where each patch measurement is also an average of a 20 mm wide scan measurement.

To quantify color degradation, the color difference formula CIEDE2000 (ISO 13655) is used. This formula corrects for the non-uniformity of the CIELAB color space for small color differences which leads to a good correlation with observer perceived color differences.

To connect the resulting color difference to observers the table published by FOGRA is used. A quality threshold of CIEDE2000 = 3 is advised to our clients in evaluating materials and printing technologies. The values are described in Table 1.

Table 1: The meaning of calculated color differences

CIEDE2000	**Impression of the color difference**
Below 0.5	Normally not noticeable
Between 0.5 and 1	Very small difference, only visible for trained color professionals
Between 1 and 2	Mediate difference, also noticeable for non-color professionals
Between 2 and 4	Noticeable color difference
Above 4	Strong color difference

3. Results and discussion

3.1 The exposure results

Figure 4 shows an example of an exposure result (process yellow). The more radiation the printed sample strikes, the higher the color degradation becomes. The degradation process is slowly building up without quick changes. Description of the color changes in CIELAB color space is done by describing the color change, starting from the unexposed color sample. Figure 4 shows that this can be done with good correlation by polynomial functions. For all tested materials and colorants the coefficients are stored in a small database.

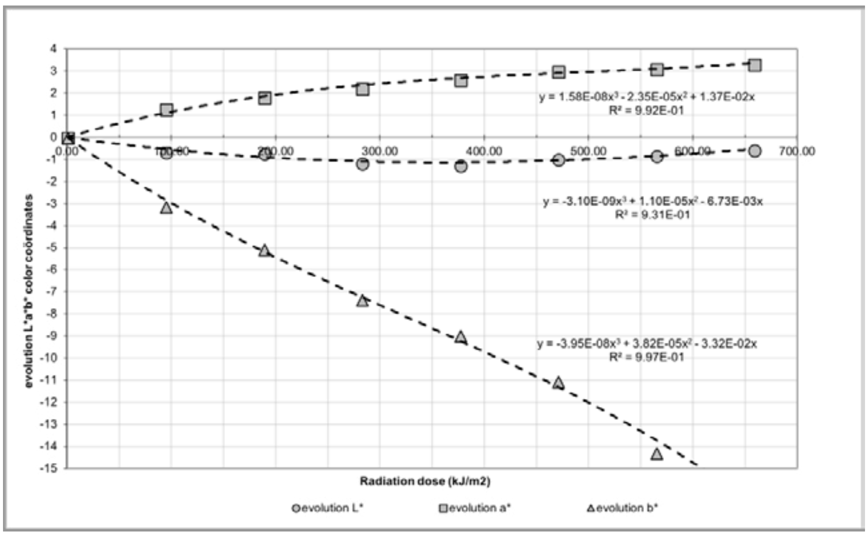

Figure 4: Description of exposure result of a production dry electrophotography printed yellow

3.2 Weathering information

As a second step in the design of a lightfastness calculator weathering information is gathered from a number of weathering stations worldwide. These stations are reporting daily radiation figures and monthly and yearly averages (Table 2) in the following format:

Table 2: Yearly radiation averages of different weathering stations

Location	300–3 000 nm Global (MJ/m²)	300–800 nm UV+visible (MJ/m²)	300–400 nm UV (MJ/m²)	340 nm Global (MJ/m²)
Florida	5 850	3 400	355	3.2
Arizona	8 000	4 600	485	4.4
Central Europe	3 550	2 050	215	1.9
South of France	5 000	2 900	300	2.7

The 300–800 nm UV+visible MJ/m^2 – format is the best spectral match with the Xenon exposure lamp and filters in the Suntest equipment. The cumulative radiation can be expressed in function of the daily measurements by weathering stations. Again, polynomial functions are suitable to describe this behavior with fine correlation, Figure 5.

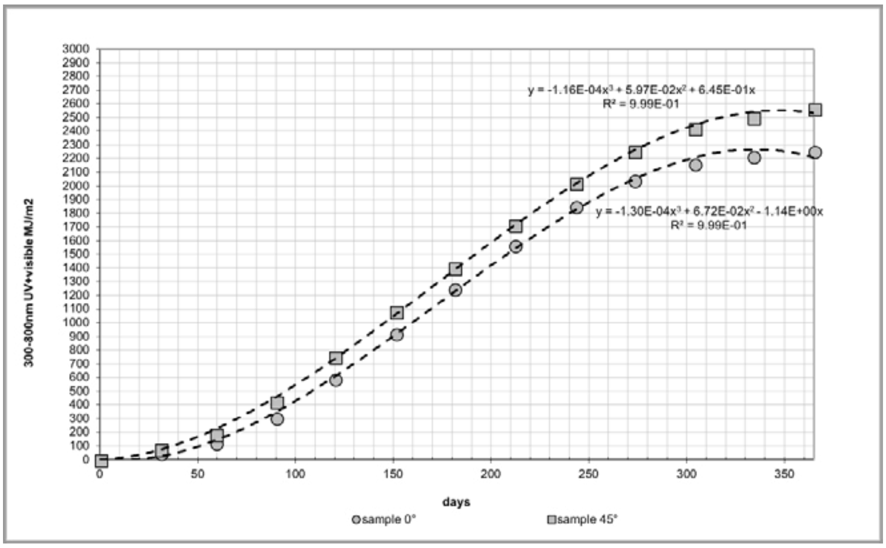

Figure 5: Increasing radiation starting on the first of January for a specific weathering station; he orientation of the print sample is also of influence (0, 45°)

3.3 Calculating performance

Exposure results and weathering information can now be used to predict sample degradation.

Following parameters have to be selected:

- Tested printing condition (type of printer, substrate,)
- Weathering location
- Outdoor start date

After selection, the calculator shows the expected color degradation as a function of time (days, starting from the outdoor start date), Figure 6. A proposed threshold for acceptance of CIEDE2000=3 is drawn as a support for customer acceptance.

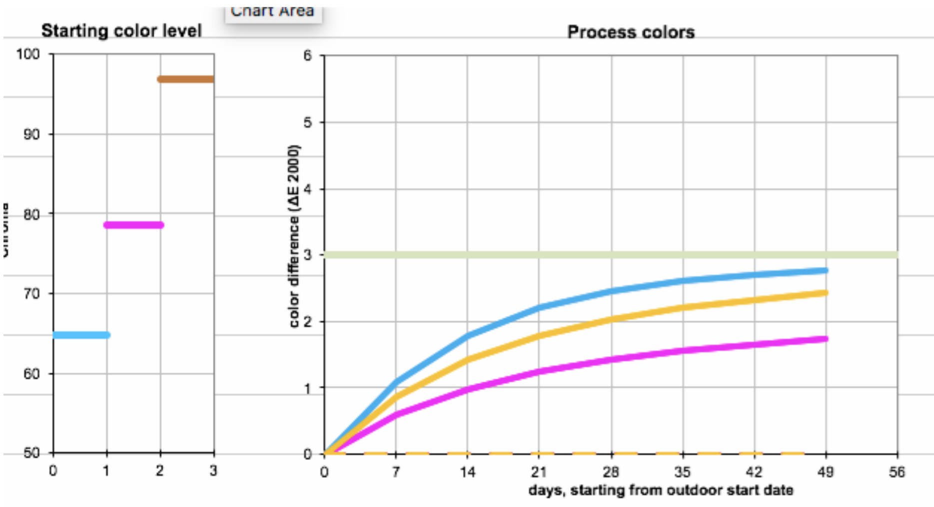

Figure 6: Output of the lightfastness calculator

3.4 Color Management

To further support the quality of the prediction, color management can be used. Here for a minimal color chart is measured during exposure, Figure 7. ICC profiles are calculated and can be used to soft and hard proof the color degradation of specific designs.

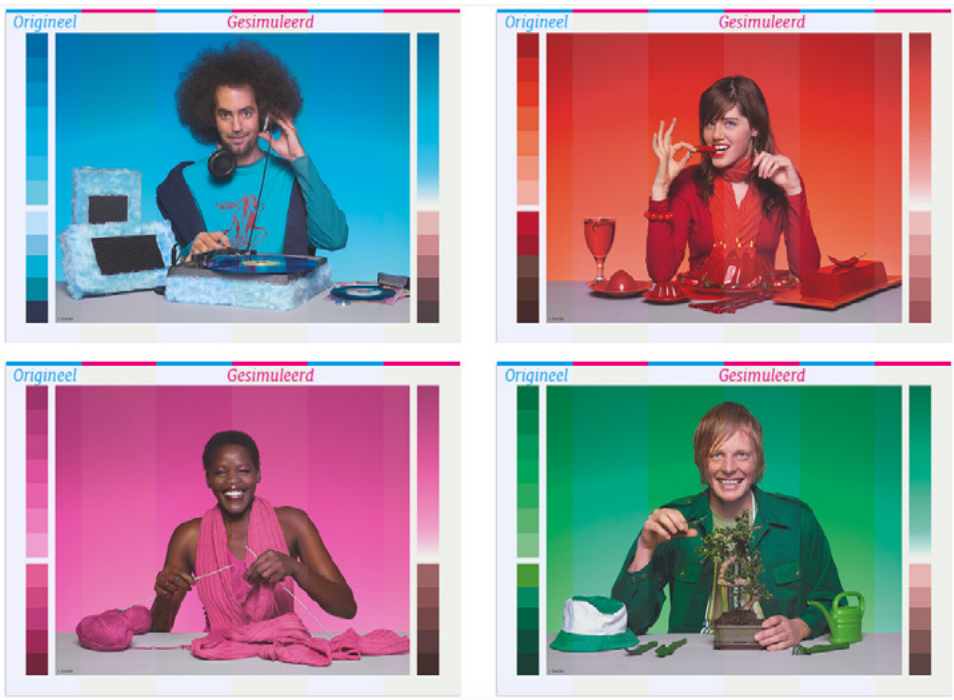

Figure 7: Simulation of color degradation by ICC color profiles.

4. Conclusions

Comparing of all the results in the lightfastness calculator shows a number of trends. Yellow is the weakest process color in offset. This could be explained by the absorption spectrum, yellow absorbs powerful UV and blue wavelengths, cyan does not. Inkjet and toner printing doesn't show these trend, yellow is in ink-jet and toner not necessary the weakest link. In choosing substrates, the presence of optical brighteners makes it vulnerable for fast degradation. The bluish tint will turn quickly to yellow. When adding finishing layers, these can dramatically reduce the lightfastness properties of a print. Especially vanish is prone to yellowing.

As a general conclusion the lightfastness calculator appears to be a quick and easy tool to compare and evaluate print in specific outdoor conditions.

References

Koltai, L., Horváth, C. and Bartha, E., 2017. Accelerated weathering tests of parking vignettes. In: P. Gane and C. Ridgway, eds. *Advances in Printing and Media Technology: Proceedings of the 44th International Research Conference of iarigai. Fribourg, Switzerland, September 2017. Darmstadt: iarigai, pp. 39–44.*

Kraushaar, A., Geßner, F., Bickeböller, C. and Karp, P., 2008. *Untersuchung moderner Farbabstandformeln: Fogra-Forschungsbericht Nr. 60.054*. München: FOGRA.

Rosenberg, A., Pertler, H. and Steger, E., 2002. *Light - and weatherfastness of printed products: Fogra - Research Report No. 52.024.* München: FOGRA.

International Organization for Standardization, 1997. *ISO 12040:1997(en) Graphic technology - Prints and printing inks - Assessment of light fastness using filtered xenon arc light*. Geneva: ISO.

International Organization for Standardization, 2009. *ISO 13655:2009(en) Graphic technology - Spectral measurement and colorimetric computation for graphic arts images*. Geneva: ISO.

DNA and DNA Staining as a Test System for the Development of an Aptamer-based Biosensor for Sensing of Antibiotics

Jacqueline Stamm[1], *Dieter Spiehl*[1], *Jeannine Jaeger*[2], *Florian Groher*[2], *Tobias Meckel*[3], *Beatrix Suess*[2] *and Edgar Dörsam*[1]

[1] Institute of Printing Science and Technology, Technische Universität Darmstadt, Magdalenenstraße 2, 64289 Darmstadt

[2] Department of biology, synthetic genetic circuits, Technische Universität Darmstadt, Schnittspahnstraße 10, 64287 Darmstadt

[3] Macromolecular and Paper Chemistry, Technische Universität Darmstadt, Alarich-Weiss-Straße 8, 64287 Darmstadt

E-mails:stamm@idd.tu-darmstadt.de;spiehl@idd.tu-darmstadt.de;jaeger.jea@bio.tu-darmstadt.de;groher@bio.tu-darmstadt.de; meckel@cellulose.tu-darmstadt.de; bsuess@bio.tu-darmstadt.de; doersam@idd.tu-darmstadt.de

Short abstract

It has become necessary to create a quick, efficient and low-cost verification procedure for antibiotics detection, because of increasing resistance and multiple resistance of bacteria against antibiotics duo to their excessive use on food-producing animals. We propose an inkjet-printed aptamer-based biosensor initially adapted for the detection of the fluoroquinolone ciprofloxacin (CFX). To obtain starting parameters for the open questions on the printing process, the carrier material, required concentrations and fluorescence detection preliminary experiments with different DNAs and DNA dyes are executed. The printing process is analyzed by characterizing DNA and buffer solutions and by comparing printed with unprinted DNA using an agarose-gel test. The carrier materials are preselected by analyzing the auto fluorescence excitation and emission spectra of 10 different materials out of which three with the lowest intensity at the CFX excitation and emission peaks are chosen. On these materials the fluorescence of CFX as well as DNA and DNA dyes are measured. The experiments show that nucleic acids can be inkjet-printed without damage and that many foils and papers commonly used in the laboratory show auto fluorescence when excited in the UV-spectrum. The inconsistent results with DNA and DNA dyes on suitable materials illustrate that not all relevant parameters are taken into consideration yet.

Keywords: Inkjet printing, functional printing, RNA

1. Introduction and background

Antimicrobial drugs are used on food-producing animals for therapeutic, prophylactic or growth promoting purposes. They include disinfectants, antiseptics and antibiotics. It is an almost inevitable consequence that bacteria constantly exposed to antibiotics become resistant and the antibiotics ineffective. Since 1990 the resistance and particularly multiple resistance to several antibiotics has increased drastically in developed countries leading to numerous outbreaks of serious diseases (Threlfall, et al., 2000). In fact, antibiotic resistance is known to be one of the main public health problems (Novais, et al., 2010). Most antibiotics used are sulfonamides (20 %) or fluoroquinolones (19 %), followed by aminoglycosides (15 %), phenicols (15 %), β-lactams (15 %), tetracyclines (8 %) and oxazolidinones (8 %) (Cháfer-Pericás, Maquieira and Puchades, 2010).

To control and determine the propagation of antibiotics in food a quick, efficient and low-cost verification procedure is needed. Biosensors fulfil these requirements and have already proven themselves in different areas including but not limited to food quality control (Kivirand, Kagan and Rinken, 2013). A biosensor consists of three parts: the sensitive biological element, which binds to the target molecule; the transducer, which transforms the interaction into a measurable signal; and the signal processor, which displays the result in a user-friendly way (Kivirand, Kagan and Rinken, 2013).

Currently established methods of detecting antibiotics can be divided into two groups. Most frequently used are confirmatory methods, generally involving mass spectrometry. They are, however, time consuming, expensive and require specific equipment as well as training. Second are screening methods such as microbiological assays and immunoassays. While microbiological assays lack specificity and require long incubation times, immunoassays require the *in vivo* production of antibodies and are restricted in possible targets to antigens. The development of other screening methods is increasing considerably, with biosensors currently taking up 8 % of all used methods (Cháfer-Pericás, Maquieira and Puchades, 2010).

The possibility for a new biosensor method has arisen twenty years ago with the development of synthetic aptamers. Their properties and advantages in antibiotics detection are discussed in section 2.1.

There are several components to consider when developing a printed biosensor. On the one hand the proper printing technology has to be selected, as well as an appropriate carrier material and its pretreatment, both of which need to be compatible with the bio selective material, i.e. in our case, the aptamer. On the other hand, the aptamer has to be developed precisely for the antibiotic to be detected including a detector system that produces readable output (Groher and Suess, 2016). A straightforward approach is given by the fluoroquinolone antibiotic ciprofloxacin (CFX) and an aptamer developed to bind CFX (Groher, et al., 2018), as the auto fluorescence of CFX is quenched after binding with its aptamer, thereby producing a direct detector system. Hence, only the change in intensity of the fluorescence has to be determined to obtain the concentration of CFX in a liquid applied onto the aptamer-based sensor.

The preliminary tests presented in this abstract concern themselves with the alternative system, namely DNA and DNA dyes, which similarly produces an altered fluorescence intensity after binding to one another. The idea is to learn about nucleic acid behavior while printing and on materials, as well as about concentrations needed before starting actual experiments with the CFX binding aptamer.

2. Materials and methods

2.1 A CFX-binding aptamer

Aptamers are approx. 25 – 100 nucleotide-long deoxyribonucleic acids (DNA) or ribonucleic acids (RNA), that bind specifically to molecular targets. They possess a complex three-dimensional structure, which entwines around its specific target, its ligand, upon binding (Garst, Edwards and Batey, 2011). Other interactions are also involved in recognizing the target molecule (Edwards, Klein and Ferré-D'Amaré, 2007). Additionally, aptamers can be denatured reversibly. This means that changing the surrounding conditions will only cause aptamers to temporarily unfold, while – upon returning to the original binding conditions – they are able to regain their functionality (McKeague and DeRosa, 2012).

The *in vitro* procedure of generating aptamers enables a great control over the binding conditions and the target selection. They can be generated de-novo for a specific ligand via a procedure called systematic evolution of ligands by exponential enrichment (SELEX). Usually 6 to 20 cycles of this procedure are needed (Ellington and Szostak, 1990).

We have developed a CFX-binding RNA-aptamer using SELEX. CFX belongs to the fluoroquinolones and is used to treat a wide variety of bacterial infections on animals and humans.

After 10 rounds of SELEX specific clones were selected and analyzed concerning their dissociation constant (K_D). The smaller the KD-value, the higher the affinity between aptamer and ligand. The best affinity and titration curves were given by a clone called R10K6 with K_D = 31.2 nM shown in Figure 1 (Groher, et al., 2018). In the discussed experiments the mutant R10K6_V11 is used, which was selected as minimal motif in previous works (Jaeger, 2017) and is also shown in Figure 1.

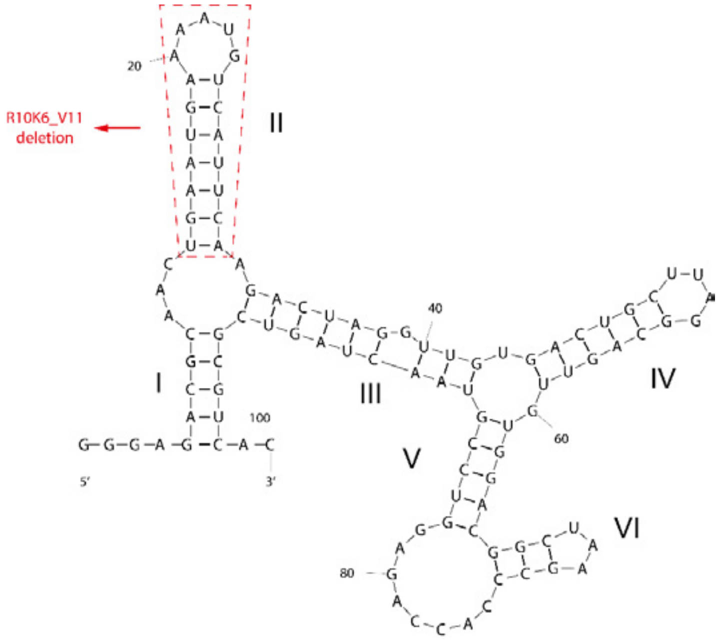

Figure 1: The secondary structure of the CFX-binding aptamer R10K6; the minimal motif R10K6_V11 has strain II deleted

Importantly, while handling aptamers, any contact with RNase has to be strictly avoided, as this enzyme breaks down RNA. Before handling the aptamer solution, it has to be thawed from its storage temperature of -20 °C to room temperature followed by an initiation of the folding. This is achieved by placing the solution at 95 °C for 5 minutes, followed by snapcooling by placing it on ice.

In the presented preliminary tests experience is gathered in handling and printing nucleic acids as well as its behavior on different carrier materials by using an alternate system with DNA.

2.2 DNA and DNA dyes

DNA is a pair of polynucleotide biopolymer strands that form a so called double helix, RNA is a single strand of said polymer. DNA dyes are used to make DNA visible. They intercalate in the DNA, meaning they insert themselves between the bases and fluoresce after excitation.

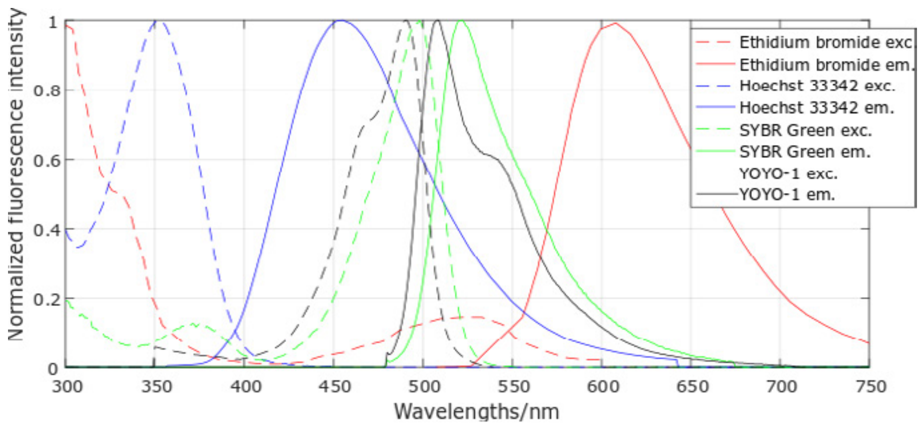

Figure 2: Excitation and Emission spectra of selected DNA dies; the normalized fluorescence intensity is given over the wavelengths in nm, data taken from Thermo Fisher (n.d.)

Figure 2 shows the excitation and emission spectra of a selection of DNA dyes. All of them increase their fluorescence after binding. The experiments mentioned and shown here use Hoechst 33342 (Thermo Fisher Scientific, Waltham, MA, USA), because of its similar fluorescence excitation and emission spectra to CFX; and YOYO-1 iodide (Thermo Fisher Scientific, Waltham, MA, USA), because of its significantly higher intensity increase after intercalating.

There are three different kinds of DNA we use for different experiments: DNA with low molecular weight ($m_w \approx 1.3$ to 7.9 million g/mol), DNA V11 and a plasmid solution. Their properties and usages are listed in Table 1.

Table 1: The used DNA and RNA solutions with their properties and applications

Name	Properties	Usage
DNA low m_w	Salmon sperm, low priced	Analyzing fluid properties
DNA V11	R10K6_V11 as DNA	Functional tests
Plasmid	Circular DNA	Shear force stress test
R10K6_V11	CFX aptamer	CFX detection

2.3 Printing methods & carrier materials

The established printing processes can be divided into conventional printing, which requires a printing plate and non-impact printing (Kipphan, 2001). Considering the requirements of transferring small amounts of nucleic acids in a clean environment, one option of each group seems most promising: Inkjet and gravure printing. In both methods, it is possible to have all materials coming into contact with the ink made from inert plastics like PTFE and PP, chromium, stainless steel or silicone. We will focus on inkjet printing because of its variable dispensing options.

The used inkjet printer Autodrop from Microdrop Technologies is equipped with piezo-based drop-on-demand single nozzle print heads. Each drop has a volume of approx. 260 pl. The drop space can be varied to create different volume per area concentrations. The driving voltage of the printhead is set to 68 V, the pulse length is 24 µs and the frequency is 100 Hz.

Ten different materials were initially chosen from the categories paper, plastic and combinations of both. Their names are listed in Table 2 together with the manufacturer and material general name.

Table 2: The materials initially chosen as possible carriers to print on; in the text called by their specific name

Specific name	Manufacturer	Material	Thickness
Hostaphan GN 4600	Mitsubishi Polyester Film	Polyethylentherephthalat (PET)	125 µm
Hostaphan GUV 4600	Mitsubishi Polyester Film	Polyethylentherephthalat (PET)	50 µm
Melinex 339	DuPont Teijin Films	Polyethylentherephthalat (PET)	250 µm
Melinex Q65FA	DuPont Teijin Films	Polyethylennaphthalat (PEN)	125 µm
SyntiTec 3900	Sihl Direct	Polypropylen (PP)	180 µm
SFT 40 T	Taghleef Industries	Biaxially oriented polypropylene (BoPP)	40 µm
Rotilabo 601	CARL ROTH	Paper	160 µm
Whatman Grade 1	GE Healthcare	Paper	180 µm
Amersham Hybond RPN2020N	GE Healthcare	Nylon membrane	160 µm
HF 120	Millipore	Nitrocellulose	230 µm

3. Results and discussion

Two kinds of experiments are carried out. One concerning the printing process and one involving fluorescence measurements. The printing experiments aim is to show that DNA can be printed without taking damage. With the fluorescence experiments CFX-suitable carrier materials and concentrations are preselected. Here two devices are used for fluorescence detection. For fluid measurements a microplate reader (CLARIOstar, BMG LABTECH), is chosen, as it allows for precise recordings of both excitation and emission spectra. However, the device records the spectral properties of each sample on a single point, making it suitable for measurements of homogeneous fluids but not for potentially inhomogeneous solid samples. For inhomogeneous samples a space-resolved imaging method is needed given by the imager Fusion FX Edge from Vilber.

3.1 Printing

First the DNA with low m_w, single fold concentrated buffer and water from the Milli-Q processing plant are characterized. The density is determined with a pycnometer, the surface tension (ST) and its polar and disperse parts are measured with the tensiometer DSA 100 from Krüss. The results are shown in Table 3. Within their measurement errors all fluids have the same properties. It is assumed that all printing techniques suitable for water should also work with nucleic acid solutions. First printing tests show no problems after filtration of the ink prior to printing using a PES-filter having a pore size of 0.2 µm.

Table 3: Fluid characterization of water, buffer and DNA in buffer

	Water	**Buffer**	**Buffer + DNA low m_w**
Density in g/ml	0.997541	1.00 ±0.02	1.01 ±0.02
ST in mN/m	70 ±5	68 ±4	70 ±4
ST disperse	30 ±5	28 ±4	33 ±5
ST polar	40 ±8	40 ±6	36 ±6

Whether the molecules are damaged during inkjet printing, is tested with a plasmid solution. One part is kept at the Biology department, another is transported and stored, the last part is printed. The printing was done over several minutes at a constant position into a test tube to collect 200 µl. An agarose-gel assay test (Figure 3) shows no difference in the molecular sizes of all solutions. It is concluded, that the shear stress from inkjet printing does not tear plasmid molecules apart and will not damage similar molecules such as aptamers. This is also suggested by other works on inkjet printing DNA micro-arrays (Goldmann and Gonzalez, 2000), fabricating microfluidic paper-based analytical devices (Yamada, et al., 2015) and depositing nucleic acids to fabricate DNA chips (Okamoto, Suzuki and Yamamoto, 2000).

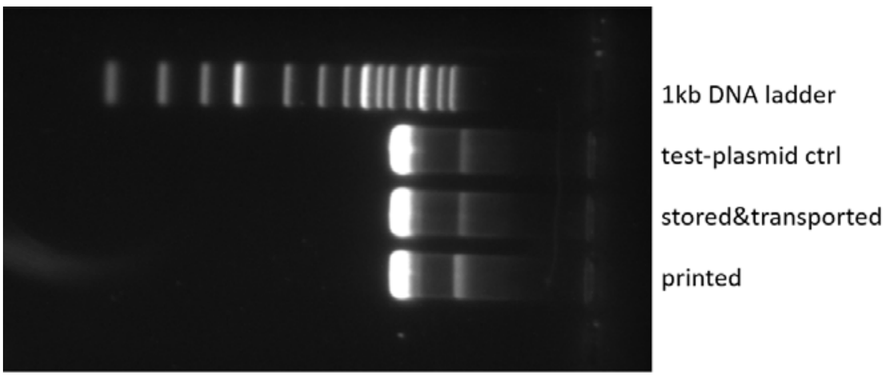

Figure 3: Plasmid test with 1 % Agarose-gel in TBE buffer; the stored, transported and printed solutions show a similar behavior

3.2 Fluorescence measurements

First the fluorescence of CFX is measured. With known maximum excitation and emission wavelengths of CFX, the fluorescence of all the carrier materials that could interfere with the CFX detection can be determined. In the end, different combinations of DNA dyes and materials, as alternative system, are tested in their ability to distinguish between different DNA concentrations.

3.2.1 CFX

The fluorescence of CFX is measured with the microplate reader. The excitation spectrum recorded at an emission of 422 nm and the emission spectrum recorded at an excitation of 328 nm are shown in Figure 4. Based on these spectra, the optimal combination of light source (UVB transillumination, yellow) and emission filter (F440, blue) are chosen to achieve the best sensitivity for imaging CFX.

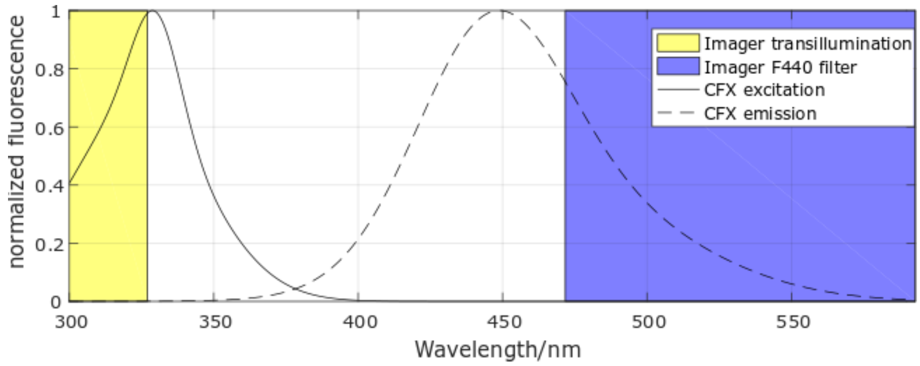

Figure 4: Fluorescence of CFX measured in the microplate reader and corresponding wavelength range for illumination and detection in the imager; the data is extrapolated below 320 nm with a two term Gauss fit

3.2.2 Carrier materials

To determine which carrier material has the lowest auto-fluorescence in the range of the illumination and detection wavelength of CFX, all materials listed in Table 2 are examined at the maximum excitation and emission wavelength of CFX by an illumination at 328 nm and a detection at 450 nm, respectively. The measurements are carried out with punched-out pieces of the materials placed in a microplate and the measured fluorescence intensities are shown in Figure 5 in logarithmic scale to illustrate the broad range in intensities.

Especially paper, because of its lignin content, but also certain plastics show a high fluorescence, which correlates with their thicknesses as seen by the three PET foils. The normalized spectra are shown in Figure 6 and Figure 7 and show the behavior at different wavelengths, they are grouped accordingly. In Figure 6 the excitation maxima lie at around 330 nm and 350 nm; the emission maxima are lower than 400 nm. All included materials are made from paper, nitrocellulose and nylon membrane, with the exception of one foil. All other foils show different spectra shown in Figure 7. The excitation maxima are around 370 nm and there are several different emission maxima between 400 nm and 450 nm.

Three different materials with least fluorescence are selected for further experiments: the nitrocellulose HF 120, Hostaphan GUV 4600 and the paper Whatman Grade 1. The PET foil was chosen over the BoPP foil SFT 40 T, because the latter is only produced in unpractically thin films.

Other works on depositing biological materials use nitrocellulose and nylon membrane (Goldmann and Gonzalez, 2000) or filter paper and chromatography paper (Yamada, et al., 2015). They are composed of pure cellulose without additives such as brighteners, which might interfere with fluorescence-based detection.

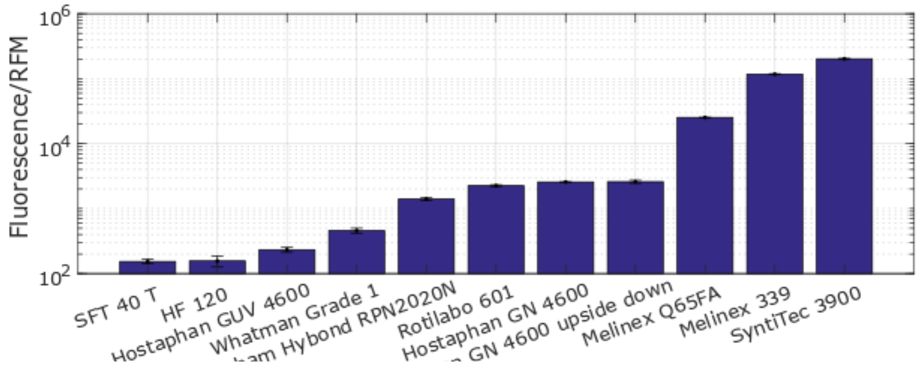

Figure 5: Fluorescence of the different materials at CFX excitation (328 nm) and emission maxima (450 nm) taken with the microplate reader and shown in logarithmic scale

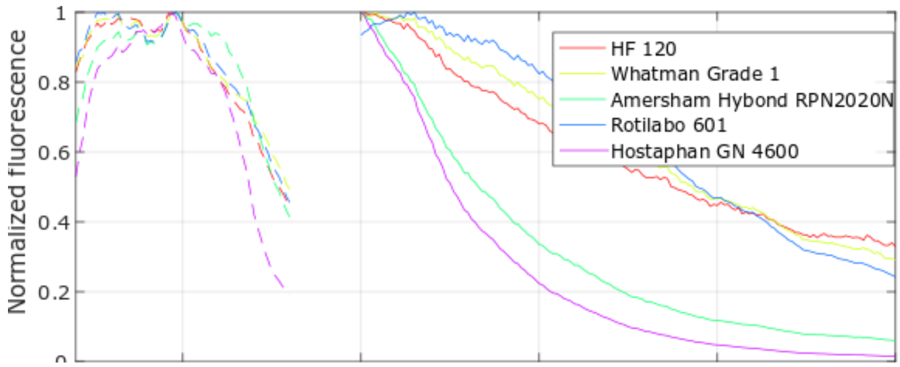

Figure 6: Normalized excitation (dotted) and emission (continuous line) spectra of different potential carrier materials, measured at 328 nm excitation and 450 nm emission

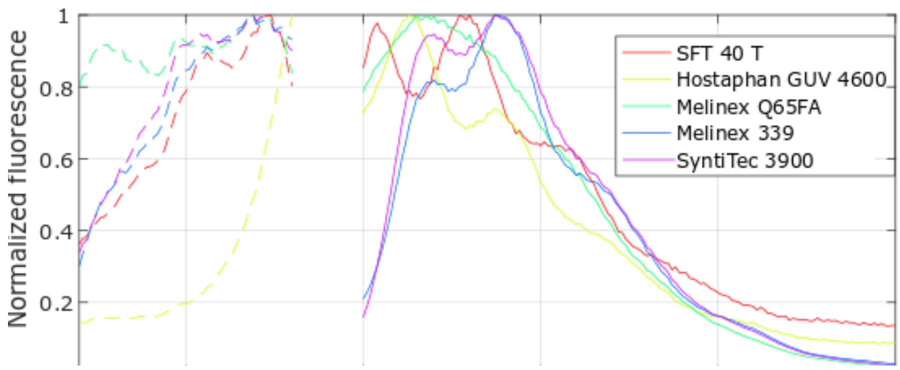

Figure 7: Normalized excitation (dotted) and emission (continuous line) spectra of different potential carrier materials, measured at 328 nm excitation and 450 nm emission

3.2.3 DNA & DNA dyes

Hoechst 33342 has the most similar fluorescence spectrum to CFX and seems promising to function as an alternative system for doing pre-tests for printing of aptamers and detection of CFX. Measurements in Figure 8 using the microplate reader show the characteristic rise and saturation of fluorescence when increasing the DNA concentration while holding the amount of 178 nM Hoechst constant. The problem is the relatively high fluorescence of the DNA dye alone when no DNA is present. The fluorescence intensity of Hoechst 33342 bound to DNA is not even twice the intensity of the unbound one, which was not expected, as the literature claims a twentyfold increase after binding. This is probably the case because DNA dyes are usually used with gel assays or inside cells, where the DNA concentration is a lot higher than the tested solutions with up to 1 µM. Furthermore, gels or assays are washed after staining to have only the dyed DNA left for detection.

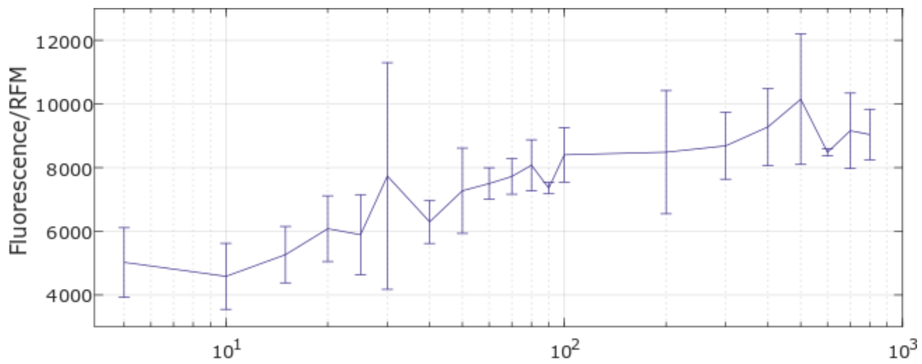

Figure 8: Fluorescence of different DNA V11 concentrations mixed with a constant amount of Hoechst 33342 dye, averaged over three microplate reader measurements

Nonetheless the experiment is conducted with Hoechst, since different lower DNA concentrations can be distinguished by fluorescence. A solution containing 10 µM DNA is printed onto the three selected carrier materials and left to dry, using the parameters in Table 4. Onto the same spots different solutions of Hoechst concentrations, 10 nM, 100 nM, 1 µM, 10µM are pipetted and the fluorescence is measured with the imager in wet and dry state. Unfortunately, all materials containing foils filter out the UVB transillumination, leaving only the paper as possible carrier. On Whatman Grade 1 only the highest Hoechst concentration is visible, with small changes between the different DNA concentrations. The integrated intensity of the wet area increases between zero, 0.01 µl and 0.1 µl DNA-solution, but falls to its initial value at 1 µl and 10 µl, with the difference that the fluorescence of the last one is spread more evenly instead of accumulating in the middle, see top left in Figure 9 .

Table 4: Inkjet printing parameters for four 5 mm × 5 mm squares with increasing DNA concentration

Drop space	**Grid size**	**Drop volume**	
mm	drops	ml/m^2	µl
1.180	6 × 6	0.2	0.01
0.354	20 × 20	2	0.1
0.114	62 × 62	20	1
0.036	196 × 196	200	10

Hence, the DNA dye YOYO-1, from Thermo Fisher Scientific, is chosen as an alternative to Hoechst 33342 because of the fact that it is stated to have an enormously larger difference in fluorescence between the bound and unbound state. For excitation epi-illumination with an LED with 460 nm ± ≈15 nm is used and for detection the filter F-590, which passes through 530–600 nm wavelengths.

The best results are obtained on Whatman Grade 1 with the 1 µM YOYO-1 dye. The integrated density of the fluorescence intensity increases steadily for bigger DNA drop volume. Again, the fluorescence is more evenly spread for bigger DNA drop volumes.

The general drop spreading is the greatest on Whatman Grade 1 paper, as expected from its medium porosity when compared to PET and nitrocellulose, which is used in lateral flow tests. It was suspected, that less of the DNA would be available for intercalation because of its spreading and possibly other interactions with the paper. But these factors prove to be less significant than the immobilization potential of the filter paper. A work on detecting viruses of dried serums, compares Whatman Grade 1, nylon membrane and nitrocellulose membrane as possible carrier materials and comes to the same result (Wang, Giambrone and Smith, 2002).

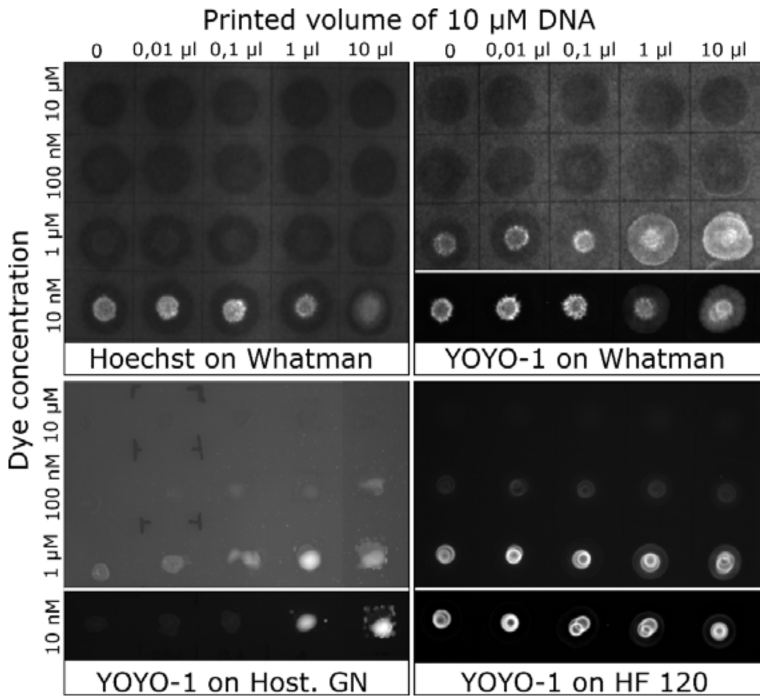

Figure 9: Different DNA volumes printed onto different carrier materials, where the dies, varying in concentration, are added onto the dried DNA spots; all shown sub-pictures are taken with different exposure times to avoid over- and under- exposure

4. Conclusions and outlook

On our way to printing a functional biosensor with aptamers we were able to answer a few questions. Inkjet printing is a suitable method for transferring variable amounts and concentrations of nucleic acid solutions without damaging the molecules. The work with fluorescence substances which require excitation in the central UV sector identified several problems to consider in the future. CFX and Hoechst are both excited in a wavelength range that is provided by a UVB, rather than a UVA light source. Using the UVB transillumination lamp of the imager, however, impeded the use of all examined materials containing foils. Thus, next to the auto fluorescence of the carrier material, its transmittance for the wavelength required to excite the fluorescent compound have to be considered.

It was shown that DNA solutions can be left to dry on suitable carrier materials and still display their usual response to DNA dyes after renaturation. This procedure, did, however, not work on every material.
Another problem is building a detector system based on minimal fluorescence changes. Even after finding good conditions, the detected intensity was often hard or impossible to distinguish from the auto fluorescence of the DNA dye. An ideal detector system would produce a much better contrast between positive and negative probes.

Acknowledgements

We thank the Technische Universität Darmstadt for funding this work within the project Forum for Interdisciplinary Research and the Merck Lab for the permission to use equipment.

References

Cháfer-Pericás, C., Maquieira, Á. and Puchades, R., 2010. Fast screening methods to detect antibiotic residues in food samples. *Trends in Analytical Chemistry,* 29(9), pp. 1038–1049. http://doi.org/10.1016/j.trac.2010.06.004.

Edwards, T.E., Klein, D.J. and Ferré-D'Amaré, A.R., 2007. Riboswitches: small-molecule recognition by gene regulatory RNAs. *Current Opinion in Structural Biology,* 17(3), pp. 273–279. http://doi.org/10.1016/j.sbi.2007.05.004.

Ellington, A.D. and Szostak, J.W., 1990. In vitro selection of RNA molecules that bind specific ligands. *Nature,* 346, pp. 818–822. http://doi.org/10.1038/346818a0.

Garst, A.D., Edwards, A.L. and Batey, R.T., 2011. Riboswitches: structures and mechanisms. *Cold Spring Harbor Perspectives in Biology,* 3(6), article id. a003533. http://doi.org/10.1101/cshperspect.a003533.

Goldmann, T. and Gonzalez, J.S., 2000. DNA-printing: utilization of a standard inkjet printer for the transfer of nucleic acids to solid supports. *Journal of Biochemical and Biophysical Methods,* 42(3), pp. 105–110. http://doi.org/10.1016/S0165-022X(99)00049-4.

Groher, F. Bofill-Bosch, C., Schneider, C., Braun, J., Jager, S., Geißler, K., Hamacher, K. and Suess, B., 2018. Riboswitching with ciprofloxacin-development and characterization of a novel RNA regulator. *Nucleic Acids Research*, 46(4), pp. 2121-2132. http://doi.org/10.1093/nar/gkx1319.

Groher, F. and Suess, B., 2016. In vitro selection of antibiotic-binding aptamers. *Methods,* 106, pp. 42–50. http://doi.org/10.1016/j.ymeth.2016.05.008.

Jaeger, J., 2017. *A fluoroquinolone binding aptamer as a biosensor for detecting antibiotic-contaminations in food*. Master's Thesis.

Kipphan, H., 2001. *Handbook of print media: Technologies and production methods*. Berlin, Heidelberg: Springer.

Kivirand, K., Kagan, M. and Rinken, T., 2013. Calibrating biosensors in flow-through set-ups: studies with glucose optrodes. In: T. Rinken, ed. *State of the art in biosensors*. Rijeka: InTech. https://doi.org/10.5772/54127.

McKeague, M. and DeRosa, M.C., 2012. Challenges and opportunities for small molecule aptamer development. *Journal of Nucleic Acids,* 2012, article id. 748913. https://doi.org/10.1155/2012/748913.

Novais, A., Comas, I., Baquero, F., Cantón, R., Coque, T.M., Moya, A., González-Candelas, F. and Galán, J.-C., 2010. Evolutionary trajectories of beta-lactamase CTX-M-1 cluster enzymes: predicting antibiotic resistance. *PLOS Pathogens,* 6(1), article id. e1000735. https://doi.org/10.1371/journal.ppat.1000735.

Okamoto, T., Suzuki, T. and Yamamoto, N., 2000. Microarray fabrication with covalent attachment of DNA using bubble jet technology. *Nature Biotechnology,* 18, pp. 438–441. https://doi.org/10.1038/74507.

Thermo Fischer, n.d. *Thermo Fischer Scientific*. [online] Available at: <https://www.thermofisher.com/si/en/home.html> [Accessed January 2018].

Threlfall, E.J., Ward, L.R., Frost, J.A. and Willshaw, G.A., 2000. The emergence and spread of antibiotic resistance in food-borne bacteria. *International Journal of Food Microbiology,* 62(1–2), pp. 1-5. https://doi.org/10.1016/S0168-1605(00)00351-2.

Wang, C.-Y.J., Giambrone, J.J. and Smith, B.F., 2002. Detection of Duck Hepatitis B Virus DNA on Filter Paper by PCR and SYBR Green Dye-Based Quantitative PCR. *Journal of Clinical Microbiology,* 40(7), pp. 2584–2590. https://doi.org/10.1128/JCM.40.7.2584-2590.2002.

Yamada, K., Henares, T.G., Suzuku, K. and Citterio, D., 2015. Paper-based inkjet-printed microfluidic analytical devices. *Angewandte Chemie*, 54(18), pp. 5294–5310. https://doi.org/10.1002/anie.201411508.

Overcoming Printing Challenges related to Fabrication of Inkjet-printed Coated Microfluidic Reaction Platforms

Eveliina Jutila[1], Risto Koivunen[1], Roger Bollström[1,2] and Patrick Gane[1,2]

[1] Aalto University, School of Chemical Engineering, Department of Bioproducts and Biosystems, FI-00076 Aalto, Helsinki, Finland
[2] Omya International AG, Baslerstrasse 42, CH-4665 Oftringen, Switzerland
E-mails: eveliina.jutila@aalto.fi; risto.koivunen@aalto.fi; roger.bollstroem@omya.com; patrick.gane@omya.com

Short abstract

Microfluidic paper-based assays composed of a hydrophilic substrate and patterned hydrophobic barriers, which guide the capillarity-driven flow of liquids, provide miniaturised test platforms for multiple fields of application, such as microanalytics and diagnostics. In this study, we utilise a highly porous coating especially designed for microfluidic purposes, composed of functionalised calcium carbonate (FCC) bound with micro (nano)fibrillated cellulose (MFC), combined with inkjet printed barriers fabricated with alkyl ketene dimer (AKD) and polystyrene (PS) inks. We present challenges experienced during the progress toward a printed design for enzymatic testing of pharmaceutical compounds, comprising an impermeable initially blue-dyed (Blue 807) AKD barrier and a semi-permeable red-dyed (Sudan Red G) PS barrier. These challenges related primarily to the instability of the blue-dyed AKD ink, the printing direction variation and the required heat-treatment of the coating at 105 °C to ensure full hydrophobisation of AKD. The presence of blue dye in fresh AKD ink caused jetting instability and thus leaking AKD barriers, while in aged ink dye precipitation resulted in hue shifts in printed patterns. The blue dye was replaced with a more stable yellow dye (wood stain 157), with care taken to identify the differential mobility of AKD versus dye. Printing direction affects the functionality of the semi-permeable PS barrier due to concentration of the PS at the start of the printing head traverse, which, if oriented parallel to the flow direction, renders the trailing edge in the liquid flow direction impermeable. Placing the pattern with the flow direction perpendicular to the print direction eliminates the problem, as PS concentrates at the hydrophobic channel edges. Heat-treatment also shrinks the underlying polypropylene film causing misalignment of the subsequently printed PS semi-barrier. Printing both barriers assuming constant geometry before heat-treatment is, therefore, not viable. Instead, the positioning of the PS semi-barrier is adjusted based on the known film shrinkage. These challenges highlight the importance of establishing ink preparation and printing protocols, which should be followed strictly to ensure batch-to-batch reproducibility of the samples.

Keywords: microfluidics, porous coating, inkjet printing, hydrophobic barriers, reaction platform

1. Introduction and background

Paper-based microfluidic assays offer an inexpensive, simple, rapid, portable alternative to traditional laboratory tests. Hydrophilic paper substrate can be transformed into a microfluidic device by fabricating hydrophobic barriers, which guide the liquid flow via capillary action without the need for external pumps. (Martinez, et al., 2007). Such devices have been developed for various applications including point-of-care (POC) diagnostics (Bedin, et al., 2017; Syedmoradi and Gomez, 2017; Zhang, et al., 2017), environmental analysis (Chen, et al., 2016; Meredith, et al., 2016), food safety (Hua, et al., 2018) and forensics (Ansari, et al., 2017; Garcia, et al., 2017).

Paper-based assays allow miniaturisation and integration of complex functions, often without sophisticated laboratory infrastructure or highly trained personnel. Such assays are especially essential in remote and resource-limited areas, such as developing countries, where simple and inexpensive assays are needed for detecting diseases and for improve public health, (Martinez, et al., 2010; Sharma, et al., 2015). Despite their huge potential, paper-based microfluidics have limitations including varied reproducibility, low sensitivity (Liana, et al., 2012; Sher, et al., 2017), non-uniformity of paper (He et al., 2015) and limited fabrication resolution (Bracher, Gupta and Whitesides, 2010). Instead of using filter or chromatography paper, which most researchers utilise in their assays (Li, Ballerini and Shen, 2012; Yamada, et al., 2015), a specially designed highly porous coating provides a more homogeneous surface, a finer and designable pore structure and better controlled optical properties, thus enabling improved fabrication resolution, use of smaller sample volumes and potentially improved sensitivity, especially in colorimetric detection due to increased whiteness.

Several patterning techniques can be used for creating well-defined channels including photolithography (Martinez, et al., 2007), laser printing (Oliveira, et al., 2016), plasma treatment (Li, Nguyen and Shen, 2008), wax printing (Carrilho, Martines and Whitesides, 2009; Phillips, et al., 2016), flexography (Olkkonen, Lehtinen and Erho, 2010) and inkjet printing (Abe, Suzuku and Citterio, 2008; Koivunen, et al., 2016). The most popular fabrication methods are wax printing and inkjet printing due to their low cost, high fabrication resolution and simplicity (He, et al., 2015; Li, Ballerini and Shen, 2012). The advantage of inkjet printing over wax printing is that in addition to fabricating the hydrophobic barriers, inkjet printing can also be used to deposit the reagents (He, et al., 2015; Li, Rossignol and Macdonald, 2015; Yamada, et al., 2015). The most commonly used hydrophobising agents used in inkjet patterning are wax and alkyl ketene dimer (AKD), which work well with non-challenging aqueous solutions (Li, Rossignol and Macdonald, 2015; Wang, et al., 2014), though other agents, such as siloxane (Rajendra, et al., 2014) and methylsilsesquioxane (MSQ) (Wang, et al., 2014) are better suited for organic and lower surface energy solvents as well as surfactant solutions.

This research is a follow-up on previous work (Jutila, et al., 2016) in which we developed an inkjet printed reaction platform for enzymatic testing of pharmaceutical compounds. The detection method for quantitation adopts UV fluorescence, in which the natural fluorescence of the reaction product 7-hydroxycoumarin in response to an excitation wavelength of 355 ± 5 nm, using a detection emission wavelength range spanning 400–700 nm, is recorded. In this paper, we introduce the final design of the printed pattern and some inkjet-printing related challenges encountered while fabricating the samples as well as solutions to the problems. The hope is that by communicating these, others following these learnings might enjoy an easier path to their goal.

2. Materials and methods

2.1 Coating materials and formulations

The coating formulation consists of a highly porous form of pharmaceutical grade functionalised calcium carbonate (FCC) pigment, which contains hydroxyapatite (52.7 %) and calcium carbonate (47.3 %), and a mechanically produced micro (nano)fibrillated cellulose (MFC) binder (Schenker, et al., 2016; 2018) provided by Omya International AG (Oftringen, Switzerland). Previous experiments by Jutila, et al. (2016) showed that the optimum binder level is 5 parts of MFC by weight in respect to 100 parts by weight of FCC (pph). This binder level is sufficient for binding the particles to each other and to the base substrate while maintaining good absorption and wetting capabilities, which are crucial properties for paper-based microfluidic devices.

Impermeable SuperYUPO® (Yupo Corporation), a pigment filled polypropylene (PP) film with a thickness of 80 µm and a basis weight of 62 gm^{-2}, was used as a base substrate for the coatings. The coating was applied with a K202 Control Coater (RK PrintCoat Instruments Ltd., Litlinton, UK) employing a spirally wire wound rod applying a 400 µm wet coating layer with a speed setting of 6 m·min^{-1}. The coated sheets were dried in laboratory atmosphere. Figure 1 shows scanning microscope (SEM) images of the FCC + 5 pph MFC coating.

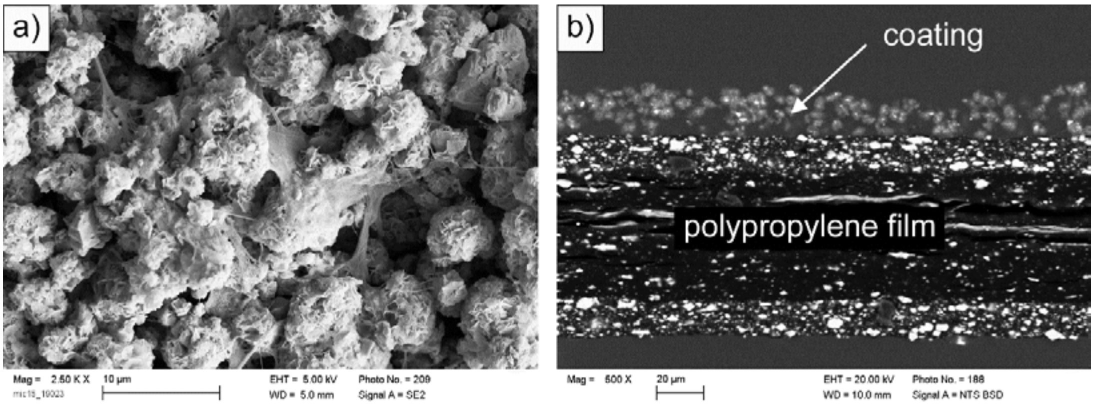

Figure 1: SEM images of (a) the surface and (b) the cross-section of a polypropylene film coated with FCC + 5 pph MFC

2.2 Functional inks and printing

Two functional inks prepared using hydrophobising agents (a mass fraction of 5.0 %), alkyl ketene dimer (AKD, Basoplast 88 (BASF, Ludwigshafen, Germany)) and polystyrene (PS, Sigma-Aldrich, St. Louis, USA, product code 331651) dissolved in p-xylene solvent (VWR, Vienna, Austria, product code 28984.292) were used to pattern the coating. Both inks in pure component form are clear and therefore the patterns would be almost invisible on the coating. For the sake of visual study of the ink-applied areas, the PS ink was coloured with Sudan Red G (Sigma-Aldrich, St. Louis, USA, product code 17373), and the AKD ink was first coloured with Blue 807 Dye (Kremer Pigmente GmbH, & Co. KG, Aichstetten, Germany, product number 94030) and later with a yellow dye, wood stain colourant 157 (Kremer Pigmente GmbH & Co. KG, Aichstetten, Germany, product number 94010). The inks were printed with a DMP-2831 research inkjet printer (Fujifilm Dimatix, Santa Clara, USA) employing DMC-11610 ink cartridges with ten picolitre nominal drop volume. More details regarding the ink preparation, polymer content and printing details can be found from publications by Koivunen, Jutila and Gane (2015) and Koivunen, et. al. (2015; 2016).

The AKD ink hydrophobises the coating more efficiently than the PS ink (Koivunen, et al., 2016), and so was used as the main patterning ink to create impermeable barriers with two printed layers. Four printed layers of PS ink were used to create a controlled semi-permeable barrier, which prevents or allows the passage of fluids depending on the liquid volume applied.

2.3 Pigment coating characterisation methods

The solids content of the coating colour was determined with a Precisa HA 300 Moisture Balance (Precisa Gravimetrics AG, Dietikon, Switzerland). Coat weight was calculated by measuring the weight of coated pieces (5 cm × 5 cm) of polypropylene film, using a Mettler AE260 analytical balance (Mettler-Toledo International Inc., Columbus, Ohio, the United States), and deducting the equivalent proportional basis weight of the film. Five measurements were taken. The total dry coating plus substrate thickness was measured with an SE250D micrometer (Lorentzen & Wettre, Kista, Sweden), having a 2 cm^2 measurement area spindle and measurement pressure of 100 kPa. The dry coating thickness was determined from the measured coated film by subtracting the nominal thickness, 80 µm, of the polypropylene film. Ten measurements were taken.

Scanning electron micrographs (SEM) were obtained with a Sigma VP field emission scanning electron microscope (Carl Zeiss AG, Oberkochen, Germany). Samples were scanned with Epson Expression 1680 (Epson, Suwa, NGN, Japan). Coating pore volume was measured with an Autopore IV mercury intrusion porosimeter (Micromeritics, Norcross, USA) from coating sample dried in a petri dish (diameter 5.5 cm) in normal laboratory conditions.

3. Results and discussion

The findings from the experimental procedures are reported here, beginning with the characterisation of the coating, followed by introduction of the final design of the printed pattern for enzymatic testing and some inkjet-printing related problems and their solutions.

3.1 Coating properties

The optimum coating formulation was chosen from four coating formulations based on previous experiments (Jutila, et al., 2016). The coating consists of FCC and 5 pph of MFC and has a solids content of a mass fraction of 7.8 %, Brookfield viscosity of 298 mPa·s, dry thickness of 137 ± 11 μm and coat weight of 43.2 ± 2.3 gm^{-2}. The FCC-based coating has a bimodal pore size distribution, i.e. the coating consists of both intraparticle and interparticle voids (Figure 2). Compared to coarse ground calcium carbonate (cGCC), which has a unimodal pore size distribution, the FCC-based coatings offer not only high capillarity, but also high permeability facilitating fast absorption of liquids within the coating structures (Ridgway, Gane and Schoelkopf, 2004; 2006), thus making the functionalised FCC-based coatings suited for paper-based microfluidic applications.

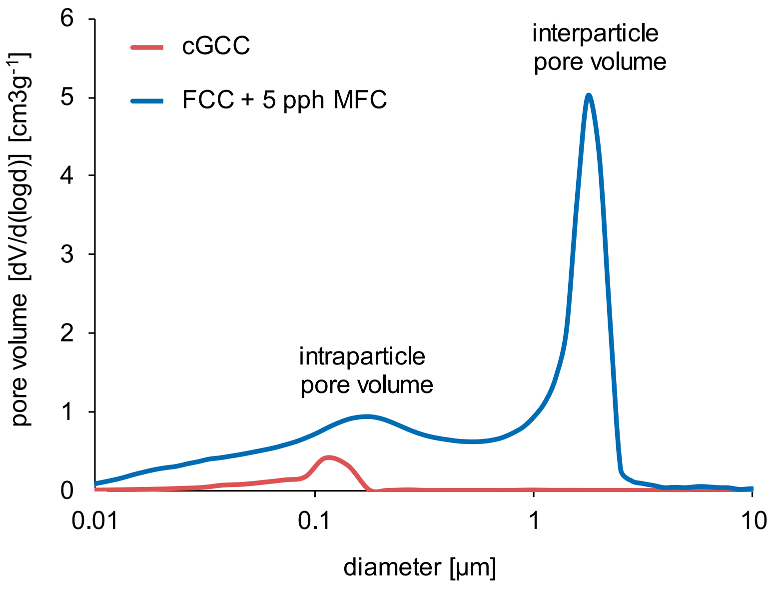

Figure 2: Pore size distribution of the FCC + 5 pph MFC coating showing bimodal nature with both intra-particle and inter-particle voids in comparison with unimodal pore size distribution of cGCC (cGCC values obtained from Ridgway, Kukkamo and Gane, 2011)

3.2 Inkjet-printed pattern

The final design consists of an impermeable barrier printed with blue-dyed AKD ink, a semi-permeable barrier printed with red PS ink as well as separate areas for wetting, reaction and detection. Figure 3 represents the physical characteristics of the test design. Reactions occur on the microscale within the pores, having the distribution shown in Figure 2, which includes micro and nano features. This defines the behaviour as microfluidic. The larger overall scale of the device (in mm) is to accommodate the volumes of liquid and reactants required to provide sufficient enzymatic breakdown product (metabolite) for subsequent fluorescent analysis, and to provide sufficient surface area to undertake the chromatographic separation of the metabolite to enable that analysis.

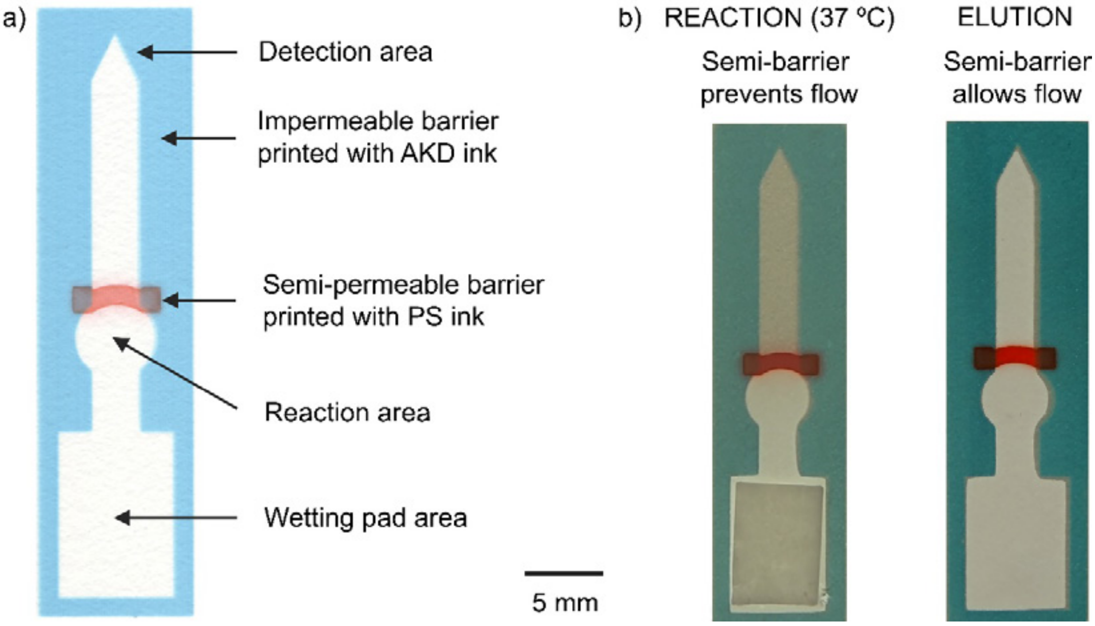

Figure 3: Final pattern design for enzymatic testing (a) and the functionality of the semi-permeable barrier during reaction and elution stages (b)

The impermeable AKD barrier keeps the fluids inside the pattern and guides the fluid flow towards the detection area. The semi-permeable PS barrier prevents fluid passage during the reaction phase, when the sample is heated to 37 °C and kept wetted using a wetting pad. After the reaction, when the sample is no longer heated, the semi-permeable barrier allows the transfer of the reaction products and the eluent to the detection area. The reaction product is detected using a fluorescence-based method.

The fluid volumes were optimised so that (i) the reaction area stays wetted during the heated reaction with the aid of the pre-wetted pad, but the fluids do not pass the semi-barrier, and (ii) the applied elution volume is sufficient to pass through the semi-barrier and reach the detection area in approximately 5 min. During initial trialling, however, we encountered several setbacks while fabricating the samples to function with the liquid as wished, which revealed some unforeseen problems relating to the functionality of both the impermeable AKD barrier and semi-permeable PS barrier. The next section introduces the causes and solutions found for the most important inkjet-printing relating challenges.

3.3 Inkjet printing-related challenges

3.3.1 Instability of the blue dyed AKD ink

The AKD ink is prepared by dissolving 5 % mass fraction of AKD and 0.1 % mass fraction of blue dye overnight without agitation (Koivunen, et al., 2016). The first image in Figure 3a corresponds to a pattern printed with freshly made AKD ink. Over time, however, the blue dye crystallises and precipitates on the bottom of the ink container, thus changing the concentration of the dye in the AKD ink and changing the shade of the blue AKD barrier. The shade of the AKD barrier not only changes the visibility of the pattern, but also affects quantification of the reaction products in fluorescence-based detection. The positioning of the microfluidic device for detection becomes more challenging if the tip of the arrowhead where the reaction product concentrates cannot be clearly seen. This can be overcome relatively easily by positioning the device when the tip has been wetted if a fluorescence microscope with a light source is used. The effect of the dye concentration in the AKD barrier on the fluorescence background intensity measured from the tip of the arrowhead occurs due to the large detected area, which not only covers the tip where the reaction product has concentrated but also some area of the AKD barrier. AKD itself gives a high fluorescent background intensity, and the blue dye layer formed on and between the coating pigment particles results in scattering of the blue and UV light. This may be enhanced by newly re-crystallised dye particles, if such are formed during the drying of the ink. Variation in the blue dye concentration thus causes differences in the background intensity between samples from different batches. This problem can be overcome by measuring the background of each individual tip before measuring the fluorescence intensity of the reaction products, and deducting the background intensity, though a stable ink would be preferred for good reproducibility. It was also found that the mobility of the AKD in the wet ink on contact with the coating was greater than that of the dye, which affected detection because AKD alone gives a higher fluorescence background than the dyed AKD.

The presence of the blue dye in the AKD ink also made jetting unstable forming accumulations within or around the outside of the nozzles, thus causing eventual misalignment and/or non-jetting of the nozzles (Figure 4b). This effect was most significant for freshly prepared ink batches, as aged ink had a lower dye concentration due its crystallisation and precipitation, and so jetting became more stable after storage. Jetting instability resulted in the print quality gradually decreasing making the samples unusable since the AKD barriers became permeable and were not able to prevent leakage of liquids. Therefore, the chosen dye was changed to a more soluble yellow one, which proved to be more stable. The yellow dye, however, as expected, absorbed shorter wavelength light, including UV. This, too, was overcome by recording the background fluorescence level prior to sample measurement. In addition, the AKD concentration was increased to a mass fraction of 10 % so that only one printed AKD barrier layer was needed to achieve a complete barrier.

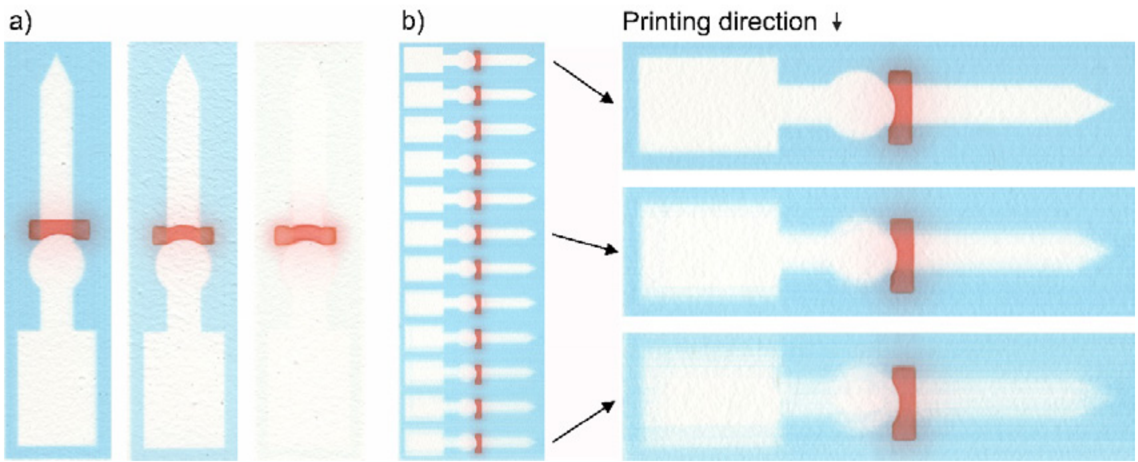

Figure 4: Challenges related to the AKD ink: (a) re-crystallisation of the blue dye changes the dye concentration in the AKD ink resulting in lighter blue AKD ink, and (b) clogged and/or misaligned nozzles resulting in poor printing quality and leaking AKD barriers

3.3.2 Printing direction-related hydrophobe concentration

The printing direction was changed to fit more printed samples onto a single coated polypropylene film. Originally 52 samples were printed perpendicular to the microfluidic flow direction. The number of patterns, however, could be increased to 60 samples per film when the direction of print was changed to parallel with the flow direction, which was naturally thought to be an advantage. However, this made the semi-barriers impermeable. A close inspection revealed that this was caused by concentration of the PS at the start-point of the printing head traverse, and so at the trailing edge of the semi-barrier (Figure 5), which meant that the test liquid was able to transfer into the semi-barrier area but not out through it according to design. The issue was related to the long printing time, resulting from a combination of hardware (relatively slow moving printhead with a limited number of nozzles), ink (stably jettable only at low frequencies) and substrate (a thick and porous coating requiring a large ink volume per unit area to achieve full-depth hydrophobisation). The high ink volume likely leads to flow inside the porous structure transporting ink from the freshly printed droplet to the still wet previously printed area. In a roll-to-roll printing process at high speed and frequency such transport, if taking place, would be directed more uniformly to the edges of the pattern. The problem was solved by changing the printing direction back to perpendicular to the fluid flow direction. This way the PS concentrated to one side of the semi-barrier in contact with the impermeable channel wall, and thus no longer interfered with the liquid flow.

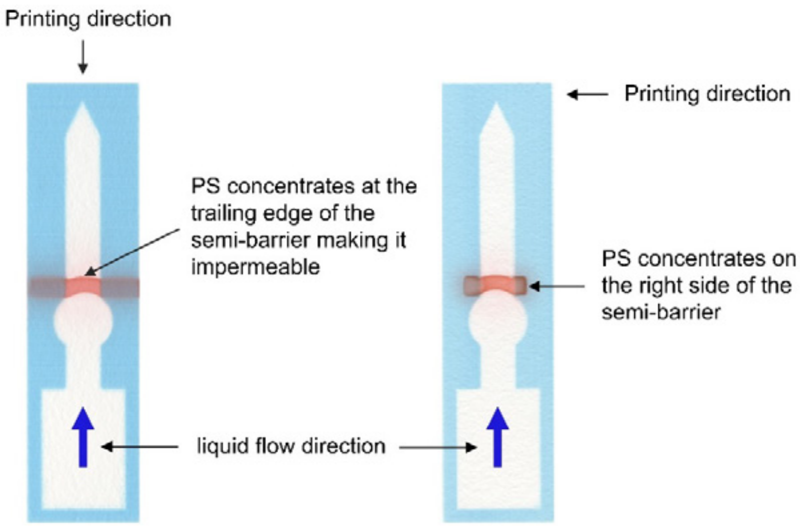

Figure 5: The effect of the printing direction on the permeability of the semi-barrier due to concentration of the PS ink

3.3.3 Heat-treatment-related effect

The AKD ink needs to be heat-treated to ensure that AKD reacts with hydroxyl groups present in the coating (Koivunen, et al., 2016). This, however, causes the polypropylene substrate film to shrink approximately 0.77 ± 0.03 % in one dimension at 105 °C, thus causing misalignment of the red semi-permeable PS barriers. This problem could be solved in two ways: either printing both AKD and PS layers before the heat-treatment or by adjusting the positioning of the PS barriers according to the shrinkage of the film. Heating both AKD and PS ink seemed to be the easier option, however, the heat-treatment affected the functionality of the semi-barrier adversely. Prior to the heat-treatment, the liquid passed the semi-barrier correctly and reached the detection area without problems. When the PS ink was heat-treated, the semi-barrier became almost impermeable. By the time the liquid had reached the detection area on the non heat-treated sample, the liquid had barely passed the semi-barrier on the heat-treated sample (Figure 6). As a result, the liquid front never reached the detection area.

The softening/melting point (ASTM E 28) of the PS in question was known to be 123–128 °C and, therefore, heat-treatment for the AKD barrier at 105 °C was initially considered to leave the PS inert. However, later literature research revealed that the glass transition temperature (T_g) of polystyrene with a similar molecular weight is in the range of 100–106 °C (Claudy, et al., 1983; Hitachi High-Tech Science Corporation, 1995). PS changes from a glassy to a rubbery state once the temperature is above T_g (Brun, et al., 2011). When the PS barrier is heated to 105 °C, the material property of the PS barrier changes making the barrier less permeable, possibly due to PS flow and coagulation, resulting in an uneven distribution over the high pore surface area. The problem was solved by first printing the AKD barrier, treating the sample at 105 °C, and then printing the semi-permeable PS barrier by adjusting its position according to the shrinkage of the polypropylene film.

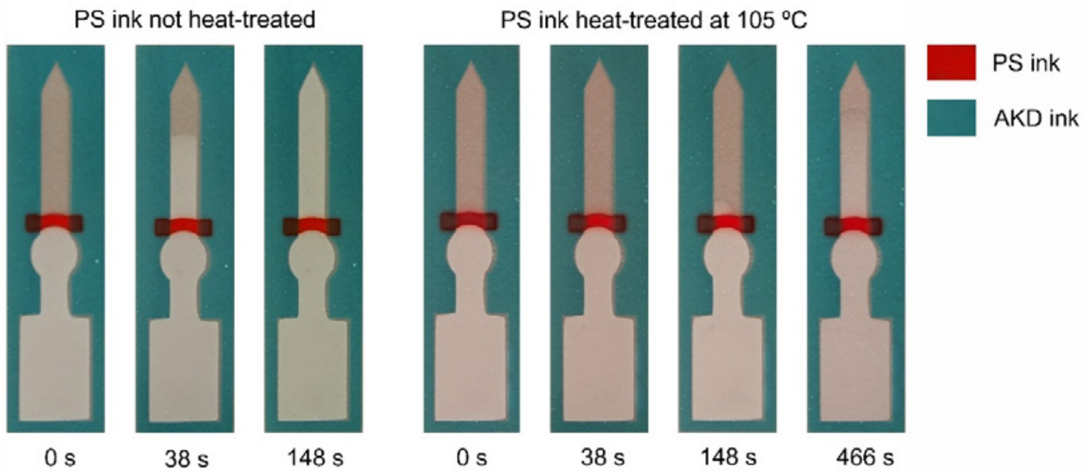

Figure 6: The effect of heat-treatment at 105 °C on the functionality of the semi-permeable PS barrier

The shrinkage of the filled polypropylene film is a result of polymer coiling in response to the supplied energy, thus increasing entropy. In the case of the substrate used in the work, the shrinkage occurs in one dimension and is calculated and corrected for. However, should higher temperatures be needed in general then it would be preferable to choose a substrate having a low coefficient of expansion/contraction, e.g. glass. Considering point-of-care diagnostic applications such thermal effects are unlikely to be encountered, enabling a broader choice of substrate to be considered.

4. Conclusions

Some of the inkjet printing related challenges revealed during the design and multiple fabrication of printed microfluidic patterning are presented and solutions discussed with the aim of assisting others working in the field to avoid at least part of the time-consuming "learning curve". Jettability was seen to be susceptible to ink colorant formulation, and semi-barrier design in turn susceptible to print direction layout for the given print hardware used. Other encountered design needs requiring optimisation include the shape of a measurement zone, resulting in this case with the choice of an arrowhead into which the reaction product can concentrate. Variation in background fluorescence needs careful attention, for example differential mobility of the hydrophobising agent (AKD) compared with the surface adsorbing dye in contact with the coating pores resulted greater fluorescence background coming from AKD alone versus dyed AKD regions. Inhomogeneity in thermal response of the materials also requires careful planning of the work sequence.

These findings highlight the importance of ensuring the stability of the inks, finding optimum printing conditions and establishing ink preparation and printing protocols, which should be followed strictly to ensure batch-to-batch reproducibility of the microfluidic device.

Acknowledgements

Funding for the project was supported by Omya International AG. Tiina Sikanen (Helsinki University) is acknowledged for collaboration in elaborating the requirements for enzymatic testing, Silvan Fischer (Omya International AG) for the SEM analysis and Cathy Ridgway (Omya International AG) for porosimetry.

References

Abe, K., Suzuki, K. and Citterio, D., 2008. Inkjet-printed microfluidic multianalyte chemical sensing paper. *Analytical Chemistry*, 80(18), pp. 6928–6934.

Ansari, N., Lodha, A., Pandya, A. and Menon, S.K., 2017. Determination of cause of death using paper-based microfluidic device as a colorimetric probe. *Analytical Methods*, 9(38), pp. 5632–5639.

Bedin, F., Boulet, L., Voilin, E., Theillet, G., Rubens, A. and Rozand, C., 2017. Paper-based point-of-care testing for cost effective diagnosis of acute flavivirus infections. *Journal of Medical Virology*, 89(9), pp. 1520–1527.

Bracher, P.J., Gupta, M. and Whitesides, G.M., 2010. Patterned paper as a template for the delivery of reactants in the fabrication of planar materials. *Soft Matter*, 6(18), pp. 4303–4309.

Brun, N., Bourson, P, Margueron, S. and Duc, M., 2011. Study of the thermal behaviour of syndiotactic and atactic polystyrene by Raman spectroscopy. In: *XXXVII JEEP - 37th Conference on Phase Equilibria*. Saint -Avoid, France, 30 March – 1 April 2011. EDP Sciences, pp. 0004-p.1-0004-p.5.

Carrilho, E., Martinez, A.W. and Whitesides, G.M., 2009. Understanding wax printing: a simple micropatterning process for paper-based microfluidics. *Analytical Chemistry*, 81(16), pp. 7091-7095.

Chen, W., Fang, X., Li, H., Cao, H. and Kong, J., 2016. A simple paper-based colorimetric device for rapid mercury(II) assay. *Scientific Reports*, 6, Article number 31948, 1-7 p. http://doi.org/10.1038/srep31948.

Claudy, P., Létoffé J.M., Camberlain, Y. and Pascault, J.P., 1983. Glass transition of polystyrene versus molecular weight. *Polymer Bulletin*, 9, pp. 208–215.

Garcia, P.T., Gabriel, E.F.M., Pessôa, G.S., Santos Júnior, J.C., Mollo Filho, P.C., Guiduqli, R.B.F., Höehr, N.F., Arruda, M.A.Z. and Coltro, W.K.T., 2017. Paper-based mi crofluidic devices on the crime scene: a simple tool for rapid estimation of post-mortem interval using vitreous humour. *Analytica Chimica Acta*, 974, pp. 69–74. http://doi.org/10.1016/j.aca.2017.04.040.

He, Y., Wu, Y., Fu, J.-Z. and Wu, W.-B., 2015. Fabrication of paper-based microfluidic analysis devices: a review. *RSC Advances*, 5(95), pp. 78109–78127.

Hitachi High-Tech Science Corporation, 1995. *DSC Measurements of Polystyrene – The Effects of Molecular Weight on Glass Transition. Application Brief, TA No. 68*. Hitachi.

Hua, M.Z., Li, S., Wang, S. and Lu, X., 2018. Detecting chemical hazards in foods using microfluidic paper-based analytical devices (μPADs): the real-world application. *Micromachines*, 9(1), 32, pp. 1–14.

Jutila, E., Koivunen, R., Bollström, R., Sikanen, T. and Gane, P.A.C., 2016. Reaction platforms for enzymatic testing. In: P.A.C. Gane and C. Ridgway, eds. *Advances in Printing and Media Technology: Proceedings of the 43th International Research Conference of iarigai*. Toronto, 23–27 August 2016. Darmstadt: International Association of Research Organizations for the Information, Media and Graphic Arts Industries, pp. 39–48.

Koivunen, R., Jutila, E. and Gane, P.A.C., 2015. Inkjet printed hydrophobic microfluidic channelling on porous substrates. *Journal of Print and Media Technology Research*, 4(1), pp. 7–17.

Koivunen, R., Jutila, E., Bollström, R. and Gane, P.A.C., 2015. Inkjet-printed reaction arrays on pigment coated substrates. In: P.A.C. Gane and C. Ridgway, eds. *Advances in Printing and Media Technology: Proceedings of the 42nd International Research Conference of iarigai*. Helsinki, 6–9 September 2015, Darmstadt: International Association of Research Organizations for the Information, Media and Graphic Arts Industries, pp. 107–114.

Koivunen, R., Jutila, E., Bollström, R. and Gane, P.A.C., 2016. Hydrophobic patterning of functional porous pigment coatings by inkjet printing. *Microfluidics and Nanofluidics*, 20:83, pp. 1-21 p. https://doi.org/10.1007/s10404-016-1747-9.

Li, J., Rossignol, F. and Macdonald, J., 2015. Inkjet printing for biosensor fabrication: combining chemistry and technology for advanced manufacturing. *Lab on a Chip*, 15(12), pp. 2538–2558.

Li, X., Ballerini, D.R. and Shen, W., 2012. A perspective on paper-based microfluidics: current status and future trends. *Biomicrofluidics*, 6(1), pp. 011301–1130113.

Li, X., Tian, J., Nguyen, T. and Shen, W., 2008. Paper-based microfluidic devices by plasma treatment. *Analytical Chemistry*, 80(23), pp. 9131–9134.

Liana, D.D., Raguse, B., Gooding, J.J. and Chow, E., 2012. Recent Advances in Paper-based Sensors. *Sensors*, 12(9), pp. 11505–11526.

Martinez, A.W., Phillips, S.T., Butte, M.J. and Whitesides, G.M., 2007. Patterned paper as a platform for inexpensive, low-volume, portable bioassays. *Angewandte Chemie International Edition,* 46(8), pp. 1318–1320.

Martinez, A.W., Phillips, S.T., Whitesides, G.M. and Carrilho, E., 2010. Diagnostics for the developing world: microfluidic paper-based analytical devices. *Analytical Chemistry*, 82(1), pp. 3–10.

Meredith, N.A., Quinn, C., Cate, D.M., Reilly III, T.H., Volckens, J. and Henry, C.S., 2016. Paper-based analytical devices for environmental analysis. *Analyst*, 141(6), pp. 1874–1887.

Oliveira, K.A., Damasceno, D., de Oliveira, C.R., da Silveira, L.A., de Oliveira, A.E. and Coltro, W.K.T., 2016. Dengue diagnosis on laser printed microzones using smartphone-based detection and multivariate image analysis. *Analytical Methods*, 8(35), pp. 6506–6511.

Olkkonen, J., Lehtinen, K. and Erho, T., 2010. Flexographically printed fluidic structures in paper. *Analytical Chemistry*, 82(24), pp. 10246–10250.

Phillips, E.A., Shen, R., Zhao, S. and Linnes, J.C., 2016. Thermally actuated wax valves for paper-fluidic diagnostics. *Lab on a Chip*, 16(21), pp. 4230–4236.

Rajendra, V., Sicard, C., Brennan, J.D. and Brook, M.A., 2014. Printing silicone-based hydrophobic barriers on paper for micro fluidic assays using low-cost ink jet printers. *Analyst*, 139(24), pp. 6361–6365.

Ridgway, C., Gane, P.A.C. and Schoelkopf, J., 2004. Modified calcium carbonate coatings with rapid absorption and extensive liquid uptake capacity. *Colloids and Surfaces A Physicochemical and Engineering Aspects*, 236(1-3), pp. 91–102.

Ridgway, C., Gane, P.A.C. and Schoelkopf, J., 2006. Achieving rapid absorption and extensive liquid uptake capacity in porous structures by decoupling capillarity and permeability: nanoporous modified calcium carbonate. *Transport in Porous Media*, 63(2), pp. 239–259.

Ridgway, C.J., Kukkamo, V. and Gane, P.A.C., 2011. Effect of binders and additives on inkjet coating pigment pore structure. In: *Proceedings Paper Conference and Trade Show 2011 (PaperCon 2011)*. Covington, Kentucky, USA, 1–4 May 2011. Tappi Press GA, pp. 1305–1319.

Schenker, M., Schoelkopf, J., Mangin, P. and Gane, P., 2016. Rheological investigation of complex micro and nanofibrillated cellulose (MNFC) suspensions: discussion of flow curves and gel stability. *Tappi Journal*, 15(6), pp. 405–416.

Schenker, M., Schoelkopf, J., Gane, P. and Mangin, P., 2018. Influence of shear rheometer measurement systems on the rheological properties of microfibrillated cellulose (MFC) suspensions. *Cellulose,* 25(2). https://doi.org/10.1007/s10570-017-1642-x.

Sharma, S., Zapatero-Rodríguez, J., Estrela, P. and O'Kennedy, R., 2015. Point-of-care diagnostics in low resource settings: present status and future role of microfluidics. *Biosensors*, 5(3), pp. 577–601.

Sher, M., Zhuang, R., Demirci, U. and Asghar, W., 2017. Paper-based analytical devices for clinical diagnosis: Recent advances in the fabrication techniques and sensing mechanisms. *Expert Review of Molecular Diagnostics,* 17(4), pp. 351–366.

Syedmoradi, L. and Gomez, F.A., 2017. Paper-based point-of-care testing in disease diagnostics. *Bioanalysis*, 9(11), pp. 841–843.

Wang, J., Monton, M.R.N., Zhang, X., Filipe, C.D.M., Pelton, R. and Brennan, J.D., 2014. Hydrophobic sol–gel channel patterning strategies for paper-based microfluidics. *Lab on a Chip*, 14(4), pp. 691–695.

Yamada, K., Henares, T.G., Suzuki, K. and Citterio, D. 2015. Paper-based inkjet-printed microfluidic analytical devices. *Angewandte Chemie - International Edition*, 54(18), pp. 5294–5310.

Zhang, H., Qiu, X., Zou, Y., Ye, Y., Qi, C., Zou, L., Yang, X., Zhu, Y., Yang, Y., Zhou, Y. and Luo, Y., 2017. A dye-assisted paper-based point-of-care assay for fast and reliable blood grouping. *Science Translational Medicine*, 9(381), pp. 1–11. https://doi.org/10.1126/scitranslmed.aaf9209.

Surface Energy-guided Patterning for Printed Electronics Applications

Zhiqing Xin[1], Jianghao Liu[1], Lingya Gu[1], Yi Fang[1], Lixin Mo[1] and Li Yang[2]

[1] Beijing Institute of Graphic Communication (BIGC), School of Printing and Packaging and Beijing Engineering Research Center of Printed Electronics, Beijing 102600, People's Republic of China

[2] Research Institutes of Sweden (RISE), RISE Bioeconomy, Drottning Kristinas väg 61, 11486 Stockholm, Sweden
E-mail: li.yang@ri.com

Short abstract

We demonstrated patterning method for silver nanoparticle ink by wire-wound rod coating on commercial paper substrate. The hydrophobic and hydrophilic zones (patterns) on the paper surface were created by combining coating of hydrophobic dispersion with selective plasma treatment using a mask. Thanks to the surface energy difference in different zones, the silver nanoparticle ink self-aligned to form desired patterns, e.g. a matrix of lines of 0.5 mm wide with 0.3 mm spacing.

Keywords: Printed electronics, rod coating, surface energy, printing dynamics

1. Introduction and background

Paper-based packaging is dominant in our every life, which is still growing. Paper and board are the major materials for primary and/or secondary packaging. Besides the primary functions of packaging namely protection, storage, loading and transport, there is a growing interest and market demand on extending the functions beyond the conventional ones by means of e.g. intelligent features which enable tracing and tracking, monitoring of shelf life and product safety, and more effective storage and transport management.

While the device performance of printed electronics on plastic and glass substrates has been improved, printing electronic on paper substrates remains challenge (Bollström, 2013; Öhlund, 2014). Compared to other materials, e.g. plastics and glass, paper substrate has quine characteristics (difficulties) e.g. rougher surface and porous structure, which impact on transferring of conductive ink from a print drum to the paper surface and more complicated interactions between the conductive ink with the paper substrate. Unlike on a plastic or a glass surface, the ink not only spreads on the surface but also penetrates the bulk structure either as whole or partially. All of factors make it difficult to obtain well-defined patterns or material stacks on the paper, which are essential for desirable performance of electronic components or devices. While paper-making-based solutions were in focus of researches (Bollström, 2013), e.g. multi-layer-coated paper substrate, little has been done in developing alterative ink application methods to the existing printing techniques for paper-based electronics. It is necessary to investigate novel printing and processing techniques enabling devices with good electrical and mechanical properties while maintaining minimal variability and high device yields.

Device reliability and performance is found to improve through the use of surface energy patterned (SEP) substrates to self-align inkjet-printed or spin-coated electrodes (Sele, et al., 2005; Diao, et al., 2013) and pattern zone-casted semiconductor for partially printed devices on smooth and non-porous substrates like plastics and glass. (Minari, et al., 2008; Sirringhaus, et al., 2000; Kim, et al., 2008). Yet, this technique has not been tested or verified on paper-based substrates. In this work, we demonstrated how to create printed-electronics patterns or structures on paper substrates which are of higher geometric accuracy and better performance, using surface energy guided patterning techniques.

2. Materials and experiments

Commercial coated papers, 128 g/m^2, were used as substrates. The paper surface was first coated with transparent super hydrophobic dispersion FC3120, provided by Solmont Technology Wuxi Co., Ltd, Wuxi, China, to turn the paper surface into hydrophobic (This step could be skipped if the paper surface was originally hydrophobic). The surface was then covered by mask of stripy patterns, made of stainless steel. The line width of the stripes was 0.5 mm and interval between two adjacent stripes 0.3 mm. The masked paper substrate was then treated by plasma at 15 W for 15–30 s to make the open substrate areas into hydrophilic. As the results the paper surface was divided into alternating zones of hydrophobic (light grey) and hydrophilic (dark grey) forming invisible patterns with surface energy difference, see Figure 1. The contact angles of the hydrophobic and hydrophilic zones were measured with water. Their corresponding values were 125^o and 34^o, respectively.

The topographic characteristics of the paper substrate was measured by a L&W OptiTopo device.

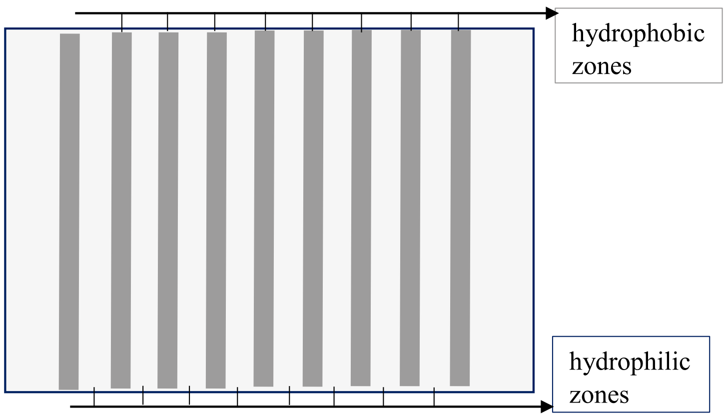

Figure 1: Schematic illustration of the paper surface after treatments with hydrophobic dispersion and plasma; the line width of the hydrophobic zones is 0.3 mm and that of the hydrophilic zones 0.5mm

Silver nanoparticles conductive ink made at BIGC was used in this study. The spherical silver nanoparticles (Ag NPs) were first synthesized by phase reduction method and the mean particles size is about 50 nm in diameter. Detailed preparation method had previously been reported elsewhere (Mo, et al., 2016). The conductive inks having different concentrations of Ag NPs, 20 %, 40 % and 60 %, were obtained by addition of different amount of solvent. The rheological properties of the conductive ink, i.e. viscosity was measured by Brookfield Cap2000+ Viscometer and the surface tension by Krüss K100 Tensiometer.

The nano-Ag conductive ink was applied onto the plasma-treated surface employing a Mayer coater with 3# Mayer-bar. The wet film thickness was about 20 μm. Sheet resistance (Ω/sq) of the coated layer (after drying) was measured with RTS-9 four-point probe.

3. Results and discussion

The rheological characteristics of the conductive inks, i.e. viscosity and surface tension, are listed in Table 1. The sheet resistance of the conductive layers (after drying) are also shown in the table. It is natural that a higher Ag NPs content of the conductive ink led to higher conductivity or lower sheet resistance of the ink layer. While the surface tensions of the conductive inks were in large independent of the solid content of Ag NPs, their viscosities increase dramatically with the solid content of Ag NPs.

Table 1: Viscosity and surface energy of the nano Ag inks

	Concentration of nano Ag (%) of the conductive inks		
	20 (%)	40 (%)	60 (%)
Viscosity (Pa•s)	0.27	0.59	10.71
Surface tension (mN/m)	48	48	47
Sheet resistance (Ω/sq)	33.4	17.0	5.6

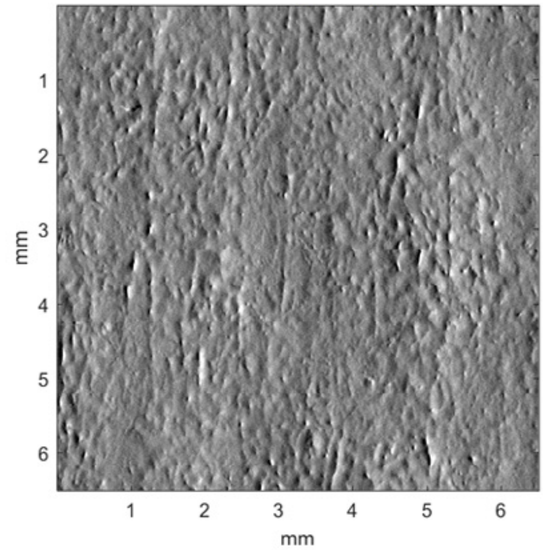

Figure 2: A close-up of the topographic gradient image of the substrate surface, obtained with L&W OptiTopo device

Figure 3: An examples of surface energy guided pattern created by Mayer-bar coater with nano Ag inks (Ag NP content 40%)

Figure 2 shows how the substrate's surface looks like. The small scale rough surface features would of course have strong impact on ink transferring and ink-layer thickness hence surface resistance, if a printing technique, like flexography was applied. It is obvious that rough surface features are particularly harmful when the thickness of ink-layer is shallow. Therefore, to print on ordinary commercial paper boards large ink volume in combination with high nip pressure had to be applied in order to achieve sufficiently think ink-layer. This would in turn lead to difficulties in creating narrow line features and lines with narrow spacing. Having said that, ink application by surface coating is advantageous because a thicker ink layer could be achieved yet without scarifying narrow line features as no external (nip) pressure was involved.

Figure 3 depicts the nano Ag lines created by surface-energy guided patterning technique. Experiments had indicated that surface energy and viscosity were crucial for surface-energy guided patterning process, in addition to the substrate's hydrophobicity/hydrophilicity. It is important to work with the ink formulation and coating parameters so that the conductive ink has both optimal rheological characteristics and conductivity. We have achieved line-patterns of narrower line spacing than 0.3 mm.

4. Conclusions

We demonstrated a patterning method for printed electronics on paper substrate. The hydrophobic and hydrophilic zones (patterns) were created by combining coating of hydrophobic dispersion with selective plasma treatment. Thanks to the surface energy difference between different zones, the silver nanoparticle ink self-aligned to form the desired patterns, e.g. a matrix of lines of 0.5 mm wide with 0.3 mm spacing.

Acknowledgments

This work has been financed by NSFC through project: Printing dynamics for high-definition printed electronics (61474144). Support from 2017 Cultivation and development of innovation base (Z171100002217032) is also acknowledged.

References

Bollström, R., 2013. *Paper for printed electronics and functionality*. Doctoral Thesis. Åbo Akademi University.

Diao, Y., Tee, B.C.-K., Giri, G., Xu, J., Kim, D.H., Becerril, H.A., Stoltenberg, R.M., Lee, T.H., Xue, G., Mannsfeld, S.C.B. and Bao, Z., 2013. Solution coating of large-area organic semiconductor thin films with aligned single-crystalline domains. *Nature Materials,* 12(7), pp. 665–671.

Kim, S.H., Choi, D., Chung, D.S., Yang, C., Jang, J., Park, C.E. and Park, S.-H.K., 2008. High-performance solution-processed triisopropylsilylethynyl pentacene transistors and inverters fabricated by using the selective self-organization technique. *Applied Physics Letters,* 93(11), article id. 113306.

Minari, T., Kano, M., Miyadera, T., Wang, S.-D., Aoyagi, Y., Seto, M., Nemoto, T., Isoda, S. and Tsukagoshi, K., 2008. Selective organization of solution-processed organic field-effect transistors. *Applied Physics Letters,* 92(17) article id. 173301.

Mo, L., Ran, J., Yang, L., Fang, Y., Zhai, Q., Li, L., 2016. Flexible transparent conductive films combining flexographic printed silver grids with CNT coating. *Nanotechnology*, 27(6), article id. 065202.

Öhlund, T., 2014. *Metal films for printed electronics: ink-substrate interaction and sintering*. Doctoral thesis. Mid Sweden University.

Sele, C.W., von Werne, T., Friend, R.H. and Sirringhaus, H., 2005. Lithography-free, self-aligned inkjet printing with sub-hundred-nanometer resolution. *Advanced Materials,* 17(8), pp. 997–1001.

Sirringhaus, H., Kawase, T., Friend, R.H., Shimoda, T., Inbasekaran, M., Wu, W. and Woo, E.P., 2000. High-resolution inkjet printing of all-polymer transistor circuits. *Science,* 290(5499), pp. 2123–2126.

About Deinking of Paper-based Printed Electronics

Anne Blayo, Nathalie Marlin and Céline Chrétien

Univ. Grenoble Alpes, CNRS, Grenoble INP*, LGP2, F-38000 Grenoble, France
*Institute of Engineering Univ. Grenoble Alpes
E-mails: anne.blayo@pagora.grenoble-inp.fr; nathalie.marlin@pagora.grenoble-inp.fr

Short abstract

Despite its rough and porous characteristics, paper can be considered as a potential substrate for some applications in printed electronics. The main advantages of paper are its low cost, general availability, flexibility and recyclability. Depending on the desired properties, paper recycling may include a step of deinking. In the case of conventional printing, i.e. with conventional inks such as offset, flexo or gravure inks, different deinking techniques are efficient and well-monitored. With the growth of printed electronic components, one can expect an increase of paper-based electronics share in the waste papers, and therefore comes the issue of recycling, with the apparition of new challenges due to the presence of functional inks. In this study, an evaluation of the potential amount of functional materials in cellulose-based substrates is proposed. Then, in order to investigate whether current deinking lines are adapted to paper electronics, deinking tests were performed on a mix of inkjet- and screen-printed electronics on coated and uncoated papers with a silver-nanoparticles based ink. A deinking strategy was identified after the study of the different existing technologies: (i) pulping, (ii) hyperwashing and (iii) centrifugation were used to recover as much nanoparticles as possible from the substrate. Fillers coming from the coating were also removed from the substrate, which was proved to be detrimental for silver recovery. The rate of silver in the centrifugation deposit is low. Micro-analysis demonstrated that nanoparticles are mainly removed thanks to hyperwashing, meaning that fillers may play an important role in silver retrieval.

Keywords: deinking, printed electronics, silver –based conductive ink, paper

1. Introduction and background

In the context of an increasing demand for low-cost flexible electronic devices, printing processes have proved to be efficient as an alternative to conventional micro-electronics processes. A lot of applications already exist on polymer substrates such as polyethylene terephthalate, polyethylene naphthalate and polyimide. Despite its rough and porous characteristics, paper can be considered as a potential substrate for some applications in printed electronics, often designated as "paper electronics". Some devices are already described in the literature: transistors, diodes, passive components, RFID antennas, sensors, medical diagnosis equipment, etc. (Tobjörk and Österbacka, 2011; Li, et al., 2014; Mahadeva, Walus and Stoeber, 2015 ; Lin, et al., 2016). The main advantages of paper are its low cost, large availability, flexibility and recyclability. The possibility of printing disposable electronic devices on a cellulose-based material (paper or board) opens the road to connected packaging or printed objects; it allows electronics to be integrated as part of other printed media by printing them on a same press, for instance. The significant technologies in functional printing are inkjet, screen-printing and some coating techniques. Printing functionalities on paper-based substrates implies that functional inks may be used as well as conventional ones. Therefore, new questions arise:

- Are the current paper de-inking strategies adapted to these functional materials?
- Once the recovered electronic papers are collected, does a treatment or a relevant way of valorisation for the high added-value electronic ink exist?

The issue of recycling electronic devices starts to be discussed in a global way, but the specific topic of recycling functional printed cellulosic materials is relatively few documented. For example, some authors only mention the possibility of incinerating the final disposed devices (Lin, et al., 2016).

Printed electronics already raised the question of recyclability, researches were carried out to create recyclable devices, and the use of paper is described as an environment friendly approach.

Bollström, et al. (2009) developed a recyclable multilayer-coated fibre-based substrate combining sufficient barrier and printability properties for printed functional devices using reel-to-reel techniques. Recent researches demonstrated that cellulosic nano-fibres (CNF) used for enhancing the substrate surface properties of a paper exhibit the required properties for a printed electronic substrate. The CNF coated films possess better smoothness and lower porosity than the traditional paper. Nanocellulose films could also be used and are promising for processing transparent conductive flexible films either by coating of by impregnation of the composites. They have a better thermal stability than plastic substrates and their great advantage is that they contain recyclable materials (Hoeng, 2016).

Some researchers have also evaluated the sustainability of the electronic components. Zhou, et al. (2013) studied the possibility of recycling a transparent smooth CNC (Cellulose Nanocrystals) substrate used in a solar cell device. Recycling was done by a simple immersion of the solar cell in water leading to the swelling and dissolution of the CNC substrate. Then the solar cell components can be separated by washing and filtration, showing a recycling process very easy and green (Zhou, et al., 2013). CNC potential to be used as a scaffold for silver nanoparticles production in a silver-based inkjet ink was evaluated thanks to the good dispersing properties of CNC. Moreover, CNC coated cardboard has been studied to propose a new alternative for the printing of conductive tracks onto a porous substrate such as cardboard (Hoeng, et al., 2017). Jung, et al. (2015) demonstrated a new method for the degradation of nanocellulose substrates by biological degradation. The electronic components consisted of CNF coated epoxy substrates. Fungus degradation was evaluated for 100 % CNF films and epoxy films and was found to be efficient for both films. After an extended time (84 days), the encapsulated electronic component can be recovered (Jung, et al., 2015).

Another research related to our project is an investigation on the possibility of recycling conductive ink-printed paper substrate previously used in printed electronics, and reworking it into a conductive paper. Firstly, paper printed with conductive carbon ink was re-pulped. Substrate was torn into small pieces. Secondly, paper handsheets were prepared with additional amounts of conductive material (Husovska, et al., 2016). It was demonstrated that it is possible to reuse graphite printed substrates formerly used in printed electronics for building new conductive structures such as a capacitors.

Keskinen and Valkama (2009) raised the question of the end of life of printed electronics with solutions such as the reuse of products, the recycling of components and/or materials, the recovery of energy content and landfill. The study is not focused on paper substrates (Keskinen and Valkama, 2009).

A paper-making technique was used for the manufacture of low cost and low environmental impact all-paper-based Li-ion cells. The cells were composed of two paper-like electrodes, prepared using micrometric-sized graphite (anode) and $LiFePO_4$ (cathode) as active materials and truly natural micro-fibrillated cellulose as binder, and paper hand-sheets soaked in a standard liquid electrolyte solution as separator between them. The specific capacity obtained is even superior to that of standard PVdF (Polyvinylidene fluoride)-binded cell assembled with the same electrodes, and remains stable over prolonged cycling, indicating that the cellulose fibers do not affect the cycling stability. In this study, no organic solvents or synthetic polymer binders were used all along the production of the cell components which, in addition, can be easily re-dispersed in water by simple mechanical stirring as well as common paper hand-sheets (Zolin, et al., 2014).

The steps of this project are:

i. to make an inventory of the different functional materials that are likely to be printed on cellulosic fibre-based substrates, and that could possibly contaminate regular paper and board collection;
ii. to select some typical functional ink formulations in order to identify the components that could be recovered;
iii. to find elimination or valorisation strategies adapted to these products, staying within the framework of the current deinking lines.

The strategy is to focus on the most used inks. Our purpose is not to study the recycling ability of the fibre fraction of the electronic papers, but to evaluate how it is possible to extract the added value components of the functional ink for reuse and valorisation. Thus, the final objective will be to determine whether the current strategies used for de-inking can be used for printed electronics or not. To achieve these goals, separation/de-inking tests have been carried out on a mixture of electronic printed papers, collected from several companies, and unprinted mixed office papers in order to simulate a paper collection contaminated by functional inks. To simplify this first study, no regular printed paper was introduced in the mixture. The focus will be made on the recovery of silver since the commercial electronic papers collected all contain silver-based inks. The rapid progress and development of silver nanoparticles ink has been leading to concerns about the potential risk associated with the use and application of nanoparticles on human health and the environment. The issue is also economical because silver nanoparticles are very expensive and their recovery could spare money to suppliers and customers.

2. Materials and methods

2.1 De-inking line: the main steps

Recycling processes for conventional printed papers are well established. Deinking is carried out using flotation or washing technologies depending on the ink properties (oil- or water-based inks). Additional unit operations complete the fibre suspension cleaning, using the size and the density of the contaminant to be removed as separation criteria (Hüke and Schabel, 2000).

To our knowledge, the recycling of paper-based printed electronics has not yet been studied. However in the context of the strong development of such products, the evaluation of their recycling ability becomes inevitable, the final objective being the recovery of the ink components, especially metals like silver. The finality of this work is to evaluate if the added value components, after their separation from fibre, could be extracted and reuse in other applications. The methodology adopted in this work has been to start with current and available recycling technologies applied in the paper and board industry. Before testing the conventional recycling operations on paper based printed electronics, the different operations present in regular industrial deinking lines will be described.

2.1.1 Re-pulping

Pulping is always the first step. Fibres are separated and all the additives added to the paper during the printing and converting process should be separated from the fibres. This is a key operation leading to ink particle detachment from the fibre. If ink is correctly separated, its extraction from the fibre suspension will be favoured. Due to lack of material (paper based printed electronic) and time, the optimization of the pulping condition, i.e. electronic ink detachment optimization, could not be carried out. We will focus on the operations leading to ink removal/extraction from the fibre suspension.

2.1.2 Removal of contaminants

In conventional de-inking lines, removal of contaminants is based on the different properties of the contaminants:

- Differences in size: particles smaller than fibres can be removed by washing/particles larger than fibres can be removed by *screening.*
- Differences in density: if they are large enough, particles having a density different than 1 can be removed by centrifugal *cleaning*.
- Differences in surface properties: for particles between 10 μm and 250 mm, *flotation* can remove hydrophobic particles, additives (surfactants or soaps) are generally used to improve flotation efficiency.

In the case of this project, we will try to remove mainly silver nanoparticles from a paper substrate. A description of the common contaminant removal operations (screening, cleaning, etc.) will be done in a further section and their potential application for silver extraction will be discussed.

Screening

Screening is basically a physical separation technology; it consists in removing contaminants by keeping them on a screen while fibres go through the openings of a screen. Considerable progress has been achieved recently in screening techniques, especially with slots. Screen surfaces can be flat (disk screens) or cylindrical (cylindrical screens). Slots down to 0.10 or 0.15 mm width are currently used in mills (reduction by a factor 3 during the 3 last decades). Criteria such as separation ratio, enrichment, and cleanliness efficiency define and assess separation processes including screening.

In the case of the present study, silver nanoparticles (50–150 nm) would probably pass through the screen with the fibre fraction; consequently, this technique will not be studied.

Cleaning

Cleaning is a separation method based on particle separation in a centrifugal flow field. A swirling motion is created by the tangential inlet flow. The vortex motion creates centrifugal forces which cause the particles heavier than the stock to migrate to the outside of the cleaner, while lightweight particles migrate toward the vortex core. Centrifugal cleaning eliminates high densities (sand, metal fragments…) and low densities (plastics).

The flow containing contaminants is separated from the principal flow, at the base of the hydrocyclone or at the top. The centrifugal separation can eliminate particles with different properties:

- Particles of several densities;
- Ranging from slushing screen perforation diameters of 8–20 mm to 5 μm or less (centrifugal cleaning can remove smaller particles than screening, as low as 10 μm);
- Deformable particles that cannot be eliminated by screening.

Because of the high density of silver or other metals encountered in electronic ink formulations, cleaning may be a potential solution for ink extraction. However, the nanometric size of the particles to be removed may also affect the cleaning efficiency. Yet, the separation of fibres and electronic ink particles using centrifugation has been tested.

Flotation

Flotation consists in removing hydrophobic particles (namely ink particles), by floating them up to the surface of the cell with air bubbles. Flotation aids are used to improve the attachment of ink particles to air bubbles. Flotation can remove ink (oil-based ink with hydrophobic characteristics), varnishes and some adhesive particles, provided that their size is in the right range (10–250 μm roughly).

Because of the nanometric particle size and the absence of any hydrophobic character of the ink, electronic ink particles could not be removed by flotation. This operation has not been tested in this study.

Washing

Washing is a filtration process removing small particles (size < 30µm) from the fibre suspension using a screen with a calibrated pore size (10-500 µm); larger particles including fibres are retained on the wire of the washing device. Water acts as a carrier medium for the fine particles to be removed.

In this project, the washing operation has been studied to transport nanometric ink particles from the fibre suspension to the water filtrate. Then the filtrate will be centrifuged to concentrate the separated ink particles.

2.2 Materials: collection of electronic papers

A first difficulty in this project was to collect a large quantity of electronic papers. The paper substrate, generally a specialty paper, and the ink are expensive and the production of printed electronic rather limited. Arjowiggings and VFP ink provided printed electronics material. The totality of the samples gathered weights 9 kg, with more or less ink depending on the type of print. The majority of the samples provided were printed with nanosilver ink using mainly the inkjet and screen-printing processes. The main issue of the provided samples is their coating layer (paper Powercoat®).

For one pulping batch, 850 g of office paper were mixed with 150 g of electronic printed paper. A calculation based on the ink thickness and the coverage rate was made and estimates that the resulting fibre blend contained around 3 g to 10 g of nanosilver ink particles. This amount cannot be exactly evaluated because the bulk density of nanoparticles varies from 1.2 g/cm^3 to 8 g/cm^3.

In a second set of assays, a non-coated paper substrate, bearing a silver-based ink deposit (manually), was also submitted to deinking trials. In that case no fillers will interfere with the ink extraction. The ink is a silver nanoparticle-based ink.

2.3 Deinking of a paper collection containing commercial printed electronic papers

The purpose of the project is to use as much as possible the processes of the traditional de-inking line and to show if they are compatible with the recovery of silver. The tests carried out are mapped on Figure 1.

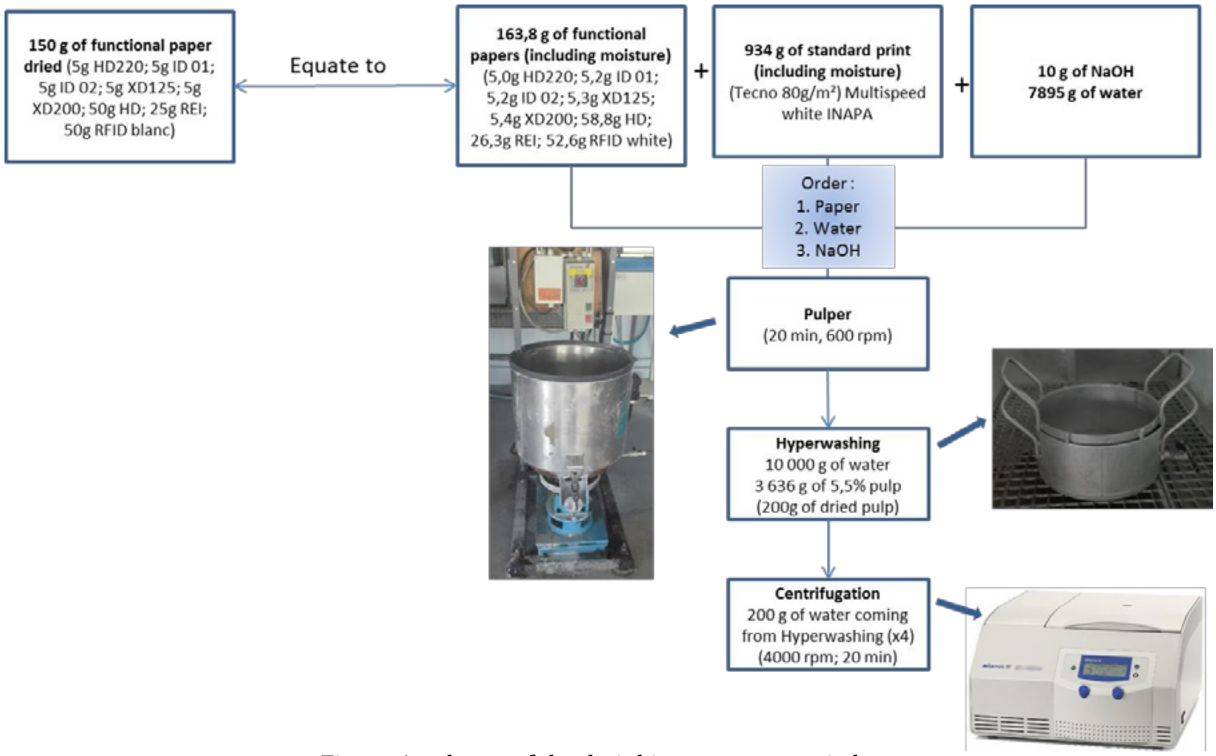

Figure 1: scheme of the de-inking process carried out

2.4 Analysis of the results

2.4.1 Percentage of ash in paper

Usually the ash content of a sample of wood, pulp or paperboard consist of:

- Various residues from chemicals used in manufacture
- Metallic matter from piping and machinery
- Mineral matter in the pulp from which the paper was made
- Filling, coating, pigmenting and/or other materials

The purpose of this experiment is to quantify the percentage of nanoparticles in the resulting pulp. The percentage of ash before/after pulping, after hyperwashing and of the centrifugation deposit is measured. A blank test is made to figure what is the percentage of ash in the substrate (Powercoat®) and the traditional print paper.

The blank test was performed on the paper mixture pulp, after the pulping step, on a pad formed after filtration. To ensure that most of the fillers and nanoparticles are retained on the pad, the filtrate was re-circulated 4 times on the pad.

The combustion of cellulose to form volatile combustion products occurs at about 300 °C. Both ignition at 525 °C and 900 °C were made. At 520 °C, only cellulose is eliminated but calcium carbonates remain. Ignition at 900 °C transforms calcium carbonates in calcium oxides; only fillers that are not carbonates remain. In a first approximation the difference in weight between the 550 °C and 900 °C ashes may be assumed to result from loss of carbon dioxide during carbonate mineral break-down. Because calcium carbonate is the dominant form of carbonate in most coatings, weight losses at 900 °C may nonetheless be used to estimate calcium carbonate content.

2.4.2 SEM and X-ray micro-analysis

The previous tests are made to recover as much as possible nanoparticles and fillers. But the presence of silver in the recovered samples is not verified, microscopic tests were made with a scanning electron microscope (SEM) to detect silver and to see whether there is any possibility to recover it. Analysis of the X-ray signals is used to map the distribution and estimate the abundance of elements in the sample.

3. Results and discussion

3.1 Prospective study of the potentially recovered printed electronics in collected papers

From calculations based on statistical data and hypothesis, it can be estimated that selective collections in 2017 in Europe could contain 0.002 % paper electronics (weight %). Although this ratio is still low, the recovery of metals from conductive ink formulations remains a challenge from economical and environmental points of view, given the expected growth of printed electronics.

3.2 Deinking of a paper collection containing commercial printed electronic papers

Commercial paper electronics were gathered from different manufacturers to conduct deinking tests. After a careful analysis of typical formulations of functional inks, hyperwashing was selected to separate the ink from the substrate. The first tests were conducted on a mix of office and electronic papers. After pulping, hyperwashing and centrifugation of the filtrate, a deposit is obtained. This residue contains mainly fillers from office papers and electronic papers, which are highly coated. A low fraction of Ag was detected. It was estimated that the rate of Ag recovered by centrifugation is only 2 % to 6 %. Unfortunately, the deinking method proved to be inefficient and water consuming.

3.3 Deinking of a paper mixture containing a printed electronic paper free of fillers

To understand the source of this lack of efficiency, deinking test using the same method were carried out on paper containing no fillers coated with conductive silver nanoparticle ink. After the deinking steps, X-ray analysis showed that the deinked fibres did not contain any silver. It means that most of the silver is in the filtrate, which was proved after an X-ray analysis of the filtrate centrifugation deposit.

4. Conclusions

The purpose of the project was to determine whether the classical de-inking techniques are viable for paper electronics. On the basis of the results obtained it may be concluded that the presence of fillers on paper surface and in the paper bulk affects the extraction of Ag from the fibrous matrix. The limiting factors could be: (i) the poor detachment of the ink from the paper coating (phenomenon that is often observed when highly coated print are deinked), (ii) the difficulty to drag the particles in the hyperwashing filtrate and (iii) the complexity to separate fillers from silver nanoparticles by centrifugation. Quantifying Ag throughout the different steps could also be improved.

Eventually, this project demonstrated that given the growth of printed electronics on paper substrates, it is worth asking the question of their end of life. Separating Ag from fillers is an issue that merits further investigations.

Acknowledgements

This work has been partially supported by the LabEx Tec 21 (Investissements d'Avenir – grant agreement n°ANR-11-LABX-0030).

We are grateful to Arjowiggings and VFP ink who provided us with the printed electronic paper samples.

References

Bollström, R., Määttänen, A., Tobjörk, D., Ihalainen, P., Kaihovirta, N., Österbacka, R., Peltonen, J. and Toivakka, M., 2009. A multilayer coated fiber-based substrate suitable for printed functionality. *Organic Electronics*, 10(5), pp. 1020–1023. http://doi.org/10.1016/j.orgel.2009.04.014.

Hoeng, F. 2016. *Potential of nanocellulose for conductive ink preparation*. Ph.D. thesis. Ecole doctorale Mécanique des fluides, Energétique, Procédés, Grenoble INP.

Hoeng, F., Bras, J., Gicquel, E., Krosnicki, G. and Denneulin, A., 2017. Inkjet printing of nanocellulose silver ink onto nanocellulose coated cardboard. *RSC Advances*, 7(25), pp. 15372–15381. http://doi.org/10.1039/c6ra23667g.

Hüke, U. and Schabel, S. eds., 2000. Recycled fiber and deinking. In: L. Göttsching, and H. Pakarinen, ser. eds., 2000. *Papermaking science and technology: Book 7*. Helsinki: Fapet Oy.

Husovska, V., Pekarovic, J., Pekarovicova, A. and Fleming, P.D., 2016. Capacitors out of recycled printed electronics paper substrates. In: *Proceedings of TAGA 68th Annual Technical Conference.* Memphis, 20–23 March 2016, pp. 202–211.

Jung, Y.H., Chang, T.-H., Zhang, H., Yao, C., Zheng, Q., Yang, V.W., Mi, H., Kim M., Cho, S.J., Park, D.-W., Jiang, H., Lee, J., Qiu, Y., Zhou, W., Cai, Z., Gong, S. and Ma, Z., 2015. High-performance green flexible electronics based on biodegradable cellulose nanofibril paper. *Nature Communications*, 6, article no. 7170. http://doi.org/10.1038/ncomms8170.

Keskinen, M. and Valkama, J., 2009. End-of-life challenges of printed electronics. In: *IEEE International Symposium on Sustainable Systems and Technology*. Phoenix, Arizona, 18-20 May 2009. http://doi.org/10.1109/ISSST.2009.5156737.

Li, R.-Z., Hu, A., Zhang, T., and Oakes, K.D., 2014. Direct writing on paper of foldable capacitive touch pads with silver nanowire inks. *ACS Applied Materials & Interfaces,* 6(23), pp. 21721–21729. http://doi.org/10.1021/am506987w.

Lin, Y., Gritsenko, D., Liu, Q., Lu, X. and Xu, J., 2016. Recent advancements in functionalized paper-based electronics. *ACS Applied Materials & Interfaces*, 8(32), pp. 20501–20515. http://doi.org/10.1021/acsami.6b04854.

Mahadeva, S.K., Walus, K. and Stoeber, B., 2015. Paper as a platform for sensing applications and other devices: a review. *ACS Applied Materials & Interfaces*, 7(16), pp. 8345–8362. http://doi.org/10.1021/acsami.5b00373.

Tobjörk, D. and Österbacka, R., 2011. Paper Electronics. *Advanced Materials*, 23(17), pp. 1935–1961. http://doi.org/10.1002/adma.201004692.

Zhou ,Y., Fuentes-Hernandez, C., Khan, T.M., Liu, J.-C., Hsu, J., Shim, J.W., Dindar, A., Youngblood, J.P., Moon, R.J. and Kippelen, B., 2013, Recyclable organic solar cells on cellulose nanocrystal substrates. *Scientific Reports*, 3, article no. 1536. http://doi.org/10.1038/srep01536.

Zolin, L., Destro, M., Curtil, D., Chaussy, D., Penazzi, N., Beneventi, D. and Gerbaldi, C., 2014. Flexible cellulose-based electrodes: towards eco-friendly all-paper batteries. *Chemical Engineering Transactions,* 41, pp. 361–366. http://doi.org/10.3303/CET1441061.

Secure Printing for Labels and Packaging using Industrial Digital Printers: authentication of printed matrix codes with smartphone cameras

Slavtcho Bonev[1,2] *and Sviatoslav Voloshynovskiy*[1]

[1] Stochastic Information Processing Group, Computer Science Department, University of Geneva

[2] Epyxs GmbH, Gutacher Ring 4, 68239 Mannheim, Germany

E-mails: s.bonev@epyxs.com; svolos@unige.ch

Short abstract

In a previous publication the feasibility of a product security concept based on authentication of printed matrix codes was demonstrated. The security features were printed using an offset press and scanned by a flatbed scanner. A comparison of the extracted authentication signatures has confirmed the high discriminative power (very low Equal Error Rates (EER) achieved) and leaded to a successful validation of the product protection approach using both standard (DataMatrix) and special (DataGrid) matrix codes. Two main issues remained a subject of further improvements. First, the used offset printing process led to similarities of the authentication signatures within a printed batch introduced by the printing plate, which resulted in multiple matches causing an ambiguity at conducting a database search. Second, to check the security features a high-resolution scannig was necessary, which required the usage of special scanning devices and made the verification more difficult for the end-user. In the current work we extend the previous findings to industrial digital printing and image acquisition by smartphone cameras.

Keywords: product protection, industrial digital printing, authentication, matrix codes, smartphone cameras

1. Introduction and background

Millions of dollars a year are on the line for companies as they seek ways to ensure that the products sold with their logos and branding are authentic and are delivered via the authorized distribution chains. The proliferation of counterfeiting requires brand owners and their converter/printer partners to work together to create a multi-layered protection plan so that their packaging and labels protect their brands and deter those trying to profit at their expense (Weymans, 2013; Bonev, et al., 2010).

The improvements in industrial digital printing and smartphone cameras over the last years require an adaptation of the product security concept towards economic efficiency, usability and environmental sustainability.

Recent trends show that many brand owners are looking for a complement to traditional offset printing - a solution that matches the desired output to the right technology efficiently and cost effectively. Printing tests on the industrial digital printer Primefire 106 (Lohmann, 2017), which uses the SAMBA™ drop-on-demand printhead of the FUJIFILM Group (Yoshinori, 2014), have shown that a 95 percent coverage of the Pantone color space is possible. In addition, an offset-like result was achieved on the substrates used. The technology also has other advantages, so for example, the water-based inkjet ink is recyclable and thus contributes to even higher environmental friendliness of cardboard boxes. In addition, material will be saved, since there would be little waste and resource efficiency could be increased.

Since their introduction in the latter half of the 2000s, smartphones have consistently gained market share and become more than simple gadgets, as they combine the best features of cellular phones, personal computers, and digital cameras. The built-in megapixel camera sensors combined with high-quality optics and autofocus lenses can meanwhile be used to solve complex document examination tasks. Therefore, it is natural to expect that the smartphone can be used for the verification of the brand protection features.

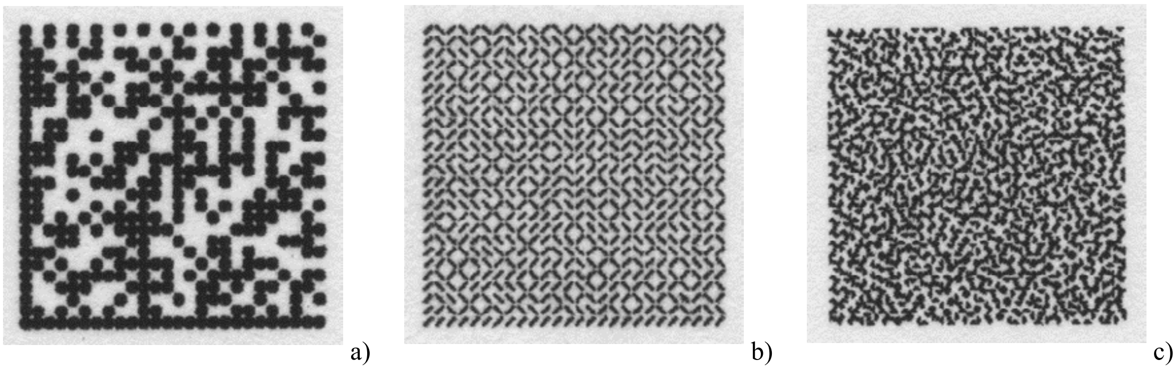

Figure 1: Printed matrix code samples: DataMatrix (a), DataGlyphs (b), and DataGrid (c)

There are substitutes (Figure 1) for the standard codes (International Organization for Standardization, 2006) used as DIN 66401 product identifiers (Deutsches Institut für Normung, 2011) in the last decades. DataGlyphs (Xerox) and DataGrid (Epyxs) represent a new class of differential codes which have two crucial advantages over the unipolar DataMatrix and QR codes. First, the proportion of printed to non-printed area in the code symbol is constant (Figure 2). This allows to check the dot gain and the uniformity of the symbols for the purpose of printing quality control just by calculating the mean value of the symbol pixels in the scanned image.

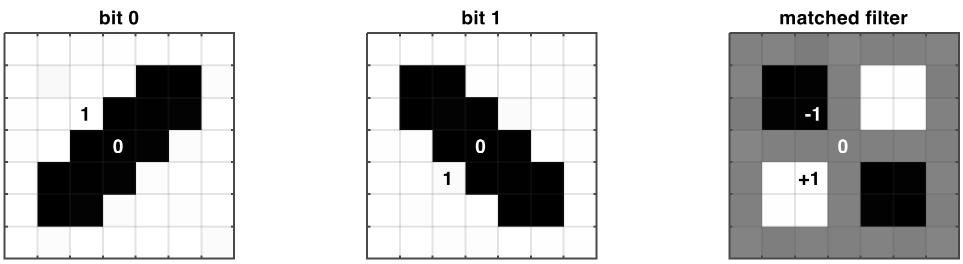

Figure 2: Graphical information encoding using DataGlyphs symbols

Second, after applying the matched filter (Figure 3) and sampling the corresponding symbol values, a bit decision is made using a constant zero-threshold. Thus, the bit decision is robust against dot gain and non-uniform illumination. The decision threshold for unipolar codes, which has to be calculated for each scanned code leads to great bit error rates for high dot gain levels or non-uniform illumination.

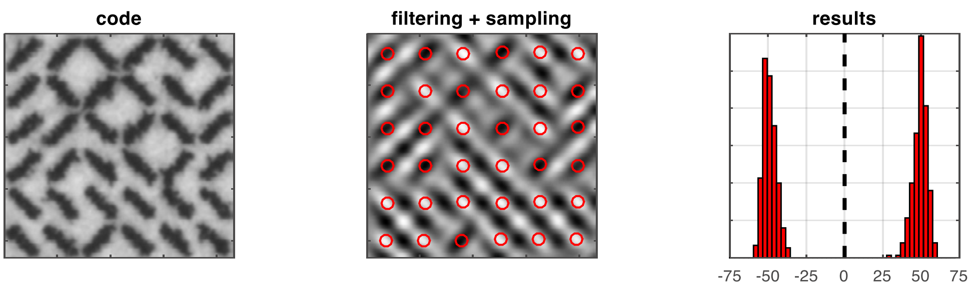

Figure 3: Information decoding from printed DataGlyphs using matched filter

The increase of data storage density represents an additional advantage (Table 1).

Table 1: Matrix codes and their properties

Nr.	Matrix code	Symbol size	Bits/symbol	Modulation	Communication theory
1	DataMatrix	6 × 6 dots	1	amplitude	OOK: On-Off Keying
2	DataGlyphs®	7 × 7 dots	1	phase	BPSK: Binary Phase-Shift Keying
3	DataGrid	6 × 6 dots	2	phase	QPSK: Quaternary Phase-Shift Keying

The terms identification and authentication (Figure 4) are widely used in the area of human biometry, but are often misused when it comes to matrix codes as printed security features. The content of the matrix code is used as a product identifier (ID). At the same time, the stochastic signal caused by the interaction between medium (ink) and substrate (paper) is unique for each print and can be used as an authentication signature (AS) of the printed matrix code.

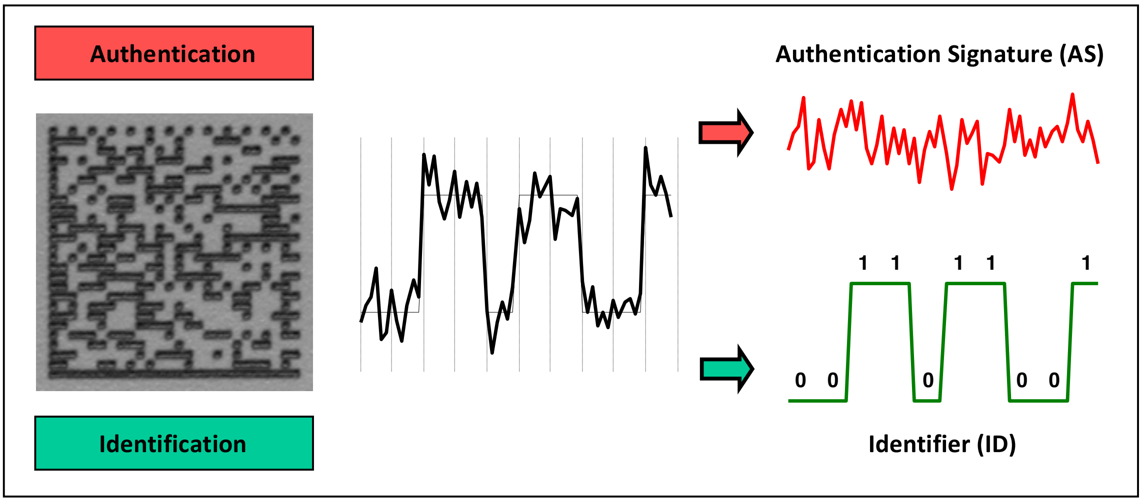

Figure 4: Identification and authentication using matrix codes

We formulate some new research questions regarding the product security concept and try to address them in this publication:

- Which discriminative power can be achieved with industrial digital printing using the authentication signatures of different matrix codes?
- How good we distinguish originals from copied codes on counterfeited products?
- Can the digital printing press be identified based on the extracted stochastic signal?

2. Materials and methods

2.1 Printing devices

In a previous article (Bonev, et al., 2010) an offset printing press at 2 400 dpi was used. The codes were printed very small to produce enough process deviations (fingerprint) and were not suitable for scanning with smartphone camera. Real serialization cannot be realized since the offset image remains the same for all items on each printed sheet. Even if each item on a sheet is marked individually, there are N identical items in a batch which leads to ambiguous authentication results.

Through the usage of digital printers with VDP (Variable Data Printing) option (Bennett, 2006), a unique identifier (Deutsche Institut für Normung, 2011) is printed on each item and printed sheet. The authentication effort is reduced from a 1:N comparison (offset printing, check all authentication signatures in a batch of N sheets) to a 1:1 comparison (digital printing, check only the authentication signature corresponding to the registered ID).

Office inkjet printers are used in the proof of concept phase and industrial printers in the product development phase. The binary code images are generated as 1-bit TIF images and are printed using the native resolution according to device datasheet without the usage of printer-specific image optimization.

Table 2: Home office digital printers

Nr.	Digital printer	Abbreviation	Print technology	Native resolution
1	Canon PIXMA iP7200	CA	thermal inkjet	600 × 600 dpi
2	Epson WorkForce WF-2010	EP	piezo inkjet	720 × 720 dpi
3	HP OfficeJet Pro 8210	HP	thermal inkjet	600 × 600 dpi

Table 3: Industrial digital printers

Nr.	Digital printer	Abbreviation	Print technology	Native resolution
1	FX DocuColor 1450 GA	FX1	EA toner xerography	2 400 × 2 400 dpi
2	FUJIFILM Jet Press 720S	FJ7	high-speed piezo inkjet	1 200 × 1 200 dpi
3	HP Indigo 20000	HP2	liquid ink electrophotography	812 × 812 dpi

2.2 Scanning devices

Flatbed scanners at 1 200 dpi were used to achieve optimal scanning conditions implying low spatial distortion and uniform illumination. A scanning resolution of 1 200 dpi was also reached using a smartphone camera (Table 4) at a distance of 90 mm. This was considered as an indication that the authentication is possibly practicable for the end-users of the protected products.

Table 4: Scanning devices

Nr.	Scanning device	Type	Optical resolution	Scanning resolution
1	Canon CanoScan 9000F	flatbed scanner	4 800 dpi	1 200 dpi
2	Epson Perfection V850	flatbed scanner	4 800 dpi	1 200 dpi
3	Samsung Galaxy S6	smartphone (mobile)	1 200 dpi	1 200 dpi

Two scanning scenarios (Figure 5) were simulated:

a) Optimal scanning: the smartphone is parallel to the substrate (0° tilt), no image distortions

b) Freehand scanning: the smartphone is tilted to the substrate, perspective image distortion

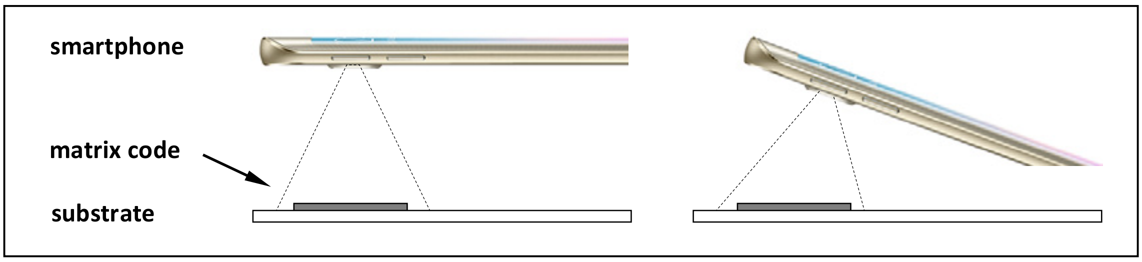

Figure 5: Scanning scenarios

2.3 Methodology

DataGrid codes (Wirnitzer and Bonev, 2007) are used as reference codes with maximized discriminative power through high-detail code symbols. Similar differential matrix codes DataGlyphs (Bloomberg, et al., 2000) consisting of low-detail code symbols are used for comparison. Both matrix codes consist of 24 × 24 information symbols. According to the recommendations of DIN 66401, only single module DataMatrix and QR codes with a maximum of 24 × 24 code symbols and maximum size of 11 mm × 11 mm can be used as Unique Identification Marks (UIM) for product marking and track-and-trace purposes.

The copies (counterfeits) of each matrix code are created using the original binary image and printing device, and are printed in the neighborhood of the original code to make batch scanning easier. This approach differs from the usual procedure of scanning, (optional) binarization, and reprinting of the codes and represents the worst case counterfeiting scenario whereby the original pattern and the printing technique are known to the counterfeiter.

The evaluation procedure was fully described in a previous work (Bonev, et al., 2010). The first scanning device according to Table 4 is used for AS registration, and both other devices – scanner and smartphone – are used for AS verification. The authentication signature (AS) represents the decoding error signal using an optimal filtering method (Figure 4). The correlation coefficient of different AS represents the authentication result. Respective EERs are calculated for each pair of printing and scanning devices using Gaussian result distribution models (Figure 7). The aim is to show that the discriminative power of the authentication signature is significantly higher than those achieved for human fingerprints (Pankanti, Prabhakar and Jain, 2002) and human iris (Daugman, 2015), which both have worst-case EER values of around 10^{-3}.

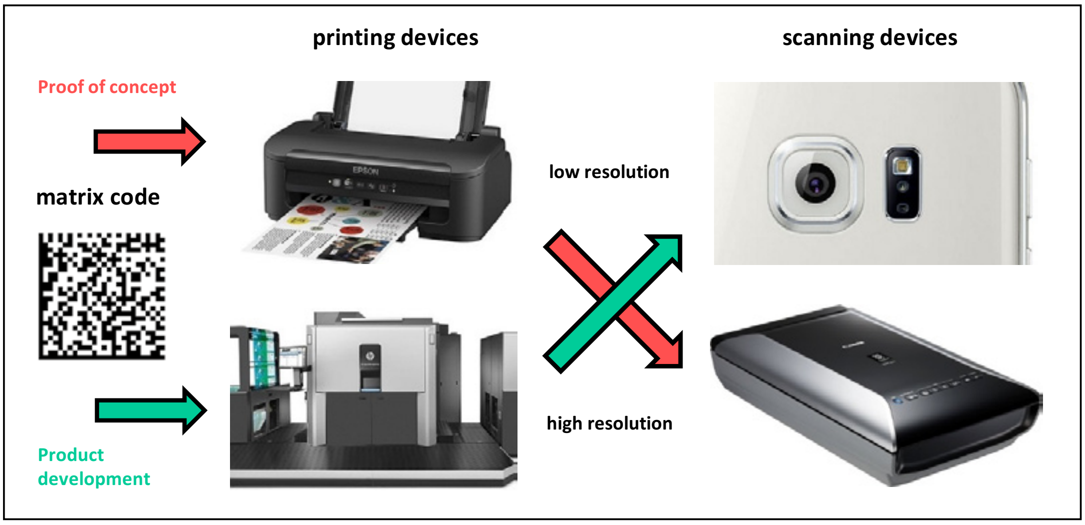

Figure 6: Two-step evaluation methodology

Preliminary tests (print, scan, authenticate) will be carried out (Figure 6) using 3 office inkjet printers and an early Proof-of-Concept will be delivered long before presentation (October 2018) and publication (January 2019). The symbol shapes will be optimized to handle with different dot gains (DG = Aprint – Aform, tonal value increases) of the used printers. In the mean time (April–August 2018) the printing tests will be conducted using industrial digital printers and the evaluation will be completed. Additional codes or patterns can be included for internal test purposes.

3. Results and discussion

The experimental results for a single printing device results are exemplary presented in Figure 7 in order to emphasize the main characteristics of the authentication approach. The authentication performance is expressed by its corresponding EER value, and is presented in Table 5 for each combination of components – matrix code, printer, and scanning device. For each involved component a clear systematical influence on the EER was expected and identified.

The type of matrix code has an influence on the EER achieved. Due to the higher detail content of the code symbols, DataGrid leads to systematically lower EER values compared to DataGlyphs. The type of used scanning device also shows a clear tendency regarding the authentication results achieved. Due to better optical transfer function (OTF) the scanner leads to systematically lower EER values compared to the smartphone camera. The JPEG image compression artifacts, which are introduced in the digital images by the mobile scanning device OS, additionally reduce the digital image quality.

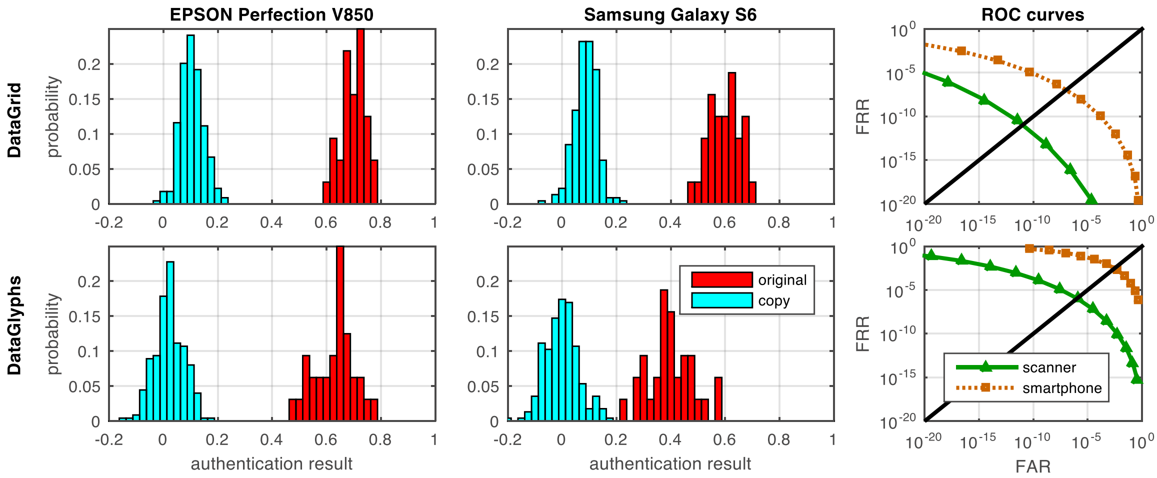

Figure 7: Authentication result distributions and corresponding ROC curves for the CA printer

The used printing device has the greatest influence on the EER. The CA and HP printer show EERs of 10^{-11} and 10^{-21} (third column of Table 5), respectively. The great EER difference of several decades cannot necessarily be derived from the difference between the printed code patterns with an area of 5 × 5 mm shown in Figure 8.

Table 5: Authentication performance using different codes and printing/scanning devices

Nr.		EER DataGrid		EER DataGlyphs			EER DataGrid		EER DataGlyphs	
	device	scanner	mobile	scanner	mobile	device	scanner	mobile	scanner	mobile
1	CA	10^{-11}	10^{-7}	10^{-6}	10^{-3}	FX1	10^{-4}	–	–	–
2	EP	10^{-10}	10^{-6}	10^{-11}	10^{-4}	FJ7	10^{-5}	–	–	–
3	HP	10^{-21}	10^{-15}	10^{-13}	10^{-6}	HP2	10^{-7}	–	–	–

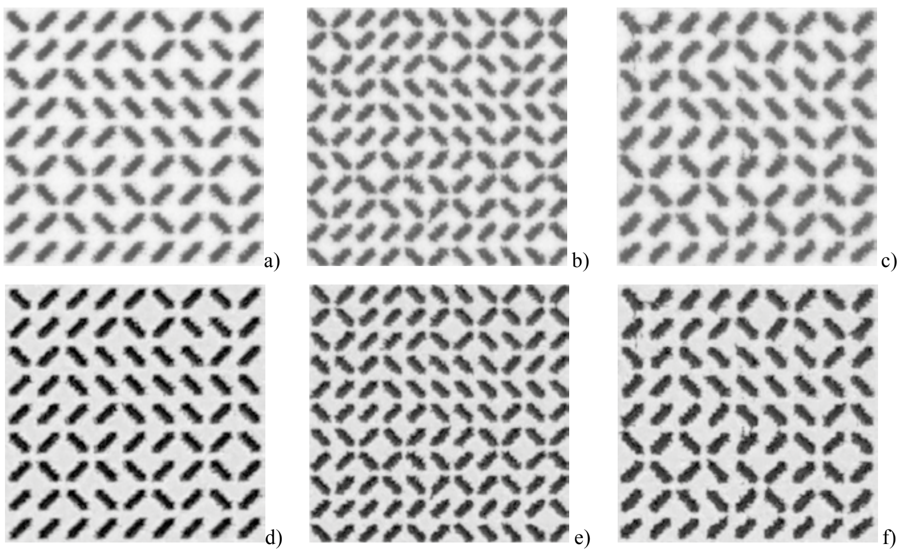

Figure 8: Typical distortions of DataGlyph symbols printed by different home office printers and scanned using scanner (upper row) and smartphone (lower row): CA (a, d), EP (b, e), and HP (c, f)

The interaction between ink and paper is a stochastic process which is expressed by different types of distortions of the printed patterns compared to the original binary patterns of the code symbols shown in Figure 2. The resulting EER depends highly on the AS extraction algorithm and can be estimated only empirically.

Acknowledgements

We gratefully acknowledge the experimental support of Mr. Hongyu Sun and Mr. Pai Peng from Shenyang AnChuang Information Technology Co. Ltd. in the area of industrial digital printing.

References

Bennett, P.K., 2006. *The handbook for digital printing and variable-data printing*. Pittsburgh, Pennsylvania, USA: Graphic Arts Technical Foundation.

Bonev, S., Gebhardt, R., Maleshliyski, S., Reinhold, G. and Wirnitzer, B., 2010. *Quality measurements in secure offset print production.* In. N. Enlund and M. Lovreček, eds. *Advances in Printing and Media Technology: Proceedings of the 37th International Research Conference of iarigai*. Montreal, Canada, September 2010. Darmstadt: iarigai.

Bloomberg, D.S. Hecht, D.L. Tow, R.F. and Flores, L.P., Xerox Corporation. 2000. *Self-clocking glyph shape codes*. U.S. Pat. 6,076,738.

Daugman, J., 2016. Information theory and the IrisCode. *IEEE Transactions on Information Forensics and Security*, 11(2), pp. 400–409. http.//doi.org/10.1109/TIFS.2015.2500196.

Deutsche Institut für Normung, 2011. *DIN 66401:2011-02 UIM - Unique Identification Mark - Application standard for very small items using matrix symbols*. Berlin: DIN.

International Organization for Standardization, 2006. *ISO/IEC 16022:2006 Information technology - Automatic identification and data capture techniques - Data Matrix bar code symbology specification.* Geneva: ISO.

Lohmann, F., 2017. *Heidelberg: MPS Obersulm erster Pilotanwender der Primefire 106.* [online] Available at: <http://www.print.de/News/Produkt-Technik/Heidelberg-MPS-Obersulm-erster-Pilotanwender-der-Primefire-106_4049> [Accessed February 2018].

Pankanti, S., Prabhakar, S. and Jain, A.K., 2002. On the individuality of fingerprints. *IEEE Transactions on Pattern Analysis and Machine Intelligence*, 24(8), pp. 1010–1025. http.//doi.org/10.1109/TPAMI.2002.1023799.

Weymans, F., 2013. *Label and packaging security: brand protection tools in printing and packaging*. [online] Available at: <http://whattheythink.com/articles/62758-label-packaging-security-brand-protection-tools-printing-packaging/> [Accessed February 2018].

Wirnitzer, B. and Bonev, S., 2007. *Method for encoding data via matrix print data storage*. European Patent EP 1771813.

Yoshinori, K., 2014. FUJIFILM Group's Inkjet Printhead and Technology. *Fujifilm Research & Development, 59*. [online] Available at: <http://www.fujifilm.com/about/research/report/059/pdf/index/ff_rd059_007_en.pdf> [Accessed February 2018].

Image Watermarking using a Cover Work with Replicated Elements

Elena Yakovleva[1], *Anton Makarov*[1], *Valery Gorbachev*[2] *and Elena Kaynarova*[2]

[1] Saint-Petersburg State University, St. Petersburg, Russia

[2] High School of Print and Media of St. Petersburg State University of Industrial Technology and Design, St. Petersburg, Russia

E-mails: e.s.yakovleva@spbu.ru; a.a.makarov@spbu.ru; valery.gorbachev@gmail.com; helenkainarova@gmail.com

Short abstract

Widespread digital images have to be protected from unauthorized copying. Numerous image types result in great number of suggestions of how to do it. We focus on steganographic technique that protects images by visible or invisible watermark. The standard steganographic system includes an algorithm that embeds a watermark into an image that is called cover or cover work. The usual problem is to detect the invisible watermark or to retrieve the cover by removing the visible watermark. Embedding algorithms exploit the digital images or covers in spatial and frequency domain representation, which have its particular features as for security, payload and watermark robustness. In this work we consider an idea of a particular prepared cover image that has the replicated elements. It may be some of the image representation components as a bit plane from the spatial domain and a frequency band achieved by an orthogonal transform like DWT (Discrete Wavelet Transform). Thanks to features of human visual system and the image redundancy the prepared cover image and original may be visually indistinguishable and in this way more effective solutions can be achieved. The aim of this work is to consider the image representation and to find which of their items can be replicated for watermarking. We present two schemes for spatial and frequency domain watermarking and consider a new representation of cover image over the basic wavelet matrices.

Keywords: steganography, digital image, DWT

1. Introduction and background

The modern steganography considers the problem of the digital data embedding that the first of all is exploited for protection of media information, particularly digital images by watermarking. The watermarking techniques are based on the features of Human Visual System and use the digital representation of images. Together with media protection steganography may be useful for another problem. For example, some information such as written guarantees, instructions, which are often difficult to find when user needs them, could be embedded inside an image. The user cannot see it by viewing but can extract it when it is necessary. It is attractive because it does not need to keep or to search for saved documents.

Being a digital matrix, the same digital image has a great number of its mathematical representations in the computer and also graphical formats to store it. Using orthogonal transforms we can achieve the frequency domain representation in contrast to spatial one, that includes, for example, the image bit planes. In this work we will consider grayscale images.

The works (Gao and Jiang, 2010; Liu and Ying, 2012; Ram, 2013; Sakthivel and Sankar, 2016; Kim, Park and Park, 2017) rely to embedding digital watermarks into digital grayscale images using Discrete Wavelet Transform (DWT). In papers (Gao and Jiang, 2010; Liu and Ying, 2012), the grayscale watermark needs preliminary data pre-processing before embedding. An approach with using DWT together with artificial neural network is cited in the paper (Sakthivel and Sankar, 2016). In the work (Ram, 2013) some demands are made to digital watermark, then it transforms into pseudo-random binary sequence.

In our work we introduce a scheme for digital image watermarking. The scheme is developed for grayscale image and allows us to embed invisible and visible marks. Now we focused on digital images. The question of whether our scheme would be useful for printed matter is open.

2. Materials and methods

In the digital image some of its fragments can be replicated without introducing visual changing. The identical areas are useful for embedding information, for extraction which the original is not needed. These features result in a set of the blind steganographic schemes.

2.1 General scheme

Assume C = {a, b, c, d} to be a representation of a digital image, consisting of elements a, b, c, d whose order may be important. E.g. elements a, b, c, d can be frequency blocks consisting of approximation and the sets of horizontal, vertical and diagonal details from DWT. Assume that some of these elements, say b, is replicated or doubled by a mapping C ⇒ $C2$ = {a, b, c, d} so that both images C and $C2$ are visually undistinguishable, C = $C2$.

Then the prepared image is watermarked by embedding a message M into b. The order of choosing of b depends on task. We can receive either visible watermark or not. The message can be presented by an image and can be visible or invisible.

Let introduce two algorithms ***emb*** and ***det*** for embedding and detection message. The embedding algorithm input is (b, M, K), where K is a set of parameters that perhaps includes a secrete key, the output is the replicated element with inserted message bM = emb(b, M, K). The detection algorithm extracts M =det(b, bM, K). By this way we get the watermarked image S = {a, b, bM, d}. The inserted data bM may be invisible, $C2$ = S, or visible, $C2 \neq S$, where equality and inequality mean the visual difference between two images. The standard watermarking task is to detect invisible message and to retrieve original by removing the visible message.

Two next features result in exploiting the replicated cover image $C2$. The first is a blind detection algorithm and the second is a high visual quality pattern when retrieving the original. It follows from the simple reasons. As for detection the watermarked image$S$ has elements b andbM needed for detection, then message may be extracted without the cover image $C2$ and detection algorithm is blind.

Indeed, numerous steganographic systems do not have blind detection. As for quality the removing of visible watermark, task of which is to make worse visual perception of image, can be done by replacing bM with b. As result we get the retrieved image $C2$ = C.

Two next versions of the considered general scheme illustrate the presented observations.

2.2 Spatial domain watermarking

The scheme exploits the grayscale image bit planes. Indeed, any 8-bit grayscale image C can be represented by a set of eight bit planes

$$C = \{B_1, \ldots, B_8\} = B_8 \cdot 2^7 + \ldots + \mathrm{B}_1 \cdot 2^0, \qquad [1]$$

where each bit B_v, v = 1,…, 8 is a binary image of size C and has its weight given by 2^{v-1}. Set of planes has hierarchic structure.

So, bit planes of v = 1, 2, 3 are the least significant, their weights are small and they look as noise, in contrast to planes of v = 8, 7, 6, which have semantic information. In this representation a bit plane can be chosen as the replicated element b.

Then we create new image $C2$ with two identical bit planes B_v

$$C \rightarrow C2 = C - B_u \cdot 2^{u-1} + B_v \cdot 2^{v-1}, \qquad [2]$$

where u is not equal to v. Let us introduce a function $bitget(C, v)$ that computes the bit plane v = 1,2… of grayscale image C. Then $bitget(C, v) = bitget(C, u) = B_v$ and we get the replicated plane B_v.

Assume that the watermark M is a binary image, and, for example, embedding algorithm is addition by modulo 2. Then bit plane with embedded image is $BM = (B_v+M) \bmod 2$ and two types of watermarking, visible and invisible are available by varying u and v.

If v, u refer to the least significant planes, v, u = 1, 2, 3, then watermarking of u

$$S = C2 - B_v \cdot 2^{u-1} + BM \cdot 2^{u-1}, \qquad [3]$$

results in invisible watermark. Really, in this case the introduced changing is small, no more than $2^3 << 2^8 = 128$, and visually imperceptible. The watermark is extracted by blind detection
$M = (bitget(S,v) + bitget(S,u)) \bmod 2$.

If plane v is chosen significant, v = 8, 7, 6, and v = 1, 2, 3 we can get a visible mark by watermarking v. The obtained image S will have two significant planes B_v, one of which has M. The goal of this scheme is to retrieve $C2$. It needs to replace the watermarked bit plane with replicated B_v. It is clear that difference between the original C and the retrieved image $C2$ is given by least significant planes B_u, u = 1, 2, 3, it may be small and results in the good visual quality retrieved original.

2.3 Frequency domain watermarking

We consider DWT, a particular orthogonal transform, that represents the cover grayscale image C by four frequency blocks $\{cA, cH, cV, cD\} = DWT(C)$,where cA is approximation, cH, cV and cD are sets of horizontal, vertical and diagonal details. These blocks are called also LL, LH, HL and HH from Low and High frequencies. The blocks keep different information about image.

So, cA that is a low frequency, includes semantic information that refers to main visual characters and plays an important role for visual perception. The other blocks are high frequency; they keep information about details so that they could be replicated without noticeably altering the visual quality of the image. Assume cD be replicated, then we get, for example, $C2 = iDWT(cA, cH, cD, cD)$, where iDWT is inverse of DWT.

To achieve a watermarking scheme we take a simple embedding algorithm, that replaces a part of the replicated block coefficients, say cD, with message M. Assume the watermarked block be $cDM = emb(cD, M, K)$, where K is a scale parameter, that is strength of the inserted watermark. By varying K we can increase or decrease the pixel brightness of M. The introduced changing arises from two parameters at last K and the chosen replicated block. They result in visible or invisible watermark.

2.4 Basic wavelet watermarking

In our works (Gorbachev, et al., 2017a; 2017b; Yakovleva, et al., 2018) it was found that any orthogonal transform of a grayscale image C of size $M \times N$ can be described by a set of basis matrices or grayscale images $C = \{E(kp)\}, k = 1,..., M, p = 1,..., N$.

In the case of DWT such basis has four sets from the basic wavelet images $\{E(kpA), E(kpH), E(kpV), E(kpD)\}$ where indexes A, H, V and D accordingly refer to cA, cH, cV and cD frequency blocks given by DWT(C). Note this image representation cannot be reduced to spatial or frequency one. Nevertheless, some basic images can be replicated and new watermarking schemes can be achieved. The features of these schemes are still open question.

3. Results and discussion

In the case of visible watermarking the retrieved image quality plays important role. It can be examined visually and with the help of distortion measures, that describes quantitatively the difference between the original C and $C2$, where $C2$ is an image obtained from C by replicating. For our calculation the original 8-bit grayscale image C is presented in Figure 1. We considered a set of distortion measures and present here the results on PSNR (Peak Signal Noise Ratio) that is often used.

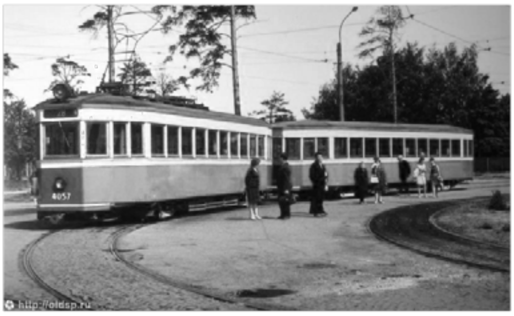

Figure 1: Original grayscale image

If PSNR has value about 20–40 dB, then one usually tells about the good visual quality.

We calculated PSNR(C, $C2$) for spatial domain watermarking, where $C2$ is grayscale image with two bit planes B_v. For this case $C2$ depends on two integers v and u, so we denote it as $C2(v, u)$, where $v, u = 1, 2, ..., 8$ and $C2(v, v) = C$. Figure 2 shows the found results for PSNR as function of v and u.

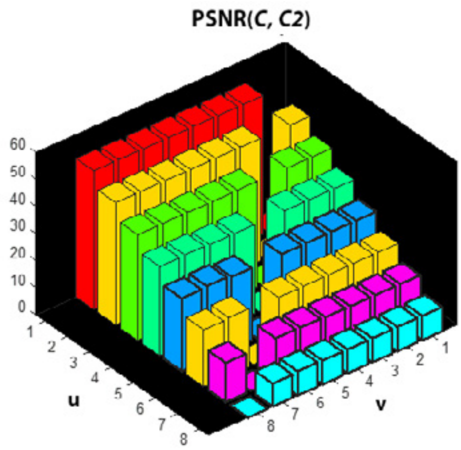

Figure 2: Spatial watermarking scheme; bit plane is replaced with bit plane B_v, u, v = 1, 2, ..., 8

We have to omit the diagonal items, $v = u$, because they are equal to PSNR(C, C) that is infinity. Note that PSNR(v, u) is degradation introduced by replacing of the bit plane B_u with B_v.

It follows that PSNR is around 60 dB and 40 dB, when the least significant plane B_1 and the plane B_4 is replaced with B_8, ..., B_1. This large PSNR is in accordance with high visual quality of $C2$.

Also we calculated PSNR(C, $C2$) for frequency watermarking based on DWT. Together with previous case $C2$ depends on two integers v and u but they refer to the DWT coefficient block v, u = A, H, V, D. For example, if $v = H$, $u = D$, then $C2(H, D)$ = iDWT(cA, cH, cV, cH). It means that cD is replaced with cH. Figure 3 presents the found results for PSNR, wavelet *db6* was used.

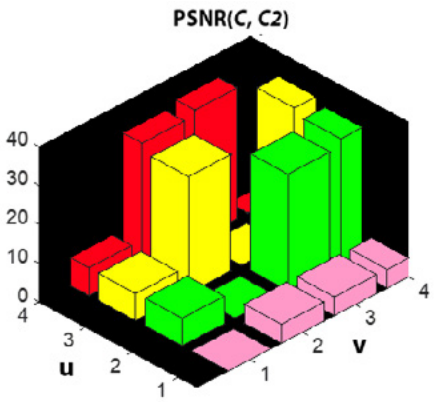

Figure 3: Frequency watermarking scheme, replicating of the DWT block of coefficients

It follows that replacing cA results in small PSNR of 10 dB that is agreed with low visual quality of image $C2$. In the same time large values of 40 dB are achieved when, for example, block cD is replaced with cV and cH.

For both schemes the found results tell us that the good visual quality of the replicated image can be possible.

4. Conclusions

The digital image has numerous representations that can be exploited for embedding information by steganographic techniques. Some of image representation elements can be replicated without loss of visual quality. This observation could result in watermarking schemes, particularly for visible and removal watermark when the high quality retrieved original is achieved.

References

Gao, G. and Jiang, G., 2010. Grayscale watermarking resistant to geometric attacks based on lifting wavelet transform and neural network. In: *Proceedings of 8th World Congress on Intelligent Control and Automation (WCICA)*. Jinan, China, 7–9 July 2010. IEEE, pp. 1305–1310.

Gorbachev, V., Kaynarova, E., Metelev, I. and Yakovleva, E., 2017a. On Color-to-Gray transformation for distributing color digital images. In: *FRUCT'20: Proceedings of the 20th Conference of Open Innovations Association* FRUCT. Saint-Petersburg, Russia, 3–7 April 2017. Helsinki: FRUCT Oy, pp. 77–82

Gorbachev, V., Kaynarova, E., Makarov, A. and Yakovleva, E., 2017b. Digital image watermarking using DWT basis matrices. In: *Proceedings of the 21st Conference of Open Innovations Association FRUCT*. Helsinki, Finland 11 June – 11 October 2017. Helsinki: FRUCT Oy, pp. 127–133.

Kim, J., Park, H. and Park, J.-I., 2017. Image steganography based on block matching in DWT domain. In: *Proceedings of 2017 IEEE International Symposium on Broadband Multimedia Systems and Broadcasting (BMSB)*. Cagliari, Italy, 7–9 June 2017, pp. 36–39.

Liu, Q. and Ying, J., 2012. Grayscale image digital watermarking technology based on wavelet analysis. In: *Proceedings* of 2012 IEEE Symposium on Electrical & Electronics Engineering (EEESYM). Kuala Lumpur, Malaysia, 24–27 June 2012. pp. 618–621.

Ram, B., 2013. Digital image watermarking technique using discrete wavelet transform and discrete cosine transform. *International Journal of Advancements in Research and Technology*, 2(4), pp. 19–27.

Sakthivel, S.M. and Sankar, A.R., 2016. Real time watermarking of grayscale images using integer DWT transform. In: *Proceedings of the 2016 International Conference on VLSI Systems, Architectures, Technology and Applications (VLSI-SATA*). Bangalore, India, 10–12 January 2016. IEEE.

Yakovleva, E.S., Makarov, A.A., Gorbachev, V.N. and Kainarova, E.M., 2018. Wavelet methods in steganography. *Russian Forum of Young Scientists, KnE Engineering*, pp. 318–330. http://doi.org/10.18502/keg.v3i4.2255.

Information Construction of MBD-based 3D Additive Manufacturing Process Model

Linlin Liu, Meng Li, Qiumin Wu, Jie Ma and Xiang Liu

School of Printing, Packaging Engineering and Digital Media Technology, Xi'an University of Technology, Xi'an 710048, China
E-mails: liulinlin1978@gmail.com; 849097977@QQ.com

Short abstract

Compared with the traditional processing molding, 3D printing (Additive Manufacturing) is a technology for the near-net shape of complex three-dimensional components and FDM (fused deposition modeling) is one of the widely used additive manufacturing technologies. The molding surface accuracy is affected by the process parameters of piece molding printing material characteristics and other factors, can't meets the demand of design. In order to reduce he decline in molding surface accuracy of pieces, buckling deformation and other phenomena due to the process parameters of piece molding, printing material characteristics and other factors, this paper establishing a process information model of FDM piece based on MBD, it uses a 3D solid feature model as a carrier and simultaneously achieves the correlation the surface molding quality requirements (surface roughness, flatness, roundness) of the design model, the traditional geometric model can be improved as the MBD model possessing the manufacturing process of products and provides the basis for the subsequent selection and optimization of FDM process pieces. The common components of the twin-cylinder engine with different planes and complex rotary surfaces in the engineering field are printed by the method and the surface molding quality is improved accordingly.

Keywords: FDM, MBD, process information model, molding surface accuracy

1. Introduction

Model-based Definition (MBD) is a technology that uses 3D models as a source of information and a single source of data throughout the product's life cycle. Because of its establishment of a unified definition of the three-dimensional model form, to achieve from the design to test the advantages of paperless, MBD technology at home and abroad for a wide range of studies. In MBD, the three-dimensional geometric model is used as the carrier to integrate the non-geometric information such as dimensions, tolerances, material properties and manufacturing requirements, which cover subsequent processing, assembly and testing, with the geometric model. The MBD technology integrates non-geometric information such as dimensions, tolerances, material properties and manufacturing requirements, which cover the subsequent processing, assembly and testing, with the geometric model based on the three-dimensional geometric model. In the absence of two-dimensional drawings of the situation, to achieve the description of product features, process data sharing, and process data in the information system, the soulution is shown by Zhongyi (2010), Guo and Mei (2011), and Zhang, et al. (2011).

Boeing engineer Clark Briggs (Briggs, et al., 2010) pointed out in his research that commonly used commercial CAD software has provided model-based environmental support for products. However, MBD is just beginning to be applied in the field of machining technology. They analyzed the role of MBD in the product's life cycle, and pointed out that the use of MBD can save the cost of human resources and reduce waste caused by improper design and manufacture of communication problems, companies need reusable, unified data in the form of three-dimensional model. Alemanni, Destefanis and Vezzetti (2011) proposed an MBD model approach to defining product quality functions and improved the data structure of MBD for different production needs.

Professor Yuqing Fan and his team (Zhou and Fan, 2008) after years of research to create consistent with China's aviation industry, presented three-dimensional digital product design and manufacture of a unified application system. The system includes three major MBD technical specifications of digital coordination, data organization and process design. Then the technology development of MBD is carried out to form a three-dimensional modeling system, a three-dimensional product manufacturing information system and a three-dimensional process simulation system, which are integrated with the application of MBD technology. Hao Lu (Lu, et al., 2008) took the production of 787 aircraft in China as an example and deeply studied the integration of 3D digital design and manufacture based on model definition. In the background of digital design and manufacture, it is an inevitable trend to use the MBD method to fully express the definition information of products.

With the continuous development of digital manufacturing, the status of digital process design in the manufacturing industry is continuously improving, and the advantages of information technology in actual production are becoming more and more obvious, especially the 3D CAD technology and additive manufacturing (3D printing) technology which have been more and more widely used in the actual production. The digital design and manufacturing technology based on model-based definition (MBD) has become the development trend of manufacturing informatization. How to make full use of 3D CAD technology to achieve 3D process coordination and manufacturing, improve product molding quality, promote the design and process at the same time, reduce manufacturing costs of products and the development cycle has become an urgent problem that needs to be resolved.

Therefore, through establishing a process information model of FDM piece based on MBD, it uses a 3D solid feature model as a carrier and simultaneously achieves the correlation between process model and design model, process geometry information and non-geometry information, assembly process and component process, and the process model and the process resources. It enables the process model information to be recognized by the existing 3D printing system, reduces the presence of data islands, making the required and generated data information the components during the process design closely related to solid feature model and providing the basis for the subsequent selection and optimization of FDM process pieces.

2. Digital information construction

At present, the 3D digital model only contains its geometric information, and it lacks the necessary non-macro geometric information, such as dimensional tolerance, form and location tolerance, surface roughness, etc., in the manufacturing process (Zhang, et al., 2013). Thus, establish an MBD-based expression method to mark the product design requirements such as geometric dimensions, form and location tolerance, etc. on the 3D model with the integrated 3D design model as the carrier, i.e. 3D annotations. In this way, the traditional geometric model can be improved as the MBD model possessing the manufacturing process of products.

The 3D annotation on the MBD model is required being remapped to the process model for additive manufacturing. Through the mapping of the model process information, we can perform the additive manufacturing of design model according to certain process requirements, and finally obtain the product that meets the molding requirements.

The establishment of the MBD-based process information model enables the geometric information and process information to be related to each other closely, to guide the subsequent 3D model forming and manufacturing. As shown in Figure 1, the MBD model mainly contains three parts: geometric model, 3D annotation and attributes. Each part is a constraint on the molding process and an effective way to ensure the molding quality.

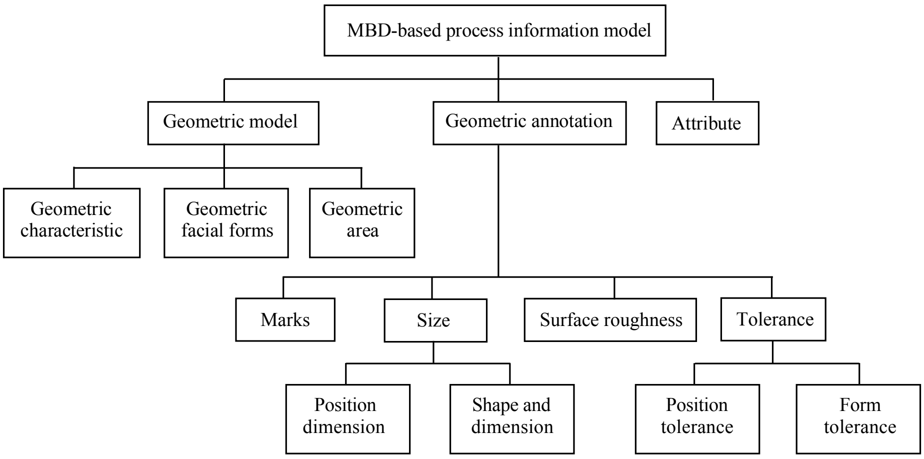

Figure 1: the MBD model contains

At present, STL is the most widely used standard file format in the additive manufacturing field. It only uses a series of unordered flat triangles to fit each other to represent the geometric information of the molded components (Chen, Quian and Ye, 2013). In this study, the 3D digitized information of components mainly contains geometric information and annotation requirements. The geometric information mainly describes the differences in the shape of the outer contours of components. The annotation requirements are to perform the design of components based on demand, so that the products with different quality of forming can be obtained. Therefore, a new additive manufacturing format 3MF (3D Manufacturing Format) is used to realize the mapping of process annotation information of the design model to a 3D process model for additive manufacturing.

3MF is a 3D data manufacturing format developed by the 3MF Alliance (software and hardware vendors such as Microsoft, Hewlett-Packard and Dassault Systemes) in May, 2015. The 3MF files aim to support interoperability and openness between design software and additive manufacturing hardware and better describe the product model. At present, 3MF files are only supported by Windows 8.1 and versions above, which lays a solid foundation (Li, et al., 2016). The 3MF file is a data format based on XML language, and it is also a new way of information transfer between design software and additive manufacturing hardware, and it has improved many functions of the traditional STL files. These functions include not only the geometric information of the product model, but also the non-geometric information such as the color definition, texture graphics, and material attributes that support the product model, which enables a full and standardized expression of the product model.

In the non-geometric information representation of the model, the 3MF file also has a great advantage over the STL file. It can define the color texture of each surface of the product model, and the color texture is consistent with the annotation information, both of which propose certain design requirements for the model surface. In this study, the transmission of additive manufacturing process model information is achieved only through the mapping of annotation information and color information. Meanwhile, the proposition to use the color description mode for representing surface finishing description and ignore color and surface properties simultaneously, because the properties is useless in manufacturing.

3. Mapping from design models to 3D process data

In this study, the surface molding quality requirements (surface roughness, flatness, roundness) of the design model are marked with RGB colorimetric values instead of directly marking the surface quality requirements in the traditional MBD. The traditional machining methods directly cut blanks according to the marked process requirements, while the additive manufacturing requires converting the design model with process requirements into 3D process data containing process information and transferring it to the 3D printing equipment for piece forming. Finally get the parts that meet the design requirements.

During the conversion of the process data, the surface roughness, flatness, and roundness of the model cannot be recorded by the subsequent 3D printing format. The RGB chromatic value has a certain commonality with these, and at the same time, it can make up for this defect. The RGB chromatic value can be used to establish the mapping relation respectively with the surface roughness, flatness, and roundness (as shown in Table 1), and the succession of model process information is achieved. First, the surface process requirements are marked on the model, and the corresponding RGB chromatic values are matched according to the mapping relationship. The unmarked surface is matched with the RGB chromatic values (255, 255, 255), and finally a 3D process model is generated for subsequent additive manufacturing.

Table 1: Mapping relation of model surface process requirements and RGB chromatic values

Accuracy class	**Roughness**		**Flatness**		**Roundness**	
Surface process requirements	Value R_a (μm)	Chromatic value R	Value (mm)	Chromatic value G	Value (μm)	Chromatic value B
Class 0	0~6.3	31	0~0.01	31	0~0.01	31
Class 1	6.3~25	63	0.01~0.02	63	0.01~0.03	63
Class 2	25~50	95	0.02~0.03	95	0.03~0.05	95
Class 3	50~100	127	0.03~0.05	127	0.05~0.1	127
Class 4	100~150	159	0.05~0.1	159	0.1~0.2	159
Class 5	150~250	191	0.1~0.2	191	0.2~0.3	191
Class 6	250~400	223	0.2~0.5	223	0.3~0.5	223
Class 7	≥400	255	≥0.5	255	≥0.5	255

In combination with the 3MF data format introduced above, a color definition is made on the surface of the design model, and different process requirements on each surface are mapped to different RGB chromatic values. Taking a regular dodecahedron as an example, first, the surface quality requirements are marked on the surface of No. 1, 2, and 3 of the design model, and the remaining surfaces are not marked (as shown in Figure 2); second, the RGB chromatic values which are corresponding to the surface quality requirements are obtained for each marked surface as shown in Figure 3 according to the mapping relation which is shown in Table 1; after the 3MF file discretizes the model, the colors of each surface are mapped to the color information of each corresponding triangular facet. Finally, the 3D process model is obtained as shown in Figure 4.

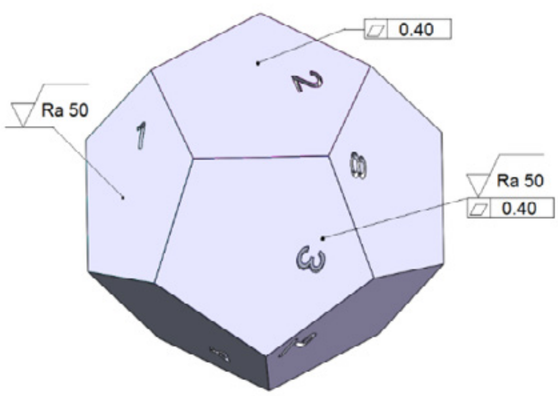

Figure 2: Regular dodecahedron MBD annotation model

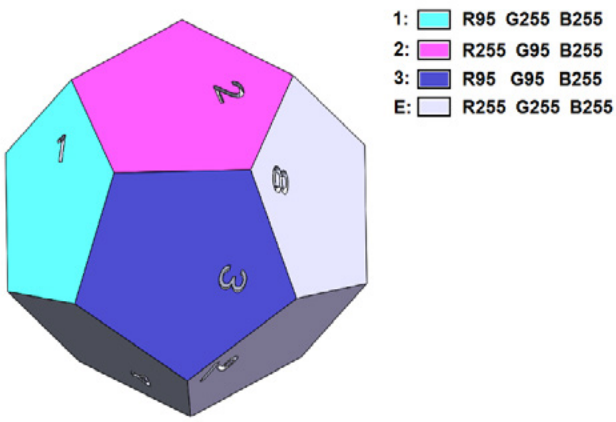

Figure 3: Matching of surface quality requirements and RGB chromatic values

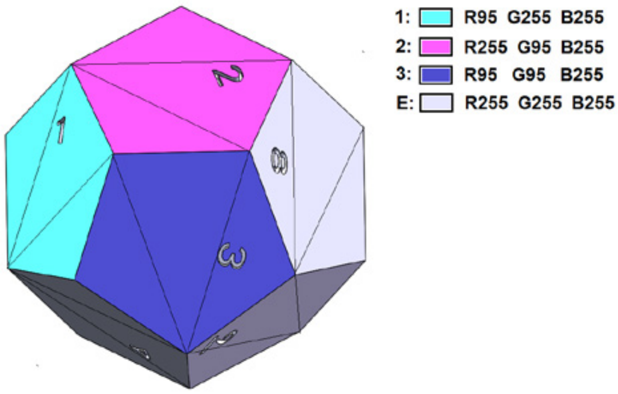

Figure 4: 3D process model

When requirements are proposed on the surface forming quality of a regular dodecahedron, 3D annotations are required on each surface of the model. Through the open source development of 3MF files, the external surface feature information of the design model is neglected. Through the mapping relation table above, the color definition of the design model surface is made in combination with the 3MF data format, and the different process requirements of each surface are mapped to different RGB chromatic values. Namely, the process requirements are mapped to the additive manufacturing 3D process model by marking the RGB chromatic values on the surface of the design model to achieve the transfer of annotation information between the upper design model and the process model so that the annotation information can be directly recognized by the molding equipment, providing the basis for the selection and optimization of the subsequent process. The partial data information of files is shown in Figure 5.

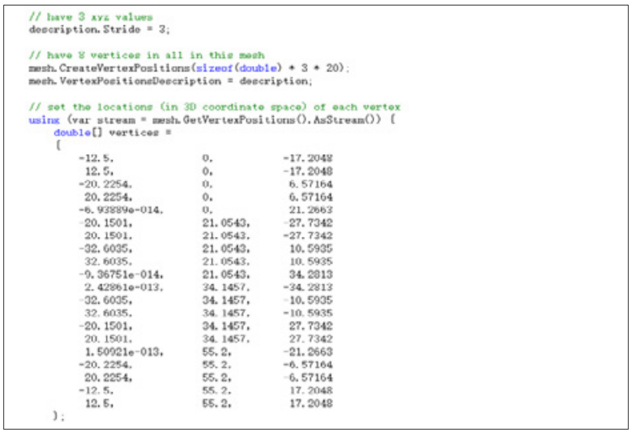

```
// have 3 xyz values
description.Stride = 3;

// have 8 vertices in all in this mesh
mesh.CreateVertexPositions(sizeof(double) * 3 * 20);
mesh.VertexPositionsDescription = description;

// set the locations (in 3D coordinate space) of each vertex
usinx (var stream = mesh.GetVertexPositions().AsStream()) {
    double[] vertices =
    {
        -12.5,            0.,         -17.2048
         12.5,            0.,         -17.2048
        -20.2254,         0.,          6.57164
         20.2254,         0.,          6.57164
        -6.93889e-014,    0.,          21.2663
        -20.1501,         21.0543,    -27.7342
         20.1501,         21.0543,    -27.7342
        -32.6035,         21.0543,     10.5935
         32.6035,         21.0543,     10.5935
        -9.36751e-014,    21.0543,     34.2813
         2.42861e-013,    34.1457,    -34.2813
        -32.6035,         34.1457,    -10.5935
         32.6035,         34.1457,    -10.5935
        -20.1501,         34.1457,     27.7342
         20.1501,         34.1457,     27.7342
         1.50921e-013,    55.2,       -21.2663
        -20.2254,         55.2,       -6.57164
         20.2254,         55.2,       -6.57164
        -12.5,            55.2,        17.2048
         12.5,            55.2,        17.2048
    };
```

Figure 5: Partial data information of files

4. Test

In order to meet the demand for the complex structure of the experimental object in this study, the common components of the twin-cylinder engine with different planes and complex rotary surfaces in the engineering field are used. Its structures and mapping process models are shown in Figure 6. The main equipment in the test is JG Aurora Z-603S printer for printing, and Keyence VHX-5000 super depth of field of the 3D microscopic system is used to accurately detect the surface of molding piece. The molding consumables are PLA material.

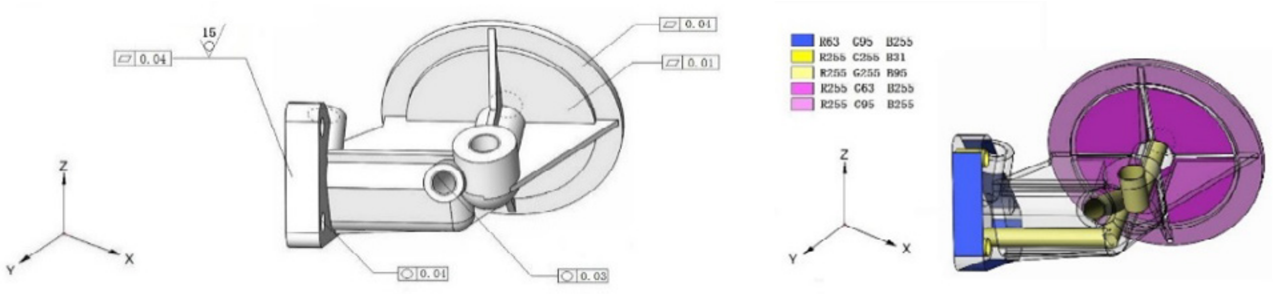

a) b)

Figure 6: Twin-cylinder engine parts; a) 3D design model of pieces, and b) process model of pieces

The pieces are printed with process parameters as shown in Scheme 1 and Scheme 2, and the number of experimental samples is 10, where Scheme 2 uses process model mapping and selects and optimizes process parameters (Tables 2 and 3):

Table 2: Scheme 1 of molding process parameters

Molding direction	Number of process layer	Thickness of layer	Width of extrusion line	Support density
$r_x = 0°$ $r_y = 0°$	1	0.1 mm	0.4 mm	$\rho_z = 0.1$

Table 3: Parameter measurement information of molding piece

Experiment Parameters / Molding Direction	Procees layer	Process requirements	Range of process layer (mm)	Thickness of layer (mm)	Width of extrusion line (mm)	Number of starting layer	Number of ending layer
$r_x = 0°$ $r_y = 90°$	G1	R63 G255 B255	0~10	0.10	0.4	0	100
	G2	R255 G255 B95	10~21.5	0.25	0.4	101	146
	G3	R255 G95 B255	21.5~29	0.15	0.4	147	196
	G4	R255 G63 B255	29~86	0.10	0.4	197	766
	G3	R255 G95 B255	86~93.5	0.15	0.4	767	823

The quality parameter measurement information is shown in Table 4.

Table 4: Parameter measurement information of molding piece

Design requirements / Process scheme	Average molding quality (R_a: *µm; r; f*: mm)					Average molding time (min)	Average molding consumables (g)
	A	B	C	D	E		
Scheme 1	$R_a = 128.50$ $f = 0.188$	$r = 0.34$	$r = 0.39$	Lack of molding surface	$f = 0.684$	217	62
Scheme 2	$R_a = 23.77$ $f = 0.029$	$r = 0.03$	$r = 0.04$	$f = 0.038$	$f = 0.027$	174	51

The accuracy class of molding is as shown in Table 5.

Table 5: Comparison of accuracy class of molding in each process schemes

Detected area / **Process scheme**		**Accuracy class**				
		A	**B**	**C**	**D**	**E**
Scheme 1	R_a	Class 4				
	f	Class 5			Lack of molding surface	Class 7
	r		Class 6	Class 6		
Scheme 2	R_a	Class 1				
	f	Class 2			Class 3	Class 2
	r		Class 2	Class 2		

The super depth of field of the 3D microscopic system was used to measure the surface quality of the molding pieces. The measurement results are shown in Figure 7.

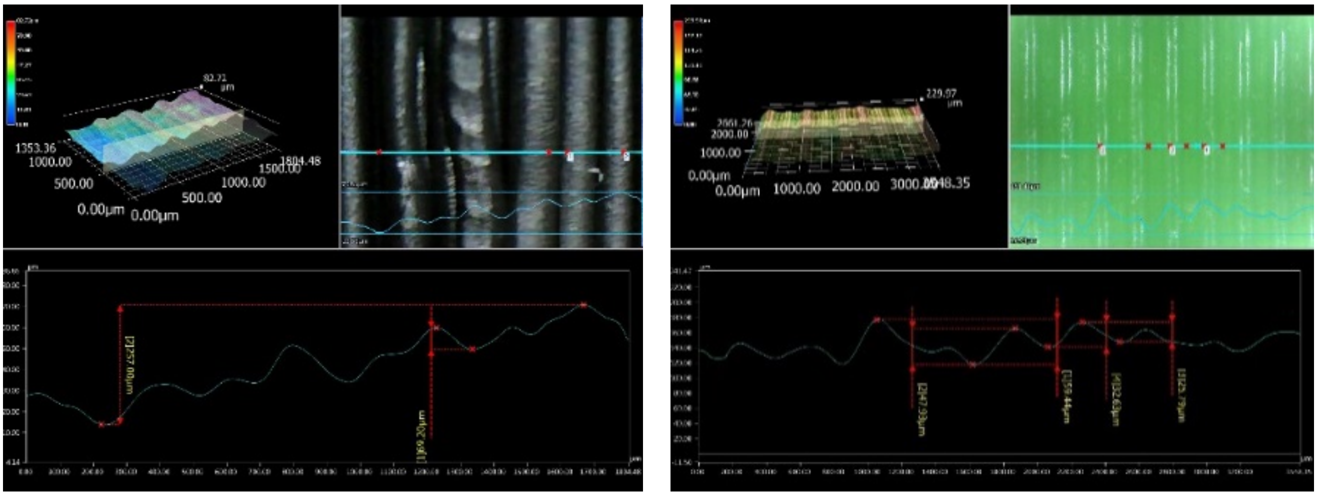

a) *b)*

Figure 7: Measurement chart of molding surface by super depth of field,
a) measurement chart of molding surface in Scheme 1, and b) measurement chart of molding surface in Scheme 2

In the Scheme 1, the surface forming quality of the piece is poor, and the mapping relationship between the process requirements and the color information in Table 1 can be used to compare the accuracy class of the various process schemes. The corresponding detected areas do not meet the design requirements. At the same time, the molding time is long and more consumables are used in Scheme 1. Compared with the accuracy class of the detected area of pieces in Scheme 2, the surface molding quality is matched with the accuracy class which proposes the process requirements during designing, and for the molding time and consumables used, the molding time is shortened by nearly 25 %, and the consumables are saved by nearly 22 % compared with the Scheme 1. Although the measurement results of Scheme 2 meet the design requirements, there are still some errors. These errors are mainly due to the accuracy of data fitting, molding accuracy of equipment, environmental temperature and humidity, material properties and other factors. The in-depth studies can be conducted later from relevant factors to further reduce errors.

Experiments have proved that the FDM piece surface forming quality optimization method used in this study can meet the user's design requirements. At the same time, after the optimization of molding direction and grading of process layer, less molding time and consumables of components are needed, which further improves work efficiency and saves processing costs.

5. Conclusion

This paper combines MBD marking information with additive manufacturing, proposes a set of color marking-based process information model for additive manufacturing field, through establishing a process information model of FDM piece based on MBD, uses a 3D solid feature model as a carrier with the help of 3 MF files, and simultaneously achieves the correlation between the process model and the design model, the process geometry information and the non-geometry information, the assembly process and the component process, the process model and the process resources, which makes the required and generated data information of the components during the process design closely related to solid feature model, provides the basis for the subsequent selection and optimization of FDM process pieces, reduces the decline in molding surface accuracy of pieces, buckling deformation and other phenomena due to the process parameters of piece molding, printing material characteristics and other factors, meets the demand of design and promotes the further development of FDM piece function applications.

Acknowledgments

The author gratefully acknowledges the support of the Key Laboratory Science Foundation of Department of Education of Shaanxi Province (16JS083), and Scientific Research Project of Key Laboratories of National Press and Publication Administration (ZBK201811), Scientific Research Project of Shaanxi Provincial Government (2018GY-162), Science Research Project (Natural Science Project) of Department Education of Shaanxi Provincial Government (2018JM5119),Scientific Research Project of Xi'an City (2018JM5119), Scientific Research Project of Xi'an City (2017080CG/RC043(XALG006).

References

Alemanni, M., Destefanis, F. and Vezzetti, E., 2011. Model-based definition design in the product lifecycle management scenario. *The International Journal of Advanced Manufacturing Technology*, 52(1-4), pp. 1–14.

Briggs, C., Brown, G., Siebenaler, D., Faoro, J. and Rowe, S., 2010. Model Based Definition. In: *51st AIAA/ASME/ASCE/AHS/ASC Structures, Structural Dynamics, and Materials Conference*. Orlando, Florida, 12–15 April 2010, article no. 3138.

Chen, Z.Y., Qian, J. and Ye, X., 2003. Solid modeling of STL data in reverse engineering (in Chinese). *China Mechanical Engineering*, 14(20), pp. 1760–1763.

Guo, J.T. and Mei, Z.Y., 2011, Design and application of aircraft digital assembly process (in Chinese). *Aeronautical Manufacturing Technology*, 22, pp. 74–77.

Li, Y., Yu Shang, Y., Yuan, Y., Chen, J., Li, D., Wang, Y. Liu, C. and Dou. Y., 2016. File format of 3D printing technology (in Chinese). *Journal of Beijing University of Technology*, 42(7), pp. 1009–1016.

Lu, H., Han, S. and Fan., Y.Q., 2008. Model-based digital definition technology (in Chinese). *Aviation Manufacturing Technology*, 3, pp. 78–81.

Zhang, Z., Tian, X., Huang, L. and Xin, Y., 2013. Research on 3D visualization and generation technology of machining process. *Manufacturing Automation*, 35(4), pp. 26–30.

Zhang, R.X., Zhang, S.S., Zhou, J.T., et al, 2011. Management Model of Parts Manufacturing Based on MBD (in Chinese). *Manufacturing Automation*, 33(8), pp. 6–9.

Zhongyi, M., 2010. The technology of aircraft digital assembly based on MBD (in Chinese). *Aeronautical Manufacturing Technology*, 18, pp. 42–45.

Zhou, Q. and Fan, T., 2008, Application of MBD on airplane manufacturing (in Chinese). *Aviation Maintenance & Engineering*, 10(3), pp. 55–57.

Industry 4.0: what does it mean for the graphic arts industry?

Anastasios E. Politis

HELGRAMED – The Hellenic Union of Graphic Arts and Media Technology Engineers
E-mail: politismedia@gmail.com

Short abstract

Industry 4.0 is described as the 4th industrial revolution. Industrial revolution is an old term, used principally to classify the various steps of evolution in industrial operations and processes. The concept of Industry 4.0 appears as a global trend regarding the evolution in industrial manufacturing and there is a need for various industries and manufacturing sectors to take under consideration the evolution that this concept brings. Within this context, the present research is aiming in addressing various issues arising that are listed below:

- Main elements of Industry 4.0.
- The relationship of Industry 4.0 with other strategic concepts such as Lean manufacturing.
- Suitability for SMEs, something that is of high importance for the graphic arts, printing and packaging sectors.
- Procedures to be followed for a smooth application of specific industry 4.0 elements
- Application of Industry 4.0 concept/trend in the printing, finishing, paper and packaging sectors of the graphic arts.

Based on the research conducted, the following conclusions can be illustrated:
Industry 4.0 appears as an interesting global trend regarding the evolution in industrial manufacturing in the years to come. Since it has various definitions, interpretations, and elements, there is a necessity for specific definition of the general concept into certain sectors.
In addition, as it concerns the graphic/media, printing and packaging industries, the generic Industry 4.0 trend is applied with the combination of certain elements that fit better to the nature of processes and operations in the industry. A clear message from the investigation in the graphic/media sector is that not all Industry 4.0 elements are applicable at all sectors.
Finally, further study is required for the progress of Industry 4.0 application into SMEs.

Keywords: Industry 4.0, Industrial Revolution, Lean Manufacturing, Printing 4.0, Finishing 4.0, Paper 4.0

1. Introduction and background

Industry 4.0 is described as the 4th industrial revolution. Industrial revolution is an old term, used principally to classify the various steps of evolution in industrial operations and processes. However, the concept of Industry 4.0 appears as a global trend regarding the evolution in industrial manufacturing in the years to come.

As such, it seems as a necessity for all industrial and manufacturing sectors to take under consideration the evolution that this concept brings.

Hence, the term consists of several elements, which need to be carefully addressed and analyzed. This analysis should lead to the determination of potential benefits for manufacturing operations and processes in various sectors.

Within this context, the present research is aiming in addressing various issues arising that are listed below:

- Definitions and elements that need to be considered for application within Industry 4.0.
- The relationship of Industry 4.0 with other strategic concepts such as Lean Manufacturing (LM).
- Suitability for SMEs, something that is of high importance for the graphic arts, printing and packaging sectors.
- Procedures to be followed for a smooth application of specific industry 4.0 elements
- Application of Industry 4.0 concept/trend in the printing, finishing, paper and packaging sectors of the graphic arts.

1.1 Objectives of the study

Initial research conducted reveals that there is a variety of definitions, elements and descriptions on Industry 4.0. Therefore, the present study is aiming in clarifying the basic terms and definitions of Industry 4.0 and to present the main elements of this trend. Further, the relationship with other concepts such as the Lean Manufacturing and the suitability for SMEs need to be addressed. Hence, the most significant analysis refers to the current interpretation of this generic concept into the graphic arts-printing sector.

2. Methodology

For the present study mostly internet sources have been searched. Browsing terms such as "Industry 4.0" return hundreds of millions of webpages. Therefore, the effort has been focused to find the most appropriate resources as well as those with a scientific background. This was not an easy task, since there was a difficulty to find reliable sources by combining Industry 4.0 science and research with graphic arts-printing industry. This search has mostly led to 3D printing.

For the time being, it seems that not many scientific research has been conducted for the application of Industry 4.0 in the graphic arts sector. Main initiatives are originating from manufacturers such as Heidelberg, Horizon and Müller-Martini.

3. Definitions and elements for Industry 4.0

3.1 Definitions

The original definition of Industry 4.0 comes from Smart industry or "INDUSTRIE 4.0", as it has been defined by the German Trade and Invest agency (MacDougall, 2014). It refers to the technological evolution from embedded systems to cyber-physical systems. The term Industry 4.0 has been coined at the 2011 Hannover Fair, a concept better known as the "Smart Factory". The 4.0 makes reference to be a forth industrial revolution to come (Rüttimann, 2015). Put simply, INDUSTRIE 4.0 represents the coming fourth industrial revolution on the way to an Internet of Things, Data and Services. Decentralized intelligence helps create intelligent object networking and independent process management, with the interaction of the real and virtual worlds representing a crucial new aspect of the manufacturing and production process.

As such, INDUSTRIE 4.0 represents a paradigm shift from "centralized" to "decentralized" production – made possible by technological advances, which constitute a reversal of conventional production process logic. Simply put, this means that industrial production machinery no longer simply "processes" the product, but that the product communicates with the machinery to tell it exactly what to do. INDUSTRIE 4.0 connects embedded system production technologies and smart production processes to pave the way to a new technological age which will radically transform industry and production value chains and business models (e.g. "smart factory") (MacDougall, 2014).

The definition of Industrie 4.0 as proposed in 2011 was pretty lengthy. In a paper, entitled "Industrie 4.0 – Smart Manufacturing for the Future", GTAI (Germany Trade and Invest) looked at the questions what is smart industry (a synonym of Industry 4.0) and what Industrie 4.0 means (i-scoop, 2016).

In Figure 1 the four industrial revolutions are illustrated:

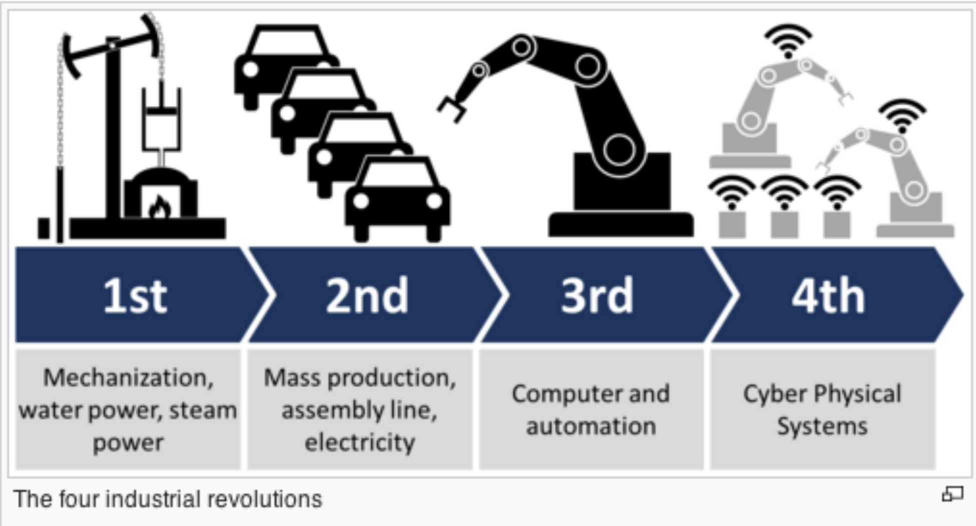

Figure 1: The four Industrial revolutions (Cheydleur, 2017)

Despite the vision aspect, 'Industry 4.0', is a very real phenomenon, transforming manufacturing and other sectors into connected and digital manufacturing (and more) with additional benefits and a range of technological evolutions and possibilities to move beyond the sheer operation dimension towards the so-called fourth industrial revolution.

3.2 Elements of Industry 4.0

Ostdick (2017) proposes 5 key elements of Industry 4.0 to better understand its place and overall value proposition in a global manufacturing stream: Greater levels of product customization, Integration of Advanced Analytics, Pushing beyond postmodern ERP, Embracing the Internet of Things, Increased reliance (and positive outcomes) on cloud technology.

Drexler (2016), suggests that new technologies, spanning mobile computing to cloud computing, have undergone vast development in the last decade and are now ready to be used as commercially available, interconnected systems within manufacturing – this is Industry 4.0. It holds the key to accessing real-time results and data that will catapult the industry into new levels of lean achievements.

Drexler continues by stating that the concept of Industry 4.0 however, is not a simple one. It envelops many pieces and is used in a variety of different contexts. There are five core pieces that define what Industry 4.0 is at its core. Each piece is similar in nature but, when integrated together, create capability that has never before been possible. In an effort to understand Industry 4.0, the following five terms are explained as they contribute to the next industrial revolution: Big Data, Smart Factory, Cyber Physical Systems-CPS, Internet of Things (IoT), Interoperability (Drexler, 2016).

However, as it is stated at an official EU document study (Smit, et al., 2016), there are certain preconditions for Industry 4.0. The presence of these preconditions, and the ability to create such preconditions where they do not exist, vary between Member States. The chart in Figure 2 presents a ranking of challenges identified based on a survey carried out in 2013:

Figure 2: Preconditions for implementation of Industry 4.0 (Smit, et al., 2016)

Further, Rüttimann and Stöckli (2016) argue that "Industry 4.0" is a fuzzy term and that the topic is poorly understood. The following are usually understood by the catchword "Industry 4.0 (without commenting the correctness): New products and new services, new business models, internet of things (IOT), big data, self-scheduled maintenance, virtual reality/augmented reality and fully automated production.

4. Industry 4.0 and Lean Manufacturing

Lean manufacturing appears in many searches related with Industry 4.0. According to Rüttimann and Stöckli, Lean Manufacturing (LM) is in reality a comprehensive manufacturing theory, which can even be modeled mathematically. Lean is also a manufacturing philosophy of continuous improvement (called Kaizen, which is performed in self-directed teams, i.e. on the shop floor level, to strive to the learning organization Industry 4.0 tries to integrate every available shop floor information via IT already with the incoming orders in the supply chain management. The strong IT-focus might be one of the origins leading to the presumed inferiority of Lean compared to the Industry 4.0 initiative (Rüttimann and Stöckli, 2016).

Netland (2015) states that "Lean will not fade with Industry 4.0. Quite the opposite, lean principles are likely to become more important. The fourth industrial revolution can enable the true lean enterprise. Industry 4.0 permits a much richer understanding of the customer demand and allows the immediate sharing of the demand data throughout complex supply chains and networks. Smart factories can produce faster with less waste. Industry 4.0 enables a much quicker one-piece flow of customized products and it has the potential to radically reduce inventories throughout the supply chain".

Netland, concludes by stating that "Industry 4.0 technologies may be exactly what we need in order to create lean supply chains and networks. Lean is about doing more with less—today and in the future" (Netland, 2015).

In accordance with the previous statement, Mrugalska and Wyrwicka (2017) conclude that "the review of literature about lean production and Industry 4.0 provided for smart product, machine and augmented operator in reference to lean production principles, indicated that these two approaches can support each other".

5. Industry 4.0 and SMEs

According to Schroeder, it can be foreseen that dynamic technological developments will give rise to substantial advances in productivity for many SMEs too. In order to realize them, small and medium-sized enterprises require flexible organisational structures because business areas that at present are clearly separated from one another are increasingly becoming interconnected. The managements of small and medium-sized enterprises must therefore try to find out how much smarter their product range can be made by Cyber Physical Systems and which new business models might emerge from that. (Schroeder, 2017).

However, according to a statement by Dr. Georg Schuettle (Bundesministerium fuer Bildung und Forschung, cited in Rüttimann, 2015), "the belief that small and medium enterprises -SMEs will benefit from Industry 4.0, is just a wishful thinking". This argument is stated for two reasons:

Firstly, due to the necessary high investment needed and the increase of the related operational break-even point (BEP) and secondly, the increased production flexibility will allow big companies to deal with smaller customized demands now usually met by SMEs. The interest of German industry for the Industry 4.0 initiative is huge due to the fact, that the government released 250 million funds to explore the potential; again, key partners of the 4.0 initiative, are not SMEs but big multi-national enterprises (Rüttimann, 2015).

6. Industry 4.0 and the graphic arts industry

Vendors, organizations and scientists from the graphic arts and media – printing sectors could not stay out of the debate for manufacturing evolution caused by the Industry 4.0 trend. Numerous manufacturers are taking position within Industry 4.0. As such Industry 4.0 is classified / translated as Print 4.0, Finishing 4.0, Packaging 4.0 and Paper 4.0 (Politis, 2017).

Niemela (2016) argues that "Printing 4.0 megatrend applies for all graphic arts / graphic communication fields, namely Design, Prepress, Print and Finishing, at an integrated and connected workflow based on full digitalization". According to Niemela, this means the integration of Computer Integrated Manufacturing, Networked production steps, Low stock levels, Just in time delivery, Innovative workflow structures and Maximum flexibility.

Further, a warning is stated by Richard Romano (WhatTheyThink, 2018): He states that "We may scoff at the idea of the 'Internet of Things'-if we are aware of it at all-but it will have many impacts on not only the market for print, but the nature of print itself," According to Romano, "Industry technology trends of specialty printing, textile printing, and industrial printing are still heating up, we do need to be aware of what is happening with technology in general and how they affect print demand. Many print businesses dismissed the importance of the Internet in the 1990s, and of mobile in the 2000s. We shouldn't make that mistake again" (WhatTheyThink, 2018).

Müller Martini, presents Finishing 4.0 which includes the following elements: Touchless Workflow, Uninterrupted print finishing, Touchless manufacture of print products in a single pass, Combination of high degree of automation with seamless connectivity, Modification of product parameters during the job run without interrupting production and Dynamic job change function.

Müller Martini's Finishing 4.0 philosophy shows that it is possible to produce customized and variable print products cost-effectively and efficiently using means of mass production. In other words, it is possible to produce customized books, brochures and magazines with high added value at low prices per copy and stay competitive. The time is not only ripe to talk about connectivity and workflows in the graphic arts industry but also to offer specific solutions (Müller Martini, 2016).

Plenz (2015), stresses the "digitized world" as the key element of Heidelberg's Smart Print Shop. He argues further that Smart Print shop is ready for Industry 4.0 with Prinect. Further, Heidelberg USA argues that "Industry 4.0 is a transformation that's sweeping every sector of manufacturing, and Heidelberg has solutions that can put its customers in the forefront of driving this transformation in printing. In this kind of print manufacturing, the essential raw material isn't paper or ink. It's data—data that connects machines to machines, machines to plant environments, plant environments to management systems, and management systems to customers. Each step of the process generates data, and all of it is captured and analyzed with one objective in mind: to make the entire manufacturing sequence as efficient and as profitable as it can be (Heidelberg USA, 2016)

In addition, as it is stated in a brochure from Horizon, "In Printing 4.0, processes happen in holistic and borderless environment. The direct connection of the service provider with its customers offers sustainable potential (Druckerei 4.0, 2015). As Druckerei 4.0, it is understood the step towards fully automated production through the mechanical and electronic networking of printing and finishing systems as well as increased transparency of the entire production environment. (Druckerei 4.0, 2015).

In a brochure from CEPI - the Confederation of European Paper Industries, the paper industry contributes in the Industry 4.0 discussion by stating that "Digital" is the major evolution for the paper industry. Industry 4.0 is a digital manufacturing revolution, leveraging the huge unrealised value potential available from the digitalisation of industrial processes, products, and services. Digitalisation is the main driver of the next industrial revolution. Everything that can be digitalised will be digitalised. The complete process of papermaking will be revolutionized, from forests to end consumers (Pantsar, Schey and Mensink, 2015).

Finally, according to X-Rite blog, Industry 4.0 means smarter print processes. With so much of the print industry transitioning to digital print processes, there's plenty of opportunity to work smarter. For example, smart front ends can grab jobs and related specifications from the cloud, incorporate variable data and adjust specifications based on job criteria like substrates and printing technology, then calibrate and color manage with embedded and near-line measurement systems. The results can then be validated to ensure they meet print specifier and/or brand owner expectations (Cheydleur, 2017).

7. Conclusions

Based on the research conducted, the following conclusions can be illustrated:

Industry 4.0 has been defined as "a name for the current trend of automation and data exchange in manufacturing technologies. It includes cyber-physical systems, the Internet of things, cloud computing and cognitive computing. Industry 4.0 creates what has been called a smart factory". Industry 4.0 appears as an interesting global trend regarding the evolution in industrial manufacturing in the years to come. Since it has various definitions, interpretations, and elements, there is a necessity for specific definition of the general concept into certain sectors.

There is a strong relation of Industry 4.0 with Lean Manufacturing. The relation lies with the share of common structures and elements for manufacturing and production operations and processes. However, there are opinions stating that manufacturing organizations are advised to implement the Lean transformation to their companies now instead of waiting for the promised land of Industry 4.0.

The integration of Industry 4.0 in SMEs, seem not to be a realistic option, since elements of Industry 4.0 are applied currently in Big enterprises such as the automotive Industry. This is supported also by the fact that Industry 4.0 concept is currently an issue for printing and graphic arts manufacturers, whereas Lean Manufacturing is applied as an operational philosophy at printing companies.

As it concerns the graphic/media, printing and packaging industries, the generic Industry 4.0 trend is applied with the combination of certain elements that fit better to the nature of processes and operations in the industry. A clear message from the investigation in the graphic/media sector is that not all Industry 4.0 elements are applicable at all sectors. The investigation for the graphic arts and related industries (printing, packaging, paper and finishing) show that generic elements of Industry 4.0 are adapted into specific applications in a more concrete manner at the level of manufacturers of graphic arts equipment and systems.

References

Cheydleur, R., 2017. *Commercial printers and industry 4.0*. [online] Available at: <https://www.xrite.com/blog/industry-4-0-commercial-printers> [Accessed November 2017].

Drexler, S., 2016. *The 5 factors of Industry 4.0: on digitizing industry and infrastructure, Industrial IoT/ Industrie 4.0 Viewpoints*. [online] Available at: <https://industrial-iot.com/2016/08/5-factors-industry-4-0/> [Accessed November 2017].

Druckerei 4.0, 2015. *Druckerei 4.0: bereit f*ür *die Revolution?*. HORIZON Druckverarbeitung. [pdf] Available at: <https://www.horizon.de/fileadmin/user_upload/horizon.de/Dateien/Pdf/Horizon_nachdruck_2015-2.pdf> [Accessed November 2017].

Heidelberg USA, 2016. Industry 4.0: the new age of prosperity for printing. [online] Available at: <https://news.heidelbergusa.com/2016/08/industry4-0/> [Accessed November 2017].

i-scoop, 2016. *Industry 4.0: the fourth industrial revolution – guide to Industrie 4.0*. [online] Available at: <https://www.i-scoop.eu/industry-4-0/> [Accessed November 2017].

MacDougall, W., 2014. *Industrie 4.0: smart manufacturing for the future*. Germany Trade and Invest. [pdf] Available at: <http://www.gtai.de/GTAI/Content/EN/Invest/_SharedDocs/Downloads/GTAI/Brochures/Industries/industrie4.0-smart-manufacturing-for-the-future-en.pdf?v=8 [Accessed November 2017].

Mrugalska, B. and Wyrwicka, M.K., 2017. Towards lean production in Industry 4.0. *Procedia Engineering*, 182, pp. 466–473.

Müller Martini, 2017. Finishing 4.0. [online] Available at: <https://www.mullermartini.com/en/gbr/company/finishing-4-0/> [Accessed November 2017].

Netland, T., 2015. Industry *4.0: what about lean?* [online] Available at: <http://better-operations.com/> [Accessed November 2017].

Niemela, B., 2016. Der Druck startet durch und wird internationaler. *Deutscher Drucker*, Nr. 13., 30. 6. 2016.

Ostdick, N., 2017. *5 Key Elements of Industry 4.0*. [online] Available at: <https://blog.flexis.com/5-key-elements-of-industry-4.0> [Accessed November 2017].

Pantsar, M., Schey, V. and Mensink, M., 2015. *Paper industry 4.0: what digital can do for the paper industry*. SITRA, StepChange and CEPI. [pdf] Available at: <http://www.cepi.org/system/files/public/documents/publications/innovation/2015/LOW_Industry%204.0_170x235mm_20151109.pdf> [Accessed November 2017].

Plenz, S., 2015. Future of Print Media Industry – Smart Print Shop. In: *Heidelberg Year-End Press Conference*. Wiesloch-Walldorf, 2 December 2015.

Politis, E.A., 2017. The Graphic-Media Communication Science - Fields, Trends and the Contribution of Research Organizations. In: *Evolution Innovation in Graphic-Media Science: Research, Industry Innovation and the Role of Education*. Athens, Greece 22 March 2017. Hellenic Union of Graphic Arts and Media Technology Engineers.

Rüttimann, B., 2015. Von Lean zu Industrie 4.0—Eine Evolution? Von einer visionären Idee zum realen Verständnis. In: *Fertigungstechnisches Kolloquium*. ETH Zürich, 26 November 2015.

Rüttimann, B.G. and Stöckli, M.T., 2016. Lean and Industry 4.0—twins, partners, or contenders? A due clarification regarding the supposed clash of two production systems. *Journal of Service Science and Management*, 9(6). article id. 72522.

Schroeder, C., 2017. *The challenges of Industry 4.0 for small and medium-sized enterprises: a good society – social democracy, a project by the Friedrich-Ebert-Stiftung 2015–2017*. [pdf] Available at: <http://library.fes.de/pdf-files/wiso/12683.pdf> [Accessed November 2017].

Smit, J., Kreutzer, S., Moeller, C. and Carlberg, M., 2016. *Industry 4.0: study for the ITRE Committee*. European Union. [pdf] Available at: <http://www.europarl.europa.eu/studies> [Accessed November 2017].

WhatTheyThink, 2018. *Printing Forecast 2018*. [online] Available at: <https://store.whattheythink.com/downloads/printing-forecast-2018/> [Accessed November 2017].

The modification of a curtain coating Formulation and its effect on Pitting

Samantha L. Schoenfelder, Alexandra Pekarovicova and Paul D. Fleming

Center for Printing and Coating Research, Western Michigan University, 4601 Campus Drive, A-217 Floyd Hall,
Kalamazoo, MI 49008
Email: a.pekarovicova@wmich.edu

Short abstract

An undisclosed recycled fiber mill installed a "two-slotted" curtain coater to replace an air knife coater, which enabled a high-quality coating without their past speed limitations. With the curtain coater's installation, however, a prominent defect arose, known as "pitting". Pitting occurs when the coating of the sheet has small holes that mar its surface, which, when clustered together or larger in size, can cause print break-up. Starch was added to the formulation to promote rheological healing properties, and advance water retention capabilities of the coating. Results showed that the starch promoted elastic and viscous properties of the coating, and increased water retention capabilities. The pitting significantly decreased during these trials, with lower overall pit counts and area pitted, but stayed generally similar in the number of pits; thus, the starch helped to decrease the size of the pits.

Keywords: curtain coating, coating formulation, pitting, air entrapment, rheology

1. Introduction and background

The utilization of recycled paperboard within the packaging industry creates a competitive need to continuously improve production by finding advancements to create a superior product in a time and cost-effective manner. These engineering capabilities assist in manipulating production while maintaining quality and trialing new applications to promote the highest optimization for the paper machine. Changes can be made at all parts of the process, from source of fiber to the coating, to actual machinery installations as new modifications are developed. It is an ever changing, developing industry, which does not have the option for complacency.

Air entrainment has been cited as the leading cause of pitting (Figure 1) in theoretical and experimental capacities, occurring between substrate and impinging coating, because of interfacial tension constraints (Urscheler, et al., 2005). The air film is unstable and breaks into bubbles, creating visible defects (pits/craters) that are usually related to the curtain's base coat that is in contact with the substrate (Urscheler, et al., 2005). Most curtain coaters have a vacuum device installed near the impingement zone, which acts as a deaerator, but these do not have the capacity to remove all the boundary air that can cause entrainment and lead to pitting. Therefore, as web speeds increase, the removal of boundary layer air becomes progressively more difficult by the vacuum and manifests itself as the onset of air-entrapment in the impingement zone (Tripathi, 2005; Tripathi, et al., 2009). For very high web speeds, steam substitution (Tripathi, 2005; Tripathi, et al., 2009), where saturated steam is injected before the impingement zone to remove boundary layer air, is needed. Furthermore, roughness of a substrate and poor wettability may lead to a higher amount of air entrainment. Without a direct metering device, the substrate does not require special strength properties for good runnability (Schweizer, 2003), but a curtain will follow the contour of low/high amplitude roughness. With a high frequency of varying roughness, the coating film becomes more complex and sometimes incapable of keeping its form, where high base sheet roughness may create craters (Figure 2) (Tripathi, 2005). Air entrainment is also synonymous with dynamic wetting failure, with critical parameters being speed and viscosity, but also found to be dependent on surface tension (Marston, et al., 2009). In order to fully understand wetting, one must look at viscosity and surface tension as tools to combat the effects of high speeds and lower the possibility of air entrapment.

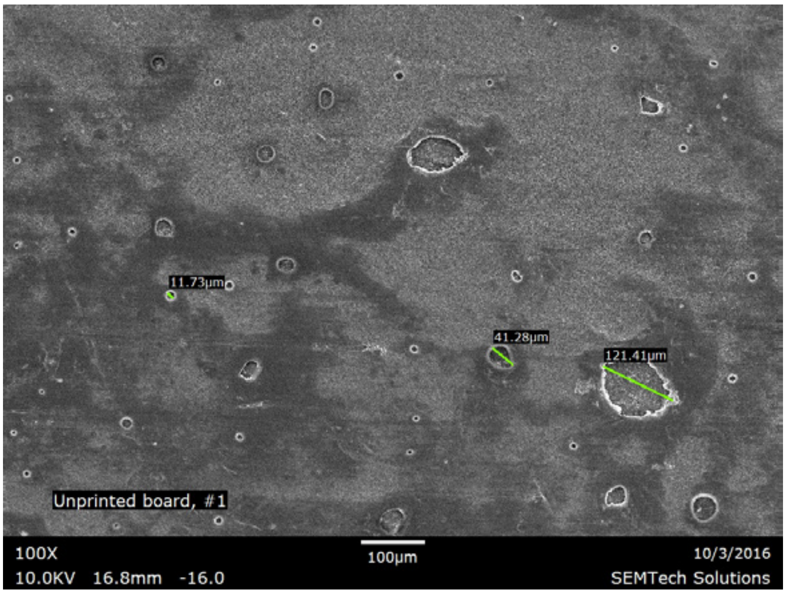

Figure 1: SEM of pitted surface of coated board

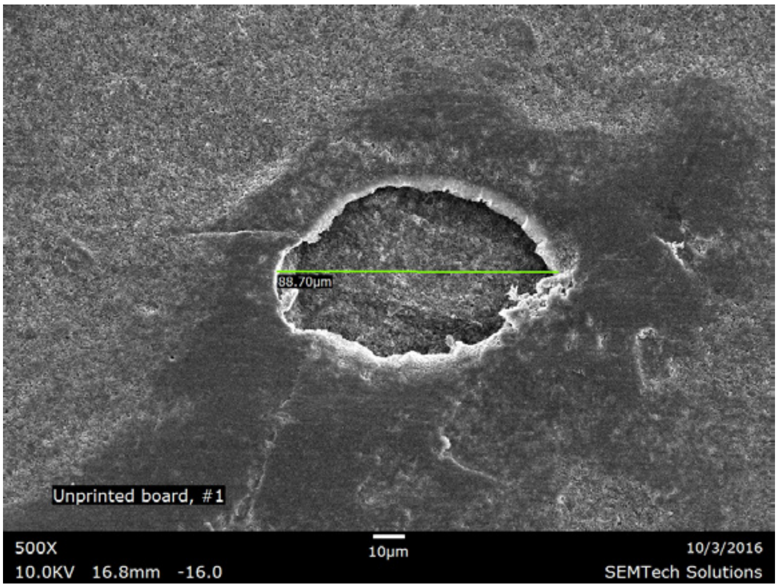

Figure 2: SEM of large pit on curtain coated board

Curtain coating suspensions are known to be pseudoplastic, which means that they are shear-thinning, or their viscosities decrease as the shear rate increases. Rheology can also help determine the coating's ability to "heal" itself through its viscoelasticity, defined by a fluid's ability to quickly return to its original state after strain is removed. It has been suggested that rheological properties of the coating are critical to avoid or reduce the presence of pitting, because they influence how easily air bubbles can be extracted from the coating color (Tripathi, 2005; Triantafillopoulous, et al., 2004; Kistler, 1983). Thus, in order to deter air entrainment, the promotion of wetting through rheological properties is critical at impingement as it affects the process in multiple ways. As the liquid coating displaces gas at a dynamic wetting line (when the coating meets the web), it will create a continuous film of coating that is deposited on the moving substrate (Kistler, 1983). Close to the respective wetting lines, there are comparatively short regions of rapidly rearranging shear and extensional flow, which is even more complicated with non-Newtonian fluid-like coating (Kistler, 1983). Low coating viscosity can cause a splash to occur at the web, while extensional viscosity is the key to preventing heel forming (Tripathi, 2005; Chen, et al, 2016), both highly affecting the amount of air that will be dragged under the film. Thus, rheological properties of the coating are critical to avoid or reduce the presence of pitting, because they influence how easily air bubbles can be extracted from the coating color (Tripathi, 2005). As previously stated, the air entrainment will then form bubbles, which lead to pitting. Curtain stability cannot only be improved with a thicker curtain, greater curtain velocity, and higher volumetric flow rate per unit width, but also with a lower coating surface tension (Brown, 1961). Thus, surface tension is an important component of a coating, particularly at slow speed. It was also found through experimentation that the air entrainment phenomenon is strongly dependent on surface tension, a fact already well established for various other coating methods (Marston, et al., 2009; Klass, 2004). Lowering surface tension can result in higher viscous drag on the curtain, increasing the radius of curvature of the pulled film over the impingement zone, and reducing total pressure, resulting in delayed and reduced air entrainment (Tripathi, et al., 2009). Without proper wettability, air entrainment is promoted between the coating and the substrate, and the coating will literally not adhere to the substrate (Joyce, 2015; Chen, 1992; BASF, 2016).

The aim of this work is to focus on a coating (and board) related defect known as, "pitting" or "pinholes," which causes an abnormal surface of the board that will not print smoothly. This issue is occurring at a recycled board plant, which has been troubleshooting it since their air knife coater was replaced by a curtain coater. In this work, coating formulations were altered to fight pitting.

2. Materials and methods

2.1 Procedures

Experiments were done on a Fourdrinier paper machine, using 100 % recycled fiber material to produce a three-ply paperboard, running at 1 500–2 000 fpm (~460–610 m/min). The three plies consisted of a top liner, filler, and back liner, with caliper of 18 pt. (18 mills or 0.457 mm). The original curtain coater formulation for the top and base coatings can be found in the Tables 1 and 2, where "pph" stands for parts per a hundred parts of pigment. The addition of 3 parts of a dry starch product was added to the Base and Top direct fountain (DF) coatings to see the effects on pitting. The control (original formula) rheology, Brookfield viscosity, high-shear viscosity, and WRV (water retention value) were tested and compared to the trial formulation's measurements. Starch origin, molecular weight and its properties are proprietary, and thus will not be revealed. However, it is expected to exhibit a typical proportion of amylose and amylopectin.

Table 1: DF Base: Original basic formulation *Table 2: DF Top: Original basic formulation*

Materials	[pph]	Materials	[pph]
Kaomax	100	Kaomax TiO_2	90 10
Latex – 3103	21	Latex – 3103	21
Thickener	0.35	Thickener	0.35
Dispersant	0.12	Dispersant	0.12
Surfactant	0.30	Surfactant	0.30

DF – The direct fountain or DF curtain coating

2.2 Pitting tests
A pitting sample was stained with a Croda manufactured red drawdown ink (MBR 10039) to better see the pitting on the sheet. (This also makes it easier for the image analysis software to read.) There are three numbers that help determine the amount of pitting on the sheet: large pit count, area % pitted, and overall number of pits per measured area, which was 6 × 6 mm.

Each test requires a paper tester to look at four random and separate areas of the sheet in the cross-machine (CD) direction. The large pit count is taken with a Barska brand handheld digital microscope (AY11336), with a 10–300 × magnification, which is placed on the stained sheet. The higher magnification, but lower resolution highlights larger pits, and dulls out the smaller pits, depending on the how many large pits are in the visual area of interest (greater than 1 mm in diameter). The paper tester rates the sample on a scale of 1–4. Thus, after four tests, the lowest pit count is ranked 4 and the highest is 16. According to claims filed against the mill, printing issues tend to occur when the large pit count reaches ranking of about an 8. There is obviously variability in data due to the dependency on human perception and opinion. The area % pitted and number of pits were both found through the use of a 200 × magnification Aven brand digital microscopic camera (Mighty Scope NIR 5M). A public domain software, ImageJ, was used to analyze these images, which is able to distinguish pits through the contrast of color (pits are darker red, filled in by the Croda ink). It digitally computes the average area % pitted and number of pits through the four measurements.

3. Results and discussion

A brief analysis of the board was performed in order to better understand the surface on which the coating is applied (Table 3). It is known that pitting only occurs when the precoat and the curtain coating are both applied and does not occur when only the precoat or the curtain coating is applied. Thus, a comparison of the coated paperboard and the precoated paperboard was completed to see any similarities and/or differences that might reveal any indications behind the pitting phenomena.

Three major properties were of interest: surface energy, smoothness/roughness, and porosity. Surface Free Energy (mJ/m^2) of the board will help to quantify the interactions between the surface and the liquid coating (surface tension), and therefore provides an insight into the wetting of the paperboard at the dynamic wetting line. Smoothness or roughness is of importance since it was noted in the theory section that a rougher sheet could allow for more boundary air entrainment. Porosity (more correctly permeability) is of interest, since a greater porosity will allow for more wetting, where the coating will tend to drive into the sheet; this could also allow air and moisture to escape through more passages, where a less porous sheet will force air and moisture through the top of the coating. The averages of 10 individual readings of all properties (besides surface energy, which is calculated using various contact angle measurements and the Owens and Wendt (1969) method) were calculated and are summarized in Table 3.

Table 3: Uncoated vs precoated paperboard – summary of paper properties

Test		Uncoated Paperboard	Precoated Paperboard
Surface Energy (mJ/m^2)		70.7	46.6
Dispersive (mJ/m^2)		31.1	43.9
Polar (mJ/m^2)		39.6	3.7
Porosity – Gurley (s/100 cm^3)	*AVG*	48	850
	STD	6	107
Roughness – PPS (µm)	*AVG*	6.6	4.5
	STD	0.4	0.3
Roughness – Sheffield (Sheffield Units (SU))	*AVG*	304	260
	STD	8	26

As seen in Table 3, the surface energy of the uncoated board is considerably higher than the precoated board, which will result in faster, more complete wetting of a liquid on the surface. This value is probably skewed, due to the high porosity of the sheet, which will contribute to the wetting of the surface and produce a false surface energy value; a Cobb test confirmed this theory, as there was complete wetting in less than 1–2 s on the uncoated surface. The original DF Top and Base coating formulations can be seen in Tables 4 and 5. The DF Top and Base coating formulations were then modified by adding ~2 parts of dry starch to an 8 000 lb. (~3.6 tonne) batch of each coating. Otherwise, the coating formulations stayed the same. Surface tension of starch coating was slightly higher than original coating (Figure 3).

Table 4: DF Base: Starch trial formulation

Materials	[pph]
Clay	100
Latex	21
Thickener	0.35
Dispersant	0.12
Surfactant	0.30
Starch	0.30

Table 5: DF Top: Starch trial formulation

Materials	[pph]
Clay	90
TiO_2	10
Latex	21
Thickener	0.35
Dispersant	0.12
Surfactant	0.30
Starch	0.30

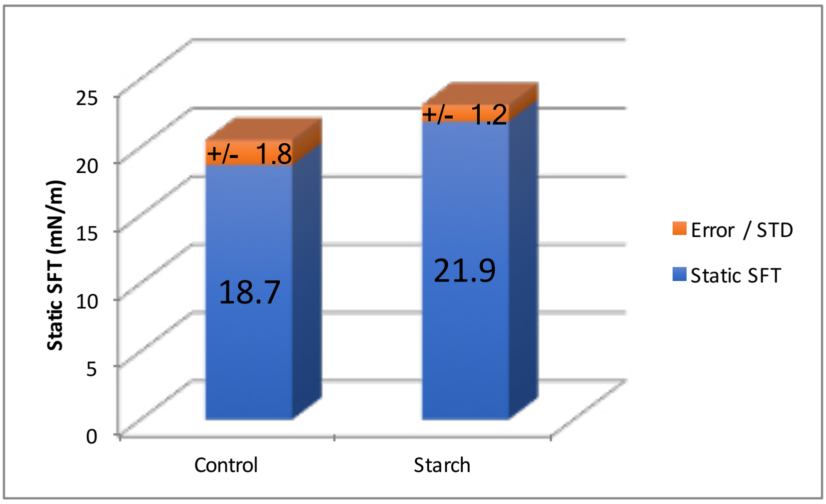

Figure 3: Static surface tension for control coating vs starch formulation

The DF Base starch formulation would run first, in order to ensure curtain stability and machine runnability. If the run was smooth, the operators would then transition the starch into the DF Top slot as well. It was planned to run on 18 pt. board, but due to the unpredictability of machine runs and customer demands, the trial was run on 14 pt. The results of the trial on pitting are seen in Table 6; there were no runnability issues, but there was a sheet break toward the end of the trial. This resulted in only 4 trial results, not 5 as initially designed. Coating samples were taken at the DF curtain head, and WRV (water retention values) were monitored to better indicate when the starch was fully integrated into the system (the WRV value was expected to decrease with the addition of starch).

Table 6: Starch trial summary – pitting averages viewed from an area of 6 × 6 mm

	Large Pit Count		% Area Pitted		Number of Pits	
	AVG	**STD**	**AVG**	**STD**	**AVG**	**STD**
Control / Pre-Trial	7	1	4.1	0.9	5 300	1 100
Trial – Starch	4	1	2.6	0.8	2 900	310

Pit counts immediately dropped from 8 to 5 when the DF Base trial coating reached the DF head; percent pitted area decreased from 5.8 % to 3.6 %. This decrease in pitting was consistent within the duration of the trial, with the overall large pit counts decreasing to an average of 4 and pitted area decreasing to 2.6 % after both DF Base and Top trial coating batches reached the DF head. The decrease in pitting was visually evident as well as seen in Figures 4 and 5.

The coating rheology could be manipulated by the addition of starch to promote further healing properties and increased water retention capabilities. It is possible that the amylose starch linear structures with no side chains in the starch mixture are responsible for such behavior, where it's also known to be hydrophilic in nature. Vinyl acrylic latex may have side chains or copolymers in their chain, with unknown amounts of –COOH groups, and side branches of various amounts and sizes, all of which may affect packing of polymer molecules in the coating and thus affecting viscosity. The original formulation (control) and the starch trial formulation (with the decreased thickener component) were both tested for the following basic coating properties: surface tension (Fig. 3), density (g/cm^3), solids (%), Brookfield Viscosity, and water retention values, and shown at Figures 6–9.

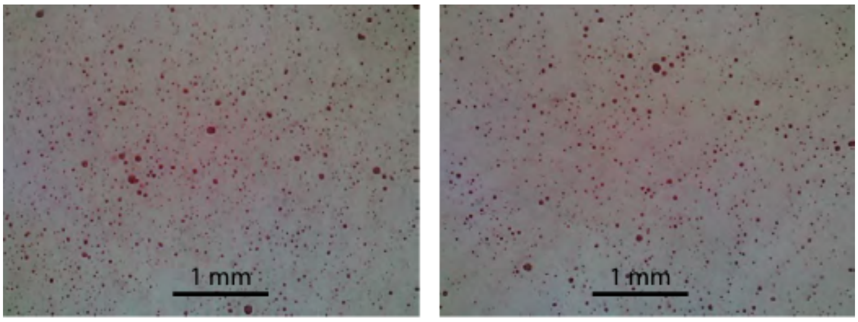

Figure 4: Pre-trial (Control) sample images

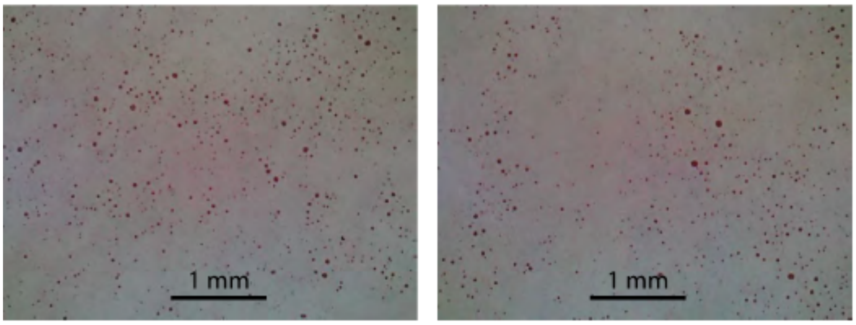

Figure 5: Trial starch sample images

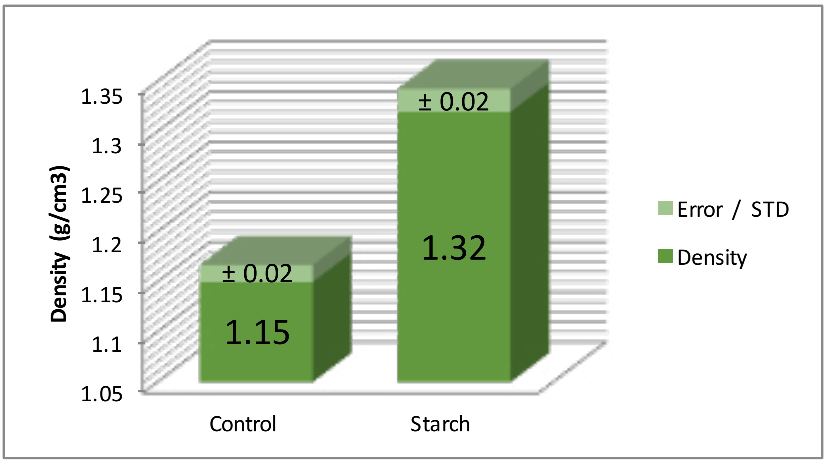

Figure 6: Density of control coating vs coating with starch

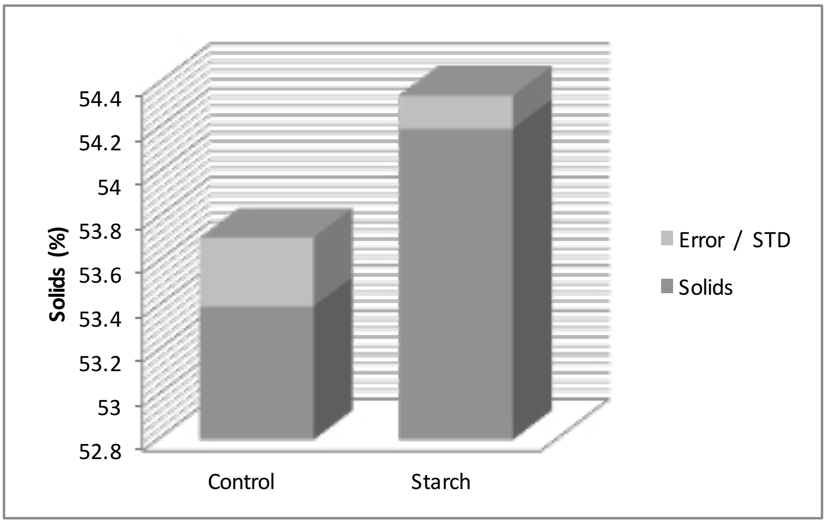

Figure 7: Solids of control coating vs coating with starch

Through these results, one can see that the starch allowed for slightly higher solids (%) and a higher density (g/cm^3) of the coating, but that it's Brookfield viscosity (@26.3 s^{-1} shear rate) was considerably lower than the original formula. This might be attributed to the decreased thickener content, which may have increased viscosity (per part) more than the starch is capable of. The pH values of the coatings are not considerably different (data not shown), with the starch being slightly closer to neutrality than the control formula. This will not change the effect of the coating performance on the machine.

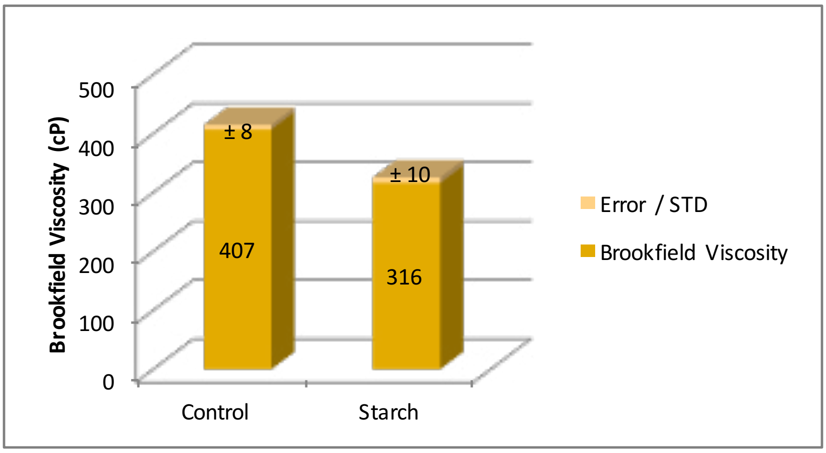

Figure 8: Brookfield viscosity of control coating vs coating with starch

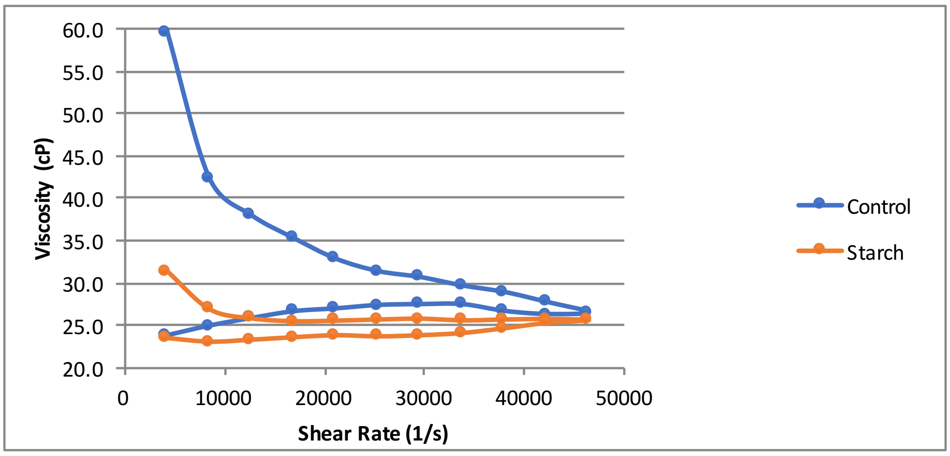

Figure 9: Viscosity vs shear rate of the control vs starch formulations

While both coatings show a pseudoplastic (shear-thinning) model curve, the control formulation has a higher initial viscosity, which quickly declines (Figure 9). This gives the control coating a larger area between the ramp up and the ramp down sections of the test; the area between the initial ramp up from 0 s^{-1} to 46.288 s^{-1} and the final ramp back down to 0 s^{-1} can help define how thixotropic a coating is – the larger the area the more thixotropic or shear thinning it obviously is (increased drop of viscosity). Thus, the control formulation is more thixotropic than the starch formulation, which seems to be almost Newtonian without much change in its viscosity during the ramp up and ramp down of the test. Low shear viscosity of coating colors usually reflects the viscoelastic region. Reducing the low shear viscosity by as much as 25 % has a large impact on converting the system from a strongly elastic rheology to a more viscous one. Such a move toward a more purely viscous system is known to prevent the elastic stretching and visible retention of coating color defects, such as bubbles.

The water retention value (g/g), or WRV, measures how much water is released by a coating after drying. In theory, if water is held in by the coating instead of being released by drainage, there is a lower probability of the water creating air/vapor and bursting through the curtain coating layers during the drying process. Starch is hydrophilic in nature, and thus it is believed that the gravimetric WRV of the coating will decrease, as the coating will be able to hold on to more water. Figure 10 shows the WRV results of the test on the control vs the starch trial formulation. The results show improved water retention capabilities of the coating through the introduction of starch. It was found through lab trials that an increase of the starch content within the coating batch did not help to lower the WRV any further, thus 150 g/g WRV seems to be where the starch's capabilities plateau. This significant drop from 200 to 150 WRV may help to decrease pitting, with water being held in the sheet/coating, not released through the coating. This also suggests that the formulation is less flocculated, and thus also less elastic.

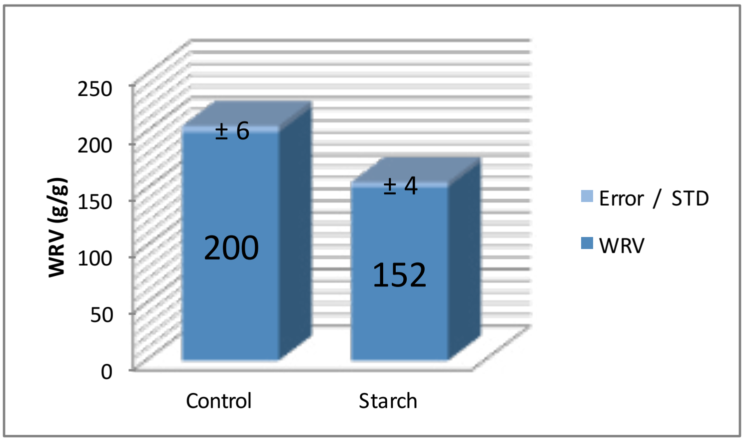

Figure 10: WRV of control and starch coating

4. Conclusions

The addition of starch and replacement of conventional thickener to base and top coating showed beneficial effects on decreased pitting area and size of pits. It was found that the pitted area decreased with increased caliper of the board (data not shown, Schoenfelder, 2017). However, addition of starch paired with decrease in the thickener addition decreased the viscosity of the curtain coating. This did not seem to have a negative effect on the pitting results, with similar results to the initial trial. The viscosity was still around/above the 300 cP (mPa·s) range. Water retention levels of coatings seem to correlate to lower pitting - as the coating holds in more water, there is most likely less air passing through the sheet, which may be a mechanism for pits formation. The coating's ability to heal is important in deterring the occurrence of large craters on its surface.

References

BASF, 2016. *Surface Control*. [online] Available at: <https://www.dispersions-pigments.basf.com/portal/basf/ien/dt.jsp?setCursor=1_564555> [Accessed May 8 2018].

Brown, D.R., 1961. A study of the behavior of a thin sheet of moving liquid. *Journal of Fluid Mechanics,* 10(2), pp. 297–305.

Chen, K. S., 1992. *Studies of multilayer slide coating and related processes*. Ph.D. Thesis. University of Minnesota.

Chen, T, Joyce, M. K., Fleming, P. D. and Bloembergen, S., 2016. Pigmented formulations containing biobased nanoparticle binders for curtain coating applications; Part 1: Rheological study. In: *Paper Conference and Trade Show (PaperCon 2016)*. Cincinnati, Ohio, USA, 15–18 May 2016. Curran Associates.

Kistler, S.F., 1983. *The fluid mechanics of curtain coating and related viscous surface flows with contact lines*. Ph.D. Thesis. University of Minnesota.

Klass, C.P., 2004. Is curtain coating ready for prime time? *Solutions - for People, Processes and Paper*, 87(12), pp. 30–32.

Marston, J.O., Hawkins, V., Decent, S.P. and Simmons, M.J.H., 2009. Influence of surfactant upon air entrainment hysteresis in curtain coating. *Experiments in Fluids*, 46(3), pp. 549–558.

Owens, D.K. and Wendt, R. C., 1969. Estimation of the surface free energy of polymers. *Journal of Applied Polymer Science*, 13(8), pp. 1741–1747.

Schoenfelder, S.L., 2017. *The modification of a curtain coating formulation: a study of rheology and surface tension, and their effect on pitting*. Master's Thesis. Western Michigan University.

Index of authors

Al Aboud 107

Backhaus 55, 115
Bilgin 55
Blass 10
Blayo 156
Bodenstein 97
Bollström 142
Bonev 164

Chrétien 156

De Groot 64
Dörsam 72, 97, 107, 132
Držková 20

Fang 152
Fernandes 97
Fischer 2
Fleming 193

Gane 88, 142
Gorbachev 171
Groher 132
Gu 152

Hakimi Tehrani 107
Hsieh 36
Hübner 2

Jaeger 132
Jiang 36
Jutila 142

Kapović 64
Karlovits 49
Kaynarova 171
Kisters 88
Koivunen 142

Lavrič 49
Li 177
Liu, J. 152
Liu, L. 177
Liu, X. 177
Lozo 64

Ma 187
Makarov 171
Marlin 156
Martinez 2
Meckel 132
Mo 152

Paap 10
Pedersen 27
Pekarovicova 193
Podsiadło 82
Politis 185
Put 125

Ridgway 88
Rosalen 115
Roudný 20

Sauer 72, 97
Schäfer 72
Schoenfelder 193
Spiehl 107, 132
Stamm 132
Suess 132

Van den Saffele 125
Voloshynovskiy 164

Warsitz 97
Wittenzellner 10
Wong 36
Wu 177

Xin 152

Yakovleva 171
Yang 152

Zakrzewska 82